وزارة التعليم
Ministry of Education
الملحقية الثقافية السعودية في المملكة المتحدة
Saudi Arabian Cultural Bureau in the UK

Newcastle University

Towards an Understanding of the Genetic Aspects of Hypoplastic Left Heart Syndrome (HLHS)

Ahlam Al-Qahtani

August 2019

A dissertation submitted to Newcastle University in accordance with the requirements for the award of degree of Doctor of Philosophy in the Faculty of Medical Sciences, Institute of Genetic Medicine.

Abstract

Hypoplastic left heart syndrome (HLHS) is a rare congenital heart defect in which the left side structures of the heart are severely underdeveloped and major, repeated surgeries throughout childhood are required for survival. Although the specific features can vary considerably, a series of abnormalities involving a diminutive left ventricle, a narrow ascending aorta and atretic or stenotic mitral and aortic valves, are always noted. Based on inheritance of HLHS in families, a strong genetic component to HLHS has been suggested. Despite this, genetic studies have failed to reveal mutated genes that cause HLHS. A novel approach was taken in this study where it was hypothesised that there might be distinct anatomical subgroups of HLHS that differed from the current clinical classification. Thus, performing analyses on specific and homogeneous subgroups might be more amenable to understand which defects in HLHS are potentially primary and which secondary, and ultimately finding the causative gene(s) for HLHS. To accomplish this, archival formalin-fixed HLHS hearts, obtained from Birmingham Children's Hospital, were carefully phenotyped and re-classified based on their ventricular morphology. It was suggested that genomic analysis of these hearts might reveal causative mutations for HLHS, but it is also recognised that formalin fixation causes damage to DNA. Consequently, a method was developed for extracting high quality DNA from formalin fixed tissue that could be used for PCR or Next Generation Sequencing (NGS). Through comparison of NGS whole exome sequencing data from formalin-fixed DNA with blood derived DNA, it was possible to determine bioinformatics processes to maximise the detection of

genomic variants with high specificity and moderate sensitivity from formalin-fixed tissue.

Finally, as a prelude to future genomic studies, the expression patterns of genes previously implicated in HLHS genes were analysed, focussing on the structures affected by HLHS and considering how they might link to the previously identified HLHS phenotypic subgroups. Although some HLHS-implicated genes, including *Gja1* and *Sap130,* showed very broad expression patterns, and thus it was hard to associate them with the HLHS phenotypes, other genes showed specific expression within the structures affected by HLHS. It was speculated that *Notch3, Hand1, Foxc2,* and *Pcdha9* would be more likely to correlate with, based on their expression patterns, the abnormalities associated with various subgroups of HLHS.

Together, these data suggest that the broad clinical spectrum of HLHS is made up of distinctive anatomical subgroups. DNA obtained from archival hearts should not be used for primary variant detection but could be used for corroboration of findings for example from family studies. Some postulated genes appear to be expressed in structures affected in HLHS and are more interesting candidates for the malformations, whilst others are more broadly expressed and may represent modifier genes or false positive findings.

Dedication and Acknowledgements

This thesis could not have been completed without the help, supervision and support of my wonderful supervisors Dr. Bill Chaudhry and Prof. Deborah Henderson. They were like a family to me and I appreciate all that they have done to make my PhD journey a lot easier. I owe them warm thanks, not only for advising and guiding me through my long and rough PhD journey, but also for all their support outside the work environment.

Thank you to my husband Jamil who has been and always will be my rock during difficult times and believed in me more than I believed in myself. Thank you Yasem for always being able to change my mood by being affectionately happy and present in the moment.

Thank you to my wonderful sisters Athba and Munira who were a major source of encouragement and support. Thank you to all my family and friends whose names were not mentioned but their kindness and support had paved my way.

Thank you to my lab mates for their continuous support, understanding and help. Special thanks to Lorraine Eley, Lindsay Murphy, Rachel Richardson, Adrian Santos and Mashael Alaradi. Also, many thanks to Andrew Skelton, Adrian Crucean, Robert Anderson and William Brawn for their help in conducting some of the studies. I wish also to extend special thanks to the Saudi Ministry of Higher Education administered by the Saudi Cultural Bureau in London for fully funding this study.

أولاً شكرًا لله تعالى الذي يسر لي كل شيء...
أهدي هذه الرسالة إلى والدي العزيز محمد ووالدتي الغالية مريم لحبهم ودعمهم اللامحدود...
شكراً لزوجي العزيز جميل وابني الرائع ياسم لجعل حياتي مليئة بالدعم والحب...

Table of Contents

List of Tables

List of Figures

List of abbrevations

A: adenine
AA: aortic atresia
AAo: ascending aorta
Ao I: aortic isthmus
Ao: aorta
AS: aortic stenosis
BCA: brachiocephalic trunk
BQSR: base quality score recalibration
C: cytosine
CC: cardiac crescent
CJ: cardiac jelly
CS: carnegie stages
DA: ductus arteriosus
DAo: descending aorta
DORV: double-outlet right ventricle
EFE: endocardial fibrolastosis
EMT: endothelial mesenchymal transition
EndoC: endocardium/endocardial cells
FHF: first heart field
G: guanine
H_2C: schiff base
HC: haplotypeCaller
HLHS: hypoplastic left heart syndrome
IC: intercalated cushions
LCCA: left common carotid artery
LSCA: left subclavian artery
LV: left atrium
LV: left ventricular heart
LVOT: left ventricular outflow tract
MA: methylol adduct
MA: mitral atresia
MC: myocardium/myocardial cells
MinV: miniaturised ventricle
MS: mitral stenosis
NGS: next-generation sequencing
PCR: polymerase chain reaction
Pul: pulmonary artery
RA: right atrium
RV: right ventricular heart
SHF: second heart field
SLV: slit-like ventricle
T: thymine
TWV: thick-walled ventricle
UNG: uracil-N-glycosylase
VCF: variant Call Format
VEP: variant effect predictor
VQSR: variant quality score recalibration

Chapter 1: Introduction to Hypoplastic Left Heart Syndrome

1.1 Overview

Hypoplastic left heart syndrome (HLHS) is a rare congenital heart defect that without intervention leads to death in the first months of life. It is characterized by an underdeveloped and functionally insufficient left-side structure of heart, including non-apex forming hypoplastic left ventricle with atretic (imperforate) or stenotic (narrowed) mitral and aortic valves, and hypoplastic aorta (**Figure 1.1**) (Crucean and Alqahtani et al., 2017).

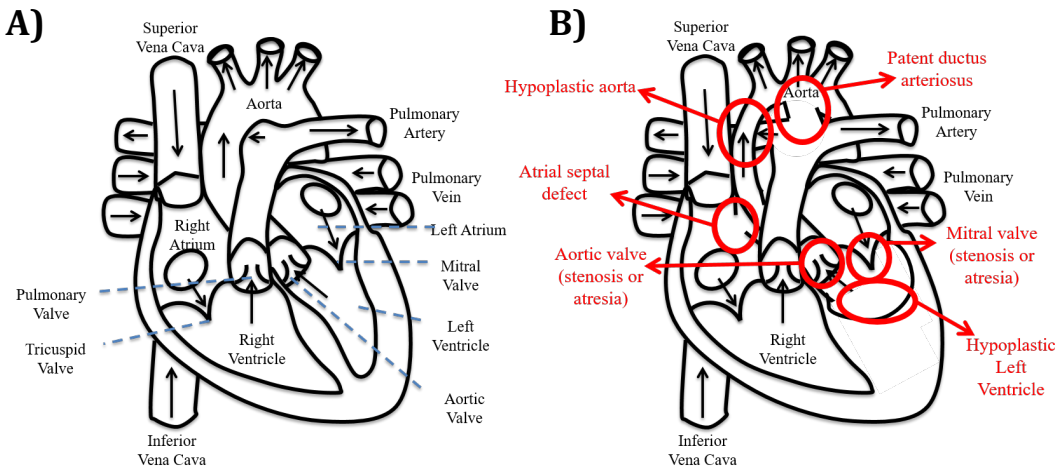

Figure 1.1: Diagrammatic sketches of a normal heart (A) and a hypoplastic left heart (B).
HLHS is characterised by hypoplasia of left ventricle and aorta, stenosis and atresia of aortic and mitral valves, atrial septal defect and patent ductus arteriosus (red labelled).

The underdevelopment of the left side of the heart is detectable antenatally and can be diagnosed as early as 15 weeks of gestation using routine sonographic scans (Andrews et. al., 2004; Galindo et al., 2009). Upon diagnosis of HLHS, parents are challenged with two options: termination or continuation of pregnancy. If continuation of pregnancy is chosen, the infant will have to either undergo an emergency three-step surgical procedure

(staged palliation) and/or a heart transplantation or go for comfort palliative care when the baby is born (Yabrodi et al., 2017). The staged palliation consists of three procedures: Norwood Procedure[1] or Hybrid procedure[2] (performed as emergency operations shortly after birth), Bi-directional Glenn Operation (six months after first surgery), and Fontan Operation (approx. 18 to 36 months after the second surgery). Thereafter, HLHS patients will require a life-long cardiac care and medications including anticoagulation and anti-arrhythmics (Karbassi et al., 2017). Unfortunately, even when the staged palliation is initially successful, there is a significant risk of requiring a heart transplant in later life. Despite improvements in the medical and surgical management of HLHS and the usually good surgical results, this remains a very complex and life-threatening clinical problem.

Remarkably, the knowledge of HLHS pathology remains limited and its causes remain unknown. Therefore, this section intends to review what is known about early heart development in order to try to understand the developmental origins of HLHS, and will outline the historical perspectives, epidemiology, and possible mechanisms and causes of HLHS.

1 Norwood procedure involves atrial septectomy, joining the aorta to the pulmonary artery and inserting a shunt between the two branching pulmonary arteries and either the right ventricle or the branch of aorta to provide blood flow to the lungs.

2 Hybrid procedure involves balloon atrial septectomy, placement of a stent to patent ductus arterious and banding the branching pulmonary arteries.

1.2 Formation of a normal heart

The heart is one of the earliest organs to differentiate and function. Generally, the heart begins to beat at around 22-23 days in human embryos (Moore et. al., 2015). The development of the heart is highly similar between different species, but it has been intensively studied in mice (Vincent and Buckingham, 2010). Therefore, this section will look at heart development from the standpoint of mouse cardiogenesis, highlighting relevant aspects of human development (**Figure 1.2**).

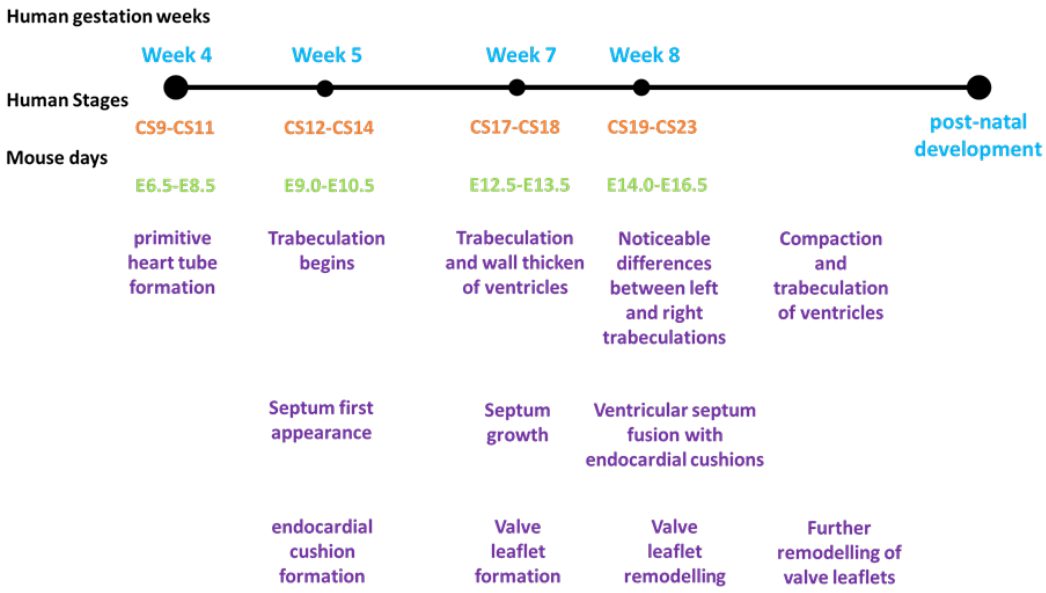

Figure 1.2: Development of heart in human Carnegie stages (CS) and mouse Embryonic days (E).
CS is a standardised and universal system for staging embryonic development. In human, there are 23 stages (first 60 days of development) and after that the term changes from embryo to fetus.

1.2.1 Overview of mouse heart development

The development of the heart in mice begins at embryonic day 6.5 (E6.5), when the cardiac progenitor cells, derived from the epiblast and located lateral

to the primitive streak, undergo an epithelial to mesenchymal transition (EMT) and enter the primitive streak (Tam et al., 1997). These cells then migrate to form clusters in the ventro-lateral region of the embryo, in the new mesenchymal layer. By E7.5, the merged clusters are located under the head folds and establish the cardiac crescent, which is a horseshoe-shaped structure (Vincent and Buckingham, 2010). Through several signals from the underlying endoderm, including fibroblast growth factor (FGF), WNT signals and bone morphogenetic protein (BMPs), expression of cardiac transcription factors such as GATA binding protein 4 (*Gata4*) and *Tbx5* are induced and differentiation of cardiac myoblasts begins (Kelly and Buckingham, 2002). As the embryo grows, it starts to fold laterally, the two ends of the cardiac crescent come together at the midline, and fuse to form a single primitive cardiac tube, which swiftly begins to pump blood (Moorman et al., 2003, Vincent and Buckingham, 2010). By E8, the cardiac tube is composed of an outer myocardial layer surrounded by an inner endocardial cell layer, and in between an extracellular matrix-filled cardiac jelly (**Figure 1.3**) (de Vlaming et al., 2012). The dorsal mesocardium, a mesenchymal fold, keeps connection between the posterior pericardial wall of the growing embryo and the cardiac tube. As embryonic development progresses, however, this attachment disappears and the heart tube suspends in the developing pericardial cavity through its connections at the venous and arterial poles (Kelly et al., 2014). At approximately E8.5, the cardiac tube undergoes a rightward looping process, which causes the developing chambers to be placed into their adult positions. The process of looping is still not fully understood although there are thoughts of cell additions that lead to elongation of the cardiac tube and extracellular

matrix irregular depositions (Taber et al., 1995) and buckling through gradual breakdown of dorsal mesocardium while growing of the heart tube between fixed poles (Garrec et al., 2017). The looping process as well as expansion of myocardium result in the formation of recognisable heart chambers (Buckingham et al., 2005). By E10.5, the heart has developed four-recognisable chambers, but is still a tube until E14.0-E16.5 when the chambers and outflow tract are separated by the fusion of myocardial and membranous septa (**Figure 1.3**) (Buckingham et al., 2005).

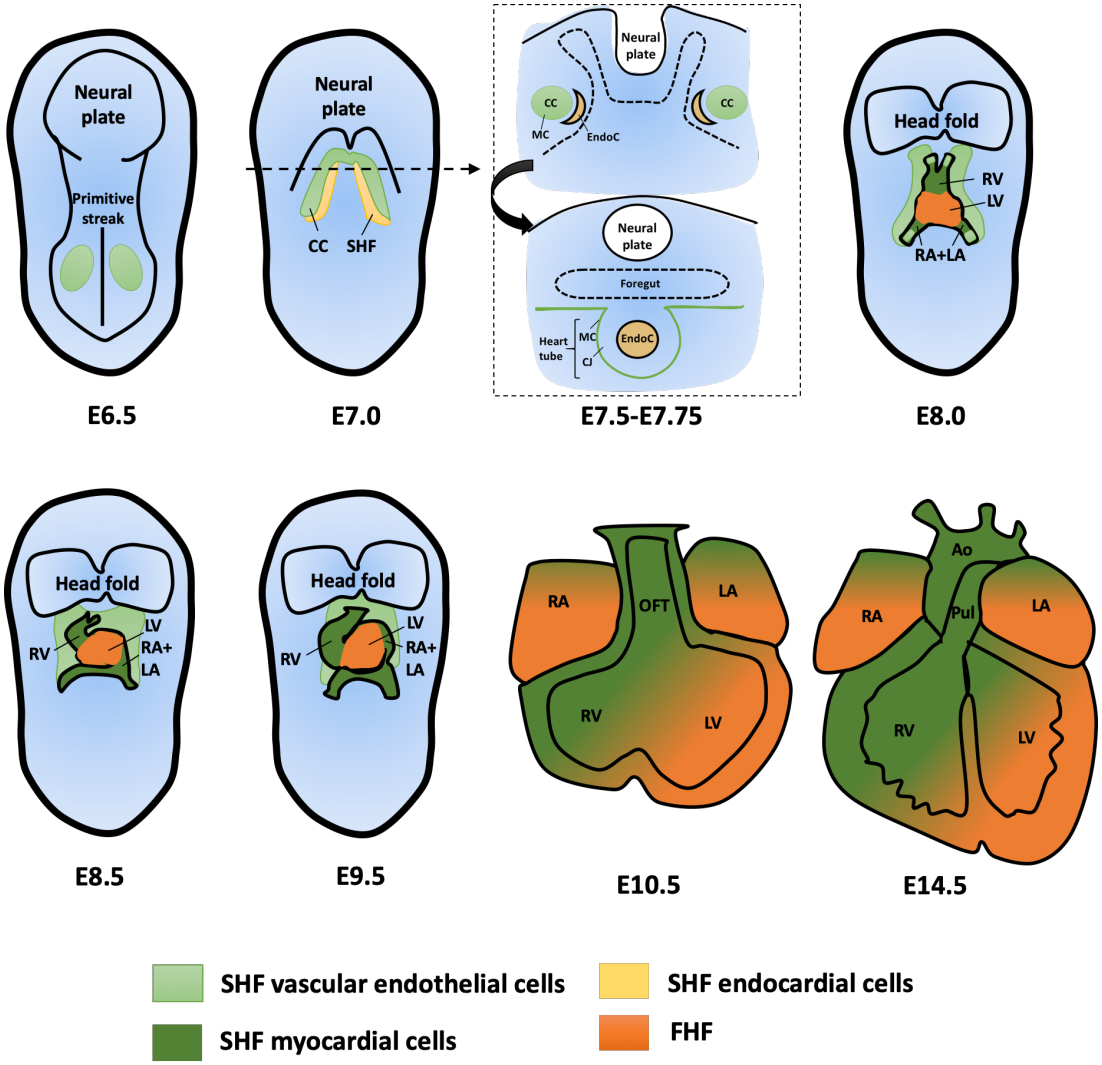

Figure 1.3: Development of the heart tube.
At E6.5, cardiac progenitor cells, located lateral to the primitive streak, undergo an epithelial to mesenchymal transition (EMT) to enter the primitive streak. At E7.0 to E7.5, cells migrate to form cardiac crescent in which the two ends of the cardiac crescent fuse to form a single primitive cardiac tube. At E8.0, cardiac tube is formed by an outer myocardial layer surrounded by an inner endocardial cell layer, and in between an extracellular matrix-filled cardiac jelly. Between E8.5 to E9.5, the cardiac tube undergoes a rightward looping and ballooning processes. By E10.5, the heart has developed four-recognisable chambers and at E14.5 the chambers and outflow tract are separated. CC, Cardiac crescent; SHF, second heart field (Dark green: myocardium and pale green: vascular endothelial cells); FHF, first heart field (Orange); MC, Myocardium/myocardial cells; EndoC, endocardium/endocardial cells; CJ, cardiac jelly; LV, left ventricle, RV, Right ventricle; LA, left atrium; RA, right atrium; OFT, outflow tract; Ao, aorta; Pul, pulmonary artery.

1.2.2 Myocardial progenitor cells and regulatory genes

Myocardial specification and differentiation are initiated in the splanchnic mesoderm, and in mouse, they continue for a 3 day period during the phases of cardiac tube elongation and heart looping (Kelly et al., 2014). The addition of cells at the end of the heart tube initiates cardiac tube growth. As mentioned previously, after the suspension of heart tube in the pericardial cavity, the mesodermal cells maintain connection with the heart tube through posterior venous and anterior arterial poles of the heart (Buckingham et al., 2005; Kelly, 2012). Retrospective lineage analysis and genetic tracing studies have shown that myocardium originates from two distinctive cell lineages: the first heart field (FHF) and the second heart field (SHF).

1.2.2.1 The first heart field (FHF)

The early wave of mesodermal cells that give rise to the initial heart tube and express muscle-specific proteins is referred to the first heart field (FHF), which originates from the cardiac crescent (Buckingham et al., 2005). The FHF cells provide a scaffold for later growth and have mainly a left ventricular identity, although they also contribute to the atria (Kelly et al., 2014).

1.2.2.1.1 Genes involved in FHF regulations

There are several transcription factors expressed in the FHF, including *Nkx2.5, Gata4, Tbx5* and *Mesp1*. Although *Nkx2*.5 is an essential transcription factor for the FHF, it is also expressed in the SHF, which indicates a central regulatory role for *Nkx2*.5 during cardiac development and losing Nkx2.5

function causes impairment of cardiogenesis (reviewed in Colombo et al., 2018). Likewise, knockout the transcription factor GATA binding protein 4, *Gata4*, caused cell migration failure and eventually led to cardiac bifida where two independent hearts started to form on either side of the embryo (reviewed in Zaffran et al., 2004; Buckingham, 2016). Furthermore, identification of transgenic genes such as *Tbx5* specific to FHF has opened the way to functional analysis not only to the FHF but also to SHF (Vincent and Buckingham, 2010).

1.2.2.2 The second heart field (SHF)

The SHF cells are detected initially lying medially and extending posteriorly to the cardiac crescent (the FHF; Hami et al., 2011). However, upon fusion of the cardiac crescent, the SHF cells relocate behind the heart tube, anteriorly adjacent to the outflow tract, and posteriorly adjacent to the sinus venosus and venous pole (reviewed in Buckingham, 2016). As the heart tube is in continuity with the dorsal mesocardium, this allows addition of undifferentiated cells from the SHF. Even after the dorsal mesocardial connection disappears, the SHF cells continue to add to the heart poles forming myocardium through the venous and arterial poles of the heart (Felker et al., 2018). This addition of SHF cells lasts for several days in mouse embryos, as myocardium of the caval veins and pulmonary is not fully formed until E12.5 or 40 days of human development (Buckingham, 2016). The SHF delivers a pool of cardiac progenitor cells that are conserved as a population of proliferating and non-differentiated cells. The behaviour of these cells is largely controlled by

transcription factors and signalling molecules, which have been identified as markers for these cells (Vincent and Buckingham, 2010).

1.2.2.2.1 Genes involved in SHF regulations

The progenitor cell population of the SHF has several genes that are specifically expressed in these cells. These genes have been considered as the key markers for the SHF population. *Islet1*, for example, has long been known to be the major marker for the SHF cells (reviewed in Vincent and Buckingham, 2010; Kelly, 2012). However, it was reported that *Islet1* was also expressed in the FHF progenitors, although transiently and at a low level, suggesting less sensitivity of this marker (Vincent and Buckingham, 2010). Therefore, other gene markers for the SHF progenitors have been identified including genes encoding for transcription factors such as *Foxc2, Mef2c-AHF-Cre, Nkx2-5-Cre, Tbx1*, and the chromatin remodelling protein SWI-/SNF-related, matrix-associated, actin-dependent regulator of chromatin, subfamily D, member 3 (*Smarcd3*) (Buckingham, 2016). All these genes are expressed in the SHF and also involved in myocardial differentiation.

Although the transcription factors and components of signalling pathways described above show essential roles in cardiogenesis, they are not necessarily cardiac specific (Buckingham and Rigby, 2014). Loss of cardiac regulatory genes can lead to embryonic lethality at early stages or cause multiple defects such as those seen in syndromes where the heart is affected, but other organ systems are also disturbed. This is the case for *Tbx1*, which in humans is associated with DiGeorge syndrome. This syndrome not only

causes cardiac defects including persistent truncus arteriosus / common arterial trunk, but also craniofacial abnormalities (Papangeli and Scambler, 2013). This is because *Tbx1* is involved in development of the endoderm and ectoderm of the pharyngeal region that is fundamental for both cardiac and cranial neural crest, as well as its role in the SHF (Buckingham, 2016). Therefore, genes that are specific to the SHF with no expression outside of this progenitor population, are the best candidates for malformations that are restricted to SHF-derived regions of the heart.

1.2.3 Development of the left ventricle

The left ventricle originates from the first heart field (FHF) and can first be seen after heart looping, as the primary heart tube elongates and bends to show an inner and outer curvature. The outer curvature gives rise to the main chamber and the apical parts of the left and right ventricles through a ballooning process (Moorman et al., 2007) (**Figure 1.3**). Eventually with remodelling, the inner curvature is very small and observed as the area between the left atrial wall and the root of the aortic valve (Crucean and Alqahtani et al., 2017).

The earliest phases of ventricular growth and development begin during the looping process (Moorman et al., 2003) as ventricular trabeculations appear. It is presumed the trabeculare network of myocardial muscle strands develop and functions to increase myocardial oxygen delivery whilst the coronary circulation is not yet established (Samsa et al. 2013), but it may also act as a preferential network for electrical activity prior to the establishment of the mature conduction system (Hatcher and Basson, 2009). Whilst the trabeculae

are forming the underlying compact myocardium also thickens, the trabeculated myocardium has a distinctive programme of gene expression that varies from that of the compact ventricular wall myocardium (Qi et al., 2007). In this section, the remodelling events that lead to formation of trabecula as well as the formation of ventricular septum will be discussed.

1.2.3.1 Left ventricular trabeculae

The initial formation of the trabeculae starts in the mouse at E9.5 and in the humans at CS12 (by the end of the fourth gestational week) (**Figure 1.2**). Because trabeculation occurs prior to ventricular septation, most of the myocardial mass and ventricular wall thickness in the embryonic heart is formed by the trabeculae (Wessels and Sedmera, 2003). In fact, the trabeculated myocardium has a distinctive programme of gene expression that varies from that of the ventricular wall myocardium (Qi et al., 2007). During cardiac development, the trabeculae undergo remodelling events that influence their arrangement and density. These remodelling events have been suggested to associate with formation of different cardiac structures, including delineation of papillary muscles, conduction system, and the coronary vasculature (Liu et al. 2010). Several genetic manipulation studies, primarily in mouse, have shown that disruptions of the normal meshwork of the trabeculae arrangement leads to severe consequences, such as an immature ventricular conduction system, dysfunctional myocardial contractility or even to embryonic lethality (Samsa et al., 2013; Liu et al. 2010).

As ventricular septation occurs, between E10.5 to E14.5 in mouse, the trabecular meshwork becomes more complex and thickly packed, with no great differences in complexity between the left and the right ventricles (Captur et al., 2016; Moorman et al., 2003). At E12.5, the left and right ventricular free walls are thickened along with the interventricular septal wall. From E14.5, this thickening in the septal and free walls is continued while the complexity of the trabeculae is reduced. Strikingly, at E14.5, the arrangement of the trabecular meshwork becomes noticeably aligned illustrating an “apex-to-base” orientation. Also, the trabecular strands now merge together providing the base for the developing papillary muscles (Towbin et al., 2015; Captur et al., 2016). At this stage, in the mouse and human, differences between left and right ventricles can be seen. For example, the surface of the left ventricular septal wall is trabeculated, whereas the surface of the right ventricular septal wall is relatively smooth. Also, in the humans, the left ventricular myocardium usually has more trabecular compaction compared to the right ventricular myocardium, with trabeculae much more obvious in the mature right ventricle than in the left (Towbin et al., 2015).

The trabeculations of myocardium in the developing heart to form the inner ventricular walls, and aggregation to generate the compact myocardium of the ventricular free walls in the mature heart, remain poorly understood. There have been, however, two models to explain the potential consolidation of myocardium from a trabecular layer to compact muscle (**Figure 1.4**). The first model proposed the expansion of the fetal compact myocardium into the trabecular layer to form the mature inner myocardial wall (Kirby, 2007). The

second model proposed merging the fetal trabeculated myocardium together to form the mature inner myocardial wall (Wessels and Sedmera, 2003). Both models suggested that the expansion of compact myocardium leads to the development of the outer myocardial wall/ventricular free wall. However, they both suggested a different mechanism for transformation of the trabeculated layer into the inner myocardial wall. Recently, a fate mapping study has proposed a new model that combines the two previous models, as well as adding a new component by identifying a middle hybrid myocardial zone (**Figure 1.5**). The new proposed model suggests that expansion of the embryonic compact myocardium into the trabecular layer in an epicardial-to-endocardial orientation causes condensation of the trabeculated myocardium, subsequently closing the spaces within the trabecular meshwork, which eventually forms the inner myocardial wall (Tian et al., 2017). In this model, the contribution of the compact myocardium to the trabecular layer that forms the inner myocardial wall is limited to the hybrid myocardial zone. The high proliferation rate of the fetal compact myocardium compared to the trabeculated myocardium allows inward expansion of compact myocardium rather than outward expansion of the trabeculated myocardium. Altogether, although there are several models that have been proposed to explain the postnatal transformation of trabeculated myocardium into compact myocardium, the cellular process of trabecular compaction remains controversial.

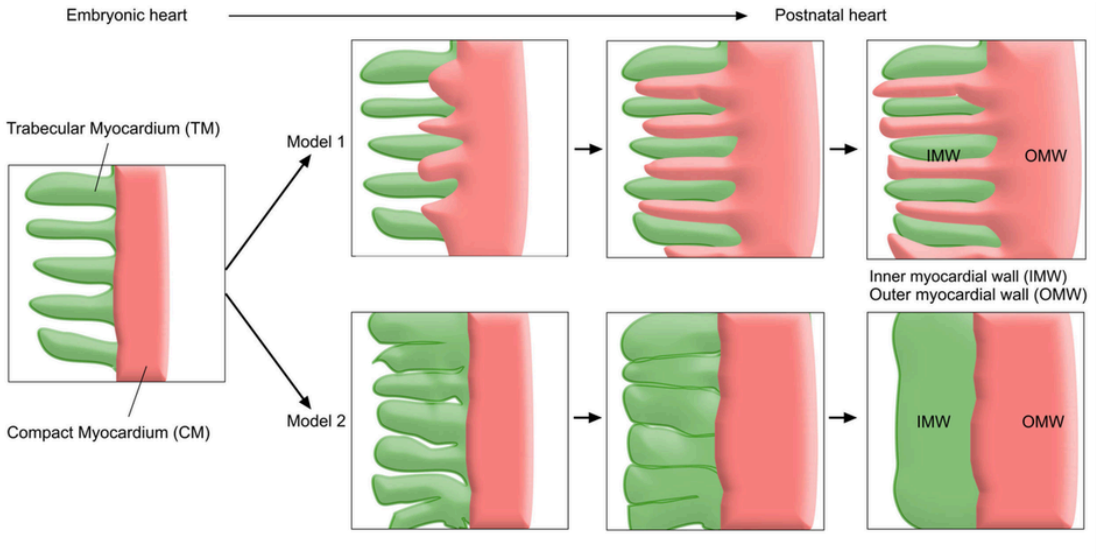

Figure 1.4: The two proposed models for myocardium compaction transformation in developing heart.
Model 1 indicated expansion of the compact myocardium from the outer wall into the intertrabcular space forming the inner myocardial wall in postnatal heart. Model 2 indicated the compact myocardium fused together to form the inner myocardial wall. IMW, inner myocardial wall; OMW, outer myocardial wall (Image obtained from Tian et al., 2017).

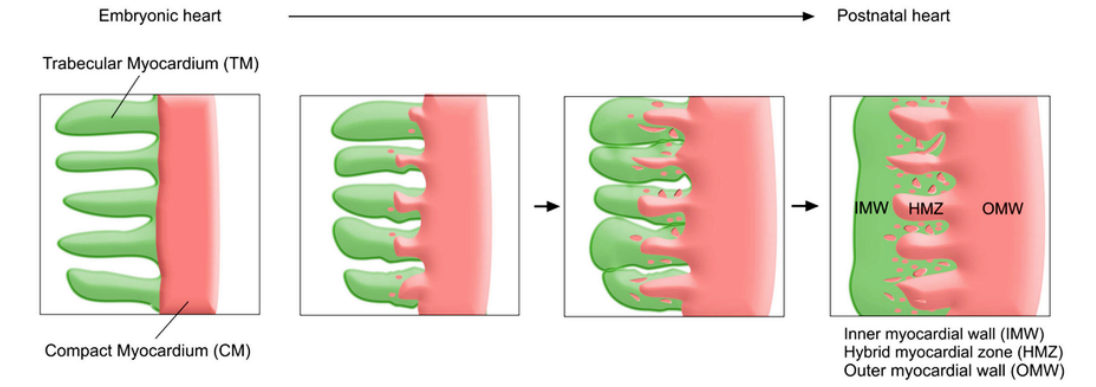

Figure 1.5: The recent model for myocardium compaction.
This model combines the two previously reported models with a novel identification of a hybrid myocardial zone that contains the contribution of compacted myocardium into the trabecular layer (image obtained from Tian et al., 2017).

1.2.3.2 Formation of the ventricular septum

The initial appearance of the ventricular septum observed is at E10.5 in mouse, and at CS12 in human (by the end of the fourth gestational week) (**Figure 1.2**). As the heart tube undergoes the looping and ballooning process, the formation of the muscular ventricular septum begins at the interventricular groove (Anderson et al., 2014), whereas the membranous region of the ventricular septum develops at the atrioventricular groove by the endocardial cushions (Wiegering et al. 2017) (**Figure 1.6 A-C**). In parallel with ventricular growth, at E10.5 to E11.5 in mouse, proliferation of cells located in the ventricular wall establishes the formation of the muscular region in the ventricular septum (**Figure 1.6 C-D**) (Franco et al. 2006). As trabecular meshwork develops and forms the inner ventricular wall, trabeculated myocardium fuse with the growing muscular ventricular septum and boost the septum growth (**Figure 1.6 D-E**) (Contreras-Ramos et al., 2008). Hence, this highlights the importance of the trabeculated myocardium and the normal development of the ventricular wall for the formation of the muscular ventricular septum (Wiegering et al. 2017). Because the ventricular septum forms between the left and right ventricles, it is composed of a combination of cardiomyocytes derived from both ventricles (Franco et al. 2006). As the muscular ventricular septum grows, the membranous ventricular septum originating from the atrioventricular endocardial cushion cells concomitantly grows to eventually fuse with the muscular ventricular septum in a yet unknown fashion (**Figure 1.6 F-G**) (Wiegering et al. 2017).

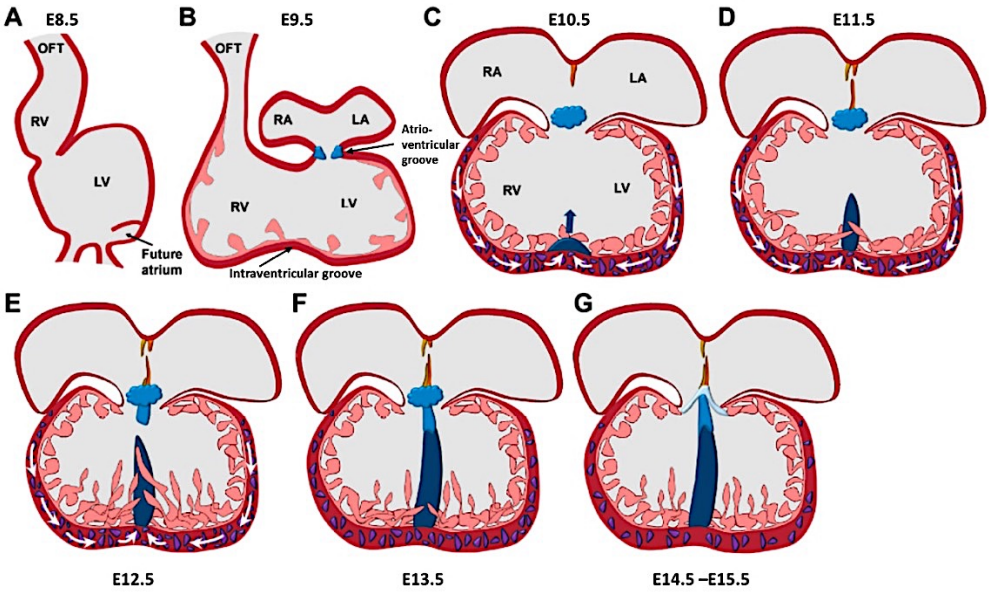

Figure 1.6: Ventricular septum formation.
(A-B) cardiac four-chambered shaped through looping and ballooning process. (C) Proliferation of myocardial cells (purple) from the ventricular wall causes outgrowth of the muscular region (dark blue) of the ventricular septum. (D) Trabeculated myocardium in the ventricular wall also contribute to the development of the septum. (E) In an unknown process, the membranous ventricular septum derived from the endocardial cushion cells (bright blue) develops and grows in the direction of the muscular ventricular septum. (F-G) Fusion of the muscular and membranous ventricular septa and development of the atrioventricular valves. OFT, outflow tract; RV, right ventricle; LV, left ventricle; RA, right atrium; LA, left atrium (Obtained and modified from Wiegering et al. 2017).

1.2.4 Development of the aortic valve

The aortic valve develops from the outflow tract cushions, which are expansions of cardiac jelly that are found in between an outer myocardial layer and an inner endocardial layer along the length of the unseptated outflow tract. The cardiac jelly is an acellular extracellular matrix; up-regulation of extracellular matrix secretion; transformation of endocardial cells to form mesenchyme and contribution of neural crest-derived mesenchymal cells leads to its expansion. SHF-derived endocardial cells undergo endothelial–mesenchymal transformation (EndoMT) and invade into the cardiac jelly, particularly at the proximal outflow tract. This process occurs at E10.5 in mouse and 28 days post-fertilization in human (**Figure 1.7**) (Henderson et al., 2018). At the same time, neural crest cells migrate into the distal part of the outflow tract to stimulate fusion of the left and right endocardial cushions and promote the septation of the outflow tract in a zipperlike fashion to form the aorta and pulmonary trunk. The aortic valve is formed at the distal part of the fused endocardial cushions, at the same level as the anterior and posterior intercalated cushions. The intercalated cushions primarily are first seen at E10.5 in mouse. Remodelling of these cushions to form the posterior (non-coronary) and anterior leaflets of the arterial valves was first described in 1942 by Kramer. Kramer also proposed that the left and right leaflets of the aortic and pulmonary valves developed from the main outflow cushions, and that these are different from the intercalated cushions. He suggested that the left leaflets of the aortic and pulmonary valves are formed by the superior main cushion, whereas the right leaflets for both valves are formed by the inferior

main cushions (**Figure 1.8**). This suggestion was supported and extended by Phillips et. al. (2013), who showed that neural crest cells and EndoMT-derived cells were observed in the left and right leaflets, but not in the posterior (non-coronary) and anterior leaflets of the aortic and pulmonary valves. Recently, it was proposed that the intercalated cushions were originated from undifferentiated SHF-derived cells, which by a Notch-Jag dependent mechanism, these cells became differentiated (**Figure 1.8**) (Eley et al., 2018). Altogether this suggests that the anterior and posterior leaflets have a distinct origin to the left and right leaflets.

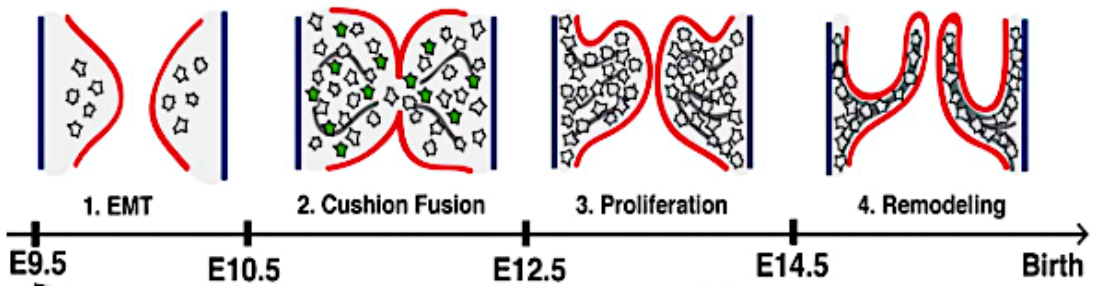

Figure 1.7: Development of aortic valve.
The endocardial cushions in the outflow tract undergo epithelial-to-mesenchymal transformation (EMT), generating the primitive valve at E9.5, and trigger proliferation of mesenchymal cells that remodel and mature into three thin valve leaflets. Image obtained from (Macgrogan et al., 2016).

By E12.5, the primitive leaflets of the aortic and pulmonary valves are developed, and the aorta and pulmonary truck are separated. By E13.5, two free-standing arterial trunks are formed along with their respective three-leaflet valves that permit unidirectional blood flow. However, at these stages the arterial valve leaflets have not matured, as they resemble solid bulky structures with no valve sinuses formed. Subsequently the cushions remodel

by a lengthening/elongation process that sustains coaptation of valve components with growth and maturation into flat thinned structures, and the sinuses form, so that by postnatal day 2, the valves are completely formed. However, little is known about these latter stages of arterial valve remodelling.

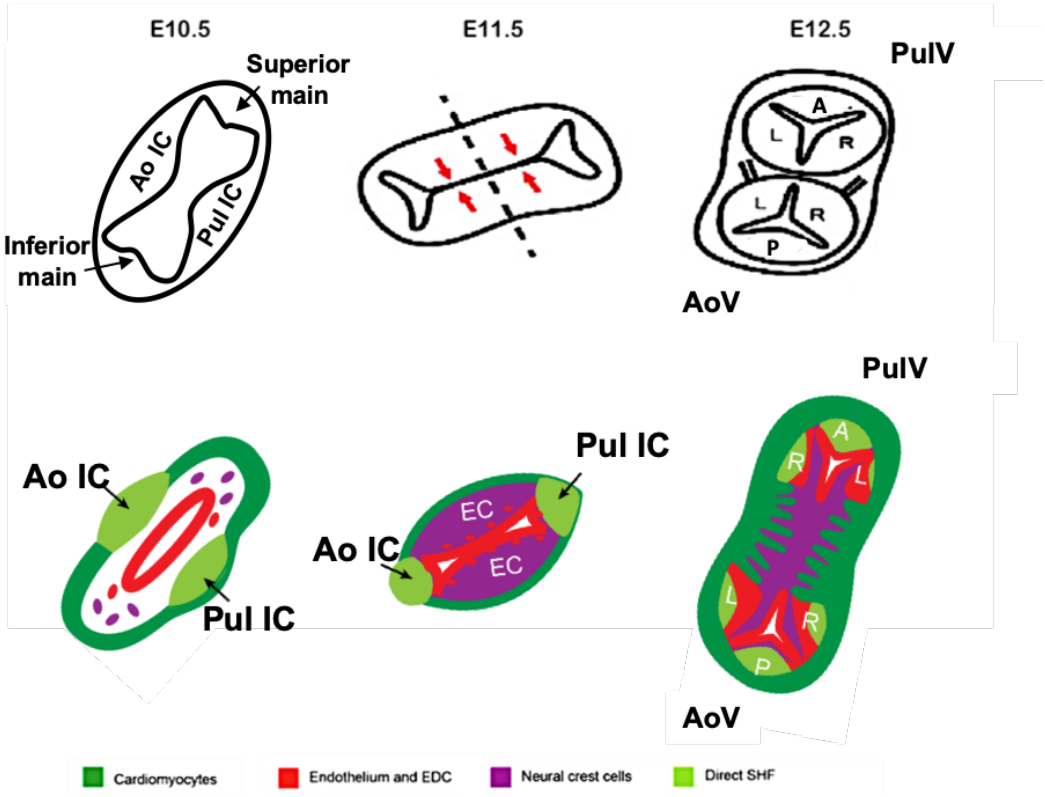

Figure 1.8: Development of aortic valve leaflets.
(A) Cartoon based on (Kramer, 1942) showing the fusion of superior and inferior main cushions along with intercalated cushion (IC) forms the three leaflets of aortic valve (AoV) and pulmonary valve (PulV). (B) cartoon based on (Eley et al., 2018) illustrating how the intercalated valve swelling, which found at E10.5 within the outer wall of the outflow tract, expands at E11.5 and by E12.5 separates from the wall remodelling the aortic and pulmonary valve leaflets. Ao IC: aortic valve intercalated cushions, Pul IC: pulmonary vavle intercalated cushions. Colour scheme summarised the contributions of cardiomyocytes (green), endothelium and EndMT-derived cells (red), neural crest cells (purple) and second heart fields (light green) in the leaflets of aortic and pulmonary valves. Image obtained from Eley et al., 2018.

1.2.5 Development of the mitral valve

Similar to the aortic valve, the mitral valve develops between the left atrium and left ventricle from endocardial cushions, although in this case in the atrioventricular canal (**Figure 1.9**). However, there are key points where development of the atrioventricular canal cushions differs from that of the outflow tract cushions. Unlike the outflow tract cushions, the atrioventricular canal endocardium is not derived from the second heart field (SHF). Lineage tracing studies have shown that only the outflow tract cushion mesenchymal cells express the SHF-specific markers: *Mef2c-AHF-Cre* and *Isl1-Cre* (Wessels and Sedmera, 2003). Moreover, the aortic valve received a large contribution of neural crest cells to the outflow cushions, whereas the mitral valve received small/no contributions from these cells. Also, the maturation process of the aortic valve and mitral valve are different, as the mature leaflets have distinct structure; the aortic valve has free edged leaflets, whereas the mitral valve retains tendinous chords leaflets (Butcher and Markwald, 2007).

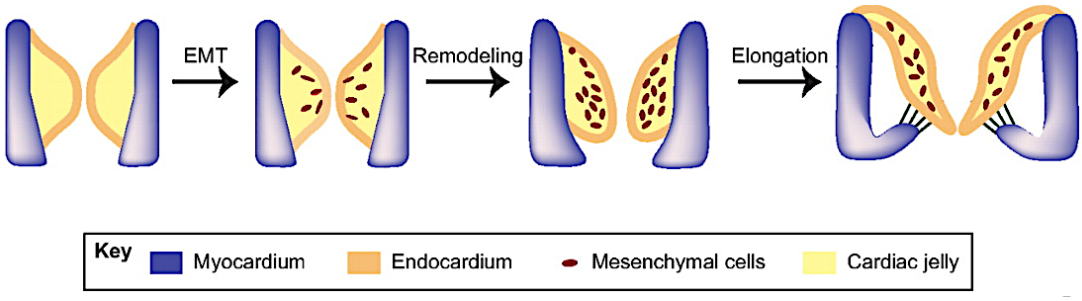

Figure 1.9: Development of the mitral valve.
Similar to the development of the aortic valve, the endocardial cells undergo endothelial-to-mesenchymal transition (EndMT) and migrate into the cardiac cushion of the atrioventricular canal to proliferate and secrete extracellular matrix proteins that lead to bend the valve leaflets along the blood flow. Further remodelling occurs as the valve develops, including formation of fibrous chordae tendineae that distinguish the mitral valve from the aortic valve.

The initial formation of the mitral valve begins by the two major endocardial cushions that develop opposite to each other at the wall of the atrioventricular canal. These two major cushions are known as the inferior cushion and superior cushion (**Figure 1.9**) (Wessels et al., 2012). As heart development proceeds, the two major cushions fuse and thus the atrioventricular canal separates into a left and right atrioventricular orifice. Also, fusion of the major cushions, particularly the inferior cushion, leads to the formation of the septal leaflet in the tricuspid (right) valve and the aortic leaflet of the mitral valve. Whereas fusion of the superior major cushion contributes only to the formation of the aortic leaflet of the mitral valve (Wessels and Sedmera, 2003; Lamers et al., 1995). At the same time, an additional set of endocardial cushions, originating from mesenchymal protrusions, begin to form on the left and right lateral aspects of the atrioventricular canal. These cushions are known by the left and right lateral cushions and composed of epicardial-derived cells that

replaced the endocardial-derived cells (Wessels and Sedmera, 2003; Butcher and Markwald, 2007). Both the left and right lateral cushions play a role in the valve morphogenesis, as the left lateral cushion contributes to the formation of the mural leaflet of the mitral valve, whereas the right lateral cushion is responsible for the formation of anterosuperior leaflet of the tricuspid valve. However, the mechanisms in which these cushions develop and differentiate remain poorly understood (Butcher and Markwald, 2007; Wessels et al., 2012).

Remodelling event occurs to form the free-moveable leaflets of the mitral and tricuspid valves through myocardial delamination. During this process, the inferior atrioventricular cushions connected to the myocardial layer separate from the myocardial wall of ventricle, whilst retaining attachment at the cranial and caudal edges, forming the papillary muscles (**Figure 1.10**) (Markwald et al., 1977; Nowak et. al., 2011). As development progresses, the leaflets gradually lose the myocardium at their ventricular side and develop mesenchymal tissue strands, which eventually progress to generate the tendinous chords (Chesler et. al., 1971; Wessels and Sedmera, 2003). However, these processes remain poorly understood.

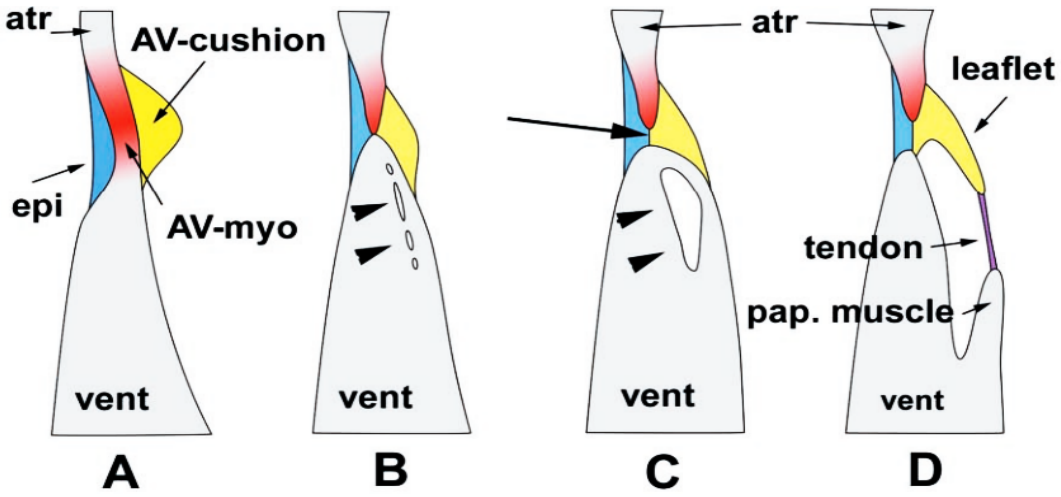

Figure 1.10: Remodelling of the atrioventricular cushions to form the atrioventricular valve.
Atr, atrium; epi, epicardium; AV-myo, atrioventricular myocardium; vent, ventricle; tendon, tendinous chords. Image obtained from (Wessels and Sedmera, 2003).

1.2.5.1 Formation of atrial septum

The atrioventricular cushions contribute to the process of atrial septation. After fusion of the major atrioventricular cushions (AVC), a large mesenchymal "bridge" is formed linking the atrioventricular canal posterior wall to the cardiac anterior wall. The mesenchymal component located posteroinferiorly connects to the endocardial cushions, and to the dorsal mesocardial projection and the mesenchymal cap (cap) on the leading edge of the primary interatrial septum (IAS) (**Figure 1.11**) (Wessels and Sedmera, 2003). At this stage, the primary interatrial foramen between left and right atrium has not closed, thus the mesenchymal bridge (cap) covers the atrial foramen between the fused major cushions (AVC) (**Figure 1.11**).

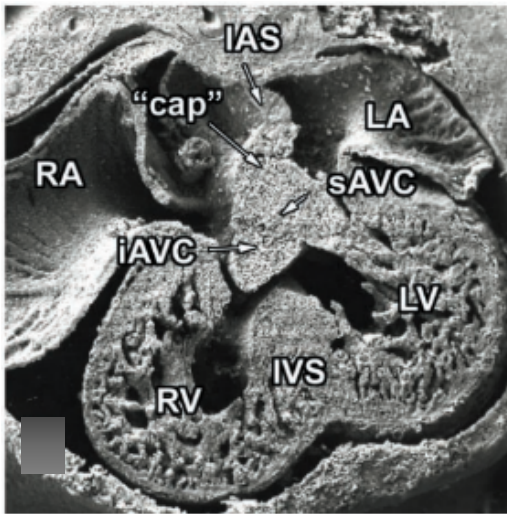

Figure 1.11: Contribution of the major atrioventricular cushions and the primary atrial septum along with the mesenchymal cap to the atrial septation at E10.5.
IAS, interatrial septum, "cap" mesenchymal cap; sAVC, superior atrioventricular cushions; iAVC, inferior atrioventricular cushions; IVS, interventricular septum; LV, left ventricle; RV, right ventricle; LA, left atrium; RA, right atrium. Image obtained from (Wessels and Sedmera, 2003).

As development continues, the atrial foramen closes by fusion of the atrioventricular major cushions and the mesenchymal cap located on the primary interatrial septum (Wessels and Sedmera, 2003; Kramer, 1942). Such remodelling eventually leads to the formation of the membranous atrioventricular septum, as it occurs between the muscular interventricular septum and the interatrial septum.

1.3 Circulation

Throughout human life, the circulatory system changes and adapts to be compatible with the needs of the body. The foetal circulation is different from the adult circulation because of the placenta, the presence of foramen ovale, and the ductus arteriosus (Kiserud and Acharya, 2004; Whitaker, 2001). The following section will look at the foetal circulation with respect to the changes that occur after birth and how these changes are important for cardiac malformations.

1.3.1 Physiology of foetal, transitional and post-natal circulations

Since the lungs in the foetus are not completely developed, the foetal circulatory system relies mainly on the placental circulation and other supporting structures, including the foramen ovale and ductus arterious, and the ductus venosus (Kiserud and Acharya, 2004) (**Figure 1.12**).

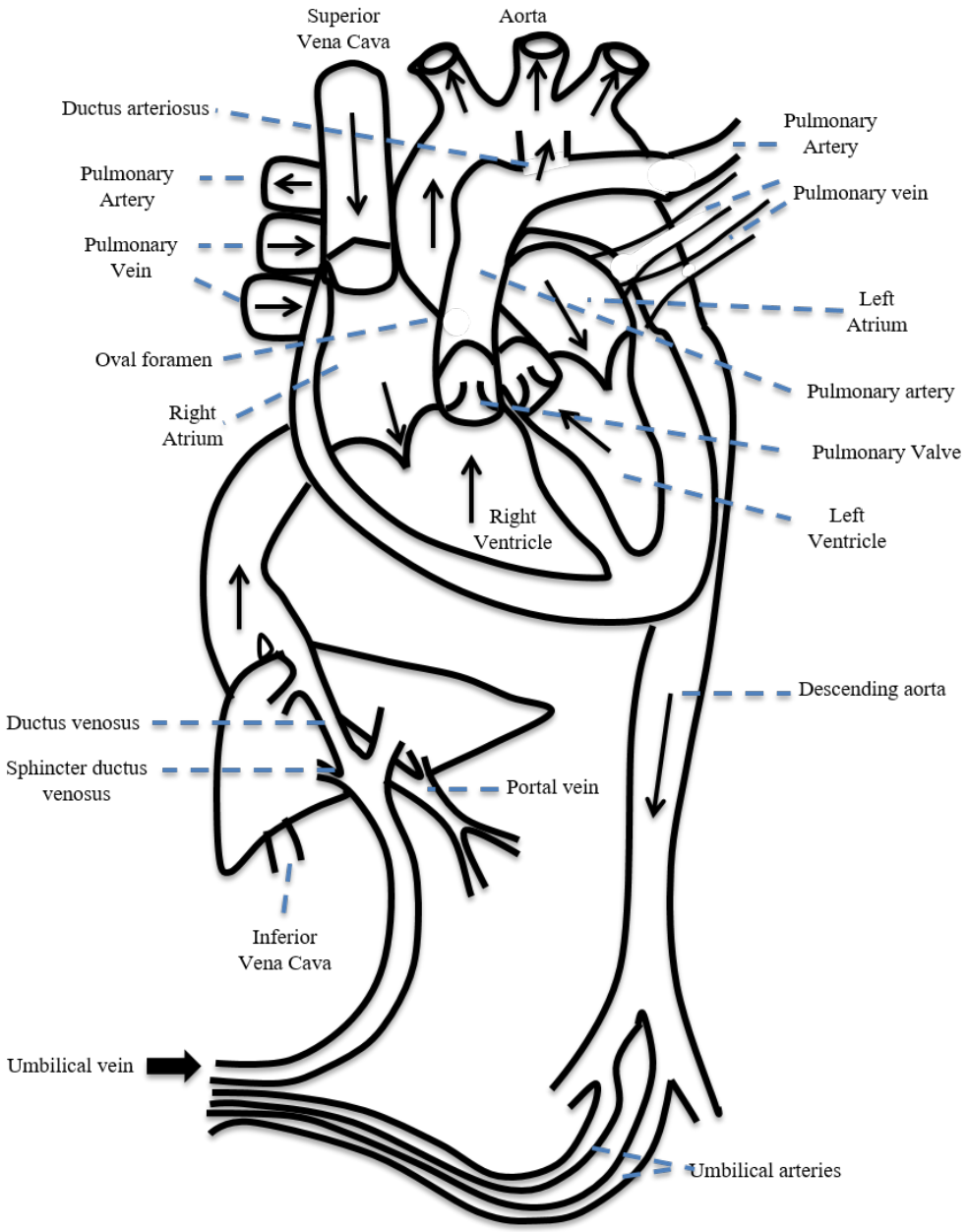

Figure 1.12: diagram shows the foetal circulation.
Modified from Murphy (2005).

In the foetus, the placenta delivers oxygenated blood through the umbilical vein to the inferior vena cava and ductus venosus in the liver. In return, a mixed of oxygenated/deoxygenated blood goes through the two umbilical arteries of the umbilical cord back to the placenta (Whitaker, 2001). Consequently, gas exchange occurs in the placenta without direct contact between the mother and fetal blood flows (Kiserud and Acharya, 2004). When the oxygenated blood from the placenta enters the right atrium through the inferior vena cava, a large stream of the blood passes to the left atrium via the patent foramen ovale. Then, it flows from the left atrium to the left ventricle into the ascending aorta to the upper regions of the foetus. Therefore, the most oxygenated blood passes mainly to the brain and upper extremities. However, the other stream of blood that enters the right atrium through the inferior vena cava joins the blood stream that comes from the superior vena cava, which is blood returning from the upper regions of the foetus. Hence, this blood stream has limited oxygen levels compared to the blood that passes to the left atrium (Whitaker, 2001). This limited oxygenated blood then passes into the right ventricle where it bypasses the lungs, shunts via the ductus arteriosus directly to the descending aorta, and finally goes to the lower part of the body (Kiserud and Acharya, 2004). The ductus arteriosus is a blood vessel connecting the pulmonary trunk to the descending aorta and it is a unique feature of the foetal circulation. At this stage, the diameter of the ductus arteriosus is comparable to that of the ascending aorta and hence the blood predominantly flows into the aorta and only a small stream goes to the lungs (Whitaker, 2001; Kiserud and Acharya, 2004).

At birth, closure of the umbilical cord eliminates the umbilical vessels, causing a dramatic drop in the blood flow through the ductus venosus and inferior vena cava (Kiserud and Acharya, 2004). This subsequently causes a passive closure of the ductus venosus within 3 to 10 days of birth. It also leads to increased blood flow in the pulmonary arteries and consequently in the pulmonary veins that direct blood to the left atrium. This therefore results in the left atrial pressure exceeding the right atrial pressure, and eventually causes the flap of the foramen ovale, located between the two atria, to push against the atrial septum (Whitaker, 2001). This effectively causes the initial closure of the foramen ovale, which occurs within a few minutes to hours of birth. Although the closure of the foramen ovale happens in the majority of babies, there are around 25% of the adult population have a patent foramen ovale (Almekhlafi et al., 2009). The permanent closure of foramen ovale occurs a few days after birth where the septum primum fuses with the septum secundum closing the foramen ovale and leaving a thin fibrous layer, termed the fossa ovalis (Kiserud and Acharya, 2004; Whitaker, 2001). As a result, the blood entering the right atrium can only flow into the right ventricle. The ductus arteriosus closes within two days of birth through a complicated process involving removal of prostaglandins (relaxation hormone) and a rise in blood oxygen tension (Coceani and Baragatti, 2012).

Overall, although there are several aspects where the foetal circulation differs from the neonatal circulation, and the foetal circulation is essential for normal foetal development. However, a healthy foetal circulation does not guarantee a normal foetal heart as the foetus with a malformed heart can survive

pregnancy by relying on the foetal aspects of the circulation, such as the ductus arteriosus. Thus, babies with severe heart malformations such as Hypoplastic Left Heart Syndrome (HLHS) can survive pregnancy and birth without problems, as long as the ductus arteriosus is open. However, after birth, when the ductus arteriosus closes, the baby can become acutely ill, and will die if untreated, as there is no systemic circulation (Murphy, 2005).

1.4 Hypoplastic left heart syndrome

Hypoplastic left heart syndrome (HLHS) is a rare congenital heart defect that without intervention leads to death in the first months of life. It is characterized by an underdeveloped and functionally insufficient left heart-aorta complex, including hypoplastic aorta and none-apex forming hypoplastic left ventricle with atretic or stenotic mitral and aortic valves (Crucean and Alqahtani et al., 2017). In this section, HLHS will be described taking a historical and nomenclature perspective. In addition, epidemiology, potential causes, and main genes implicated in HLHS will be discussed.

1.4.1 Nomenclature and historical perspectives of HLHS

Hypoplastic left heart syndrome (HLHS) was described by Lev in 1952, as underdevelopment of the aortic arch with a small ascending aorta and small left atrial and ventricular chambers. At that time, HLHS was known as “hypoplasia of the aortic tract complexes” (Lev, 1952). However, in 1958, it was recognised as a syndrome by Noonan and Nadas. They broadly defined HLHS to include a range of lesions that included vestigial left ventricle with aortic and mitral atresia and hypoplasia or atresia of the aortic arch (Noonan and Nadas, 1958). Henceforth, several other definitions have been suggested to describe HLHS, which eventually made the specific definition of this syndrome complicated. For example, Feinstein and colleagues described HLHS as “genetically inherited abnormalities in the valves, such as aortic valve atresia and mitral valve regurgitation, accompanied by dilated left atrium and a hypoplastic and fibrotic left ventricle, and usually a small patent foreman

ovale" (Feinstein *et. al*., 2012). However, Nemes and colleagues defined HLHS as "defects during cardiogenesis causing enlargement of the right ventricle and atrium, pulmonary venous hypertension, atrial septal defect, hypoplastic left ventricle and ascending aorta, and stenotic or atretic valves" (Nemes *et. al.,* 2014). These two definitions differ based on the author's ideological theory of HLHS; the Nemes's theory was mainly about defects in the right-sided structures that lead to defects in the left-side of the heart, whereas in Feinstein's theory the defects were predominantly in the left-sided structures of the heart. Therefore, there was no clear agreement as to how precisely HLHS should be described, although recently the term "classical HLHS" had gained some recognition. Classical HLHS was defined as a spectrum of cardiac structural anomalies with a common obstructive lesion including atresia or stenosis of the left-sided heart structures (Simpson, 2000). According to Simpson, the term "classical HLHS" should only be used to describe two cases: (1) atresia of mitral and aortic valves with indemonstrable or slit-like left ventricular cavity, and (2) atresia of the aortic valve with patent mitral valve and detectable hypoplastic left ventricle. Other instances, where hypoplastic left ventricle was accompanied with severe aorta coarctation, critical aortic stenosis, or unbalanced atrioventricular septal defect, should be termed HLHS variants (Simpson, 2000). Additionally, Tchervenkov and colleagues referred to the mild degree of left ventricle hypoplasia with small mitral and aortic valves, but without core valve stenosis, as hypoplastic left heart complex (HLHC) (Tchervenkov *et al*, 2000). Most recently, the Eleventh Iteration of the International Classification of Diseases (ICD-11) (Franklin et al. 2017), which has gained a globally accepted nomenclature tree for CHD and

recognised by the international nomenclature committee, has defined HLHS as a spectrum of heart malformations that involve a small non-apex-forming left ventricle with atresia, stenosis or reduction in size of the mitral and aortic valves, and hypoplasia of the aorta. This definition required normally aligned great arteries without atrioventricular septal defect (Franklin et al. 2017). Therefore, the ICD-11 has provided the most definitive definition for HLHS.

Although there have been various suggested definitions for HLHS, they all shared a common approach which reflected clinical approaches to treatment. As a result, HLHS has for many years been clinically classified into four subgroups: aortic and mitral atresia (AA/MA), aortic atresia and mitral stenosis (AA/MS), aortic stenosis and mitral atresia (AS/MA), and aortic and mitral stenosis (AS/MS) (Tchervenkov *et al*, 2000). However, there have not been any attempts to classify HLHS into discrete subtypes based on the anatomical features of the hypoplastic ventricle or its developmental origin. Hence, this study intends to evaluate HLHS based on its anatomical features, ignoring approaches to treatment, and thereby to attempt to shed light on whether it is a spectrum of abnormalities or falls into discrete subtypes. In order to do this, HLHS was characterised according to the ICD-11 definition. The hypoplasia of the left heart causes malformation of the left-sided structures, leading to non-apex forming left ventricle, a combination of the mitral and aortic valve atresia or stenosis, hypoplasia of the ascending aorta, and atrial septal defects (Franklin et al. 2017). Other HLHS variants, double outlet right ventricle, atrioventricular septal defects, ventricular septal defect, transposition of the great arteries, and common arterial trunk were excluded (Franklin et al. 2017).

1.4.2 Epidemiology

Epidemiology is the study of how and when diseases or conditions occur and is often used to suggest causative factors, through incidence rate and the outcome of relevant managements as survival or mortality rate. In this section, the incidence, and survival and mortality of HLHS will be discussed with emphasis on any suggested aetiological factors.

1.4.2.1 Incidence

Several studies have reported the frequency of HLHS over the last 40 years (**Figure 1.13** and Appendix Table 1). Some have reported the incidence within the whole population, whereas others have indicated the frequency within patients with congenital heart defects (CHD). According to Hoffman (2002), the population incidence of CHDs is 0.8% and this therefore was used as a basis for comparing these studies. Whilst no studies have specifically sought to determine variations in the incidence of HLHS, or CHD in general, between countries or over time, the incidence of HLHS in European-based studies has remained at approximately 2-3% of all CHD or 4/100,000 live births since 1980 (Grech, 1999).

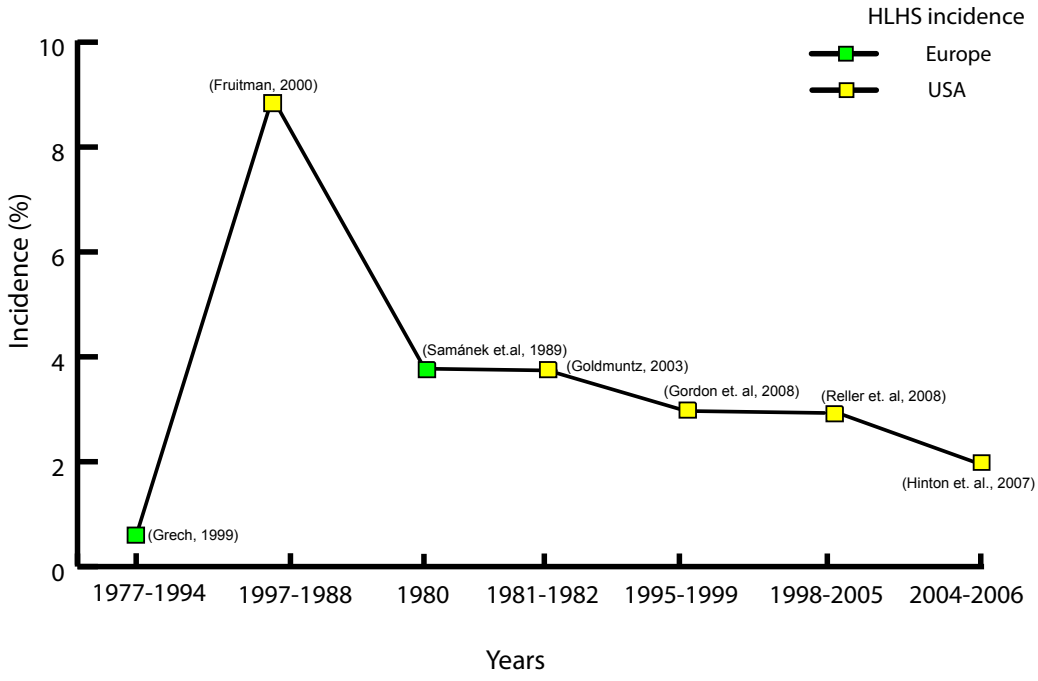

Figure 1.13: the line chart shows the incidence percentage of HLHS of all CHD between 1977 and 2006.
Colour scheme represents the population-based region: green, Europe; yellow, USA and Canada.

There are many factors that can influence the incidence rate of HLHS including gender, twinning, and association with chromosomal abnormalities. Based on clinical and population studies, HLHS is predominantly found in males and has an approximate ratio of male to female (1.5:1) (Karamlou et.al, 2010; Ohye et. al., 2010). The overall reported incidence of HLHS in all CHD was 7% according to a population-based study, with 1% prevalence of HLHS (Lopriore et.al., 2007). Of interest, HLHS has been reported in monozygotic twins in which both foetuses had HLHS diagnosed at week 15 of gestation (Andrews et. al., 2004). Another study also reported monozygotic twins in which only one foetus had HLHS, whereas the other had pulmonary atresia and tricuspid

regurgitation (Negishi et.al., 1995). These studies not only suggest the possibility of a genetic explanation, but also showed that HLHS incidence is relatively affected by twinning particularly when they are affected with other CHDs (see section 1.4.3.2.2). In addition, it has been reported that 20% of CHDs are associated with chromosomal abnormality, where HLHS accounted for 2.4% of all CHDs that are associated with chromosomal abnormalities; such as Turner, DiGeorge, and Downs syndromes (Brenner and Kuehl, 2011). Overall, although all these factors suggest a genetic aetiology for HLHS, they also play a major role in conflicting the incidence rate for HLHS.

1.4.2.2 Survival and mortality

Currently, the three to five-year survival rates for infants undergone the stage I repair of HLHS is estimated at 70%, whereas around 90% for of children (up to 12 months) survive the stage II repair (Siffel et al 2015). However, it is generally accepted that HLHS is a severe form of CHD and is the leading cause of cardiac death in the first month of life (Surmiak *et al,* 2015). In general, the mortality rate of HLHS without surgical intervention accounts for 25% to 40% of death from all CHDs, whereas it accounts for whilst 4% -16% of HLHS death occur during the surgical interstage period (Siffel et al., 2015; Simsic et al., 2005). Since there are different clinical subgroups of HLHS, the frequency of each HLHS subgroup could be related to the mortality rate. The frequency of the clinical subgroup with aortic atresia and mitral atresia (AA/MA) has been suggested to account for 50% of HLHS patients, whereas the subgroups with aortic atresia and mitral stenosis (AA/MS) and aortic stenosis and mitral stenosis (AS/MS) are found in 26% and 23% of HLHS

patients, respectively (Glatz et. al., 2008). Strikingly, the mortality rate of the AA/MS subgroup during the surgical interstage period was suggested to be higher (21%) than that for other HLHS subgroups (6% for AA/MA and 0% for AS/MS) (Glatz et. al., 2008). Similarly, another study had also shown a high mortality rate (29%) for the AA/MS subgroup compared to the other HLHS subgroups (7.9% for AA/MA and AS/MS) (Vida et. al., 2008). The high mortality rate in this specific subgroup (AA/MS) of HLHS has been investigated and some possible causes were suggested. This involved the presence of pathological abnormalities within the left ventricle, such as interstitial fibrosis, calcifications, and myocardial necrosis (Sugiyama et al., 1999). Also, angiographic and pathologic studies have suggested the appearance of abnormal left ventricle–subepicardial coronary artery communications causing the failure in HLHS treatment management (Baffa et al., 1992). Overall, although the mortality rate of HLHS varies based on the HLHS clinical subgroups, the overall mortality rate for all HLHS subgroups remains high compared to the other CHDs.

1.4.3 The causes of HLHS

Two factors have been considered to influence the occurrence of HLHS: environmental and genetic (Gladki et al., 2015; Hinton et al., 2007). The following section will discuss these factors and how they may influence HLHS.

1.4.3.1 Environmental factors

Several studies have suggested associations of HLHS with various environmental factors including ambient air pollution, viral infections,

consumption of medications and alcohol, and teratogens (Gładki et al., 2015; Agay-Shay et al., 2013). Although there have been intensive studies to investigate the association between maternal exposure to air pollution, such as sulphur-dioxide, carbon monoxide, ozone, and nitrogen-dioxide, these studies could not link the air pollution to a specific form of CHD (Dadvand et al., 2011; Agay-Shay et al., 2013; Dolk et al.,2010; Gilboa et. al., 2005; Hansen et al., 2009). A recent study based on analysing 100 infants with HLHS compared to 100 new-borns without CHD showed no association between the occurrence of HLHS and other factors including marital status, consumption of tobacco, medications and alcohol, or parent's age (Gladki et al., 2015). However, the Towbin group suggested an association between viral infections and the occurrence of endocardial fibroelastosis, which is frequently reported in HLHS (Ni et al., 1997). The study was based on analysing 29 samples from patients with diverse CHDs and autopsy-proven endocardial fibroelastosis, to detect the presence of various viral genomes. Interestingly, 70% of the samples were positive for mumps virus, whereas 28% were positive for adenovirus. This therefore indicated a connection between maternal viral infection, particularly mumps virus, and occurrence of endocardial fibroelastosis (Ni et al., 1997). It was suggested that transplacental mumps infection was a significant cause of endocardial fibroelastosis (Lurie, 2010). However, there was no report of decreasing the incidence of HLHS after vaccination, and thus no direct links to HLHS was concluded (Lurie, 2010; St. Geme et al 1966). Overall, there is insufficient evidence to decisively conclude that HLHS can be caused by specific environmental factors.

1.4.3.2 Genetic factors

There have been several studies that link HLHS to genetic factors (Brenner et. al., 1989; Hinton et al., 2007; Kelle et al., 2015). The original thought that genetic factors influence the aetiology of HLHS was in 1974 by Bjornstad and Michalsen. Based on analysing previous study cases of HLHS, they found that 64% of the analysed cases (102/160 cases) were boys, suggesting a strong sex-linked aetiology for HLHS. Interestingly, when they analysed specific subgroup of HLHS (aortic and mitral atresia), they found that 50% (11/22 cases) were boys, indicating a lower importance of gender in this group (Bjornstad and Michalsen, 1974). In 1976, a survey of HLHS infants (64 cases) and their pedigree (42 families) information indicated an increased recurrence of HLHS in later siblings, which gave rise to the conclusion of HLHS caused through polygenic inheritance (Brownell and Shokeir, 1976). Thereafter, the idea of a genetic aetiology for HLHS has been widely accepted. In 1989, a pilot study was carried out on 41 first-degree relatives of 11 HLHS probands. This showed that 5/41 relatives of the HLHS probands had confirmed cardiac defects. This study not only suggested a high risk of cardiac defects in the first-degree relatives of HLHS patients, but also proposed a high frequency of HLHS recurrence in siblings, compared to the earlier model of polygenic inheritance (Brenner et al., 1989). In 2005, a familial study of left ventricular outflow tract obstruction (LVOTO), including a family with HLHS and aortic coarctation, suggested a male to male inheritance for HLHS as two male family members (father and brother) had mild aortic stenosis (Wessels et al., 2005). Furthermore, examination of 38 HLHS probands with a three-generation family

history showed that 55% (21/38) of families had at least one or more family members affected by cardiac defects, with an 8% recurrence risk for HLHS in siblings suggesting heritability of HLHS (Hinton et al., 2007). According to Leary's group (2015), the familial incidence in first-degree members of HLHS probands was approximately 11.2%, as it was based on screening 152 first-degree family members of 52 HLHS probands, including 55 siblings and 97 parents (Kelle et al., 2015). Consequently, there has been increased evidence to support a genetic element underpinning HLHS.

1.4.3.2.1 Transmission patterns of HLHS

Although all of these studies had implied the genetic causes of HLHS, the proposed models for HLHS transmission pattern remains debatable. The suggested sex-linked aetiology for HLHS, for example, was based on the studies that included aortic atresia cases, which were not necessarily HLHS cases. Moreover, when HLHS was limited to a specific phenotype (aortic and mitral atresia), the sex-linked aetiology for HLHS became less significant. In addition, the polygenic inheritance was suggested through analysis of 42 families in which no phenotype for the HLHS cases was provided. Hence, it was not possible to determine the accuracy of the suggested inheritance model. The autosomal dominant inheritance model was based on analysis of a familial study of left ventricular outflow tract obstruction (LVOTO) and was not limited to HLHS. Therefore, it was difficult to conclude whether this inheritance model was applied specifically to HLHS or to LVOTO cases. Altogether, these studies had provided possible models to explain the genetic transmission patterns for HLHS, but further investigation particularly using a

specific subgroup of HLHS can provide a better insight into the genetic mechanisms of HLHS.

1.4.3.2.2 Twin study of HLHS

The study of twins in HLHS can provide an insight to further understand the genetic origin of HLHS. In the case of a birth defect such as HLHS, twin studies are a valuable source of information to explore individuals with identical genotypes. Although twin pregnancies have a higher risk of structural heart disease than singleton pregnancies, the concordance rate between twins has been revealed to be relatively low (Andrews et al., 2003).

Comparisons between monozygotic and dizygotic twins can assess the degree of genetic and environmental influence on HLHS. Monozygotic twins share 100% of their genes and have the same sex, whereas dizygotic twins share around 50% of their genes and can be either gender. Therefore, when monozygotic twins reveal a significant concordance of HLHS compared to dizygotic twins, this suggests that genes largely influence HLHS. However, when monozygotic twins and dizygotic twins share similar or equal concordance of HLHS, this provides evidence for a large influence of the environment rather than genetic factors. Analysing HLHS twin case reports, between 1973 to 2018, showed that concordance for HLHS (i.e. both twins had HLHS) was significantly higher in monozygotic twins than in dizygotic twins, (**Figure 1.14**, Table 1.1). This therefore suggets a strong influence of genetic factors.

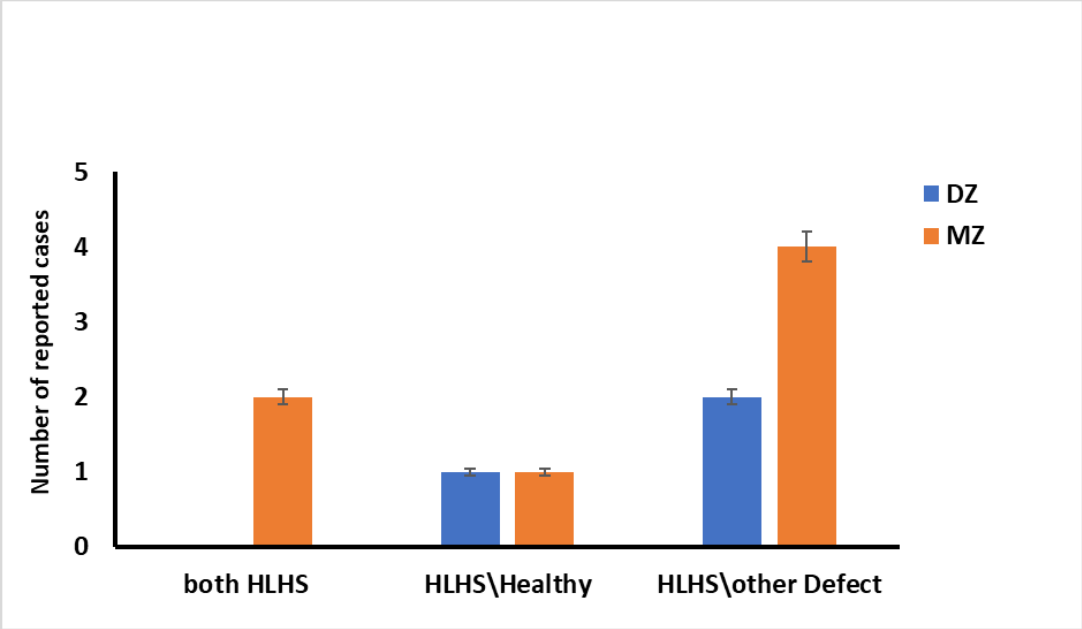

Figure 1.14: HLHS cases reported in monozygotic and dizygotic twins. There were not any dizygotic twin cases reported where both twins had HLHS, whereas there were two cases for monozygotic twins. Both monozygotic and dizygotic twins had equal cases of one twin with HLHS and a healthy co-twin. However, there were double cases in monozygotic twins, where one twin had HLHS and co-twin had other congenital heart defect (see table1.1), compared to dizygotic twins. The error bars represented the standard error.

Table 1.1: case reports for HLHS in mono/dizygotic twins between 1973 to 2018.

Twin types	Twin 1	Twin 2	Reference
Dizygotic twin	HLHS	Brain death	Blitzer et al., 2016
Dizygotic twins	HLHS	HRHS with PA	Martinovic et al., 2003
Dizygotic twins (25 out of 413)	HLHS	Not specified	Dawson et al., 2016
Monozygotic diamniotic twin	HLHS	HLHS	Andrew et al., 2003
Monozygotic diamniotic twin	HLHS	HLHS	Andrew et al., 2004
Monozygotic Monoamniotic twin	HLHS	Not specified	Young et al., 2001
Monozygotic monoamniotic twin	HLHS	TTTS	del Río et al., 2005
Monozygotic twin	HLHS	BAV	Mu et al., 2005
Monozygotic twin	HLHS	OEIS	Mathew et al., 2009
Monozygotic diamniotic twin	HLHS, TGA, PA, sirenomelia	Healthy	Al Yaqoubi et al., 2018
Monozygotic twins (4 out of 10)	HLHS	Right kidney dysplastic with cysts	AlRais et al., 2011
Not specified	HLHS	HLHS	Leake et al.,1973
Not specified	HLHS	AVSD	Digilio et al., 1999

Key: HLHS: hypoplastic left heart syndrome; AVSD: atrioventricular septal defect, PA: pulmonary atresia; TGA: transposition of the great arteries; BAV: bicuspid aortic valve; TTTS: twin-twin transfusion syndrome; OEIS: omphalocele-exstrophy-imperforate anus-spinal defects; HRHS: hypoplastic right heart syndrome.

1.4.4 Candidate genes for HLHS

As there are a growing body of evidences to show genetic causes for HLHS, several genes have been suggested to associate with HLHS. This includes *GJA1* (Dasgupta et al., 2001), *NKX2.5 (*Elliott et al., 2003; McElhinney et al., 2003), *NOTCH1/NOTCH3/NOTCH4* (Garg et al., 2005; Yang et al., 2017; Durbin et al., 2017)*, HAND1 (*Reamon-Buettner et al., 2008), *FOXC2/FOXL1 (*Iascone et al., 2012; Yu et al., 2010; Finegold et al., 2001), *SMAD3* (Fitzgerald et al., 2014), *TBX5* (McCulley and Black, 2012), *ETS1* (Ye et al., 2010*), RBFOX2* (verma et al., 2016) and *PCDHA9/SAP130* (Liu et al., 2017). This section will briefly discuss the HLHS suggested genes and further discussion will be in chapter 4.

Since the above suggested genes were proposed to cause HLHS, some of these genes, such as *HAND1, NKX2.5, GJA1* and *PCDHA9/SAP103,* were used to generate experimental animal models for HLHS. The reported HAND1 frameshift mutation ($Hand1^{A126fs}$), which was originally identified in 24 of 31 formalin-fixed hypoplastic left ventricles, was modelled in mice (Reamon-Buettner et al., 2008). Although the $Hand1^{A126fs}$ mice showed abnormal cardiac development including a thin ventricular myocardium, defects in the outflow tract, and ventricular septal defect, the size of the left ventricle in these mice was normal and eventually this mutation caused embryonic lethality (Firulli et al., 2017). In addition, generating a mouse model for a ventricular-restricted knockout of *Nkx2.5* exhibited no structural defects or HLHS, but had overgrowth of the trabecular muscle (hypertrabeculation) of the left ventricle and complete heart block (Pashmforoush et al., 2004). Similarly, another study

had used a semi-automatic software to study the effect of the *Nkx2.5* deletion on the trabeculated mass of mice model. This study showed that inducing the *Nkx2.5* mutation during early embryonic development led to dramatically increased trabeculation but not HLHS (Frandon et al., 2016). Furthermore, targeted mutagenesis of *GJA1* revealed that its presence was essential for survival of mouse embryos. The mutant embryos of *GJA1* displayed several heart defects including blockage of the right ventricular outflow tract and eventually caused embryonic death at birth (Reaume et al, 1995). The fact that *GJA1* caused decreased flow in the developing ventricles through blocking the pulmonary venous connections was compatible with the flow theory (Wessels et al., 2005). Altogether this finding indicated an important role of *GJA1* during heart development, it did not exhibit classic symptoms of HLHS. More recently, the digenetic interactions between *Pcdha9* and *Sap130* was proposed to cause HLHS in mice (Liu et al., 2017). It was also suggested that mutations in *Pcdha9* were responsible for causing aortic valve abnormalities, whereas mutations in Sap130 caused hypoplasia in the left ventricle. Therefore, combination of both genes together was required to produce HLHS features (Liu et al., 2017). Linking this finding to human HLHS patients revealed that one patient out of 68 HLHS patients had rare mutations in *SAP130* and in *PCDHA13*, which was proposed to be homologous to *Pcdha9* identified in HLHS mice (Liu et al., 2017). Although a digenic model for HLHS was proposed, the interaction between these two genes was not necessarily causing HLHS (Discussed further in chapter 5). Overall, all the generated animal models for HLHS revealed a weak association between the implicated genes and HLHS, and eventually led to either embryonic lethality or generating

other complex cardiac defects. Therefore, further investigations are required in order to find the causative gene(s) for HLHS.

1.5 Hypothesis and aims

Whilst several studies have supported a genetic aetiology for HLHS, there have been many unsuccessful attempts to find the specific gene(s) that cause this defect. This could be because the majority of genomic studies, which aimed to find HLHS genes, had investigated a wide variety of heart defects without limiting their study to a specific subgroup of HLHS. Although the clinical subgrouping of HLHS is broadly accepted in clinical diagnosis, for genomic studies these subgroups provide a wide range of valvular morphological malformations, which can be difficult to accurately phenotype, but ignore the ventricular phenotype. Therefore, this study hypothesises that there are distinct subgroups of HLHS, which can be identified based on the left ventricular morphology. Analysis of a discrete well-characterised subgroup of HLHS using archival formalin-fixed tissues may aid in understanding the genetic aspect behind it, and ultimately finding the causative gene(s) of HLHS. Also, since archival formalin-fixed tissues are used in characterising HLHS subgroups, it is hypothesised that DNA samples can be extracted from these samples at high quality and used in genomic downstream applications. Finally, evaluation of the expression patterns of the currently implicated genes for HLHS may provide good understanding of how these genes contribute to HLHS.

This study has several aims including: (1) to establish on morphological grounds, using archival specimens, whether there is evidence for different subtypes of HLHS; (2) to establish an improved method to extract high quality

DNA with reliable and reproducible sequence information from formalin-fixed tissues, and (3) to investigate the expression of HLHS proposed genes at relevant stages and in relevant tissues during heart development.

Chapter 2: Morphological Analysis of Hypoplastic Left Heart Syndrome Subtypes

2.1 Overview

Over the years, there has been much discussion about whether hypoplastic left heart syndrome (HLHS) is caused by environmental factors, inherited genetic factors, or a combination of genetic and environmental factors together. Further, if there are genetic factors, there is controversy about whether it is caused by disruption of a single gene, or several genes (Banner and Kuehl, 2011). Although these arguments have been going on for a long time with no definitive conclusion, there is now a greater preference for HLHS being a hereditary defect (Connor and Thiagarajan, 2007; Hinton et al., 2007; Liu et al., 2017). Analysis of published studies about HLHS revealed that the majority of these studies were not specific in their criteria for identifying and sub-classifying HLHS (Appendices Table 8.1). Some studies characterized HLHS patients according to the conventional clinical (functional) classification, which is based on the functional capacity of the valves located on the left side of the heart. Other studies either included other morphological defects such as atrial/ventricular septal defect (A/VSD) and hypertrophy of the right-sided cardiac structures, or linked HLHS to other syndromes including Down syndrome (Colquitt et al., 2016). As a result, these studies incorporated a variety of malformations affecting the relevant cardiac regions in HLHS and combined them into one group to eventually use them for genetic analysis studies (Appendix Table 8.1). This could be a reason for the delay in revealing the aetiology of HLHS. Therefore, this chapter will suggest a new way to understand and investigate HLHS. To achieve this, an alternative classification based on the anatomical abnormalities rather than the clinical functionality was

explored. The clinical classification is essential for correct surgical management. However, the new suggested classification in this chapter is particularly important for genetic and developmental studies, as it provides a well-defined and accurately characterised subgroup of HLHS that is ultimately critical for aetiology studies. Evaluation of the overall appearance and main structures affected in HLHS resulted in a classification based on the ventricular phenotype. Below, an overview of the developmental processes that underpin formation of the main anatomical segments implicated in HLHS is presented.

2.2 Main structures involved in HLHS

HLHS is a congenital heart condition that leads to underdevelopment of the left-sided structures of the heart, causing obstruction to the normal blood flow through the left ventricular outflow tract. It not only affects the left ventricle but also the valves that modulate flow into and out of the left ventricle (mitral and aortic valves) and aorta (Schoenwolf et al., 2009). Although HLHS is caused by perturbation during heart development, the main underlying processes remain unclear. Classifying HLHS subtypes according to their valvar malformation suggests that HLHS is initiated, at least in part, by perturbation during valve formation. However, it is still unclear to what extent defects in the valves can be considered as the primary cause of HLHS, as they may be secondary to malformations in the left ventricle. Therefore, this section will look at the normal development of left cardiac structures; with emphasis on the development of the left ventricle, aortic and mitral valves, and aorta, as these are the fundamental segments involved in HLHS. The knowledge of the normal heart structures allows the assessment of abnormalities associated with HLHS hearts.

2.2.1 Left ventricle

The left ventricle is one of four chambers in the heart. It functions to pump blood from the heart to most of the body. The position, form and proportion of the infant heart differs from that in adult and older children. Infant hearts tend to have a more horizontal position compared to that in adults. This is because of the large abdomen and high diaphragm in infants (Jour, 1950). In addition,

the form of infant hearts varies in several aspects. The new-born heart is broader and rounder than adult hearts. Also, the morphological right ventricular wall of the infant heart is slightly larger than the morphological left ventricular wall. Moreover, the left and right ventricles are cardiac apex forming (Jour, 1950; Huelke, 1998). At this stage, no individual features have developed in the left and right sides and hence the heart has a symmetrical structure (Jour, 1950) (Figure 2.1).

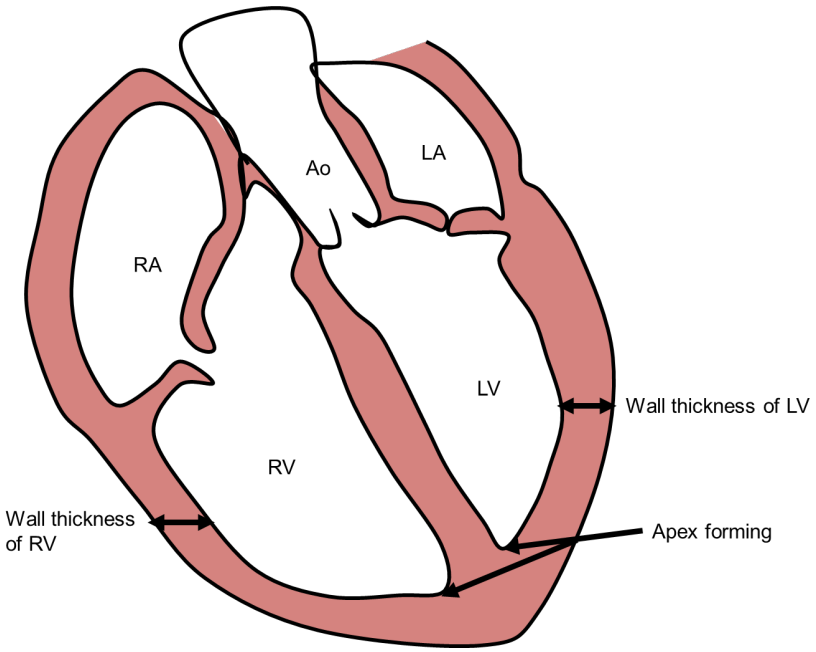

Figure 2.1: Infant Left ventricle structure.
In the infant heart the LV wall thickness is relatively similar to that in the RV. Both ventricles have the same length and are apex forming (modified from Schoenwolf et al., 2009).

2.2.2 Mitral valve

The mitral valve (or bileaflet valve) is located between the left ventricle and the left atrium and is composed of two leaflets: the anteromedial and posterolateral leaflets (Hinton et. al., 2008). These leaflets are formed from the atrioventricular (AV) cushions. The superior AV cushion develops to form the aortic leaflet, whereas the left lateral AV cushion forms the mural leaflet of the mitral valve (Snarr et. Al., 2008). The mitral valve leaflets are protected from prolapsing during blood flow by chordae tendineae located in the left ventricle. The chordae tendineae form a supportive bridge that attaches to papillary muscles at one end and to valve leaflets at the other end. There is some variability with the points of attachment on the valve leaflet and some attaching to the ventricular wall rather than the papillary muscles. The mitral annulus is a non-continuous fibrous circle surrounding the mitral valve (Hinton et. al., 2008) (Figure 2.2). It is attached to the mitral valve leaflets and helps in maintaining a complete closure of the leaflets during contraction or systole (Playford and Weyman, 2001).

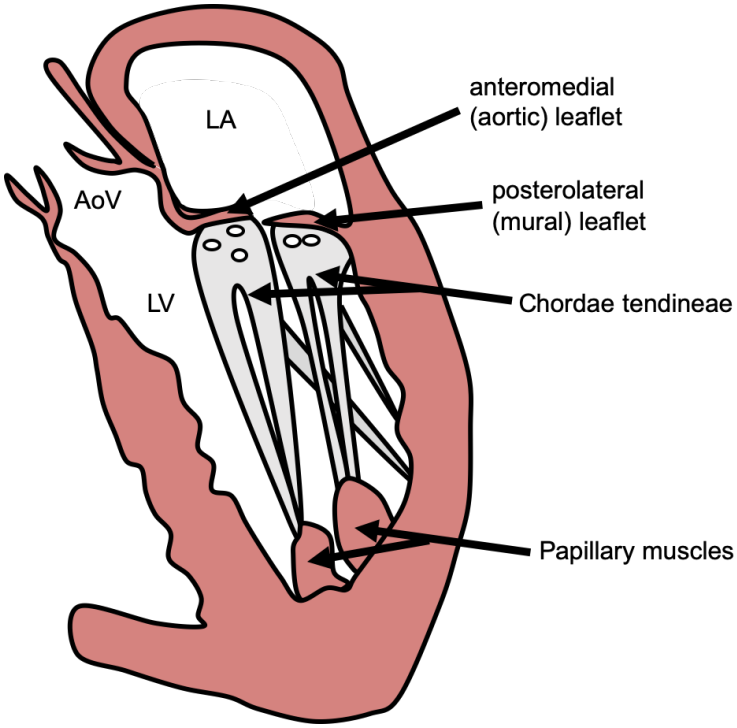

Figure 2.2: Mitral valve structure.
Mitral valve contains two leaflets known as anteromedial leaflet, which is in fibrous continuity with the aortic valve, and posterolateral leaflet. These leaflets are supported by chordae tendineae that connect to the LV wall, the leaflets and the papillary muscles that attach to the left ventricular inner wall. Abbreviations: LA: left atrium, LV: left ventricle, AoV: aortic valve (Modified from Schoenwolf et al., 2009)

2.2.3 Aortic valve

The aortic valve is located in the junction between the ascending portion of the aorta and outlet of the left ventricle. It functions to regulate blood flow from the left ventricle to the aorta and then to rest of the body (Reid, 1970). The aortic valve is composed of three leaflets which have been described in several ways. For example, the right coronary leaflet can be known as the anterior leaflet, the left coronary leaflet, can be described as the left posterior, and non-coronary leaflet can be known as the right posterior (Ho, 2009; Charitos and Sievers, 2012). However, the most common clinical terms are the left coronary, right coronary and non-coronary cusps (Ho, 2009). The left coronary leaflet and non-coronary leaflet are in fibrous continuity with the mitral valve. The aortic valve and its leaflets are all part of a complex structure called the aortic root. The aortic root joins the heart to the systemic circulation (Ho, 2009; Charitos and Sievers, 2012). In addition to aortic valve leaflets, the aortic root consists of leaflet attachments, the sinotubular junction, the ventriculo-aortic junction, the interleaflet triangles/trigones, and the sinuses of valsalva (Charitos and Sievers, 2012) (Figure 2.3).

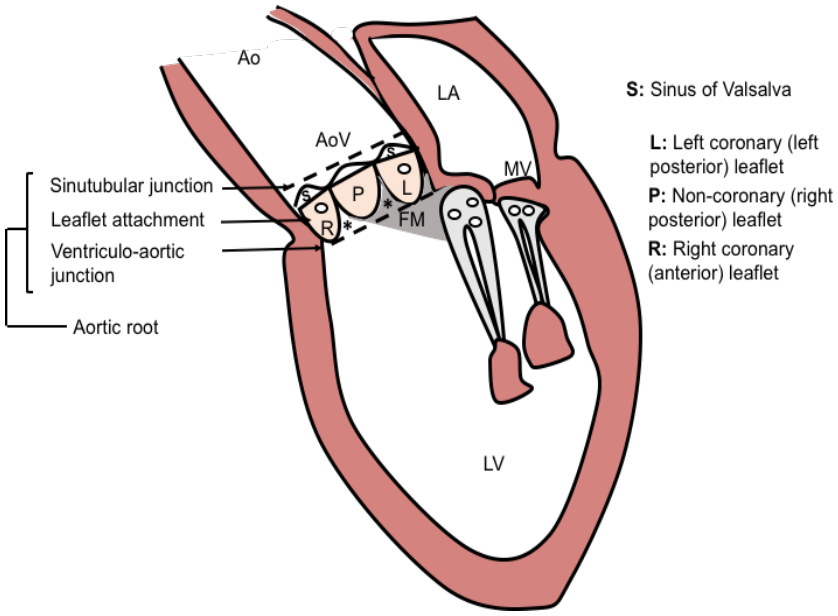

Figure 2.3: Aortic valve structure.
The aortic valve has three leaflets: left coronary leaflet (L), posterior leaflet (P) and right coronary leaflet (R). Structures between the sinutubular junction and the ventriculo-aortic junction form the aortic root. The grey area indicated the fibrous continuity between aortic valve and mitral valve. Abbreviations: LA: left atrium, LV: left ventricle, AoV: aortic valve, Ao: aorta, MV: mitral valve, FM: fibrous membrane, S: Sinus of valsalva, asterisk: inter leaflet triangle or trigone (Modified from Schoenwolf et al., 2009).

2.2.4 Aorta

The aorta is the largest artery in the body, originating from the left ventricle, to carry oxygenated blood away from the heart to the body through the aortic valve. In adults, the diameter ratio of pulmonary artery (PA) to ascending aorta (AA) is 1:1, whereas this ratio is slightly increased to 1.09:1 in the infant (Compton et. al., 2015). The aorta is normally considered to consist of three segments: the ascending aorta, the aortic arch and associated arteries, and the descending aorta. The ascending aorta is found superior to the heart exiting from the left ventricle. The transverse segment of the aorta gives rise to the brachiocephalic artery, which branches in turn to give the right common carotid artery and right subclavian artery, left common carotid artery, and left subclavian artery (Figure 2.4). The descending aorta is distal to the isthmus and has both thoracic and abdominal components.

One major difference between adult hearts and newborn hearts is the closure of the ductus arteriosus to form the ligamentum arteriosum (arterial ligament) a few days after birth. The ductus arteriosus arises from the left 6th pharyngeal arch artery, which remodels to join the pulmonary trunk (formed from the septated outflow tract) to the descending aorta (Walmsley and Monkhouse, 1988) (Figure 2.4). However, the form, length and diameter of the ductus arteriosus varies between infant hearts (Edwards, 1960). The region between the ductus arteriosus junction and the left subclavian artery is termed the isthmus (Evans, 1964). Although pathological changes in the isthmus have been described (Ho and Anderson, 1979; Bremer, 1948), the cause of these changes and origin of the isthmus remains unclear (Figure 2.4).

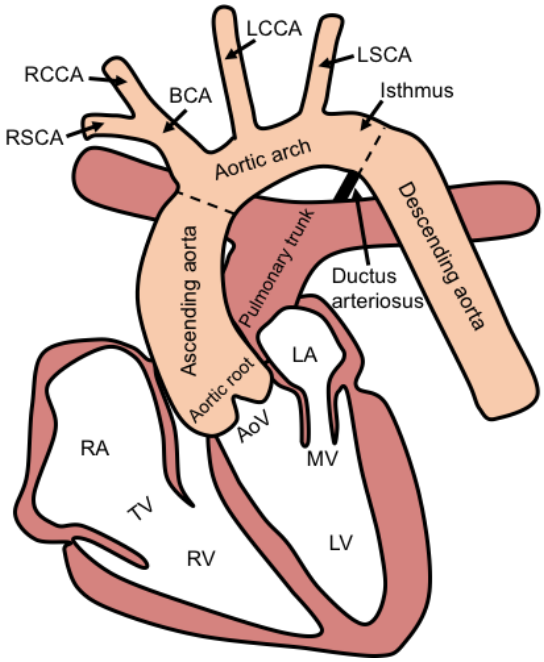

Figure 2.4: Structure of the aorta.
Three segments of aorta: Ascending aorta, aortic arch, and descending aorta. The ductus arteriosus is indicated in black. Abbreviation: LA: left atrium, LV: left ventricle, AoV: aortic valve, MV: mitral valve, RV: right ventricle, RA: right atrium, RSCA: right subclavian artery, RCCA: right common carotid artery, BCA: Brachiocephalic artery, LCCA: left common carotid artery, LSCA: left subclavian artery (modified from Schoenwolf et al., 2009).

2.3 Hypothesis and aim of this chapter

This chapter hypothesises that an anatomical analysis of HLHS will create subgroups that can be useful for genetic and developmental studies, designed to investigate the aetiology of HLHS.

The focus of this chapter is to undertake a novel approach to understanding and analysing hearts with HLHS. Therefore, this chapter aims:

- To establish on morphological grounds whether there are different subtypes of HLHS through using human archival hearts obtained from Birmingham Children's Hospital.
- To describe the morphological structure of each segment affected in HLHS.
- To correlate the various characteristics of HLHS according to a morphological classification.
- To describe a novel classification of HLHS based on ventricular morphology.

2.4 Materials and Methods

2.4.1 Archival HLHS hearts

The human congenitally malformed archival heart collection based at Birmingham Children's Hospital, contains a collection of approximately 2000 specimens collected since 1939 (the storage time for each heart was not available). Permission to perform the analysis on the HLHS heart collection was obtained from the Guardian Committee of the collection and the R&D department at Birmingham Children's Hospital NHS Foundation Trust. The collection of 183 HLHS hearts were initially analysed by Professor R. H. Anderson and Dr A. Crucean to confirm the diagnosis of HLHS. A second analysis including measurements and photography was made by A. M. S. Alqahtani and Dr. B. Chaudhry. The specimens were described according to the method of sequential segmental analysis (Anderson and Shirali, 2009) and physical measurements and analysis were performed using digital calipers, microscopic examination, and probe patency. This measurement method was novel and has not been described before. Photographs of the selected specimens were taken using either a Leica microscope (MZ16, Leica, Germany) or a digital SLR camera (Nikon 3100, Nikon, Japan).

The archival collection of 183 hearts was already prosected and fixed in formalin, no further prosection was permitted. The HLHS hearts included in this study were carefully categorised according to specific criteria. Firstly, it was important to include only non-operated hearts in good condition because only these hearts can provide a true and correct morphological description of

affected regions. Secondly, the selected hearts had to conform to the classic definition of HLHS as defined by Tchervenkov et.al, 2006 and the WHO International Classification of Diseases (ICD-11). This included a hypoplastic left ventricle with significant hypoplasia of the ascending aorta, aortic arch and at least one of the main left-sided valves; aortic and mitral. Moreover, the great arteries had to be normally aligned and there had to be a fully formed atrioventricular septum. Finally, the right-sided structures of the hearts had to be well formed with normally connected valves. Due to the original cardiac explant, it was not possible to examine the pulmonary veins or to identify the connections with the superior caval veins. The information about the gender and age of the selected hearts were not available for confidentiality reasons. Therefore, all the obtained measurements were normalised to the well-formed right-sided structure of each heart.

Therefore, in total 78 hearts (out of 183) were selected for analysis on the basis of the criteria above. These hearts were further analysed through measuring the left ventricular length and wall thickness, ascending aorta size and the distance between the left subclavian artery and ductus arteriosus (Figure 2.5.1 and Appendix Table 8.2). In addition, a morphological analysis of the overall external shape of the left ventricle in terms of hypertrophic left ventricles and the presence of endocardial fibroelastosis (EFE) was carried out (Appendix Table 8.2). Furthermore, the aortic and mitral valves were always small in HLHS hearts but with different ranges in size (no measurement were made). To accurately classify the different mitral valvar phenotypes, a semi-quantitative method was devised, describing the leaflets, papillary

muscles and chordae tendineae. Similarly, the aortic valve was morphologically evaluated based on the presence or absence of leaflets and a semi-quantitative method was devised (Appendix Table 8.2).

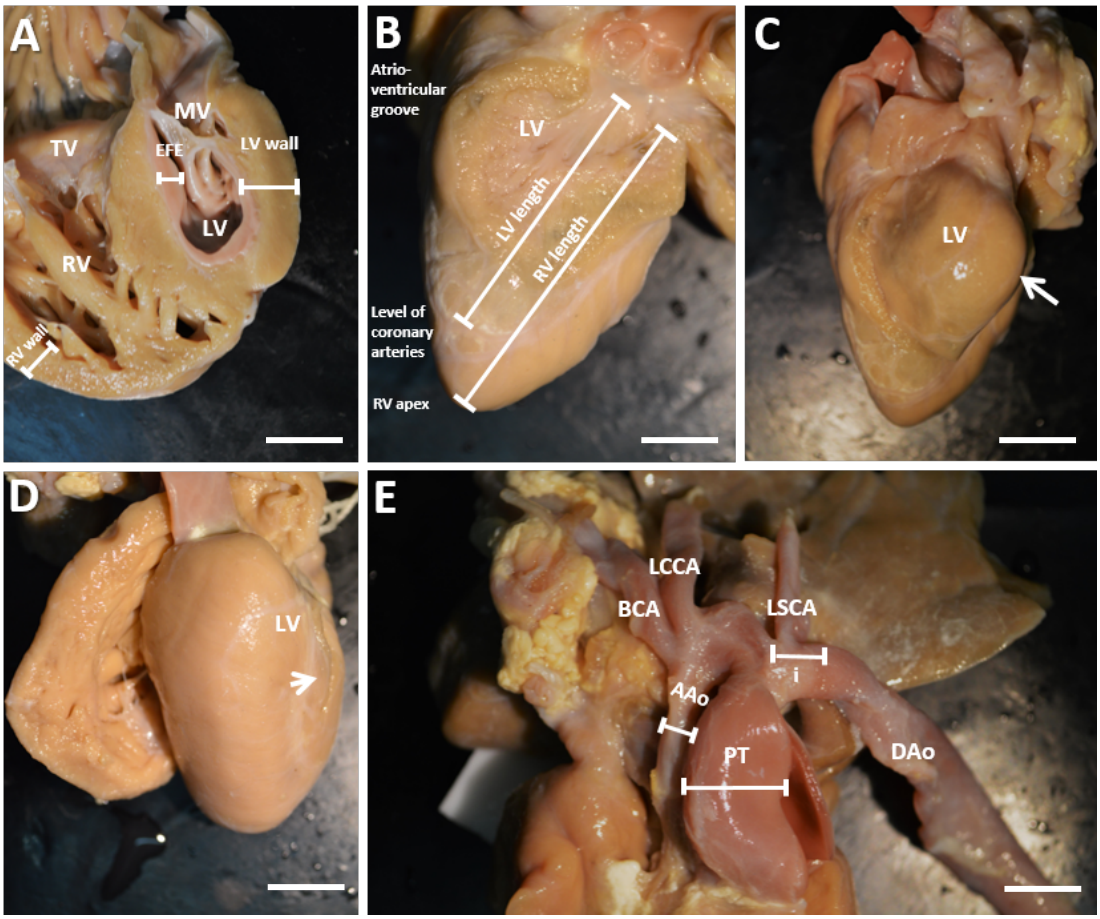

Figure 2.5.1: The measurement approach for the main characteristics of HLHS.
(A) Perpendicular measurement of LV to RV free-wall ratio and the size of EFE. (B) LV to RV length ratio, LV length starts from the atrioventricular groove and ends at the coronary artery, whereas the RV ends at the apex. (C) LV hypertrophy (arrow). (D) Non-hypertrophy LV (arrow's head). (E) Isthmus starts from the LCCA to the ductus arteriosus, AAo to PT ratio. All measurements were in millimetre (mm). Key: LV: left ventricle, RV: right ventricle, MV: mitral valve, TV: tricuspid valve, EFE: endocardium fibrosis, BCA: Brachiocephalic artery, LCCA: left common carotid artery, LSCA: left subclavian artery, DAo: descending aorta, i: Isthmus, PT: pulmonary trunk, AAo: Ascending aorta. Scale bar = 2mm.

2.4.2 Statistical analysis

All the statistical calculations were performed using SPSS (Version 22, IBM) software for Windows. Analysis was carried out using ANOVA and Tukey's multiple comparison test assuming non-parametric distributions. The statistical significance of differences between the various HLHS subgroups was assessed and only p-values less than 0.05 were considered significant.

2.5 Results

2.5.1 Selection of hearts

In total 78 hearts (out of 183) were selected for analysis on the basis of the criteria above. No additional data was collected for the excluded hearts. As a preliminary analysis, the selected hearts were initially sub-categorised according to the conventional clinical categories. This categorisation involved sub-classifying hearts on the basis of aortic and mitral valve patency using the description terms: atresia (non-patent to probe entry) and stenosis (slightly/fully patent to probe entry) (Figure 2.5).

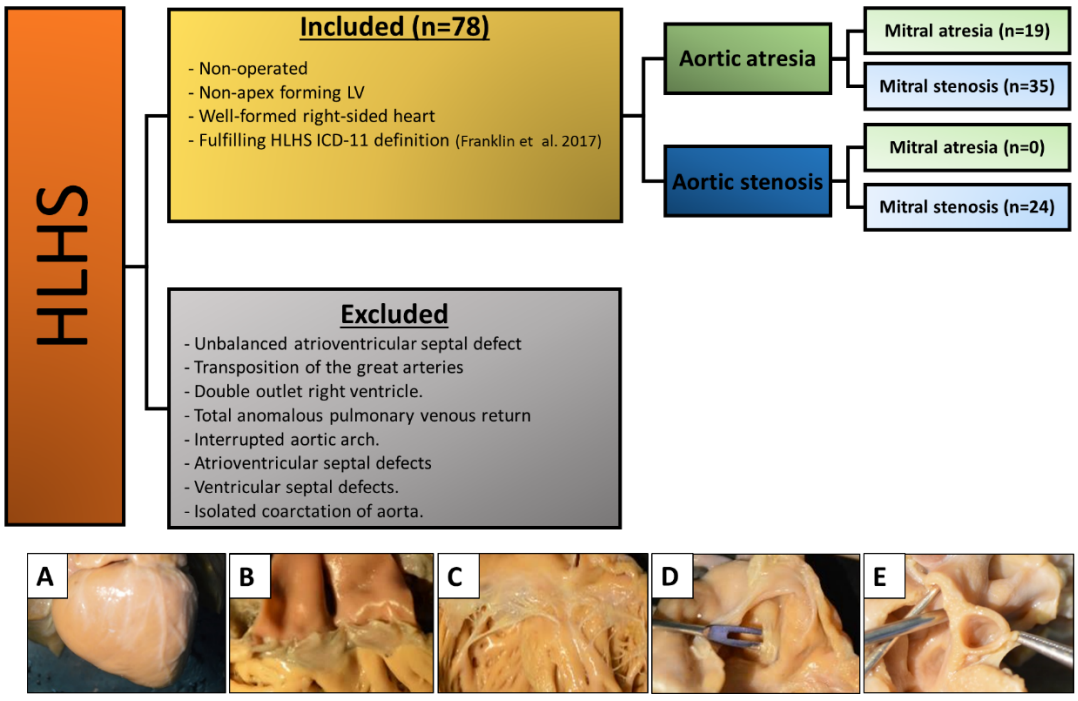

Figure 2.5: Schematic diagram showing the selection of HLHS hearts and the conventional classification of these hearts.
A total of 78 hearts were included in the study and further sub-classified according to the conventional clinical classification. Other cardiac defects associated with a relatively small or dysfunctional left ventricle were excluded. The selected hearts (n=78) maintained (A) a normal morphologically right ventricle, normal appearance of (B) pulmonary valve, (C) tricuspid valve, (D) Patent foramen ovale PFO. One heart (E) had a large coronary sinus.

2.5.2 Left ventricle

Examination of 78 hearts revealed that the morphological right ventricle was clearly apex forming in all the examined hearts. In contrast, the morphological left ventricle was not an apex-forming ventricle and showed three distinctly different appearances. A unique subset was identified by absence of the left ventricular cavity that located in the left-posterior aspect of the ventricular mass. This subset was referred to as “slit-like ventricle” (SLV) and was found in 19/78 hearts. A cross-sectional view of all of these 19 hearts exposed a thin parietal left ventricular wall with a fissure-like cavity that was identified by delimiting coronary vessels found on the surface of the hearts (Figure 2.6 G,H). All of these hearts presented with no valvular connections as non-patent probe entry was found, and hence were previously diagnosed as aortic atresia and mitral atresia (AA/MA) (Figure 2.6 I). A second subset had a small left ventricular cavity with a remarkably thick left ventricular wall (Figure 2.6 D,E). This group was referred to as “thick-walled ventricle” (TWV) and was seen in the majority of cases; 54/78 hearts (Figure 2.6 F). Of this subset, 35/54 hearts were identified with non-patent probe entry to the aortic valve and narrow patent probe entry to the mitral valve, and thus were representative of aortic atresia and mitral stenosis (AA/MS). The remaining 19/54 hearts had limited probe entry to both the aortic and mitral valves and thus were classified as having aortic stenosis and mitral stenosis (AS/MS), The final subset, which was found to be the smallest group with 5/78 hearts, had an almost normal sized left ventricular cavity and wall thickness, yet the left ventricle was not

apex-forming (Figure 2.6 A,B). While these hearts had morphologically normal-looking mitral and aortic valves with limited probe patency, they were smaller in size compared to their respective right-sided valves (Figure 2.6 C). Thus, these hearts were classified as exhibiting aortic stenosis and mitral stenosis (AS/MS) as flow would have been limited through these valves. As it is probable that these hearts could have been repaired by a biventricular surgical procedure, they were previously recognised as “hypoplastic left heart complex” (Tchervenkov 1998). Nevertheless, for the purpose of this study, these hearts were termed “miniaturised ventricle” (MinV).

Thus, examination of the ventricular morphology revealed three distinct groups; the slit-like ventricles, thick-walled ventricles and miniaturised ventricles. The ventricular-based classification provided well-defined and obvious characterised subgroups for HLHS. It also showed that the AS/MS and AA/MS groups, which have been previously considered as distinct HLHS subgroups, had in fact extremely similar morphological structures and they could be included into one group based on their ventricular morphology. Altogether, the AA/MA clinical group always have SLV and vice versa. Nevertheless, that is not the case for the other clinical/ventricular groups. Hence, this may be important for further analytical and aetiological studies.

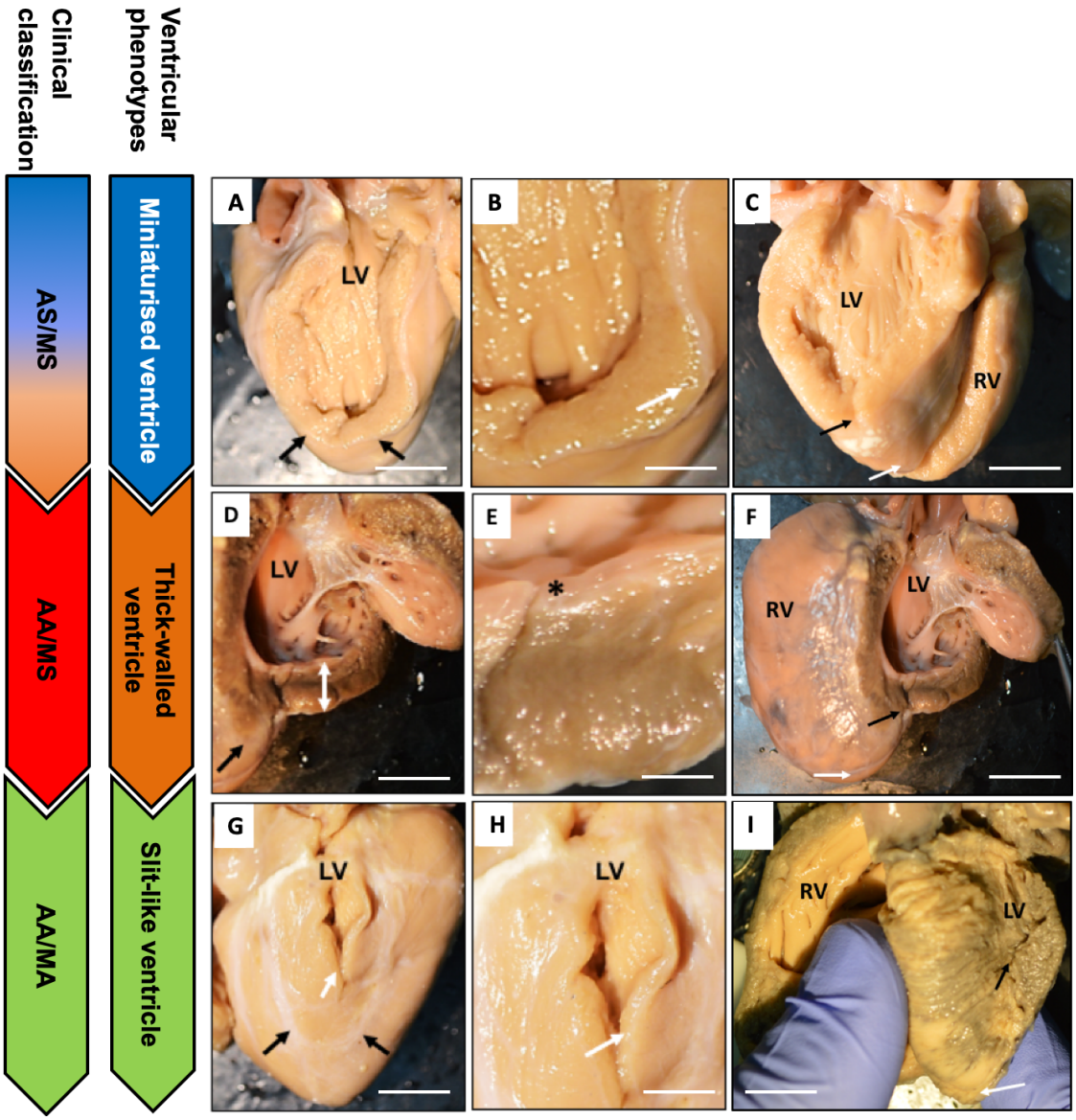

Figure 2.6: Three different left ventricular phenotypes of HLHS hearts. Examination of HLHS hearts revealed three distinctive phenotypes of ventricles: (A) slit-like ventricle detected by coronary vessels (black arrows) with no cavity (white arrow) and (B) a thin free-wall (White arrow), (C) overview of non-apex forming left ventricle (black arrow) and the apex forming right ventricle (white arrow) in the slit-like ventricles. (D) Thick-walled ventricles (white arrow) with small cavity and non-apex forming LV (black arrow). (E) Endocardial fibroelastosis (EFE) asterisk. (F) Overview of non-apex forming the left ventricle (black arrow) and the apex forming right ventricle (white arrow) in the thick-walled ventricles. (G) Miniaturised ventricle with a small cavity (black arrows) and (H) thin wall (white arrow). (I) overview of non-apex forming the left ventricle (black arrow) and the apex forming right ventricle (white arrow) in the miniaturised ventricles. Scale bar = 2mm.

2.5.2.1 Length and wall thickness of the three ventricular morphology groups

For further analysis of the three distinctive ventricular morphology groups, the length and wall thickness of the left ventricle were measured and compared between groups. The length of left ventricle was obtained by defining the anterior and posterior epicardial coronary arteries located in the inter-ventricular groove (Figure 2.7 A, B). The measurement of the coronary arteries was acquired starting from the atrioventricular groove and ending at the heart apex for both the right and left ventricles. Since demographic data (e.g. age and body size) for this heart collection were not available, the length of the left ventricle was related to the right ventricle producing a ratio-metric index that represented a normalised length value for the left ventricular size (Figure 2.7 A). Likewise, a ratio of left ventricular wall to right ventricular wall thickness was utilised to illustrate the wall-thickness of left ventricle (Figure 2.7 B).

Comparing the length of left ventricle between HLHS groups based on the usual clinical classification revealed no significant differences in left ventricular length between these groups (Figure 2.7 C). However, analysing the left ventricular length using the ventricular phenotype groups of SVL, TWV and MinV showed differences in the length between these groups (Table 8.2). The miniaturised ventricles (n=5, mean 28.4mm) were relatively longer than those with slit-like ventricles (n=19, mean 25.6mm) or thick-walled ventricle (n=54, mean 24.8mm). However, the slit-like ventricle (AA/MA) and thick-walled ventricle (which was described as AA/MS and AS/MS) groups, showed overlapping ventricular length values indicating no differences in relative

length between these groups of ventricular phenotypes (Figure 2.7 E). Therefore, this suggested that the various degree of hypoplasia presented by the relative ventricular cavity length in HLHS did not relate to the condition of the mitral/aortic valves. Thus, although both the thick-walled and miniaturised ventricular phenotypes included AS/MS cases, the length of ventricle varied. Hence, as in the conventional grouping, this parameter of relative LV length was not correlated with the valve status.

Normal development of ventricles results in equal wall-thickness of both left and right ventricles at the time of birth (Daimei et al., 2014). In the current study, based on the clinical classification groups, the ratio of the left and right ventricular wall thickness (LV/RV ratio) was significantly lower in the conventional AA/MA group compared to the AA/MS and AS/MS groups (Figure 2.7 D). However, based on the ventricular morphology grouping, the ratio of LV/RV wall thickness suggested equal wall thickness in the miniaturised ventricles (n=5, mean 4.5mm). Conversely, the LV/RV wall thickness ratio for the thick-walled ventricles (n=54, mean 7.2mm), including AA/MS and AS/MS, was increased indicating hypertrophy of the LV wall. A significant decrease in the LV/RV ratio for the slit-like ventricles (n=19, mean 2.9mm) confirmed the thin wall of LV in this group (Figure 2.7 F)**.** Therefore, the wall thickness LV/RV ratio suggested that although LV wall thickness did not relate to the conventional grouping based on stenosis or atresia of the mitral and aortic valves, it entirely correlated with the ventricular phenotypes. Hence, this implied the possibility of an alternative classification of HLHS based on the ventricular morphology: slit-like ventricle with no sign of hypertrophy and

reduced relative LV length, the thick-walled ventricle with hypertrophied LV and a reduced relative LV length, and miniaturised ventricles with no hypertrophy and reduced LV length.

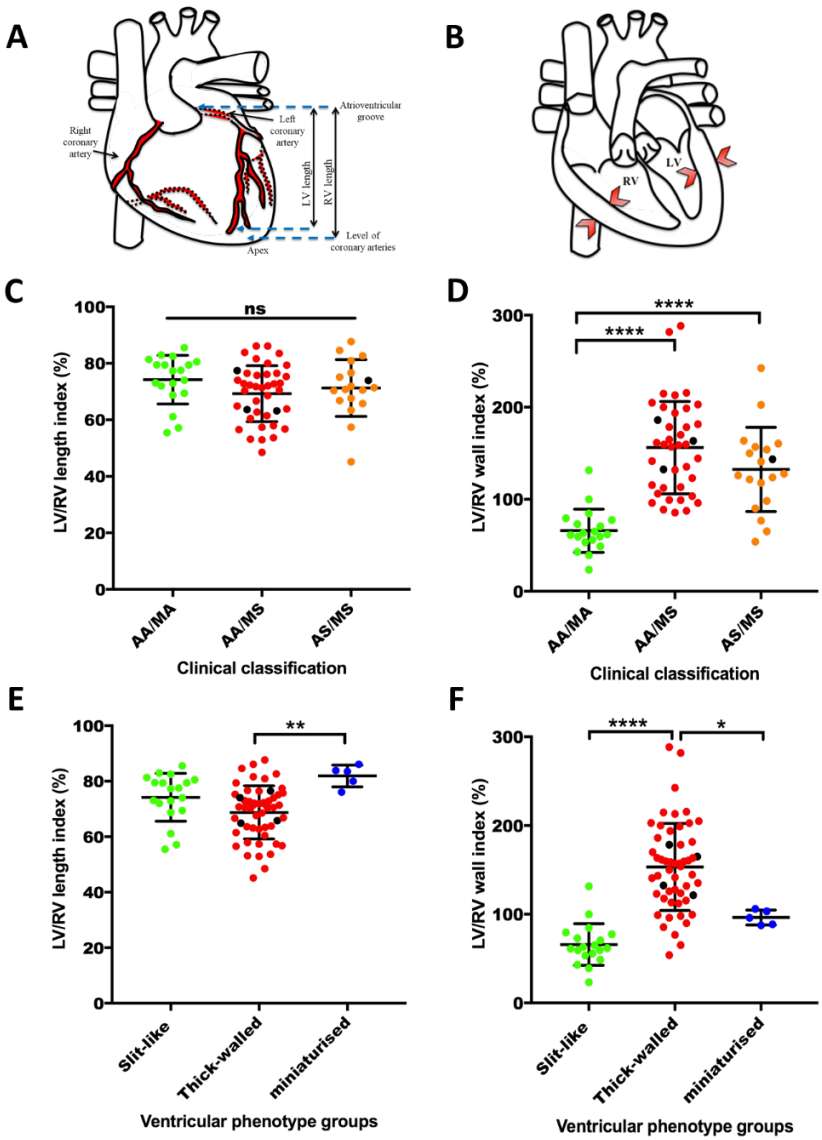

Figure 2.7: Comparison of LV length and wall thickness.
(A) A diagram showing the measurements of LV length in relation to RV length (measuring from the left coronary artery to the left anterior descending coronary artery). (B) A diagram showing LV free wall thickness in relation to RV free wall thickness. (C) The chart showed the LV length in the clinical classification group, as the left ventricular length was the same in all the different clinical groups. (D) the wall-thickness of left ventricle in the clinical classification groups, where only the AA/MA group revealed a significant difference in the thickness of LV wall. Other clinical groups showed similar wall-thickness. (E) The left ventricular length index in the ventricular morphology groups. The LV length of slit-like ventricles was the same as that of thick-walled ventricles (mean 25.6mm and 24.8mm). However, the miniature ventricle group had longer LV lengths (mean 28.4mm). (F) Left ventricular free wall thickness in HLHS grouped based on ventricular morphology. LV wall thickness in miniaturised ventricles was the same as in RV (mean 4.50mm). However, the walls of the slit-like ventricle were thin (mean 2.9mm), and the walls of thick-walled ventricles demonstrated remarkable thickening in keeping with the morphological observations (mean 7.2mm). Black markers indicated no EFE. Bars indicate median and interquartile range; *p<0.05, **p<0.01, ****p<0.0001).

2.5.2.2 Endocardial fibroelastosis

Further examination of HLHS hearts revealed the presence of endocardial fibroelastosis (EFE). The EFE appears as a firm and smooth layer on the endocardial surface of the LV. In this collection, EFE was found in the thick-walled ventricular phenotype, specifically in 50/54 thick-walled ventricle hearts (Figure 2.6 E,F). Of the remaining four hearts in the thick-walled ventricle group that did not show EFE under microscopic investigation, three hearts were clinically classified as AS/MS and one was AA/MS (Figure 2.7 C,D black dots). Strikingly, no EFE was found in any of the slit-like ventricle or miniaturised ventricle hearts (Figure 2.7 E,F). Histological examination (i.e. preparation of histological sections to look for EFE microscopically) for further analysis was not possible on these hearts, as these hearts were set up for morphological analysis only. The aetiology of EFE in HLHS remains unknown. However, it has been suggested to be caused by a primary stimulus on the endothelial layer leading to fibro-elastic thickening of the ventricular endocardium (Krenning et al., 2010). Although EFE was found in almost all of the thick-walled ventricular hearts, no relationship was drawn between the thickness in LV wall or length of LV and the presence of EFE (Figure 2.7 E,F all dots in the thick-walled ventricles excluding the black dots).

2.5.3 Aortic valve

The aortic valve was next examined for all 78 HLHS hearts within the collection. Aortic valve patency was correlated with valve appearances and ventricle morphology. Assessments of the aortic valve were made either from the ventricular aspect, proximal aorta view, or entire outflow tract view based on the condition and screening possibility of the examined hearts.

There were 24 hearts identified with aortic stenosis. In 12/24 hearts, the morphological structure of the aortic valve exhibited three thin leaflets (Figure 2.8 A, B). Relating these hearts to the ventricle phenotypes revealed 5/12 hearts had the miniaturised ventricular phenotype, with the remaining 7/12 hearts having a thick-walled left ventricular phenotype. The remaining 12/24 hearts belonged to the thick-walled ventricle group and they exhibited different appearances of the aortic valve. Of these 12 hearts, 10 hearts had dysplastic valves with thickened leaflets (Figure 2.8 C, E, F) and the remaining 2/12 hearts showed bicuspid or unicuspid leaflets (Figure 2.8 D). The size and form of valvar leaflets was proportional to the overall appearance of the aortic root. Thus, the dysplastic leaflets were found in hypoplastic aortic roots, whereas small and thin leaflets were observed within well-formed aortic roots.

There were 54 hearts identified with aortic atresia. Of the 54 hearts, 32 hearts presented with non-identifiable aortic valve structures (Figure 2.8 G,H). Referring this to the ventricular morphology grouping, there were 15/32 hearts identified with thick-walled ventricular morphology, whereas 17/32 had a slit-like ventricular phenotype. Due to their ventricular morphology (i.e. no

ventricular cavity), it was not possible to examine the outflow tract from the ventricular aspect. However, examination of some cases with previous dissected proximal aorta revealed no aortic valve tissue in the region between the coronary artery ostia. Thus, histological sectioning, although not allowed here, could be a useful for further studies. The remaining 22/54 hearts had either a slit-like (2/22) or a thick-walled (20/22) ventricular phenotype. Of the two cases with the slit-like ventricular phenotype, one case exhibited the aortic valve as dysplastic with thickened leaflets and the other case as fused valvular leaflets. In the thick-walled ventricular phenotype hearts, the aortic valve (13/20) was found as a lump of white fibrous tissues with non-distinguishable leaflets (Figure 2.8 G,H). In the remaining (7/20) hearts, the aortic valve was presented as dysplastic with thickened leaflets or with bicuspid or unicuspid leaflets (Figure 2.8 D,E,F).

A summary of the different valvar phenotypes correlating to the clinical conventional classification and to the ventricular morphology groups is presented in the following graph (Figure 2.9).

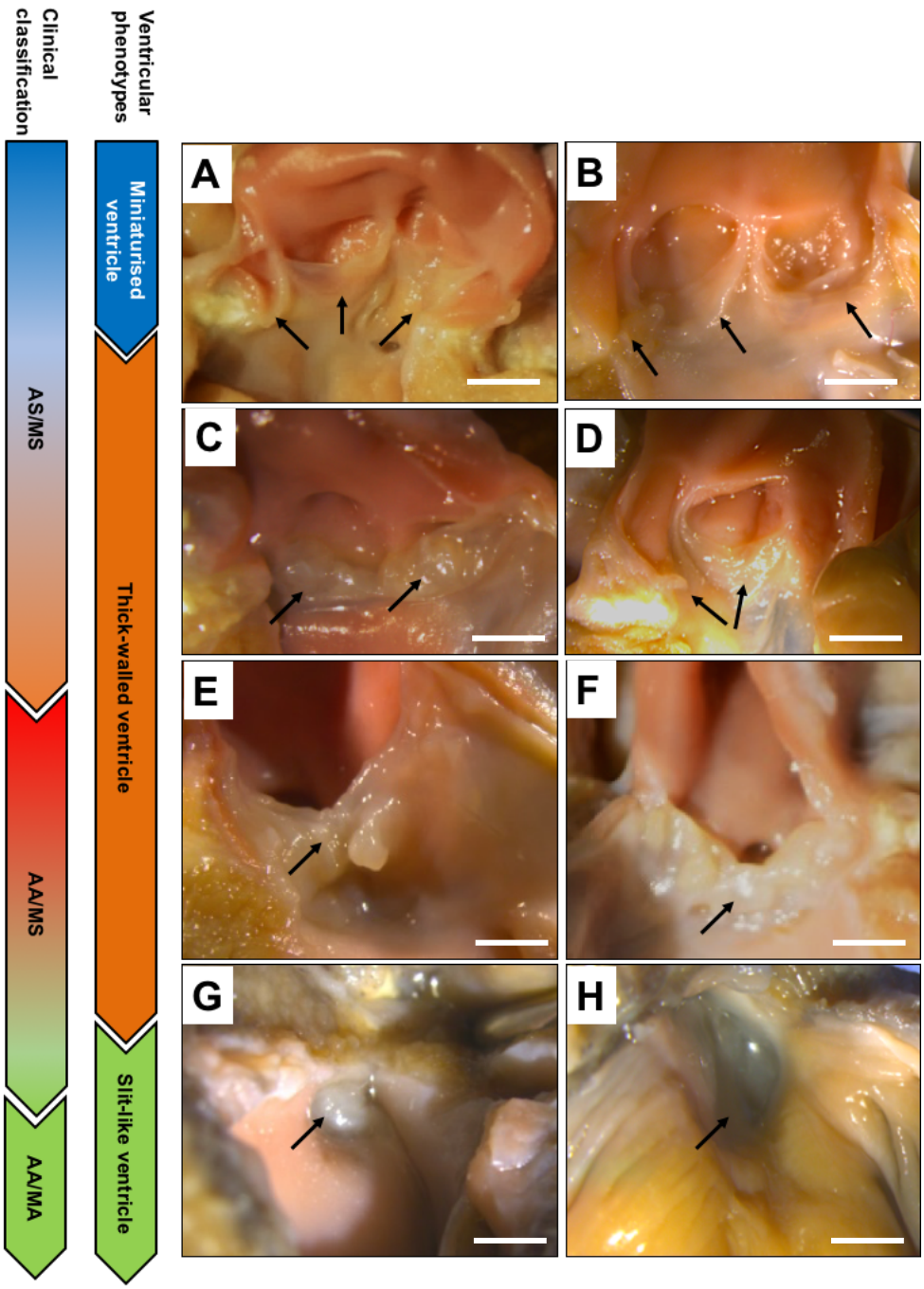

Figure 2.8: Morphological structures of aortic valve.
(A-B) small well-formed aortic valve with three leaflets (black arrows) identified in both miniaturised and thick-walled ventricles, also in AS/MS clinical grouping. (C) bobbly leaflets (D) bicuspid leaflets (E) dysplastic leaflets (F) thickened leaflets are the phenotypes seen in thick-wall ventricles and both AS/MS and AA/MS clinical grouping. The aortic valve leaflets are indicated by black arrows. (G) fibrous-tissue leaflets blocking the aortic valve and (G) imperforate leaflets were seen in mostly all the slit-like ventricular phenotype and some thick-wall ventricular phenotype. Also, these valvar phenotypes were seen in AA/MS and AA/MA clinical classifications. Scale bars =2mm.

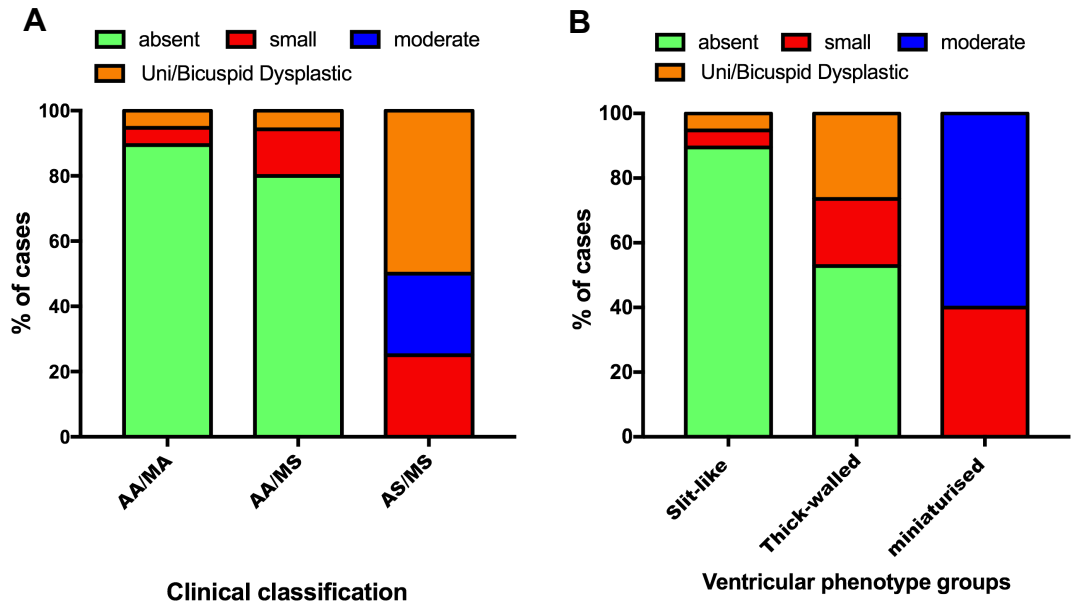

Figure 2.9: Correlation of valvar phenotypes with the clinical conventional classification and the ventricular morphology groups.
(A) The AA/MA and AA/MS groups presented with absent of aortic valve in most cases. Dysplastic valve and/or fused valve were seen across all clinical groups. In addition, the AS/MS group had moderate-size aortic valve. (B) The ventricular morphology classification, similarly, to the clinical classification, showed absence of aortic valve in most of the cases found in the slit-like ventricle and thick-walled ventricle. Also, dysplastic valve was observed across the slit-like and thick-walled ventricle. Moderate and well-form valve as well as small valves were mostly observed in the miniaturised ventricles.

2.5.4 Mitral valve

The conventional clinical classification was based on correlation between the aortic valve and the mitral valve. Hence, examination of the mitral valve was performed to relate it to the ventricular phenotype.

In 59/78 HLHS hearts, clinically classified as AS/MS or AA/MS, a range of characteristics was observed. In the thick-walled ventricle hearts with AS/MS (8/54), and the miniature ventricle hearts (3/5), the mitral valves were well-formed, the leaflets were thin, the papillary muscles were prominent, and well-formed separate chordae were apparent (Figure 2.10 A). In the remaining 2/5 hearts of the miniature ventricle group, the mitral valves were of moderate size with chordae and absent papillary muscles (Figure 2.10 B). In addition, the thick-wall ventricles with AS/MS (11/54) and AA/MS (35/54) groups represented a spectrum of mitral valve abnormalities including small mitral valve, thickened leaflets, and dysplastic leaflets (Figure 2.10 B, C, D, E, F).

Of the remaining 19/78 HLHS hearts, 15 of these hearts showed the mitral valve was either absent or existed as a small piece of non-patent fibrous tissue (Figure 2.10 G, H). All these 15 hearts had a slit-like ventricle and were clinically grouped as AA/MA. The remaining 4/19 hearts, which were also classified as AA/MA and slit-like ventricle, the mitral valve presented as dysplastic or small non-patent mitral valves (Figure 2.10 B, E, F, D). A summary of the different valvar phenotypes correlating to the clinical conventional classification and the ventricular phenotype grouping presented in the following graph (Figure 2.11).

Whilst there were similarities between the ranges of abnormalities observed in the mitral valve to that seen in aortic valve, correlation between both valves was limited. The miniaturized ventricle hearts were associated with the moderate to small valves that tended to have well-formed mitral and aortic valves, whereas the slit-like ventricles were associated with the most extreme abnormalities seen in both valves. Nevertheless, there was no clear associations between the appearances of the mitral valves in comparison to the aortic valves. In general, the aortic valve was more severely affected than the mitral valve. This could create an obstruction to the blood flow from the left ventricle with accompanying uncontrolled filling via the mitral valve.

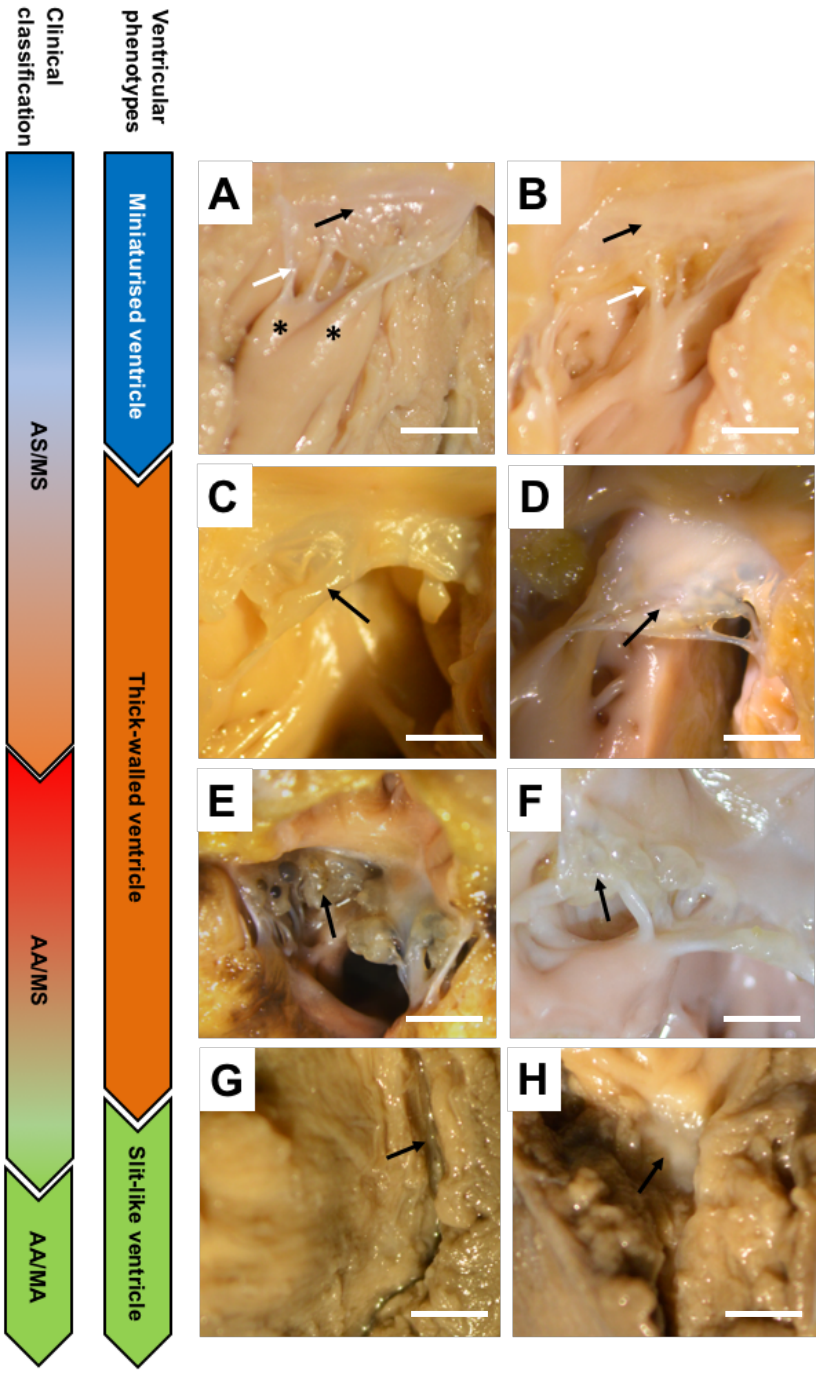

Figure 2.10: Various appearances of the mitral valve in HLHS hearts.
(A) A moderate mitral valve with thin leaflets (black arrow), short chordae (white arrow) and papillary muscles (asterisks). (B) small valve with thin leaflets (black arrow) and short chordae (white arrow) with no papillary muscles. These phenotypes are observed in miniaturised hearts, MS/AS and MS/AA. A range of mitral valve abnormalities included (C) thickened leaflets (D) dysplastic valves (E-F) bobbly leaflets (G) absent (H) fibrous-tissue. These abnormalities were demonstrated in thick-walled ventricular phenotypes and both AS/MS and AA/MS. The slit-like ventricles and AA/MA showed either absent or fibrous tissue. Scale bars = 2mm.

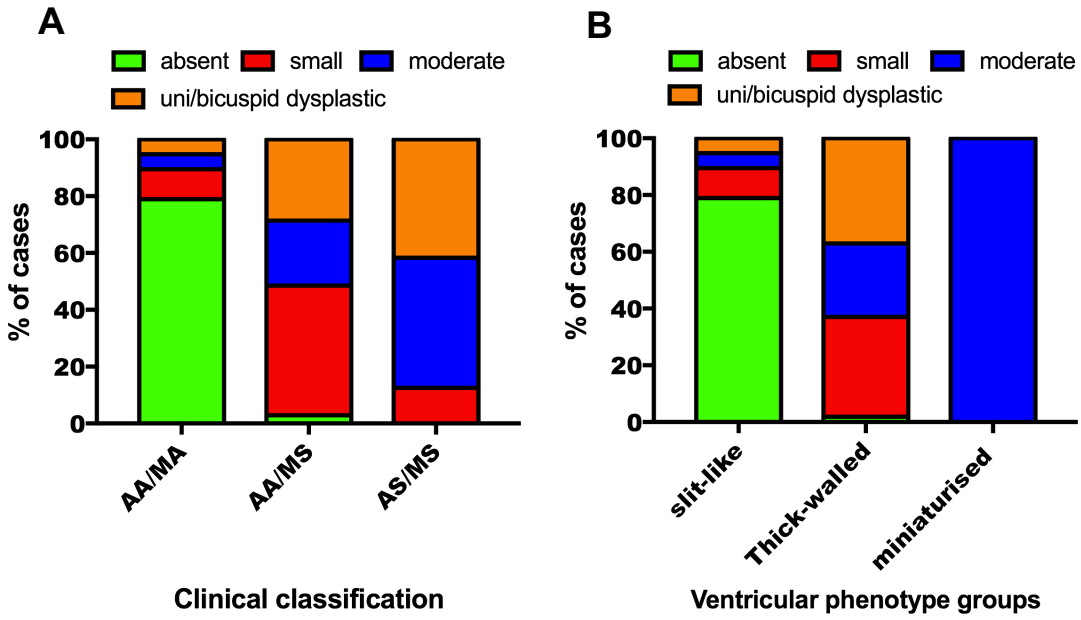

Figure 2.11: Correlation of the mitral valve phenotypes with clinical classification and ventricular phenotype groups.
(A) In the clinical classification, absent of mitral valve was seen mostly in AA/MA and some cases in AA/MS. Small and dysplastic or fused leaflets were demonstrated in mostly in AA/MS and AS/MS groups. (B) The mitral valvular phenotypes observed in the ventricular morphological groups specifically the slit-like and thick-wall ventricle groups were similar to that seen in the clinical classification. However, the miniaturised ventricles showed a specific phenotype, which was moderate mitral valve appearance, in all the cases.

2.5.5 Ascending Aorta

As previously mentioned, the normally functioning aorta serves to carry oxygenated blood from the left ventricle to the body through the aortic valve. Therefore, it has been suggested that normal aortic structure requires a fully formed aortic valve and left ventricle, as normal blood flow is required for the growth and functioning of the aorta (Chester et al., 2014). However, the counter-argument, that the abnormalities of the aorta are a primary defect that lead to malformation in related regions including the left ventricle and aortic valve, cannot be excluded (Sedmera et al., 2005).

In the collection of HLHS hearts held at Birmingham Children's Hospital, a general inspection of aorta dimension in HLHS hearts revealed a thin-looking aorta (Ao) compared to the pulmonary trunk (PT) in all the cases. This dimension did not differ throughout the ascending aorta segment (Figure 2.12). Hence, a measurement of the proximal aortic diameter close to the root should provide a representative indication of the maximal aorta size (Figure 2.12). The ascending aorta size was measured through gently flattening the aorta and taking the transverse dimension. Following the same principle, the pulmonary trunk was measured, and both measurements were expressed as the ratio of aorta: pulmonary trunk (Ao:PT) hemi circumference. This metric was sorted according to the conventional clinical groups and also to the ventricular morphological groups. All conventional clinical groups showed a significant reduction in the dimension of the ascending aorta compared to the pulmonary trunk. Upon analysis, three distinct appearances of the aorta were defined: thread-like, small and moderate aorta (Figure 2.13). The aorta size in

the AA/MA group (clinical classification), or the slit-like ventricle group (ventricular classification), which were previously labelled to represent the same group, was observed to have the smallest dimensions (Threadlike; mean Ao:PT ratio 0.2, n=19), followed by the AA/MS or AS/MS group that were part of the thick-walled ventricle group (small; mean Ao:PT ratio 0.4, n=54) and finally AS/MS that were part of the miniaturised groups (moderate; mean Ao:PT ratio 0.5, n=5) (Figure 2.14, Table 8.2). Although the relative dimension of ascending aorta varied between cases within the same ventricular phenotypic groups and conventional clinical classification, an overall increase in the ascending aorta size was observed and correlated with the expected blood flow through it (Figure 2.14). In AA/MA and the slit-like group, the forward flow through the aorta terminated early because of the atresia of both valves; this led to an extreme reduction in the ascending aorta size. However, in the AS/MS or miniaturised group, some forward flow was maintained as the aortic and mitral valve allowed flow into the left ventricle. Thus, it appeared that the more blood that was expected to enter into the aorta, the greater the size of the ascending aorta. Therefore, the observed differences in the ascending aorta dimensions suggested a flow-related feature that was secondary to abnormalities in the valves and possibly the small left ventricle.

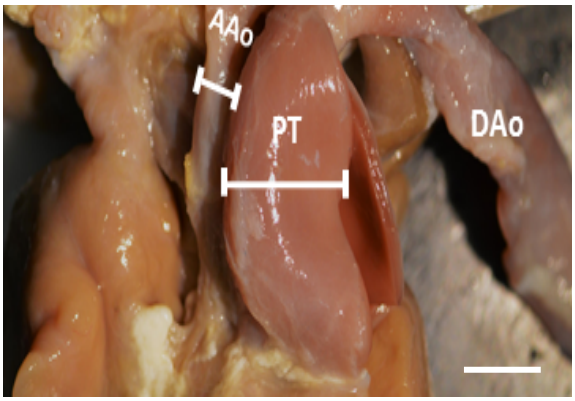

Figure 2.12: Measurement of the ascending aorta size.
The dimension of the ascending aorta was measured through calculating the proximal aortic diameter and compared to the similar proximal region in the pulmonary trunk. (AAo) ascending aorta, (PT) pulmonary trunk, (DAo) descending aorta.

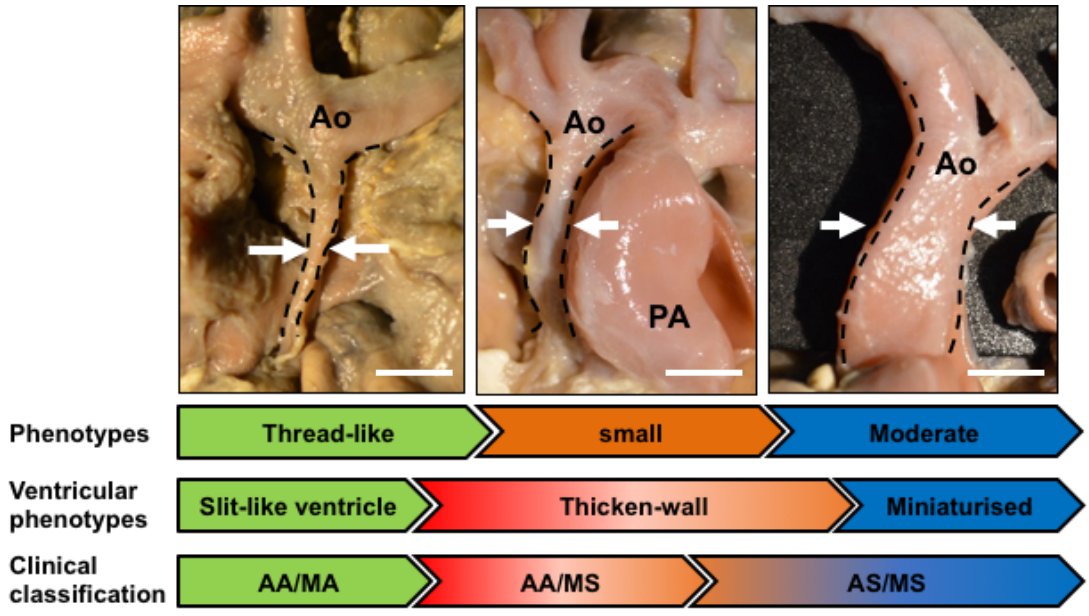

Figure 2.13: Aorta appearances in HLHS hearts.
Three main phenotypes were observed in the HLHS hearts. The thread-like aorta that was mostly seen in slit-like ventricle and some cases with AA and thick-walled ventricles. The small aorta was seen in thick-walled ventricles and cases with AA or AS. The moderate aorta was presented frequently with miniaturised ventricle, AS/MS, and AA/MS.

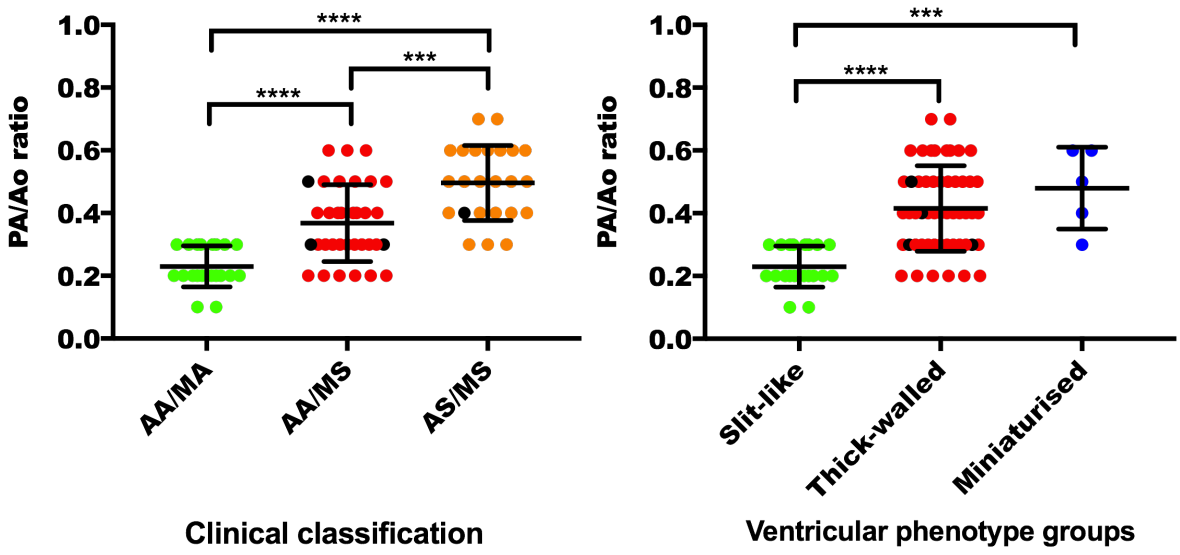

Figure 2.14: Aorta size varies between different groups of HLHS.
Quantification of aorta dimension indicating significantly reduced aorta size between the conventional clinical groups and ventricular morphological groups of HLHS. All the subgroups represented a decrease in aorta size correlated with the valve severity. Black dots represent non-EFE hearts. One-way ANOVA test (turkey and Scheffe test) was used to calculate P values, ***p<0.001, ****p< 0.0001.

2.5.6 Isthmus and ductus arteriosus

The isthmus is the region of the aortic arch between the ductus arteriosus (DA) junction and the left subclavian artery (Figure 2.16 A). Narrowing and distortion of this region in HLHS has been reported (Gobergs et al., 2016). In the current collection, all the hearts were from new-born infants and thus the DA was patent, and the isthmus was wide in all cases. Normally, the left subclavian artery (LSCA) is found adjacent to the left common carotid artery (LCCA), and both arise from the outer curvature of the aortic arch, followed by the DA attached to the inner curvature at its boundary with the descending aorta (Figure 2.15 A). Strikingly, in this collection of HLHS hearts, several positions and points of attachments of the DA were observed. For example, some cases presented with the LSCA located opposite to the DA (Figure 2.15 B), whereas in other cases the DA was located proximal to the LSCA (Figure 2.15 C). Therefore, examination of the DA location in all of the 78 hearts in this collection was performed. The DA position was investigated and expressed as a ratio of the distance from the LSCA to the LCCA and the distance from the DA to the LCCA (Figure 2.16 A-C). This ratio indicated how far the DA was positioned from the LSCA, as when this ratio is 1:1 the DA is opposite the LSCA. However, if the value of the ratio fell, the DA was located far apart from the LSCA.

Analysis of the DA position showed various points of attachments with no specific relationship to any sub-group of HLHS hearts (Figure 2.16). Hence, evaluation of the DA location according to the conventional clinical

classification or the ventricular phenotype revealed no relationship between these phenotypes (Figure 2.16 B).

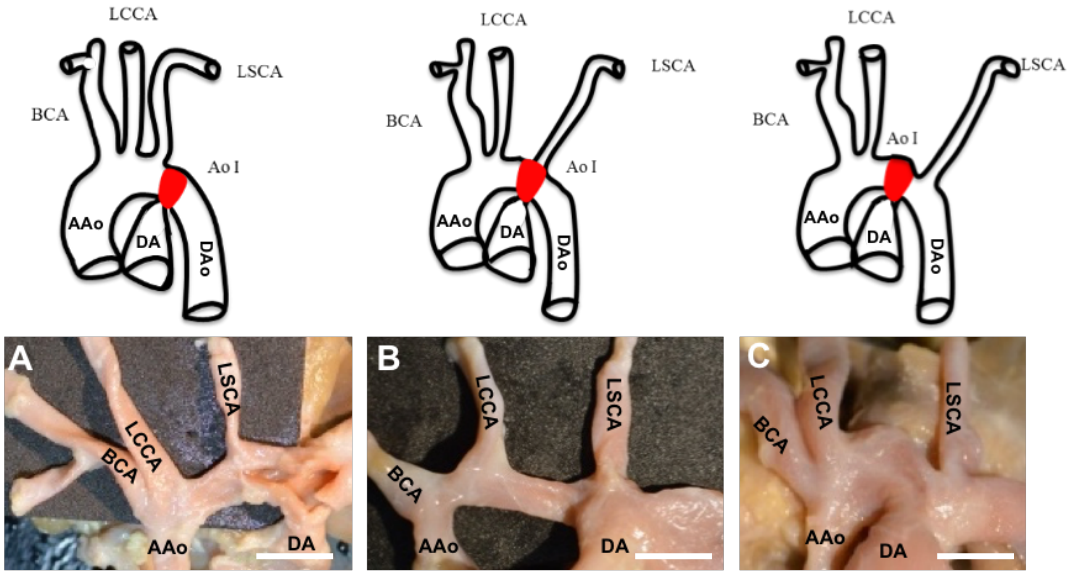

Figure 2.15: The ductus arteriosus position in relating to the left subclavian artery.
(A) The DA located after the LSCA allowing the aortic isthmus to be wide. (B) The DA located opposite the LSCA limiting the isthmus region. (C) The DA located before the LSCA. Abbreviations: BCA: Brachiocephalic trunk, LCCA: left common carotid artery, LSCA: left subclavian artery, DA: ductus arteriosus, AAo: ascending aorta, DAo: descending aorta, Ao I: Aortic isthmus (red area).

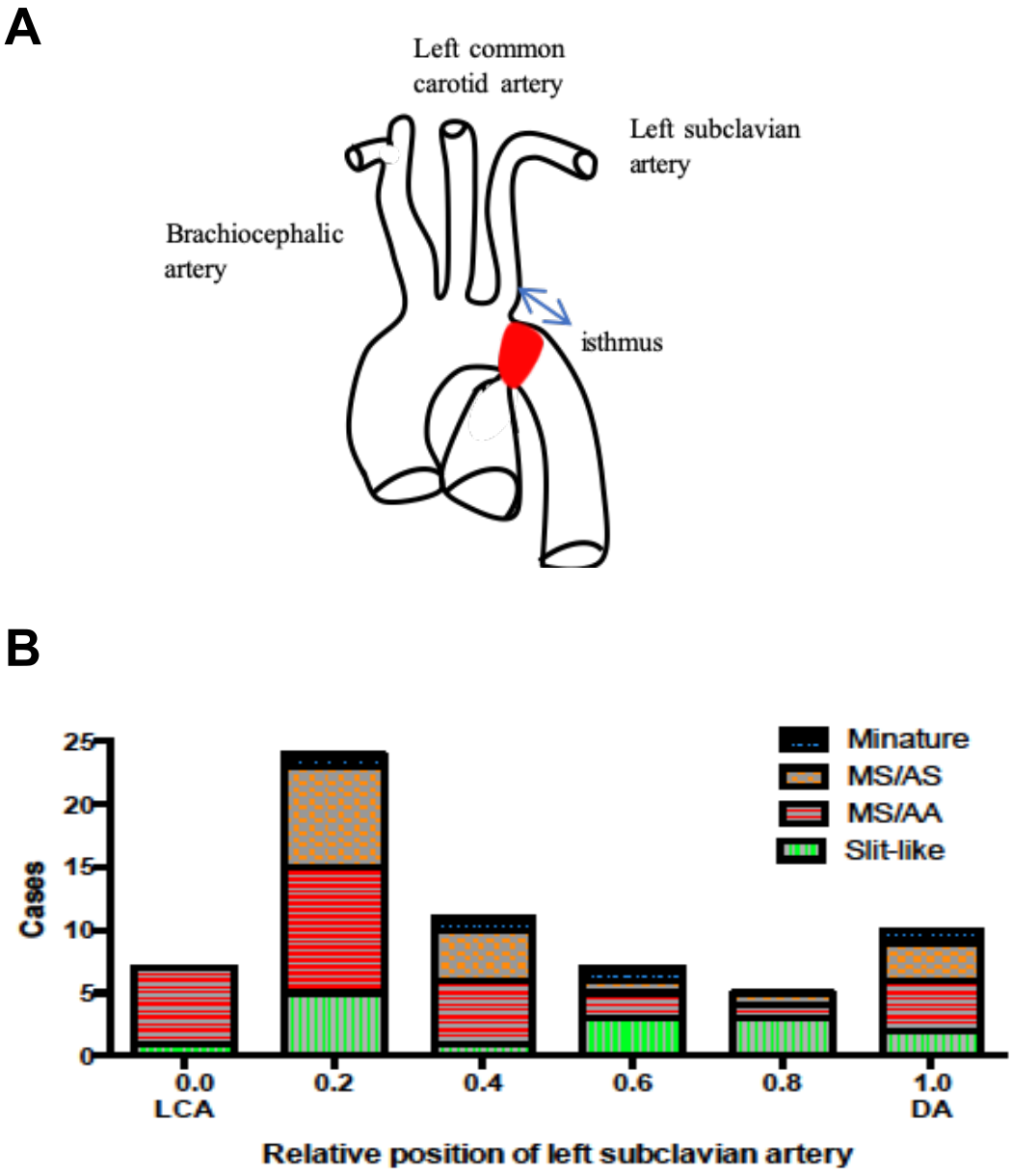

Figure 2.16: Position of ductus arteriosus.
(A) The isthmus located in the region between the ductus arteriosus (DA) junction and the left subclavian artery, measurement of DA distance in relating to the LSCA was performed. (B) The relative position of DA compared to the LSCA showed a wide range of the point of attachment and revealed no direct correlation between the DA location and the clinical classification or the ventricular phenotypes. In this graph, both MS/AS and MS/AA groups represent the thick-walled ventricular group.

2.6 Discussion

Hypoplastic left heart syndrome (HLHS) has been used to describe a heterogeneous spectrum of cardiac defects that includes various degrees of left heart-aorta complex underdevelopment (Chervenkov et al., 2000). Treating HLHS once it has been diagnosed prenatally is remarkably challenging, particularly due to the left ventricle's involvement in the systemic circulation. The placental circulation supplies essential oxygen and nutrition to the developing foetus, meaning that it is much less dependent on the function of the heart and systemic circulation in utero, than it is after birth (Ferreira et al., 2014). Therefore, signs of heart failure are not normally detected in foetuses as an abnormality affecting one side of the heart is compensated by the other normal side. Heart failure is detected after birth when the infants become entirely dependent on the systemic circulation.

HLHS was initially described by Maurice Lev in 1952, based on babies in which hypoplasia of the left heart and hypertrophy of the right cardiac structures were observed (Lev, 1952). However, in 1958, Noonan and Nadas narrowed the classification of HLHS to include a spectrum of left ventricular hypoplasia, ranging from atretic aortic and mitral valves with a vestigial left ventricle, to a mild form of left ventricular underdevelopment (Noonan and Nadas, 1958). Based on their classification, five groups of HLHS were proposed; (1) atresia of aortic valve, (2) atresia of mitral valve, (3) stenosis of mitral valve, (4) atresia of aortic arch, and (5) hypoplasia of the aortic arch. In 1996, the characterisation of HLHS was altered to take into account the varying degree

of valvar abnormalities that associate with hypoplastic development of the left ventricle (Lev, 1996; Ferreira et al., 2014). Of the different proposed classifications, the valvar abnormality-based classification that focused on mitral and aortic valves conditions has become accepted and widely used. This was predominantly due to the clinical use of this classification in the early surgical reports and by surgeons working to find a surgical solution for HLHS (Norwood et al., 1980; Doty et al., 1980). Therefore, despite the lack of specificity and difficulty in precise diagnosis, the valvular based classification has gained widespread acceptance.

Despite several HLHS genomic studies that have investigated the clinical valvular morphology, the aetiology of HLHS remains unknown. Therefore, in order to facilitate genomic and developmental studies on HLHS, this study has suggested a novel classification method based on ventricular morphology. The ventricular morphological classification presents three groups of left ventricular hypoplasia, ranging from the severest form with slit-like ventricle with atretic aortic and mitral valves, to thick-walled ventricle with EFE and mitral stenosis and either atresia or stenosis of the aortic valve, to a mild form with a miniaturised ventricle characterised by stenotic aortic and mitral valves. This classification has also showed some overlap with the clinical classification, specifically the slit-like ventricles with AA/MA, thick-walled ventricles with AA/MS and severe AS/MS, and miniaturised ventricles with AS/MS. The fact that the thick-walled ventricular group has resulted in categorising the AA/MS and severe AS/MS clinical groups together comes in agreement with Bharati and Lev study. It was proposed by Bharati and Lev in 1984, as they analysed

230 surgical hearts with HLHS and noticed almost identical anatomical features between AA/MS hearts and the severe AS/MS hearts (Bharati and Lev, 1984). Although they did not suggest the ventricular-based classification, they recommended considering the AA/MS and severe AS/MS groups as one group. The various presented parameters in this chapter including the left ventricular wall thickness, left ventricular cavity length and detection of EFE supported the alternative ventricular-based grouping. This supports the importance of the ventricular classification in developmental and genetic studies of HLHS, as this classification provides essential parameters, which are useful for detecting and proposing causes of HLHS from a developmental point of view.

Although the clinical classification is based on the functionality of the valves, from a morphological point of view this classification does not accurately describe the valve appearances. Thus, describing the valve appearances with respect to the left ventricular phenotypes provides additional information that might be relevant to diagnosis and aetiology. For example, the slit-like ventricles always showed absent or severe aortic and mitral valve malformations, whereas the miniaturised ventricles showed mild aortic and mitral valve defects. This suggested a strong correlation between the valve malformation and the ventricular size. It also provided an easy and definitive classification for the complexity of HLHS. In addition, the association of valve appearances and ventricular size suggests there could be an initial factor controlling the primary formation of the left ventricle and/or the left atrioventricular junction, or its expansion, rather than the influence of blood

flow. In the cases where the valve tissue appeared to be completely absent, as was seen in the slit-like ventricle and in some cases of the thick-walled ventricles, a failure to form endocardial cushion/valve tissue might be the primary cause. However, in the mild valvular defects including that seen in the miniaturised ventricles and some cases of the thick-walled ventricles, a deficiency in the left ventricular growth could be the primary origin for rising the defects in these groups.

The ascending aorta size was closely correlated with the severity of the abnormalities of the aortic valve, which also mapped perfectly to the ventricular phenotype classification. This correlation suggests that the hypoplasia of the aorta was secondary to a defect in the aortic valve that blocks the blood flow through the aorta and hence prevented its normal growth. This supports the hypothesis of no flow, no grow (Sedmera et al., 2005) in the hypoplastic aorta. However, the isthmus location showed no relationship to either the clinical or the ventricular phenotype classifications.

The proposed ventricular phenotype classification may help in understanding the aetiology and genomic basis underlying HLHS (Figure 2.17). The arguments about whether HLHS results from syndromic or a sequence of events (Grossfeld et al. 2019) could be explained using the ventricular classification. For example, the SLV group that showed no valves and a very small ventricular cavity might be caused by a syndromic event of gene(s) specific for all of the affected regions in HLHS. This then could lead to defects in these regions at the same time. Hence, all of these regions were severely affected, as no features of developing valves and ventricle were observed.

Alternatively, the SLV group could be due to primary defect in the aortic and mitral valves caused by first/second heart field cushions, which led to secondary developmental defects in the left ventricle following the no flow, no grow hypothesis (Sedmera et al., 2005). Similarly, the MinLV group could be caused by a syndromic event of gene(s) that act at the same time and lead to underdevelopment of the affected regions in HLHS. Thus, all these regions were moderately affected allowing similar growth-rate for all of these regions. Alternatively, the MinLV group could be originally due to defects in the myocardium and first heart field endothelium of the left ventricle leading to secondary defect in the mitral valve and the aortic valve. The TWV group, on the other hand, could be primarily caused by second heart field derived endocardium in the aortic valve, which led to secondary defects in the left ventricle and the mitral valve. Alternatively, the TWV group with its various range of valvular morphology and thick wall with small ventricular cavity might be caused by a sequence of events due to ventricular specific gene(s). This then resulted in underdevelopment of the left ventricle and eventually led to the defects observed in the valves. Therefore, based on the ventricular severity, a different range of valvular morphological defects could be observed. Evaluation of the potential genes or HLHS will be discussed in more detail in chapter 5. A unique feature of the TWV group was the presence of EFE in the left ventricle, which was not found in the other SLV and MinLV subgroups. Although there have been several suggestions for the cause of EFE including viral infections, sub-myocardial ischaemia, and excessive endocardial to mesenchymal transformation (Tian and Morrisey, 2012; Baffa et al., 1992; Xu et al., 2015) it is still unclear what the main causes of EFE is and why it is

limited to the TWV subgroup. It is speculated that EFE is a secondary response to a condition of reduced but present blood flow in the left ventricle caused by defects in the valves. Together, this indicates that the ventricular classification provides new hypotheses for each subgroup that are informative of aetiology and feasibly investigable.

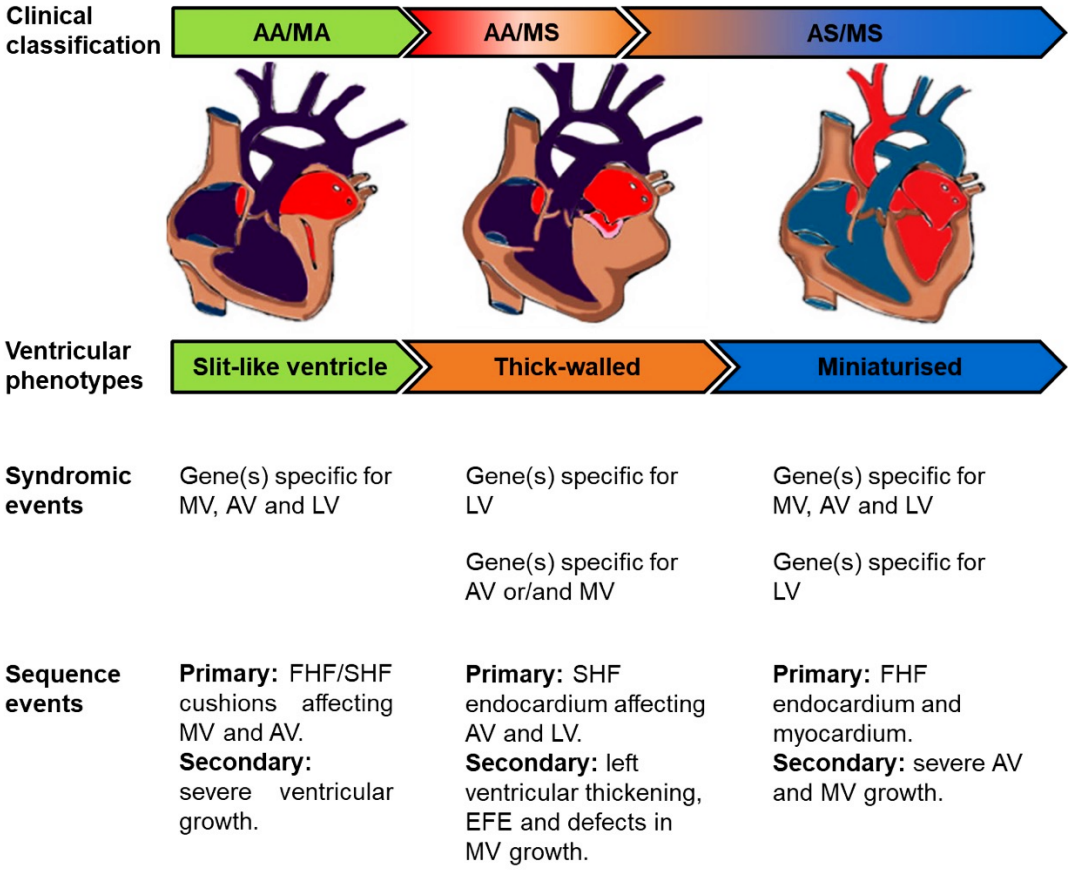

Figure 2.17: Three different ventricular classification in relation to defects and progenitor linages.
Purple represents high level of dexoxygenated blood with low level of oxygenated blood, while blue represents a mixture of oxygenated and deoxygenated blood. AV= Aortic valve, MV= mitral valve, LV= left ventricle, FHF = first heart field, SHF = second heart field.

2.7 Summary

To summarise, HLHS affects multiple regions of the hearts in which these regions are disturbed to a varying degree. In this series of 78 hearts from the Birmingham Children's Hospital, a novel classification method was proposed that was built on the basis of the ventricular phenotypes. Three distinctive ventricular morphologies were identified: slit-like ventricle, thick-walled ventricle and miniaturised ventricle (Figure 2.17). This method was not set to replace the clinical conventional classification, it was proposed to facilitate the genomic studies performed on HLHS cases as it suggested well-defined and specific anatomical subgroups of HLHS for investigating candidate genes for HLHS. The ventricular morphological classification also showed better correlation of the left ventricular wall thickness and length as well as valvular appearances, than the conventional clinical classification. This study not only suggests a novel classification of HLHS, it also shows the importance of archival heart collections in understanding the morphological appearances of HLHS in the different subgroups. The use of archival hearts made a close examination of HLHS possible and beneficial. This encourages the use of the archival hearts in other fields including histology and genetic studies.

Chapter 3: Extraction and Sequencing of Genomic DNA from Formalin Fixed Archival Tissues

3.1 Overview

In the previous chapter, a collection of hypoplastic left heart syndrome (HLHS) archival hearts, which had different abnormalities associated with left-sided valvar and ventricular development leading to different subtypes, was presented. It might be difficult to fully identify the sub-types of HLHS during early heart development, but this could be easily achieved using HLHS archival hearts. Therefore, these archival hearts could, in theory, be used as a well-defined subgroup of HLHS for genetic studies. Archival hearts are normally fixed in a chemical preserving medium, formalin that maintains the biological structure of these hearts. Although the formalin-fixed hearts are excellent resources for morphological and histological analysis, their use in molecular studies is a challenge. This is due to the fact that formalin disrupts the chromosomal DNA in these tissues by cross-linking and cleaving, which eventually leads to corrupt and short sequencing reads from that DNA. However, owing to recent advances in molecular biology, these obstacles are no longer necessarily a limiting factor. Therefore, this chapter will discuss the detrimental effects of formalin fixative on DNA with a short review of the suggested solutions to overcome these effects; both through chemical and sequencing methodological approaches. Then, an optimal method for extracting DNA from formalin-fixed materials will be developed, based on DNA yield, purity, fragment size and amplification using polymerase chain reaction (PCR). Finally, assessment of DNA sequence produced from these tissues using the gold standard Sanger sequencing and the modern next-generation sequencing is presented.

3.2 The complications of formalin fixative in respect to DNA

Fixation is the process of preserving cellular architecture and other bio-active moieties within non-living organisms with minimum alteration of their normal state (Thavarajah *et. al.,* 2012). The use of formalin as a fixative was a fortuitous discovery by Blum in 1893, when he noticed the hardening of the skin on his fingers that had had a direct contact with diluted formaldehyde (Fox *et al*, 1985). Since then formalin has been universally approved as a biological preserving solution that has a convenient and consistent effect on tissues (Puchtler and Meloan, 1985; Fox *et al*, 1985). Although formalin is used to protect tissues from damage and decay, it penetrates into tissues through a physical process that unfortunately leads to several modifications and degradation of nucleic acids within the tissue (Thavarajah *et. al.,* 2012).

3.2.1 Physical process of formalin fixation

Saturated formalin, or 100% formalin (CH_2O), is a saturated solution containing 37%-40% formaldehyde with 10-20% methanol in distilled water. The addition of methanol is essential to provide stabilisation and prevent polymerisation (Pelco, 2016). Polymerisation of formaldehyde, although it is normally a gas, produces paraformaldehyde. Formalin, formaldehyde and paraformaldehyde are fundamentally all the same, with differences in the quantity of methanol present in the former (Pelco, 2016). Owing to the presence of methanol, the fixation process has two phases: an alcohol fixation phase to dehydrate and harden tissues, and a cross-linking phase regulated

by aldehyde (Thavarajah et. al., 2012; Fox et al, 1985). Tissue immersed in formalin is penetrated by formaldehyde and methylene glycol formed by hydrated formaldehyde (Kiernan, 2000). Whilst the covalent reaction is mainly mediated by formaldehyde cross-linking to tissue components, only a minor quantity of formaldehyde is present. Therefore, the majority of methylene glycol is dissociated to form more formaldehyde, allowing more cross-links to form (Mason and O'Leary, 1991; Thavarajah et. al., 2012; Fox et al, 1985).

3.2.2 Cross linking of DNA

The chemical reaction that leads to cross-linking of proteins and DNA by formalin is the fundamental process that maintains ultrastructural detail during formalin fixation (Hassell and Hand, 1974). However, formalin has several specific effects on DNA that lead to difficulties in DNA isolation and carrying out PCR.

Formalin produces extensive aldehyde cross linking between complementary guanine (G), adenine (A), and cytosine (C) within double stranded or inter-strand DNA. It also causes non-covalent linkages between adjacent nucleotides on the same strand with the typical reaction product being a guanine residue (Figure 3.1) (Tang, 2006).

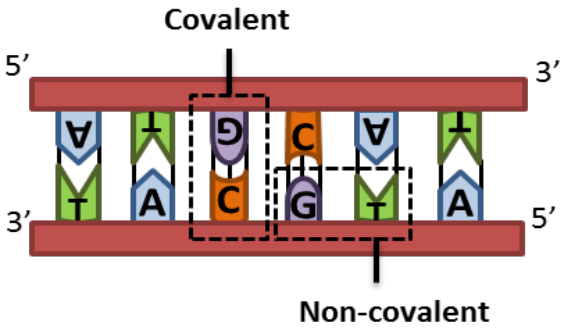

Figure 3.1: Formalin-induced cross-linking between double stranded DNA. Formalin reacts with nucleotides by forming covalent linkages between inter-strand (double stranded) and non-covalent linkages between nucleotides in the same strand (modified from Thavarajah et. al., 2012).

In DNA-protein cross-linking, the covalent linkages formed by formalin between the amino groups, particularly within guanine moieties, contribute to the cross-linking with proteins to form a stable complex. The stability of this complex is due to the other guanine moiety found in the same strand binding to formalin via a strong hydrogen bond (Zeman et al., 1998). The formation of this protein-DNA cross-linking is considered as an initial genotoxic effect after exposure to formaldehyde. There are two pathways that can be responsible for the construction of protein-DNA cross-linking. (A) The first route involves formation of a formaldehyde-induced methylol adduct on the DNA molecule nucleophilic site, which leads to generation of a hydroxymethyl compound. Due to the instability of this compound, it is dehydrolysed to form a Schiff base that interacts with proteins to establish a methylene bridge. (B) The second route involves formation of a formaldehyde-induced methylol adduct on a protein nucleophilic site leading to a direct interaction with DNA bases to form a methylene bridge (**Figure 3.2**) (Lu et. al., 2010).

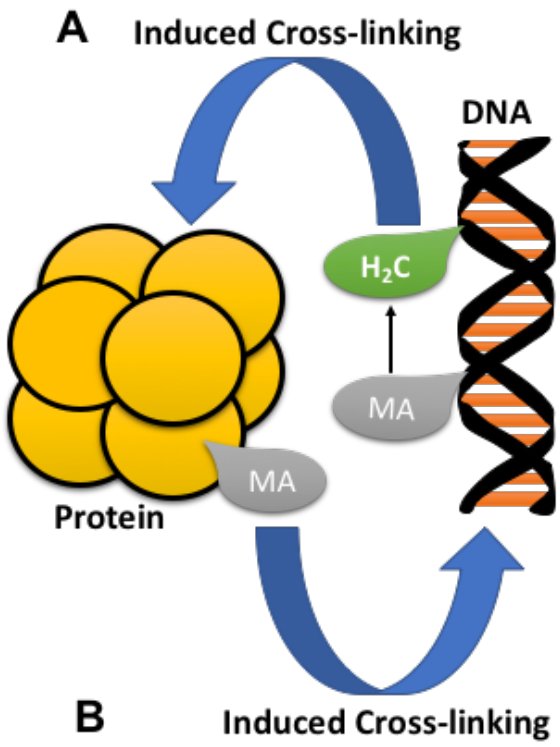

Figure 3.2: The two routes for formaldehyde-induced protein DNA cross-linking.
(A) Formaldehyde-derived methylol adduct interacts with DNA on a nucleophilic site forming an unstable hydroxymethyl compound, which is quickly dehydrated to form a schiff base. A second interaction then occurs to generate a methylene bridge between the schiff base and protein with amide moiety. (B) Formaldehyde-derived methylol adduct initially interacts with a protein in the nucleophilic site forming a hydroxymethyl compound, and then the compound interacts with DNA base to establish a methylene bridge. Abbreviations, MA: methylol adduct, H_2C: schiff base.

The cross-linking of DNA can be easily dissociated with heat, which indicates a reversible effect of formalin on DNA (Thavarajah *et. al.,* 2012). However, within the PCR reaction this has the potential to interfere with the activity of polymerisation and incorporation of DNA debris into the template DNA. Consequently, this leads to the generation of new transcripts with non-specific

hybridization of DNA fragments to the template strand (Dietrich *et.al*. 2013). However, this is a rare event and does not lead to overall misreading (Quach *et. al.,* 2004; Thavarajah *et. al.,* 2012). Whilst these processes are known to occur, they are presumed to occur sporadically and at low level such that the overall sequence within the PCR product is maintained. There is no evidence to suggest that there are sequence-specific effects that would lead to a systematic artefact. Both the covalent complementary strand and the same strand non-covalent linkage are chemically reversible, but whether their effects of the sequence reads are reversible remains unclear (Thavarajah *et. al.,* 2012; Dietrich *et.al*. 2013; Tang, 2006).

3.2.3 Covalent binding of protein

Formalin creates covalent linkage of amino and imino groups to form a Schiff's base or reacts with amides to generate hydroxymethyl compounds that contribute to a second linkage generating methylene bridges between amino acids or amides (**Figure 3.3**) (Schmiedeberg et. al., 2009; Thavarajah *et. al*., 2012). The formation of methylene bridges facilities establishment of amino acids and single nucleoside cross-links. Interestingly, cross-links induced by methylene bridges have been reported between Lys, Cys, His and Trp with G, A and C, but not with T and not Arg, Gln, Tyr or Asn with G, A, and C (Lu et al., 2010). The formaldehyde-induced cross-linking between protein and DNA is found to be specific and normally unstable at room temperature, which indicates the reversibility of protein cross-linking (Schmiedeberg *et. al*., 2009; Toth and Biggin, 2000). In addition, it is most likely that formalin interacts with

proteins primarily either to generate protein-DNA cross-linking or protein-protein cross-linking. Therefore, other molecules including nucleic acids, lipid and carbohydrates are considered to be entrapped within the complexity of protein cross-linking in a reversible manner (Ahmed, 2004).

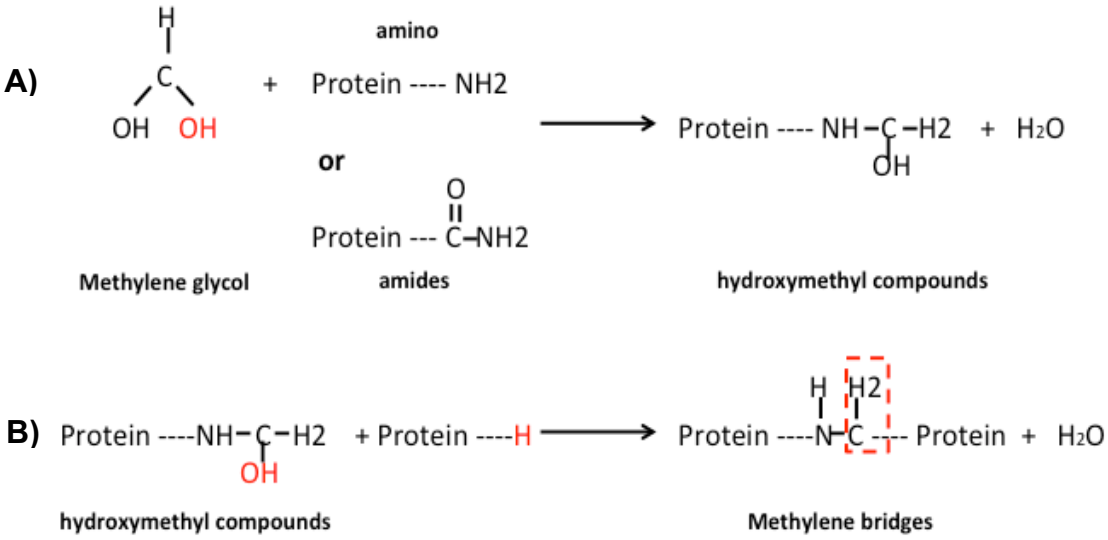

Figure 3.3: Formaldehyde-induced cross-linking between proteins.
(A) Hydrated formaldehyde forms methylene glycol that reacts fast with amino or amide groups of a protein through dehydration. This leads to the formation of hydroxymethyl compound. (B) The hydroxymethyl group on that protein then reacts slowly with other reactive atom on other proteins generating a methylene bridge (-CH2) between two proteins.

3.2.4 Severing of DNA

Whilst most of the formalin-induced genotoxic effects are reversible, there is also major irreversible damage caused by long term incubation in formalin, particularly with unbuffered formalin. The unbuffered formalin, or long-term incubation with buffered formalin, results in oxidation of formalin to formic acid, which has destabilizing properties. Formic acid de-purinates DNA such that the purine is lost from the DNA backbone through the cleavage of the N glycosidic link between the purine base and the deoxyribose in DNA (Kelly, 2006). As a result, small fragments of DNA, less than 200bp, are found. These fragments produce a poor substrate for most polymorphism and mutation-based genomic studies (Bonin et al., 2003; Tang, 2006).

3.2.5 Reliability of sequence Information

Although the reversibility of some formalin-induced DNA damage is encouraging, all the deleterious effects of formalin on DNA raise the question of whether the obtained sequence information is reproducible and reliable. Sequence modifications can occur during DNA replication, where DNA base damage is bridged by DNA polymerase by “crossover” to another strand or “fall off” its target leading to unreliable products (Pelt-Verkuil et. al., 2008; Tang et. al., 2006). Therefore, validation of sequence information is an important aspect that needs to be considered to avoid false positive or negative results.

3.3 Recommended solutions to overcome formalin complications

Formalin causes modification and interactions that are essential for preventing DNA loss during tissue preservation, however at the same time it causes DNA degradation (Srinivasan *et. al*., 2002). In fact, most of the deleterious effects of formalin on DNA are not permanent; hence these effects can be reversed with some preparatory steps. Several studies have shown varying degrees of success in extracting high molecular weight DNA from formalin-fixed samples, with some additional steps needed to breakdown formalin cross-linking and release DNA (Diaz-Cano and Brady, 1997, Wang et. al., 2013). However, these steps may expose the DNA to increased risk of contamination from the harsh detergents used to extract the DNA, and eventually lead to DNA degradation during the extracting processes. Therefore, this section will focus on the effective solutions that can be used to modify a standard DNA extraction method in order to minimise the detrimental complications of formalin while maintaining low levels of contamination, with emphasis on the impact of formalin on methodologies such as PCR.

3.3.1 Removal of excessive formalin

Tissues are normally immersed in a liquid form of formalin to ensure the hydration of tissue and efficient tissue fixation. The efficiency of fixation is mediated by formaldehyde cross-linking to the tissue components including proteins, lipids, and DNA (Kiernan, 2000). Therefore, in order to extract DNA, excessive formalin must first be removed to minimize the possibility of re-

cross-linking by formalin when the breakdown of cross-linking begins. The Sarin group (Pandey et al., 2014) suggested the use of GTE buffer that contained Glycine, Tris, and ethylenediaminetetraacetic acid (EDTA) to wash off excessive formalin, whereas the Parmar group (Shrivastava et al, 2012) and Line group (Santo et al., 2008) favoured the use of TNE buffer containing Tris, sodium chloride (NaCl) and EDTA.

The GTE buffer was recommended to use because it reduced the formation of methylene glycol, which was a source of formaldehyde, through the interactions between glycine (a component of GTE buffer) and formaldehyde. These interactions resulted in forming N-Methyleneglycine or Dimethylglycine rather than methylene glycol, which was the formaldehyde sources (Pandey et al., 2014). Moreover, the other component of the GTE buffer, Tris neutralised the DNA environment helping to reverse the DNA-protein cross-linking (Pandey et al., 2014). EDTA, which was a shared component between GTE and TNE buffers, was mainly introduced to protect and prevent degradation of DNA through neutralising the activity of DNA by binding to metal ions, such as calcium and magnesium, and inactivates DNases (Shrivastava et. al., 2012; Santo et. al., 2008; Pandey et. al., 2014). Sodium chloride, which was used in the TNE buffer, was important for removing and precipitated proteins that were loosely bound to DNA (Shrivastava et. al., 2012; Santo et. al., 2008). Thus, washing with either buffers were highly recommended for at least three days, with several changes every 6 to 12 hours or until the tissue became soft (Santo et. al., 2008; Pandey et al., 2014).

3.3.2 Digestion to remove formalin cross-linking

It is essential to break down the cross-linking between formalin and DNA or formalin and protein, and even between protein and DNA, under non-denaturing conditions and without disrupting the natural structure of DNA. Lysis buffer, which is used to digest tissue and extract cell components, allows the isolation processes of DNA, while preserving the nondenaturing conditions (Peach *et. al.,* 2015). The constituents of lysis buffer can be altered depending on the molecule of interest, and source and type of tissue. However, a standard lysis buffer contains salt solution, detergents, chelating agents and inhibitors.

The majority of lysis buffers have Tris-HCl pH 8.0, HEPES, or sodium chloride as a salt solution to stabilize pH during the digestion process. Tris-HCl is the most widely accepted salt solution due to its ability to maintain stable pH and provide alkalinity to reverse the binding between proteins and DNA (Wang *et. al*., 2013; Coa *et. al*., 2003). In a study carried out on short-term formalin-fixed human liver specimens (Duval et al., 2010), it was suggested that a combination of Tris-HCl and sodium chloride was most effective, as NaCl removed proteins that are already unbound from DNA by Tris-HCl. In addition, NaCl enhances the ionic strength of lysis buffer, which leads to a high solute concentration outside cells, and hence increases diffusion of lysis buffer across the cell membrane (Lieb and Stein, 1968; Green and Sambrook, 2012).

Detergents in lysis buffer are then used to destroy the lipid barrier in cell membranes through protein stabilisation and disruption of interactions between lipid:lipid, protein:protein, and protein:lipid (Green and Sambrook, 2012). Based on the nature of the detergent, they can be classified into three groups: ionic (anionic or cationic), non-ionic and zwitterionic (both a negative and a positive charge). Ionic detergents are favoured for their strong solubilizing ability and denaturing of proteins. Sodium dodecyl sulphate (SDS), is an anionic agent that is widely used for complete disruption of cell membranes and protein denaturing, as it adds a negative charge to all proteins leading to loss of protein functions. Similarly, sodium lauroyl sarcosinate or sarkosyl is an anionic agent that permeabilises cells and denatures proteins (Green and Sambrook, 2012).

However, non-ionic agents are mostly used for protein non-denaturing buffer. Nonidet P40 and Triton-X100 are examples of non-ionic agents. Most of the non-ionic agents interfere with UV spectrophotometry, particularly Triton-X100, as it absorbs UV light via its a phenyl ring (Lieb and Stein, 1968; Green and Sambrook, 2012). Tween 20 is also a non-ionic and polysorbate agent with lauric acid that it ideal for protein extraction as it does not affect the activity of proteins while maintaining its ability to permeabilise the cell membrane (Green and Sambrook, 2012).

Although extracting DNA from formalin fixed tissues requires the addition of several chemical detergents, it is still important to consider their interactions and inhibitions of PCR amplification processes (Alaeddini, 2012). One recommended approach to eliminate PCR inhibitors was to use Chelex-100,

which provided alkaline conditions and helped in removing heavy metals (Idris and Goodwin, 2015). Chelex-100 is a chelating agent that has the ability to purify compounds through ion exchange. The use of Chelex-100 was mostly for isolating DNA from forensic-type samples, as it yielded high DNA quantity from small starting materials (Alaeddini, 2012). In addition, Chelex-100 was reported to protect DNA from high temperature treatments and chelated a large volume of divalent ions that could be found in the lysis buffer. Because it is easy to remove the Chelex-100 beads, it is normally recommended for use with PCR as it does not interfere with PCR amplification processes (Walsh et al., 1991).

3.3.3 Reliable sequence information: Multiple clones or systematic comparison

It is very important to ensure the obtained DNA sequence is indeed representative of the original specimen. Therefore, several suggestions have been proposed in order to reduce risk of faulty DNA products (Pelt-Verkuil et. al., 2008; Tang et. al., 2006).

One approach to minimise the risk of having unreliable DNA sequence information is through cloning a DNA product extracted from a formalin fixed tissue, followed by performing a comparison between the different clones that are produced from the DNA product. This allows identification of the consensus sequence between the clones and thus reflects the original sequence (Pelt-Verkuil et. al., 2008). However, in the case of non-random and specific region alterations in DNA sequence, such as might arise following

fixation in formalin, another approach must be considered such as a comparison between a fixed sample and a fresh sample from the same individual (Tang et. al., 2006). However, fresh and fixed samples from the same individual are not always available, especially for archival studies, therefore a different methodology is required.

More recently, the advances in sequencing technology have allowed genomic studies to be performed on formalin-fixed tissues. Next-generation sequencing (NGS) provides a solution for the problem of short DNA fragments, as it requires the DNA size to be between 100-200bp. Whilst NGS has opened the possibility for sequencing DNA extracted from formalin-fixed tissues (FFT), it is still unknown whether FFT will produce reliable sequencing reads using this NGS. Although it was recently reported that reliable NGS data was obtained from formalin-fixed paraffin-embedded (FFPE) tissues, short fixation ideally for one day with 10% buffered formalin was crucial to obtain reliable NGS data using the author's protocol (Einaga et al., 2017). However, this was not the case when this protocol was used on FFPE samples that had been fixed in formalin for longer than one day. Therefore, whilst it has been shown that FFPE samples could produce reliable NGS data; but only if they were fixed for one day, it remains very important to validate DNA sequences generated by NGS from FF tissues particularly the ones that had been fixed in formalin for long periods.

3.4 Aims of this chapter

The extraction of DNA from archival FFT provides rich sources of biomolecular information enabling gene expression analysis. The use of these tissues for gene expression analysis is fundamental for understanding challenging malformations such as HLHS. However, using archival FFT collections for genomic studies remains a challenge. Breakthroughs in technology have made the use of extracted genomic DNA (gDNA) from formalin-fixed materials possible. However, the methodological constraints and practical complications demand the optimisation of protocols to enhance the yield, purity and read length of extracted DNA. Therefore, the main aim of the current chapter was to establish the most appropriate method to extract high quality DNA that will yield reliable and reproducible sequence information from FFT. The goal for the use of the optimised method is to identify genes causing HLHS using archival FFT collections of HLHS, such as those held at Birmingham Children's Hospital investigated in Chapter 2. In order to achieve this, the following aims were established:

- To establish a standard method that enables successful extraction of DNA from FFT, based on information from the published literature.
- To assess the quality of extracted DNA by quantification of DNA yield and purity using NanoDrop/spectrophotometry; DNA fragment size distribution by gel electrophoresis; and successful amplification by PCR.

- To optimise conditions of the chosen method by systematically introducing changes to the main stages involved in the extraction procedure, such as the washing step and heat treatments.
- To validate the efficiency of the optimised method by comparing the quality and quantity of extract DNA from this method to a commercial kit.
- To assess the quality and reproducibility of sequence information generated by the isolated DNA from the optimised method and to compare its efficiency to a commercial kit.
- To assess the possibility of extracting DNA from tissues with prolonged fixation period in formalin (up to 2 years).
- To validate whether NGS particularly exome sequencing can produce reliable DNA data from formalin fixed tissues by comparing DNA isolated from a formalin-fixed tissue to that obtained from a fresh blood sample of the same individual.

3.5 Methods and materials

3.5.1 Tissue samples and HTA ethics

Archival formalin-fixed human lung artery specimen (approximately 4 g) from a healthy donor was obtained from the Royal Victoria Infirmary (RVI). Immediately upon removal of donor tissue, the sample was preserved in 10% neural buffered formalin at room temperature for almost 9 months. As for the comparison of NGS, DNA extracted from 10% buffered formalin-fixed explanted heart (right ventricular myocardium) preserved for two years and DNA extracted from blood sample were obtained from the same individual. Both samples were collected from the Department of Cellular Pathology, Royal Victoria Infirmary, Newcastle upon Tyne and analyses were approved by the Newcastle and North Tyneside 1, NRES Committee; REC Reference: 15/NE/0311.

Using a disposable sterile scalpel, 10mg (approximately 15mm^2) tissue was placed on a plastic petri dish, chopped into small, equal pieces (approximately 1mm^2) and placed into a 60ml sterilin container using autoclaved forceps (Scientific laboratory supplement, CON7536, UK). To minimise risk of contamination, all used equipment were sterilised or autoclaved prior to use. The same amount of formalin-fixed tissue was used for all protocols performed in this study.

Our DNA extraction method was developed following five main stages: wash, digest, heat treatment, elution, and clean-up and storage. The wash, digest and heat treatment stages were modified from Pandey et al., 2014; Cao et al.,

2003; Idris and Goodwin, 2015; and Shi et al., 2002, followed by a traditional phenol: chloroform extraction (Green and Sambrook, 2012). The isolated DNA yield and purity were measured using a NanoDrop spectrophotometer; fragments and size range were determined by gel electrophoresis; suitability for amplification was determined based on polymerase chain reaction (PCR); and finally, reliability and reproducibility of sequence were established by a PCR-based cloning method.

3.5.2 Standard protocol (ST-100)

A modified protocol to extract DNA from formalin-fixed tissues was used as a control protocol (Pandey *et al.,* 2014). This is described hereafter as the ST-100 protocol.

Wash: tissue was washed with GTE buffer (100mM glycine, 10mM Tris-HCL pH 8.0 and 1mM EDTA, Table 3.1) for three days at 37°C in a water bath shaker (800rpm) to remove excessive formalin. Several short washes were carried out immediately after removal of tissue from formalin, followed by a fixed washing scheme performed every 12h using a disposable sterilised plastic pipette. Washing buffer was then removed and samples rinsed with 0.5mL of the lysis buffer to equilibrate samples for the next step.

Digest: samples were incubated in 3mL lysis buffer (1M Tris-HCl pH 8.0, 10% Sodium dodecyl sulphate (SDS), 0.5M EDTA) with 2mg/mL proteinase K (Sigma-Aldrich, P6556) at 55°C on a water bath shaker (Table 3.1) (Pandey *et al.,* 2014: Duval *et al.,* 2010). Following the Pandey protocol, fresh

proteinase K (to a final concentration of 2mg/mL) was added every 12h for two days. If tissue was not completely digested within this time, further addition of proteinase K (to a final concentration of 1mg/mL) was carried out every 12h until the tissue was fully digested (Farugia *et al*., 2010).

Heat Treatment: digested samples were divided into three 1mL aliquots and transferred to 1.5mL microcentrifuge tubes. Following the protocol of Cao *et al*. 2003, the samples were heated at 100˚C using a heat block for 10 minutes to inactivate proteinase K. After cooling to room temperature, incubation with 20µl of RNase A (final concentration of 40µg/mL, Sigma-Aldrich, R6513) for 5 minutes at room temperature was performed (Green and Sambrook, 2012).

Elution: samples were collected into sterilised 15mL tubes and an equal volume of phenol: chloroform: isoamyl alcohol solution (Sigma, P3803) was added and mixed gently on roller apparatus for 10 minutes. The samples were centrifuged for 15 minutes at 5000rpm (room temperature) and 0.75mL of the resulting upper aqueous layer was transferred into fresh, sterilized 1.5mL Eppendorf tubes (Green and Sambrook, 2012; Senguven *et al.,* 2014). To ensure maximum recovery of DNA, 1mL 1x TE buffer pH 7.8 (Table 3.1) was added to the remaining phenol: chloroform: isoamyl alcohol solution and mixed gently for 10 minutes using the roller apparatus. Samples were then centrifuged for 15 minutes at 5000rpm and the upper aqueous layer transferred to fresh 1.5mL Eppendorf tubes. The final step was repeated to reduce risk of carryover contamination and to maximize DNA recovery (Green and Sambrook, 2012).

Clean-up and storage: one volume (0.75mL) isopropanol and 30µL sodium chloride (final concentration at 0.2M) were added to each tube to reduce the dielectric persistent of the solution, leading to DNA precipitation. The samples were inverted several times before chilling at −20°C overnight for DNA precipitation to occur. Subsequently, samples were incubated at minus 80ºC for 2h (Green and Sambrook, 2012). Then, samples were centrifuged at 13,000rpm for 30 minutes at 4°C. The supernatant was discarded and 500µL ice-cold 70% ethanol was added to the DNA pellet. The pellet was tapped gently before further centrifugation at 13,000rpm for 15 minutes. Supernatant was removed and the wash twice repeated. The pellet was air-dried and re-suspended in 50µL 1× TE buffer, and stored at 4°C (Pandey *et al.*, 2014).

Table 3.1: List of reagents used and solution preparation.

Reagent	Preparation
1x GTE buffer	• 100 mM glycine • 10 mM Tris-HCL pH 8.0 • 1 mM EDTA
Lysis buffer	• 0.5M EDTA, pH8.0 • 1M Tris-HCl, pH8.5 • 10% Sodium dodecyl sulphate (SDS) • 2mg/ml proteinase K
1x TE buffer	• 10 mM Tris-Cl (pH 7.5) • 1 mM EDTA (pH 8) • pH to either 7.8 or 8.

3.5.3 Simple heating protocol (ST-120)

For the purpose of comparison, the ST-100 protocol was modified at the heat treatment stage. According to Shi et al. 2002, heating samples at 120˚C increased efficiency of DNA extraction. Therefore, samples were heated at 120°C using an autoclave machine for 10 minutes.

3.5.4 Chelex-100 at 100˚C protocol (CH-100)

The ST-100 was modified according to Idris and Goodwin (2015). The ST-100 protocol was followed with the exception of the heat treatment where, in addition, Chelex-100 was used. Briefly, the samples were treated with 200µl of 10% Chelex-100 (Bio-Rad laboratories) before subjecting to heat treatment at 100˚C for 10 minutes.

3.5.5 Chelex-100 at 120˚C protocol (CH-120)

The CH-120 protocol was designed to combine the techniques of Idris and Goodwin (2015) and Shi et al. (2002), along with the standard ST-100 protcol. Therefore, 200µl of 10% Chelex-100 (Bio-Rad laboratories) was added to the samples followed by heat treatment at 120˚C using an autoclave for 10 minutes (Figure 3.4).

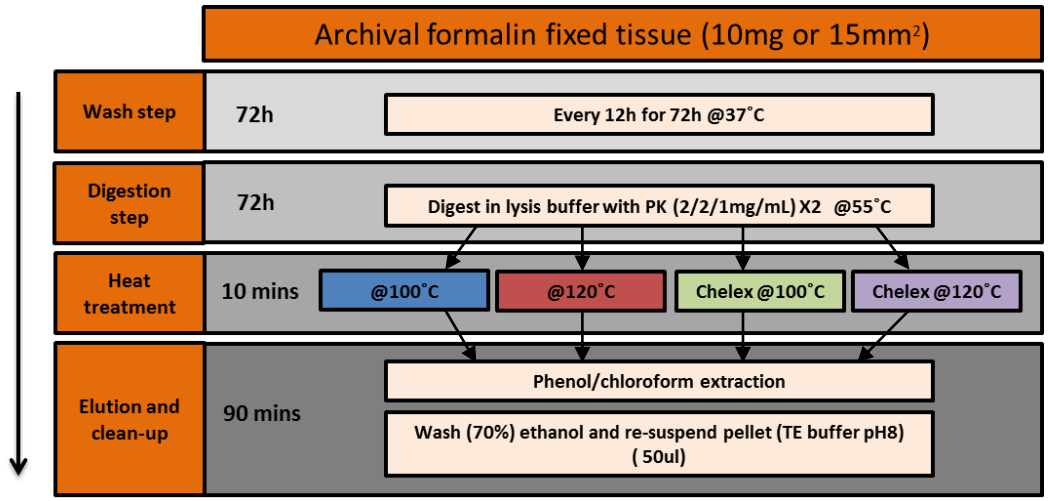

Figure 3.4: Schematic diagram of DNA extraction procedures from formalin fixed tissues.
The standard protocol involves a wash step for 72h with 1xGTE buffer at 37˚C, followed by a digestion step with lysis buffer with fresh additions of proteinase K every 12h for 72h at 55˚C. The heat treatment involves different conditions indicated by the colour scheme. The final step involves phenol/chloroform extraction and precipitation by ethanol.

3.5.6 Introduced modifications to optimise protocol

In order to improve and shorten the protocol, several alterations were introduced. The alterations were made to shorten duration period of the wash step, to reduce the concentration of proteinase K and to enhance the accuracy of sequence. Reducing proteinase K concentration was important because it would help in reducing the risk of DNA contamination and degradation, and in cutting the cost of proteinase K. The wash step was reduced to 24 hours at two different temperatures: 37˚C and 55˚C; proteinase K concentration was reduced to 1mg/mL instead of 2mg/mL; and 2U of Uracil-N-glycosylase (UNG) enzyme with 1x UNG buffer (New England BioLabs, Ipswich, MA) was added to samples and heated at 50˚C for 1 hour (Lui *et al.,*2013) (Figure 3.5).

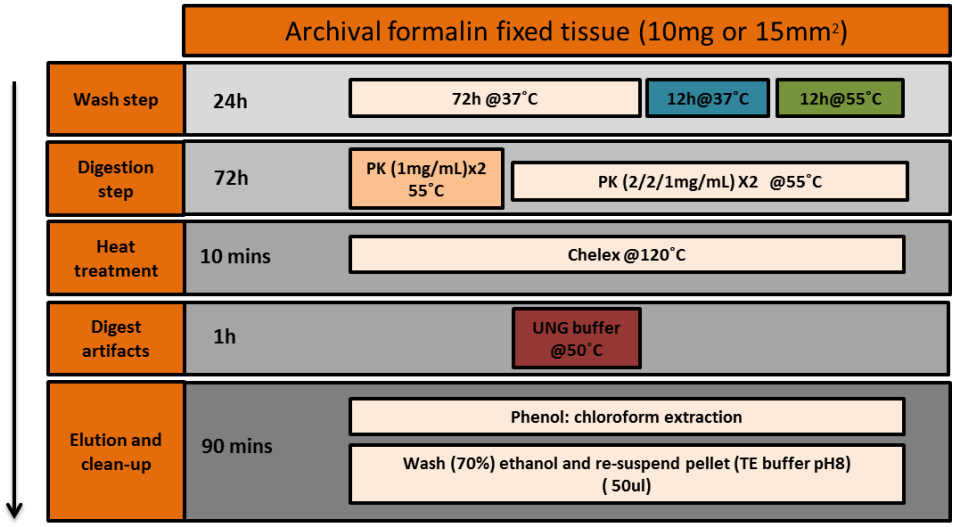

Figure 3.5: Schematic diagram of changes to the DNA extraction procedures.
The initial step to improve and shorten duration of procedure was to reduce the period of wash incubation to 24 hours with changes to incubation temperature. Samples were incubated at 37˚C (blue box) or at 55˚C (green box) for 24 hours. The procedure was then performed as indicated in the white boxes. A second alteration was the reduction in proteinase K concentration from 2mg/mL twice a day to 1mg/mL twice a day. Again, the procedure was then carried out as indicated in white boxes. The final alteration was aimed to improve the reliability of sequence; therefore, an additional step was introduced after heat treatment and involving the addition of Uracil-N-glycosylase (UNG) at 50˚C for 1 hour.

3.5.7 The DNA FFPE Kit

The QIAgen GeneRead™ FFPE kit (Cat no.180134, Valencia, CA, USA) was used to isolate DNA from formalin fixed tissues and was compared to the final optimised method. The procedure was performed according to the manufacturer's protocol (Figure 3.6). Briefly, 10mg of tissue was cut into small pieces and equally placed in two sterile 1.5mL microcentrifuge tubes. Then, a master mix of 25µl Buffer FTB, 55µL RNase-free water and 20µl proteinase K was added to each tube and incubated in a thermomixer for 1 hour at 56°C. Following a second incubation at 90°C for 1 hour, 115µL RNase-free water was added to each tube with 35µL Uracil-N-glycosylase (UNG), vortexed, and

heated for 1 hour at 50°C. After subsequent incubation with 2µL RNase A (100 mg/ml) for 2 minutes at room temperature, 250µL Buffer AL was added, followed by 250µL absolute ethanol. Samples were vortexed and transferred to the QIAamp MinElute columns. The columns were centrifuged for 1 minute at 20,000 x g and the flow-through, discarded. 500µL Buffer AW1 was added to each column, centrifuged and the flow-through discarded. This was repeated with 500µL Buffer AW2 then 250µL absolute ethanol. To remove any residual liquid, columns were centrifuged for 1 minute and then placed into fresh 1.5mL collection tubes. Finally, 25µL Buffer ATE was added to the centre of each column membrane and incubated at room temperature for 5 minutes before centrifuging for 1 minute at 20,000xg. The resulting eluted DNA was stored at 4˚C.

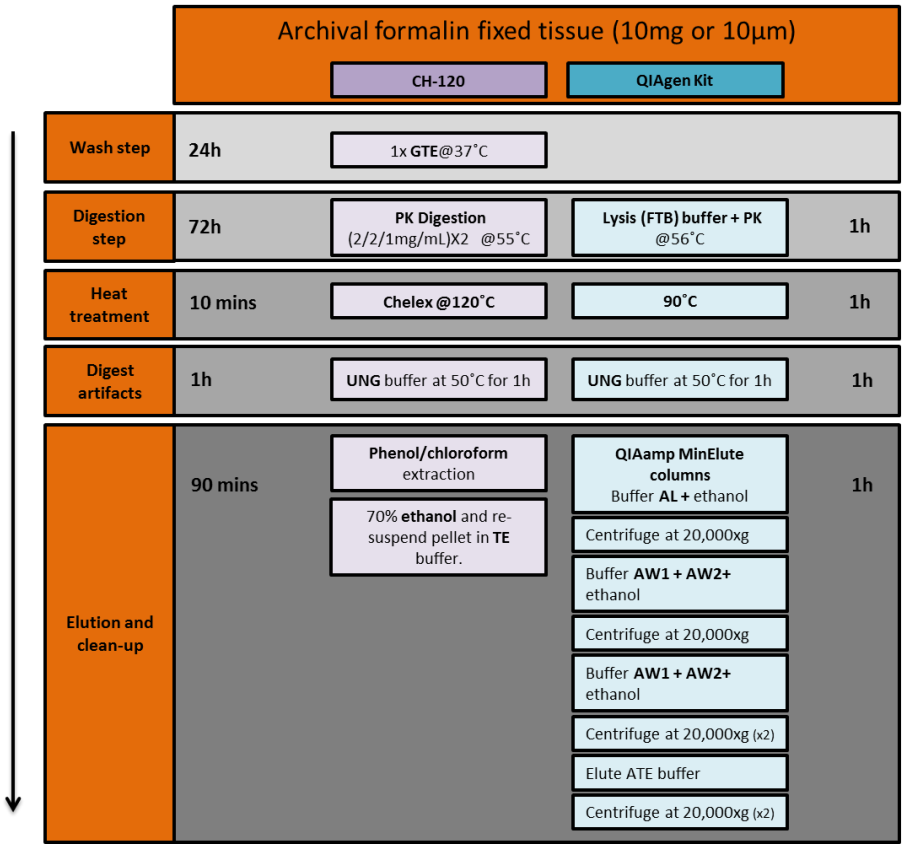

Figure 3.6: Schematic diagram showing the final optimal method and QIAgen commercial kit procedure to extract DNA from formalin fixed tissues.
The optimal method started with a wash step using 1x GTE buffer for one day, followed by digestion with lysis buffer and fresh addition of proteinase K for three days at 55˚C. Then, samples were combined with Chelex-100 and subjected to heat treatment at 120˚C for 10 minutes before being treated with UNG buffer for 1 hour at 50˚C. Finally, classical phenol/chloroform extraction was performed. The QIAgen commercial kit did not involve a wash step and samples were digested immediately after being removed from formalin. Samples were lysed using FTB buffer and proteinase K at 56˚C for 1 hour. After incubation for 1 hour at 90˚C, samples were treated with UNG buffer and incubated for 1 hour at 50˚C. Finally, a column-based protocol with intensive washes was performed to isolate the DNA.

3.5.8 Quantification of DNA

The concentration and the purity of extracted DNA from all protocols were measured using a NanoDropTM spectrophotometry. The yield was automatically measured at a wavelength of 260nm and the ratio of the reading at 260/280nm provided an estimate of DNA purity. The quantity of extracted DNA was visualised on a 0.8% agarose gel electrophoresis (SeaKem LE agarose) and gDNA fragment size was analysed using a densitometry method in ImageJ using the analyse>gels option (1.52p java 1.8.0_172, USA).

3.5.9 Polymerase chain reaction (PCR)

To determine the fragment length of extracted DNA, PCR analysis was conducted. Four sets of primers specific to the human *HAND1* gene were designed to generate amplicons of 200bp, 400bp, 600bp and 800bp when used in PCR. The reason for using *HAND1* specific primer was that *HAND1* is one of the most important associated genes in HLHS. These primers are listed in Table 3.1. All amplifications were performed using a Peliter Thermal cycler (PTC-200). Cycle conditions and primer suitability were optimised using genomic DNA extracted from fresh blood samples.

Each 25µL PCR reaction contained 2µL extracted DNA (25ng/µL), 1.25µL of 10µM each of primers, 0.5µL of 10µM each dNTPs, 2µL of 10mg/mL bovine serum albumin (final conc. 1µg/µL BSA), 5µL of 5X Q5 Reaction Buffer and 5X Q5 High GC Enhancer, and 1U DNA Taq polymerase (Q5® High-Fidelity DNA Polymerase, NEB, Ipswich, MA). The thermal cycling conditions were as

follows: denaturation at 94°C for 5 minutes, followed by 40 cycles of denaturation at 94°C for 1 minute, annealing at 60°C for 30 seconds and extension at 72°C for 1 minute, and final extension at 72°C for 10 minutes. The PCR products were separated and visualised on 1% agarose gels stained with ethidium bromide.

Table 3.2: HAND1 PCR primer sequences.

Primer	Size (bp)	Forward	Reverse
HAND1	200	GCCCTATCTCCATTTCCCTA	CAGGAAGTGCAGCGACAAAA
HAND1	400	CAACCACACACTTGGATCGC	CAGGAAGTGCAGCGACAAAA
HAND1	600	GCCCAGTCGAGAAGAGGATT	CAGGAAGTGCAGCGACAAAA
HAND1	800	ACCGGTAAGAAGACAGTGGG	ACACAGCCTCCTTCGACTAC

3.5.10 AT-cloning of HAND1 fragments from extracted DNA

A PCR-based cloning method was used to generate colonies containing the maximum length of PCR-amplified DNA. After separation of PCR products on an agarose gel, the 200bp HAND1 gene fragment from the ST-100 protocol and 400bp HAND1 gene fragment from the Chelex-100 based protocol were extracted from gels using ISOLATE II PCR and GEL Kit (BioLine, BTP0812V1, USA). Then, a polyadenylation step was performed to create a suitable substrate for TA cloning by incubating samples at 72°C for 20 minutes with 0.2mM dATP, 1X *Taq* buffer (1.5mM $MgCl_2$), and 1U DNA *Taq* polymerase (Promega, Madison, WI, USA). 5µL of polyadenylated products were then ligated into 1 µL of 50ng pGEMT-easy vector (Thermo Fisher Scientific, Inc.,

MA, USA) using 2X Rapid Ligation Buffer and T4 DNA Ligase (3 Weiss units/µl). After incubation for 90 minutes at room temperature, the mixture was transformed into JM109 competent cells (cat. M208CC85, AllianceBio) by heat shock at 42˚C for 45 seconds. Then, SOC medium was added and the newly transformed cells incubated for 1 h at 37°C with shaking at 225rpm before spreading on a LB agar plate containing 100µg/ml ampicillin, 100µL 100mM IPTG and 50µL 20mg/ml X-Gal. Following overnight incubation at 37°C, resulting white colonies were assessed by colony-PCR using identical conditions to those used for amplification of HAND1 from genomic DNA. Upon confirmation of correct HAND1 insert size, 20 selected colonies were cultured in LB broth overnight at 37°C with shaking in 225rpm.

3.5.11 Isolation of DNA from gel agarose

Isolation of DNA from gel was performed using ISOLATE II PCR and Gel Kit (Bioline, BIO-52058) following the manufacturer´s instructions. Briefly, the DNA fragment of interest was isolated using a disposable scalpel and incubated in an eppendrof tube. Based on the weight of the DNA fragment, 200uL of binding buffer was added to every 100mg of 2% agarose gel. Then, the tube was incubated at 50°C for 10 minutes with vortexing the sample every 3 minutes. After dissolving the gel into the binding buffer, the sample was loaded to a 2mL column and collection tube. Then, centrifuged for 1 minute at 11,000xg and the flow-through was discarded. Next, 700uL of the wash buffer was added to the column, centrifuged for 1 minute at 11,000xg, and the flow-through was discarded. The sample column was then centrifuged for 1 minute

at 11,000xg to remove excessive residual ethanol. Finally, the column was placed on a new tube and 30uL of elution buffer was added and incubated at room temperature for 5 minutes, before it was centrifuged for 1 minute at 11,000xg. The final product was incubated at -20°C until needed.

3.5.12 Plasmid Miniprepe purification

Plasmid preparation was accomplished using QIAprep Spin Miniprep Kit (Cat No. 27104, QIAgen group, UK) according to the manufacturer´s instructions. The overnight growth bacterial cultures were centrifuged for 10min at 1000rpm, room temperature. The pelleted bacterial cultures were then suspended in 250ul buffer P1 and transferred to Eppendorf tubes. Next, 250ul of buffer P2 was added and mixed through inverting the tube 7 times. After that, 350ul of buffer N3 was added, mixed thoroughly, and centrifuged for 10min at 13,000rpm. The supernatant then was transferred into QIAprep spin columns by pipetting and centrifuged for 30sec. The flow through was discarded and the columns were washed with 500ul buffer PB. Then, the columns were centrifuged for 30secs at 13,000rpm, washed with 750ul buffer PE and centrifuged again. To remove the wash buffer from the columns, centrifuged for 1min at 13,000rpm. Using fresh 1.5ml Eppendorf tube, the columns were placed on tubes and DNA was eluted from columns by adding 30ul buffer EB containing 10mM tris-HCl pH8.5 and left to stand for 5mins before centrifuged for 1min at 13,000rpm. The DNA samples were then stored at -20°C until needed.

3.5.13 Sanger sequencing

Plasmid insert DNA was subjected to Sanger sequencing using both forward SP6 (Cat.no. Q5011, Promega, USA) and reverse T7 (Cat.no.Q5021, Promega, USA) direction primers to confirm reliability and reproducibility of inserted nucleotide sequence. Sanger sequencing was performed by GATC biotech (Germany, https://www.gatc-biotech.com). The electropherogram was initially analyzed for good nucleotide peaks, followed by entire sequence analysis using ApE A Plasmid Editor (v2.07.47, California, USA) and Jalview (Waterhouse et al., 2009, http://www.jalview.org) to check accurate sequence of HAND1 desired size. To ensure that no cross-contamination with other vectors had occurred, the flanking region of the insert was tested for vector-specific sequences (Figure 3.6.1).

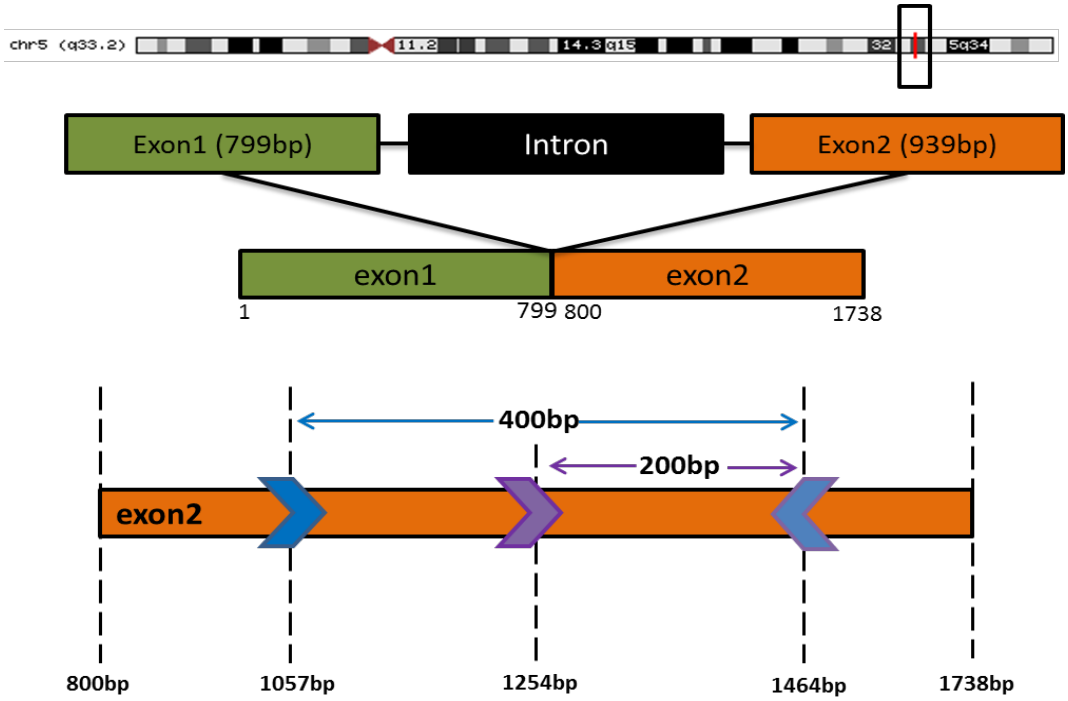

Figure 3.6.1: Diagram showing regional localization of exon 2 in HAND1 gene with markers indicating the length of cloned regions.
HAND1 is mapped to chromosome 5 (5q33.2) and consists of two exons: exon 1 is 799bp in length and exon 2 is 939bp in length. The panel shows the relative position of *HAND1* gene exons on cDNA (ensemble.org). Small regions on exon 2 are used in this study to allow determination of correct sequence read produced by the different methods of DNA extraction. The region from 1057bp to 1464bp is used to generate a 400bp PCR amplicon and the region from 1254bp to 1464bp is used to produce a 200bp PCR amplicon. The primers used to generate these fragments are indicated in Table 3.2.

3.5.14 Extraction of DNA from blood samples

Extraction of DNA from blood samples was carried out using BACC2 kit (RPN8502, GE healthcare) following the manufacturer´s instructions. The blood samples were collected in sodium EDTA tubes and 4 times the volume of the blood sample, reagent A was added. Then, the samples were rotated at room temperature for 4 minutes before it was centrifuged at 1,300xg for 5 minutes. The supernatant was discarded, and the pellet was dissolved in 2mL of reagent B by vertexing. The suspension was then transferred to 15mL

propropylene centrifuge tube and 500ul of sodium perchlorate solution was added, the tube was inverted up and down at least 7 times and then 2mL of chloroform was added. The tube was inverted, then 300uL of nucleon resin was added, and centrifuged at 1,300xg for 3 minutes. Without disturbing the nucleon resin layer, the upper phase was transferred to a 15mL clean tube. Then, 2 volumes of 100% ethanol were added. The tub was then mixed until the precipitate appeared and centrifuged at 4,698xg for 5 minutes. Discarding the supernatant, the pellet was dissolved in 70% ethanol, inverted the tube several times and then centrifuged at 4,698xg for 5 minutes. After removing the supernatant, the DNA pellet was air dried for 2 minutes and re-dissolved in 500uL of TE buffer. The final product was incubated at -20°C until needed.

3.5.15 Exome sequencing

Exome sequencing and data analysis was performed by Newcastle genomic core facility service using the Nextseq 500 platform. The NextSeq 500 platform was run on the high output flow cell modes, which enabled 10 sequencing samples in 18 hours with 40 million pair end reads of length 75bp.

Based on the type of DNA samples, different protocols were carried out. For DNA extracted from fresh blood samples, the DNA sample was processed through TruSeq Rapid Exome Kit. Whereas for formalin fixed samples, TruSeq Exome kit was used to process these samples. Before subjecting samples to exome sequencing, samples were measured using a Qubit fluorometric-based method to quantify the concentration of gDNA. The TrueSeq Rapid exome seq

kit required 50ng of total gDNA, whereas the TrueSeq exome seq kit demanded 100ng of gDNA.

The Trueseq Rapid exome seq kit was performed following the manufacture manual. This involved fragmentation of gDNA and adapter addition via Nextera transposome. Followed by purification of tagmented DNA from transposome using sample purification Beads (SPB). Then, the tagmented DNA was amplified through adding Index adapters (i7 and i5) and amplified using 10 cycles PCR programme. The product was then purified using SPB to prevent interference of unwanted products with further processes. The DNA libraries with unique indexes were then hybridised to probes followed by addition of Streptavidin Magnetic Beads (SMB) to capture specific regions of DNA hybridised to probes. The non-hybridised DNA strands were washed off and the rest were eluted. The same processes of probe hybridisation and capturing were repeated to ensure high specificity of the constructed DNA library. The DNA library was then purified with SPB before amplifying using 10 cycles of PCR amplification programme. After that, the enriched DNA library was clean-up to remove unwanted products. Finally, the quantity of enrich library was measured using Qubit dsDNA BR Assay kit and quality was validated through Agilent Technologies 2100 Bioanalyzer using a High Sensitivity DNA chip.

The TrueSeq exome seq kit was processed according to the manufacture manual. After validation of gDNA quantity and quality using Qubit, the gDNA was fragmented into 150bp fragments. This shearing generated double stranded DNA with 5’ or 3’ overhangs. The DNA fragments were then cleaned

up to be prepared for the next step. Fragmentation of DNA resulted in fragments with overhangs, therefore, End Repair Mix (ERP3) was used to produce blunt end DNA. This is achieved through removing 3' overhangs by 3' to 5' exonuclease activity and filling in 5' overhangs by the 5' to 3' polymerase activity. Then, the library size was nominated using SPB. In order to prevent 3' overhangs from binding to each other or forming chimera, a single adenine (A) nucleotide and a complementary single thymine (T) nucleotide were added to the 3' overhangs. After that, DNA fragments are ligated to multiple indexing adapters. The DNA fragments with adapter molecules at both ends were selectively amplified using PCR to construct DNA library. The PCR was made with PCR primer Cocktail (PPC) annealing to adapter ends at a low number of PCR cycles to reduce the risk of sloping library representation. The enriched DNA library was then purified and validated by Qubit dsDNA BR Assay kit for quantity and Agilent Technologies 2100 Bioanalyzer for quality. This step combines DNA libraries containing unique indexes into a single pool, and then binds targeted regions of the DNA with capture probes.

3.5.16 Statistical analysis

All the statistical calculations were performed using SPSS (Version 22, IBM) software for Windows. All experiments were run in triplicates and data were presented as an average and standard error (SEM). One-way ANOVA test and unpaired *t* test were performed to assess the statistical significance of differences between the various DNA extraction methods. Only p-values less than 0.05 were considered significant.

3.6 Results

3.6.1 Optimising procedures for DNA extraction

In order to extract DNA from tissues fixed in formalin, several fundamental steps were followed based on information in the published literature (Pandey et al. 2014; Farugia et al. 2010; Shi S et al., 2002; Idris and Goodwin, 2015; Liu x et al., 2013). Initially, intensive washes to remove residual formalin from tissues were carried out; then digestion with a high concentration of proteinase K (pK); followed by heat treatment to deactivate pK and Chelex-100 resin treatment; and finally, isolation of DNA using a salt-base method. Evaluation of the effect of heat treatment and use of Chelex-100 resin was particularly of interest because these treatments may improve the DNA quality extracted from formalin fixed tissues. Based on the published literature (Pandey et al., 2014; Farugia et al., 2010; Green and Sambrook, 2012), an initial method that had several crucial steps, including extensive washing with GTE buffer (**section 3.5.2**), multiple digestions with pK, and deactivation of pK through heat at 100°C (ST-100), was established. A similar protocol but altering the temperature to 120°C (ST-120) (**Section 3.5.3**) for the deactivation step and also including Chelex resin and heating to 100°C or 120°C (CH-100) and (CH-120) were compared to the standard protocol (ST-100) (**Section 3.5.4/ 3.5.5**) (**Figure 3.7**). For all protocols, a salt-based method, specifically sodium chloride precipitation and phenol-chloroform extraction, were implemented. All protocols had 10mg of a lung artery specimen from a healthy donor that was preserved in 10% neural buffered formalin at room temperature for 9 months

as preliminary material. To eliminate variation in tissue samples, the same specimen was used for each test group. For each test protocol, initial analyses were performed to determine efficiency of the procedure including quantification of DNA yield and purity by NanoDrop/spectrophotometry; DNA fragment size distribution by gel electrophoresis; successful amplification by PCR; and reliability /reproducibility of sequence. Each protocol was repeated three times and the average of three-repeats for each protocol was presented.

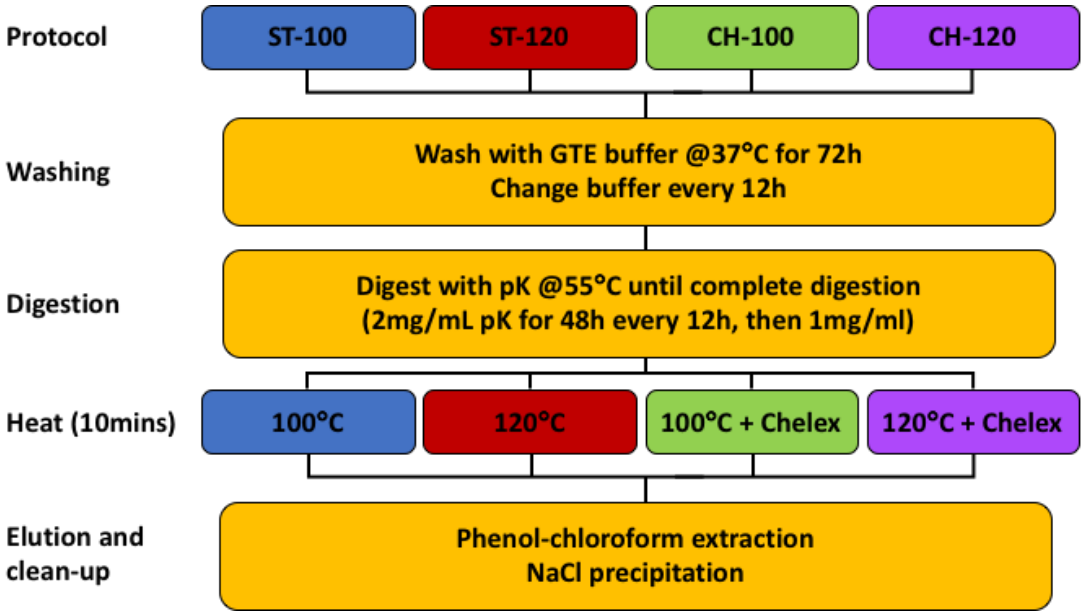

Figure 3.7: A flow chart showing the altered protocols with heating temperature and Chelex resin.
See method chapter for full protocols.

3.6.1.1 DNA yield and fragment size assessments

The quality and quantity of gDNA extracted by these different methods was compared by NanoDrop spectrophotometery and expressed in micrograms (µg) per 1mg of tissue. The DNA yield on average from the ST-100 method was significantly lower in comparison to both ST-120 and CH-100 protocols (**Figure 3.8 A**). A one-way ANOVA test (p value <0.006), indicated that higher temperature or use of Chelex-100 increased gDNA yield relative to the ST-100 method. However, comparing the yield of gDNA between ST-120 and CH-100 protocols showed no significant difference between the two protocols. Subsequently, the effect of Chelex-100 with higher temperature (CH-120) on gDNA yield was evaluated. However, the average gDNA yield was not statistically different from the ST-100 protocol (**Figure 3.8 A**).

The quality of DNA was evaluated based on the A260/A280 ratio measured via the NanoDrop spectrophotometer. Similar purity was demonstrated between all methods with no significant difference as indicated by Tukey's HSD test (p 0.3, **Figure 3.8 B**). Separation of gDNA by gel electrophoresis generated an overview of the fragment sizes produced by each method (**Figure 3.8 C**). The distribution of fragment sizes in the gel were analysed by ImageJ (Fiji, version 1.51g) and illustrated as a percentage with respect to the total gDNA yield for each method (**Figure 3.8 D**). Both ST-100 and CH-100 methods produced fragment sizes ranging from 100bp to 3000bp, whereas ST-120 and CH-120 produced a range of 100bp to 1000bp. Regardless of Chelex-100 treatment, lower temperature (100˚C) generated larger fragment

size than higher temperature (120˚C). This indicates a negative relationship between heat treatment and fragment size, as increasing the temperature leads to reducing the DNA fragment size and vice versa.

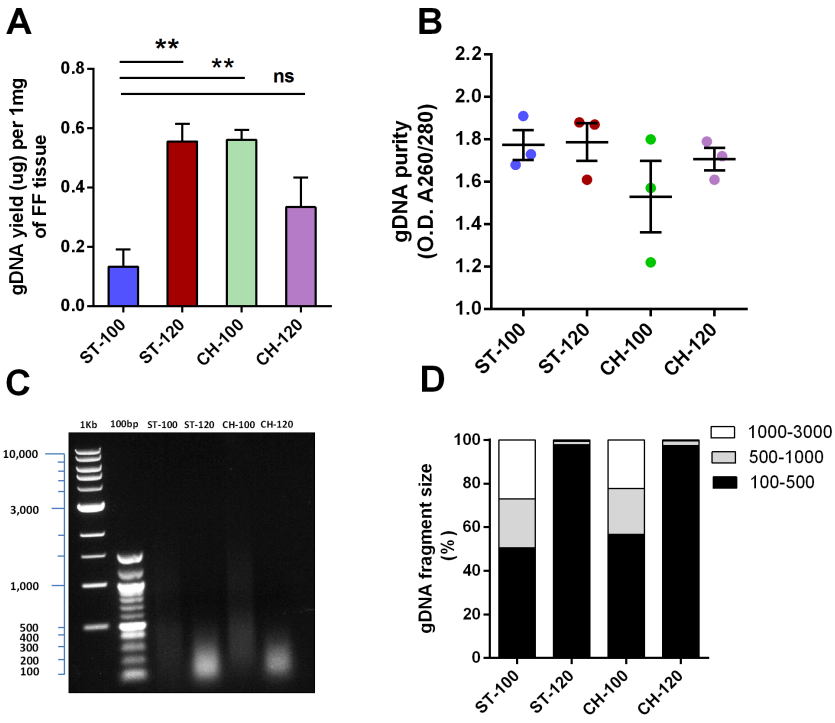

Figure 3.8: CH-120 protocol produced high quality DNA with large molecular weight.
(A) Comparisons of the genomic DNA (gDNA) yield in (µg) per 1mg volume of formalin fixed tissues from different DNA extraction methods. The difference was statistically significant for ST-120 protocol and CH-100 protocol from ST-100 protocol ($p<0.006$). (B) Comparison of the average gDNA purity for each method shows no significant difference between different protocols. (C) The gel electrophoresis image shows total gDNA fragments, separated and visualised on a 0.8% agarose gel. lane1: 1kb molecular weight marker (1-kb DNA ladder), Lane 2: 100bp molecular weight marker, Lane 3: ST-100 protocol, Lane 4: ST-120 protocol, Lane 5: CH-100 protocol, Lane 6: CH-120 protocol. (D) Size of DNA fragment generated by different methods was analysed by ImageJ and illustrated in percentage (%) with respect to the total gDNA yield for each method. The experiments were run in triplicates and data were presented as an average and standard error (SEM) of three biological samples for each protocol. FF: formalin fixed.

3.6.1.2 Evaluation of PCR mediated DNA amplification

The presence of contamination or high levels of DNA fragmentation interferes with the success of most subsequent molecular tests (Alaeddini, 2012). Therefore, assessment of the feasibility of amplification from the DNA isolated by each of the methods using the most common downstream application, PCR, was performed. In order to identify the maximum length of DNA able to be amplified by PCR, primers specific to the human *HAND1* gene, as this gene is associated with HLHS, were designed to generate amplicons of different sizes and were tested for efficacy using extracted DNA from fresh blood sample (**Figure 3.9 A**). Then, these primers were used to generate PCR products from the isolated DNA by the different protocols. All the protocols were able to generate PCR amplicon sizes of 200bp (**Figure 3.9 C**). However, the CH-100 and CH-120 gDNAs were also capable of generating amplicon sizes of up to 400bp. According to the intensity analysis performed on each amplicon band (**Figure 3.9 B**), the relative mass (ng) of an amplicon was associated with increased temperature. For example, both ST-120 and CH-120 protocols, where heat treatment at 120˚C was carried out, demonstrated higher band intensity compared to the other methods where lower temperature was used. However, the CH-100 and CH-120 methods with Chelex-100 treatment showed successful amplification of larger gDNA molecular length (**Figure 3.9 C**). This was probably because that Chelex-100 acts to release DNA from contaminating substances and at the same time protects DNA from heat damage (Walsh et. al., 1991; Turan et.at., 2015) thereby preserving it from shredding into small fragments. Also, amplified DNA demonstrated a

heat-dependent effect, as with the high temperature CH-120 protocol, the relative DNA mass obtained from 200bp and 400bp amplicons was higher than that with the low temperature CH-100 protocol (**Figure 3.9 B**). Based on these findings, heat treatment plays a major role in producing high quantity DNA and Chelex-100 is critical for isolation of larger molecular weight DNA with PCR-amplifiable behavior. Therefore, CH-120 protocol is the optimal method for extracting large and amplifiable DNA for use in downstream applications.

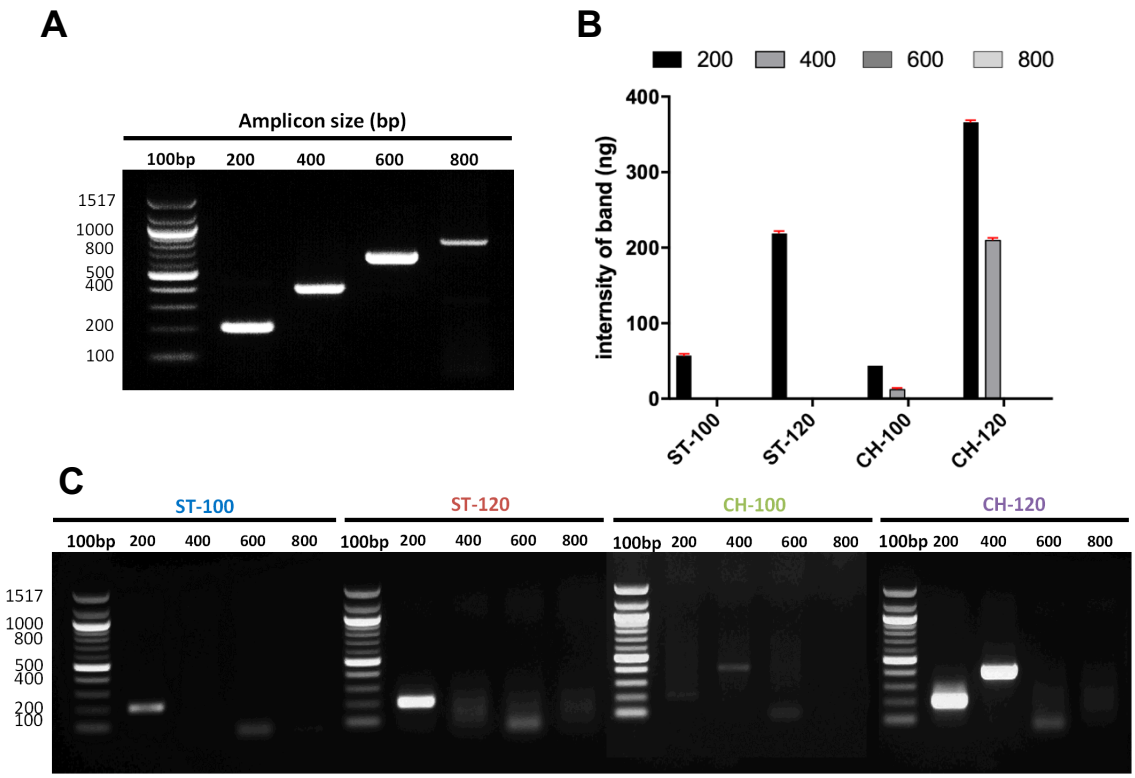

Figure 3.9: CH-120 protocol produced high quality DNA that is suitable for PCR amplification.
(A) PCR amplification of fragments of different sizes within the HAND1 gene locus was used to assess the quality of gDNA; a control gel image showing the *HAND1* gene fragment sizes of DNA extracted from fresh blood sample ranged between 200bp to 800bp. (B) A bar plot indicating the relative mass (ng) of each PCR product generated from the differently extraction methods. (C) PCR product of *HAND1* gene obtained from ST-100, ST-120, CH-100, and CH-120 protocols with a 100bp molecular weight marker. The experiments were run in triplicates and data were presented as an average and standard error (SEM) of three biological samples for each protocol. FF: formalin fixed.

3.6.2 Introduced modifications to speed-up DNA extraction

After demonstrating the effectivity of using high temperature with Chelex resin (CH-120) to generate efficient PCR template, it was important to consider reducing the duration and cost of the protocol. Several changes were introduced to the CH-120 protocol in order to reduce duration of processing and use of proteinase K. Therefore, modifications were applied to the wash step duration and temperature, and to the digestion step (**Figure 3.10 A**). The quality and quantity of gDNA was then compared to the CH-120 protocol. The first alteration was to reduce the washing duration from 72h to 12h while either keeping samples at 37˚C or increasing the temperature to 55˚C. The overall gDNA yield was not significantly changed in either alteration compared to the CH-120 protocol (**Figure 3.10 B**). After that, the effect of reduced proteinase K concentration on gDNA yield was compared. Although there was not a statistically significant difference between 1mg/mL proteinase K concentration and the standard 2mg/ml concentration used in the CH-120 protocol, this reduction in enzyme resulted in incomplete digestion of tissues, which made it necessary to extend the digestion period by 12h in order for tissues to be fully digested (**Figure 3.10 B**). Therefore, reducing proteinase K concentration did not affect gDNA yield but influenced the digest duration in a concentration-dependent manner.

Comparing the purity of gDNA obtained by these modified protocols revealed no significant difference when compared with the CH-120 protocol (**Figure 3.10 C**). This indicated that these changes did not disturb the process of

purifying DNA, hence would not interfere with the success of subsequent molecular testing, including PCR. To further confirm no alteration occurred to the fragment size of gDNA, agarose gel electrophoresis was performed separating DNA fragments according to size (**Figure 3.10 D**). The DNA fragments were then analyzed by ImageJ to detect the varying size ranges. The percentage of DNA fragment size obtained by the modified protocols in respect to their total gDNA yield are presented (**Figure 3.10 E**). Distribution of DNA fragment size was similar to the CH-120 protocol. Therefore, shortening the wash step to 24h at 37˚C and using proteinase K at a concentration of 2mg/mL revealed equal outcomes to the CH-120 protocol but time-effective alternatives, hence this improved method showed the best outcome. This is described hereafter as the improved CH-120 (iCH-120) protocol.

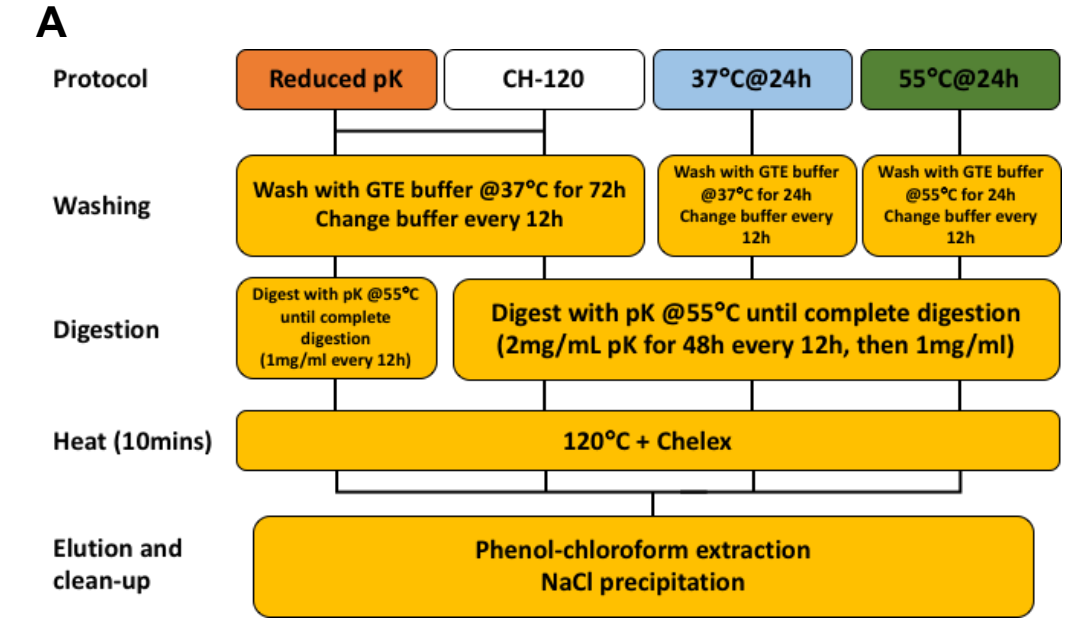
A
Protocol
Reduced pK
CH-120
37°C@24h
55°C@24h
Washing
Wash with GTE buffer @37°C for 72h
Change buffer every 12h
Wash with GTE buffer @37°C for 24h
Change buffer every 12h
Wash with GTE buffer @55°C for 24h
Change buffer every 12h
Digestion
Digest with pK @55°C until complete digestion (1mg/ml every 12h)
Digest with pK @55°C until complete digestion
(2mg/mL pK for 48h every 12h, then 1mg/ml)
Heat (10mins)
120°C + Chelex
Elution and clean-up
Phenol-chloroform extraction
NaCl precipitation

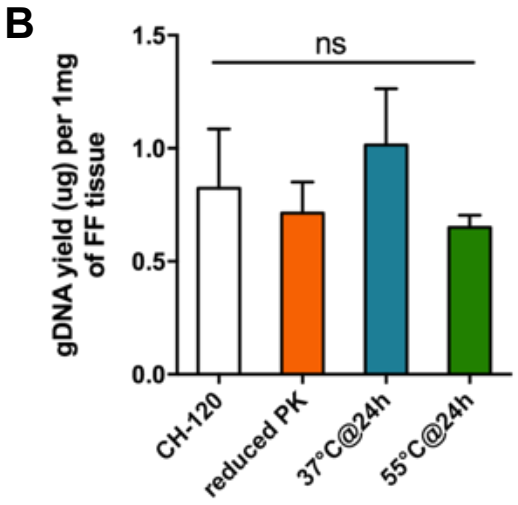
B
gDNA yield (ug) per 1mg of FF tissue
1.5
1.0
0.5
0.0
ns
CH-120
reduced PK
37°C@24h
55°C@24h

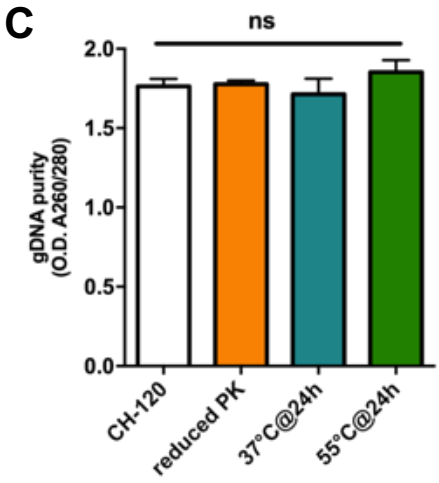
C
gDNA purity (O.D. A260/280)
2.0
1.5
1.0
0.5
0.0
ns
CH-120
reduced PK
37°C@24h
55°C@24h

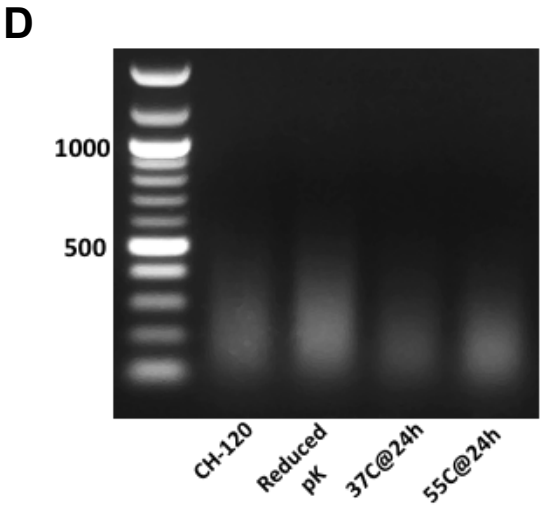
D
1000
500
CH-120
Reduced pK
37C@24h
55C@24h

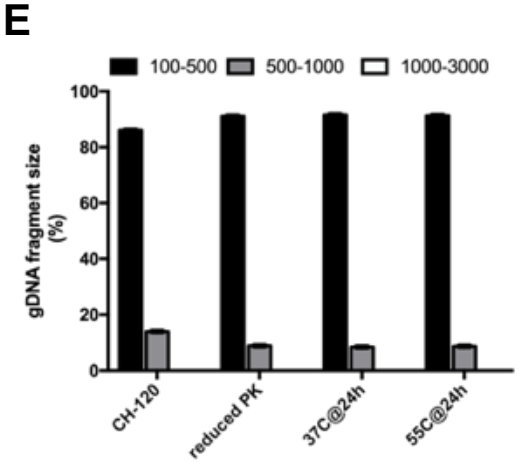
E
100-500
500-1000
1000-3000
gDNA fragment size (%)
100
80
60
40
20
0
CH-120
reduced PK
37C@24h
55C@24h

Figure 3.10: Reduction of proteinase K (PK) concentration and shortening of wash period.
(A) a flow chart of alternation procedure (see method for full protocol). (B) Comparisons of the average gDNA yield (µg per 1mg volume of AFFT) obtained by different introduced changes to protocol. Changes in the methods shows no significant difference (p=0.46) in the gDNA yield. (C) Comparisons of the average gDNA purity for each introduced change show no significant difference between protocols. (D) A gel electrophoresis image showing DNA fragments separated on a 0.8% agarose gel. Lane 1: 100bp molecular weight marker, Lane 2: CH-120 protocol, Lane 3: reduced PK concentration, Lane 4: shortened washing period to one day at 37˚C, Lane 5: shortened washing period to one day at 55˚C. (E) Fragment size generated by variations in the protocol was analysed by ImageJ and presented as a percentage (%) in relation to the total gDNA yield for each procedure. The experiments were run in triplicates and data were presented as an average and standard error (SEM) of three biological samples for each protocol.

3.6.3 Efficiency comparison of the generated protocol with UDG and a commercially available kit

The Uracil-DNA/N glycosylases (UDG or UNG) is an evolutionarily-conserved enzyme that is known to repair DNA and reverse the amination caused by formalin through a base excision-repair pathway (Schormann et. al., 2014). The UNG enzyme was suggested to reduce the nucleotide changes that resulted from formalin cross-linkage (Kim et al., 2017). This enzyme is used in the commercially-available QIAgen DNA FFPE kit. Therefore, this section will compare the improve CH-120 (iCH-120) method described in 3.5.2 section, with and without UDG enzyme, to the commercial QIAgen DNA FFPE kit. The use of UDG enzyme was made after the heat treatment for one hour at 50°C (**Figure 3.11 A**).

Similar to the previous assessment, the gDNA yield and purity for all protocols were measured by NanoDrop spectrophotometer and data presented in micrograms per 1mg of tissue. The average gDNA yield of the iCH-120+UDG

was significantly higher than that of the DNA FFPE kit that included UDG (p=0.03, **Figure 3.11 B**). However, based on NanoDrop measurement of the A260/A280 ratio, the purity of samples extracted by all methods was not significantly different, as indicated by a p value of 0.06 (**Figure 3.11 C**).

In order to assess the fragment size produced by these methods, the extracted gDNA was separated by gel electrophoresis (**Figure 3.11 D**) and the fragment size ranges, analysed using ImageJ (Fiji, version 1.51g) in respect to the entire gDNA yield. Quantification of fragment sizes produced by the iCH-120 protocol showed 80% of produced DNA was between 100 to 500bp and 20% was DNA was in the ranged of 500 to 1000bp (**Figure 3.11 E**). Conversely, the iCH-120+UDG showed 70% DNA fragment size between 100 to 500bp and 30% DNA fragment size between 500 to 1000bp (**Figure 3.11 E**). Similarly, the DNA FFPE kit (that included UDG) produced 75% of DNA size ranged between 100 to 500bp and 25% between 500 to 1000bp (**Figure 3.11 E**).

To further evaluate the suitability of isolated DNA for PCR amplification and to assess the maximum length of PCR-amplifiable DNA, the previously used sets of primers were employed to generate PCR products from the iCH-120 protocol, iCH-120+UDG protocol and DNA FFPE kit. PCR gels demonstrate that all protocols were capable of amplifying PCR products of up to 400bp (**Figure 3.11 F**). Based on intensity analysis performed on each amplicon band, the relative mass (ng) of an amplicon was illustrated as a percentage and presented in (**Figure 3.11 G**). There were no significant differences between the band intensity of 200bp and 400bp generated by any of the

protocols. This indicates that all methods produced comparable PCR-amplifiable DNA.

Based on these findings, the iCH-120, either with UDG enzyme or without it, was effective for extracting high quality gDNA with high yield and fragment length. Although the DNA FFPE kit produced comparable results to the iCH-120 protocol, the high cost (£231.00 per a kit, 2018) and small quantity (only 50 DNA samples can be done using one kit) limit its use. Therefore, the iCH-120 with/without UDG protocol provides an efficient, simple, time-effective and cheap procedure to isolate DNA from formalin fixed tissues.

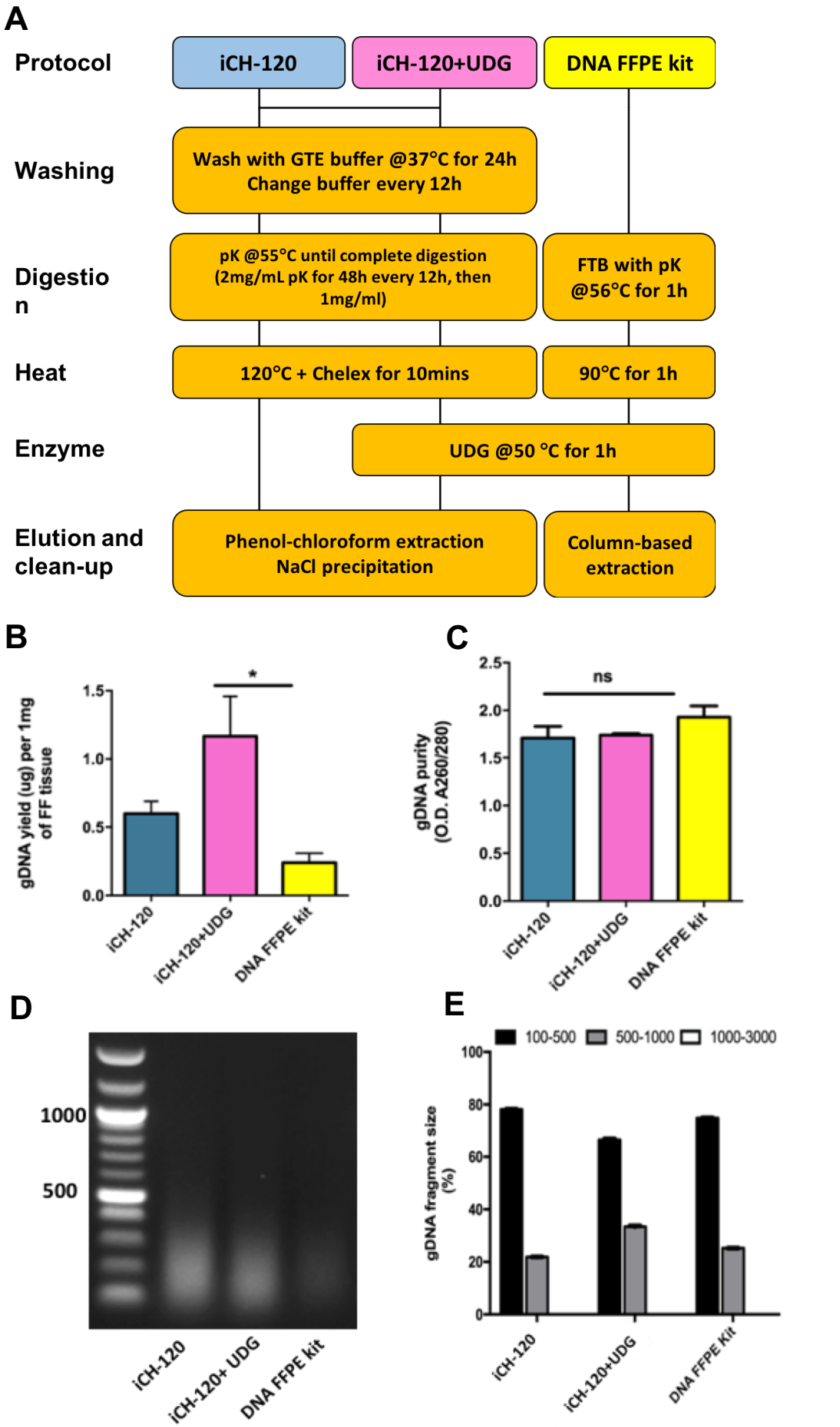
A
Protocol
iCH-120
iCH-120+UDG
DNA FFPE kit
Washing
Wash with GTE buffer @37°C for 24h
Change buffer every 12h
Digestio
n
pK @55°C until complete digestion
(2mg/mL pK for 48h every 12h, then
1mg/ml)
FTB with pK
@56°C for 1h
Heat
120°C + Chelex for 10mins
90°C for 1h
Enzyme
UDG @50 °C for 1h
Elution and
clean-up
Phenol-chloroform extraction
NaCl precipitation
Column-based
extraction
B
gDNA yield (ug) per 1mg
of FF tissue
*
iCH-120
iCH-120+UDG
DNA FFPE kit
C
gDNA purity
(O.D. A260/280)
ns
iCH-120
iCH-120+UDG
DNA FFPE kit
D
1000
500
iCH-120
iCH-120+ UDG
DNA FFPE kit
E
100-500
500-1000
1000-3000
gDNA fragment size
(%)
iCH-120
iCH-120+UDG
DNA FFPE Kit

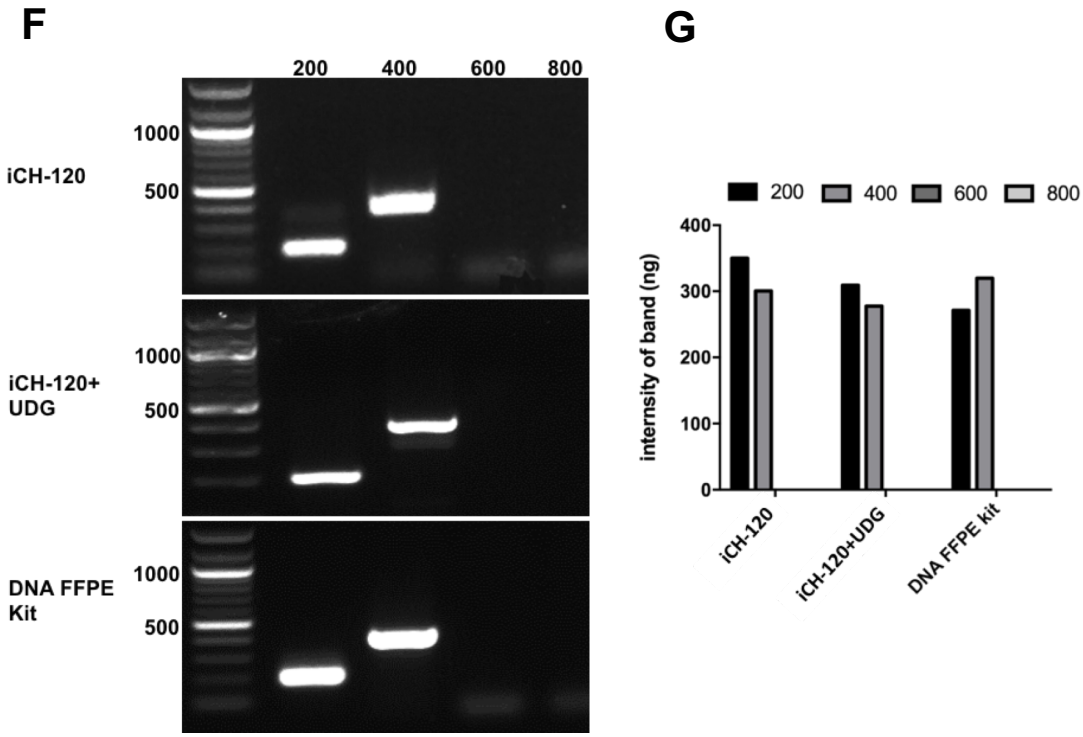

Figure 3.11: Comparable results obtained from the iCH-120 with/without UDG enzyme and the DNA FFPE kit.
(A) A flow chart showing the steps followed for each protocol. (B) Comparisons of the gDNA yield (µg per 1mg volume of FFT) between iCH-120, iCH-120+UDG and DNA FFPE kit. One-way ANOVA revealed a significant difference (p 0.03) between the iCH-120+UDG and the DNA FFPE kit methods. (C) Comparisons of the average gDNA purity obtained by the three protocols showed no significant difference (p 0.06). (D) The gel electrophoresis image showing DNA fragments separation on 0.8% agarose gel. Lane 1: 100bp molecular weight marker, Lane 2: iCH-120, Lane 3: iCH-120+UDG protocol and Lane 4: DNA FFPE kit. (E) Fragment size generated by these protocols was analysed by ImageJ and presented in percentage (%) in relation to their total gDNA yield. (F) PCR product of different sizes within the HAND1 gene locus obtained from the iCH-120, iCH-120+UDG protocols and DNA FFPE kit. All protocols amplified amplicon sizes ranged up to 400bp. (G) Quantification of the relative mass (ng) of each PCR band produced from these methods. The 200bp band generated by iCH-120, iCH-120+UDG protocols and DNA FFPE kit demonstrated a band intensity of 350ng, 309ng and 271ng, whereas the 400bp band intensity revealed 300ng, 277ng and 320ng, respectively. The experiments were run in triplicates and data were presented as an average and standard error (SEM) of three biological samples for each protocol.

3.6.4 Quality and quantitative assessments of isolated gDNA by Sanger sequencing

An important aspect of extraction of DNA from formalin-fixed tissues is the accuracy of sequence or reliability of the produced sequences from gDNA and whether the gDNA extracted is representative of the original sequence. Formalin-induced DNA damage frequently present in a small number of loci, hence, making match comparisons difficult and the distinction of real low frequency variants from sequencing artefacts challenging. Assessing the quality and validating the sequences generated by different extraction methods are fundamental for the interpretation of genomic results. Therefore, it is important to evaluate the various methods in order to understand the influence of different extraction methods on formalin-induced DNA damage. Since the possibility of distinguishing the real variants from artefacts is limited, in this study the term deviations or deviants rather than variants will be used to describe changes in the sequences. In order to determine this, gDNA was either sequenced from purified PCR products, or from PCR products that were subcloned into plasmids and then the plasmid DNA sequenced.

DNA samples extracted by ST-100 (the original protocol tested, **Figure 3.7**), iCH-120, iCH-120+UDG protocols, and the commercial Qiagen DNA FFPE kit (**Figure 3.11 A**) were used to assess quality and reproducibility of sequences. Initially, evaluation of direct sequencing from purified PCR products was carried out using the previously designed forward and reverse primers to a 200bp fragment of the HAND1 gene. The PCR was carried out as described

in the Methods section (**Chapter 2**) followed by gel extraction to purify the PCR products and finally sent for sequencing using Sanger sequencing. Despite the various protocols used for DNA extraction, all methods produced similar outcomes (**Figure 3.12**). The first few bases adjacent to the forward primer binding site were missing from the resulting sequence, which were then recovered through an additional sequencing reaction using a reverse primer to enable these missing bases to be determined. Moreover, there was one deviant found in each sequence produced from all the methods, which was again recovered using the reverse sequence (**Figure 3.12**, red highlights).

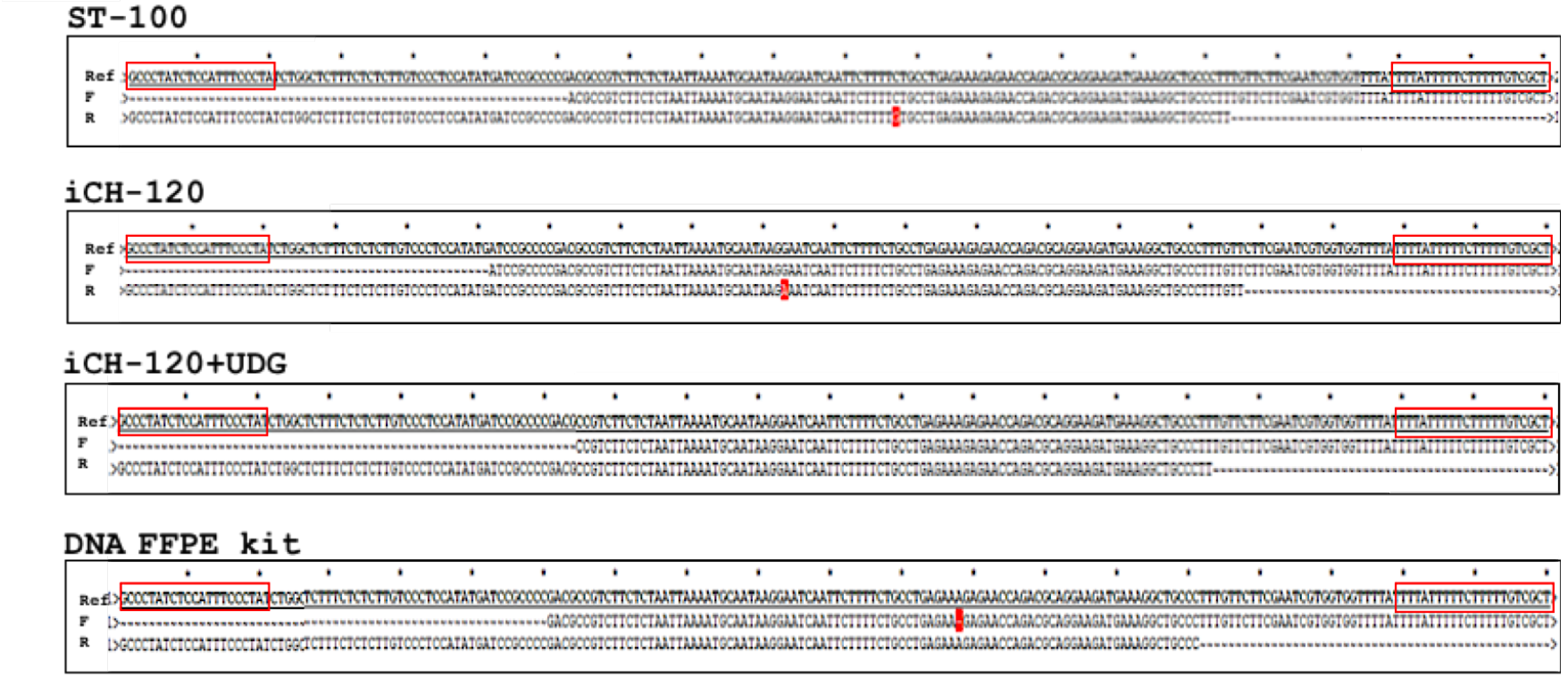

Figure 3.12: Low quality templates obtained by direct sequencing of DNA from purified PCR.
Sanger cycle sequencing for a 200bp fragment of *HAND1* exon 2 was established in DNA acquired with ST-100, iCH-120, iCH-120+UDG protocols and QIAgen DNA FFPE kit. Sequencing of DNA from purified PCR using forward and reverse primers for a 200bp fragment of *HAND1* exon2. Ref: reference sequence (*HAND1* exon2), F: forward primer, R: reverse primer, Red box: primer binding site, Red highlight: mismatches of obtained sequence compared to the reference sequence. The sequencing of purified PCR product was performed on three different samples for each DNA extraction method.

Next, a PCR based cloning method was used to generate plasmids containing the maximum length of PCR amplified gDNA. Due to difficulties in the amplification of products greater than 200bp from gDNA extracted using the ST-100 protocol, a 200bp fragment was generated using the primers in (**Chapter 2**). These primers allowed a parallel comparison between a 200bp fragment generated by the ST-100 protocol and a 400bp fragment generated by other methods. Amplification of gDNA was performed using a high-fidelity DNA polymerase, followed by addition of a poly A tail to create a suitable molecule for TA cloning. Once the molecule had been cloned into pGEM-T easy and transformed into bacteria (JM109), resulting colonies were picked and cultured. For the purpose of increasing the accuracy of results, 20 colonies per sample, which was repeated three times, were investigated by plasmid DNA sequencing. The plasmid DNA was sequenced in both forward and reverse directions and resulting sequences from each plasmid DNA were compared to a reference sequence, in this case the HAND1 gene (ENSG00000113196). Initial analysis of data was based on pairwise comparisons of forward and reverse sequences from a single plasmid DNA to a reference sequence using ApE A plasmid editor software (v2.0.47) and Jalview (v2, Waterhouse et al., 2009). Then, quantification of the overall formalin-induced DNA damages was established for each method using GraphPad prism (v6), followed by calculation of the proportions of each type of nucleotide change from each extraction method.

Upon comparison of the 200bp sequence from HAND1 gene, the percentage divergence in the overall performance of ST-100, iCH-120, iCH-120+UDG protocols and DNA FFPE kit compared to the database sequence was 5%, 6%, 9% and 17%, respectively. Comparison between the DNA extraction protocols indicated a significant difference between the ST-100 (p 0.02) and iCH-120 (p 0.03) protocols compared to the Qiagen DNA FFPE kit (**Figure 3.13 A**). The percentage divergence of the ST-100 protocol suggests increased variation between sequences leading to difficulties in distinguishing true sequencing variants from artefacts. For further analysis of sequencing variants generated by each DNA extraction methods, the percentage of nucleotide divergence was normalised to a 100bp read length. The results of specific nucleotide changes are shown in (**Figure 3.13 B**) and demonstrated a high incidence (up to 10%) of G>A changes in DNA presented by all extraction methods. In addition, an incidence of (1.8%) of A>T changes was detected in samples extracted by iCH-120 protocol, whereas 3.75%, 1.14%, and 5.20% of C>T changes were detected in ST-100, iCH-120 and DNA FFPE kit, respectively. Strikingly, a high level of A and T deletions was confined to iCH-120 (1.8% and 3.9%, respectively) and iCH-120+UDG (5.3% and 5.5% respectively) protocols and T deletions (5.8%) to the Qiagen DNA FFPE kit. This could suggest that these methods failed to correct these variants and thus delete them. Consequently, these methods showed a high prevalence to nucleotide deletions rather than alterations.

To determine if treating samples with UDG reduced sequence artefacts, a comparison of sequencing artefact divergence between the iCH-120 and iCH-

120+UDG protocols was performed. As shown in (**Figure 3.13 B**), the high range of the variant calls A>T/T>C/C>T observed from the iCH-120 protocol samples was dramatically reduced in the iCH-120+UDG protocol samples. There was, however, a consistently higher rate (up to 5.5%) of specific A and T base deletions in the iCH-120+UDG protocol samples. This suggests that although treating samples with UDG may help to minimise some of the formalin-induced sequence artefacts by removing incorrect bases, it can also cause damage to sequences by random removal of nucleotides. To further investigate whether these changes occurred due to UDG treatment and not due to Chelex-100 treatment, comparisons between the iCH-120+UDG protocol and the Qiagen DNA FFPE kit was performed. The samples from the DNA FFPE kit showed a similar range of A>T changes (less than 1%) and T deletions (less than 6%) but did not show the reduction in C>T/T>C changes (iCH-120+UDG= 0.4%, DNA FFPE kit= 6.0%), or the increase in A deletion (iCH-120+UDG= 5.3%, DNA FFPE kit= 0%) observed with the iCH-120+UDG protocol samples (**Figure 3.13 B**). This suggests that a reduction in C>T/T>C changes and an increase in A deletion may occur as a result of treatment with both UDG and Chelex-100.

Although formalin-induced nucleotide changes in gDNA from the various extraction methods seems, at first, to be random, sequence alignments of the changes from each method suggest that specific regions of DNA are affected. **Figure 3.13 C** shows alignments of a 400bp read length of 20 sequences produced from the iCH-120, iCH-120+UDG protocols and Qiagen DNA FFPE kit. Due to difficulties in amplification of a 400bp read length from the ST-100

protocol, the overlapping latter 200bp read length of sequences were aligned with other sequences and were all compared to the reference HAND1 sequence. The consensus alignment of sequences from different methods demonstrated matched and specific formalin-induced nucleotide changes that varied in frequency depending on the DNA extraction procedure. Analysis of the formalin-induced DNA damage showed a specific pattern of nucleotide changes. As seen in **Figure 3.13 C**, the AT or T rich-regions in sequences produced by different methods were susceptible to be damaged by formalin. In addition, changes of T>C or C>T were present in all methods, but with lower frequency in the iCH-120+UDG protocol. However, a high rate of G>A changes was observed in DNA isolated by all methods. This phenomenon of highly detectable bias towards G>A changes in formalin paraffin embedded tissue or formalin tissues has previously been reported (Wong et al., 2014, Qach et al, 2004).

Although UDG seemed to reduce the frequency of deamination events affecting PCR, this is not complete and, in some cases new deviations are found which may relate to different extraction methods and therefore be misleading. In addition, whilst comparing several sequence transcripts could overcome some of formalin-induced artefacts, in some cases the artefacts could be persistence and appeared in most of the transcripts making determination of real variants difficult (**Figure 3.13 C**, white lines). Therefore, it is still risky to rely on Sanger sequencing and cloning transcripts to identify unknown and rare variants, but they remain useful for confirmation of known variants.

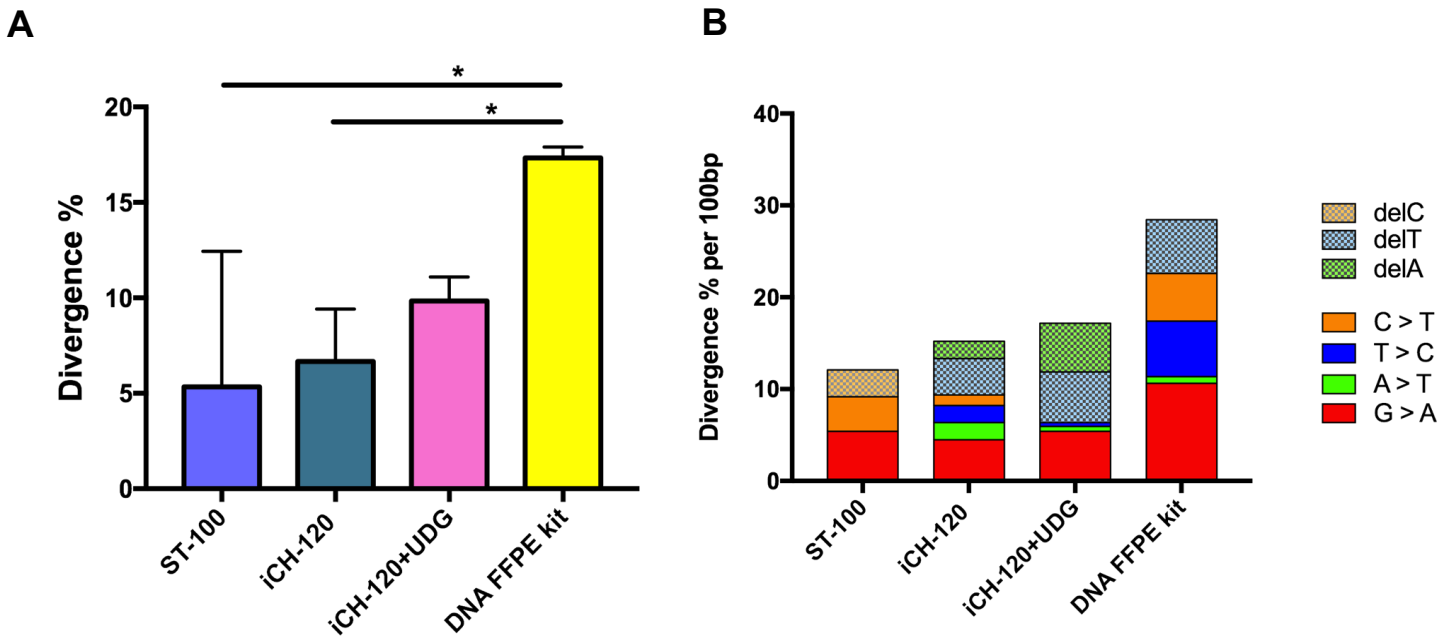
A
B
Divergence %
Divergence % per 100bp
0
5
10
15
20
30
40
*
*
ST-100
iCH-120
iCH-120+UDG
DNA FFPE kit
delC
delT
delA
C > T
T > C
A > T
G > A

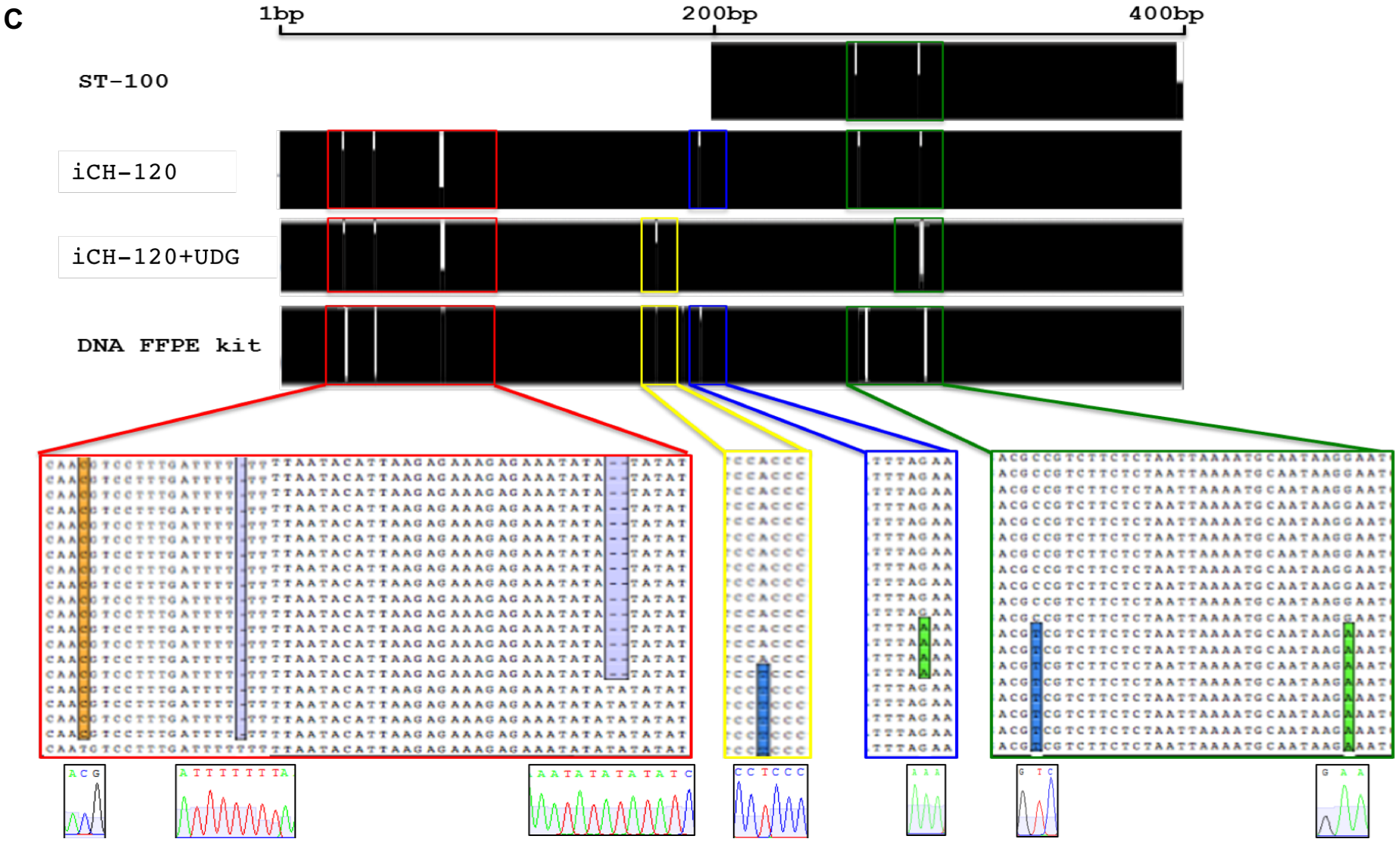
C
1bp
200bp
400bp
ST-100
iCH-120
iCH-120+UDG
DNA FFPE kit

Figure 3.13: Assessment of sequencing artefacts produced from plasmid DNA extracted by ST-100, iCH-120, iCH-120+UDG protocols and DNA FFPE kit.
Assessment of sequencing artefacts produced from plasmid DNA extracted by ST-100, iCH-120, iCH-120+UDG protocols and DNA FFPE kit. (A) Comparisons of the overall divergence (%) of different extraction methods. All DNA extraction protocols excluding ST-100 protocol show a consistent level of divergence within their group, which indicates a constant frequency incidence of sequencing artefacts generated by these methods. Tukey's multiple comparisons test showed a p value of 0.02 for the ST-100 protocol and p 0.03 for iCH-120 protocol compared to the DNA FFPE kit. (B) Stacked columns represent the prevalence (%) of each type of nucleotide divergence per 100bp read length. A high prevalence of guanine (G) changing to adenine (A) was observed in all protocols, followed by thymine (T) changing to cytosine (C) in ST-100, iCH-120 protocols and DNA FFPE kit or deletion of T in iCH-120, iCH-120+UDG and DNA FFPE kit. (C) Alignment of sequences generated by Sanger cycle sequencing for a 200bp or 400bp read length of HAND1 exon 2 was performed on DNA isolated with ST-100, iCH-120, iCH-120+UDG protocols and DNA FFPE kit. Plasmid DNA was extracted from 20 different colonies and sequenced in forward and reverse directions. Boxes show the nucleotide changes in sequences from each acquired method. Electropherograms detect the nucleotide peaks of sequencing artefacts

3.6.5 Qualitative and quantitative assessments of isolated gDNA by Next-Generation Sequencing (NGS)

The analysis of exome sequencing data found in this section was carried out by Andrew Skelton from the Bioinformatics Support Unit in Newcastle University.

Although it was feasible to extract high quality DNA with long amplifiable PCR products from formalin-fixed tissues that could be used for Sanger sequencing, the generated sequence information might contain formalin-induced artefacts that could not be discriminated from real disease-causing variants. These difficulties maybe overcome through the advances in sequencing technology, in the form of NGS. This is because NGS can perform paired-end reads, which means NGS allows sequencing of both fragment ends, then detects the common DNA rearrangements, and finally generates high-quality alignable sequence reads. In order to address the potential of NGS, the whole exome sequencing data of a DNA sample extracted from a fresh blood sample (FB-DNA) was compared to that extracted from a piece of explanted right ventricular heart fixed in formalin for 2 years (FF-DNA) from the same patient. The extraction of DNA from the explant formalin-fixed heart tissue was performed using the iCH-120 protocol previously described (**Figure 3.11 A**), as this method provided less nucleotide alternations compared to other methods.

For equal evaluation of the FB-DNA and FF-DNA samples, quantification and assessment of gDNA integrity in both samples was performed using an automated electrophoresis system (Agilent 2200 TapeStation system). This system provided a distribution of gDNA fragment length and aided in determining whether pre-library preparation shearing was necessary. The FB-DNA samples showed a mean fragment length of 280bp (**Figure 3.14 A**), whereas the FF-DNA sample had a mean of 141bp (**Figure 3.14 B**), which was anticipated from the previous results (**Figure 3.11 F**). As the FF-DNA sample showed small fragment length, no shearing was required. However, the FB-DNA sample required shearing to obtain a median fragment-length of 150bp before library preparation; thus, a transposonase-based system was used (TrueSeq Rapid exome kit, Illumina). Both samples were then processed using NextSeq 500 platform (Illumina) at high output mode to produce 40 million pair reads of 75bp length. Construction of exome data was made using the GATK best practice pipeline and both library preparations were made from identical bed files (**Figure 3.14 C**).

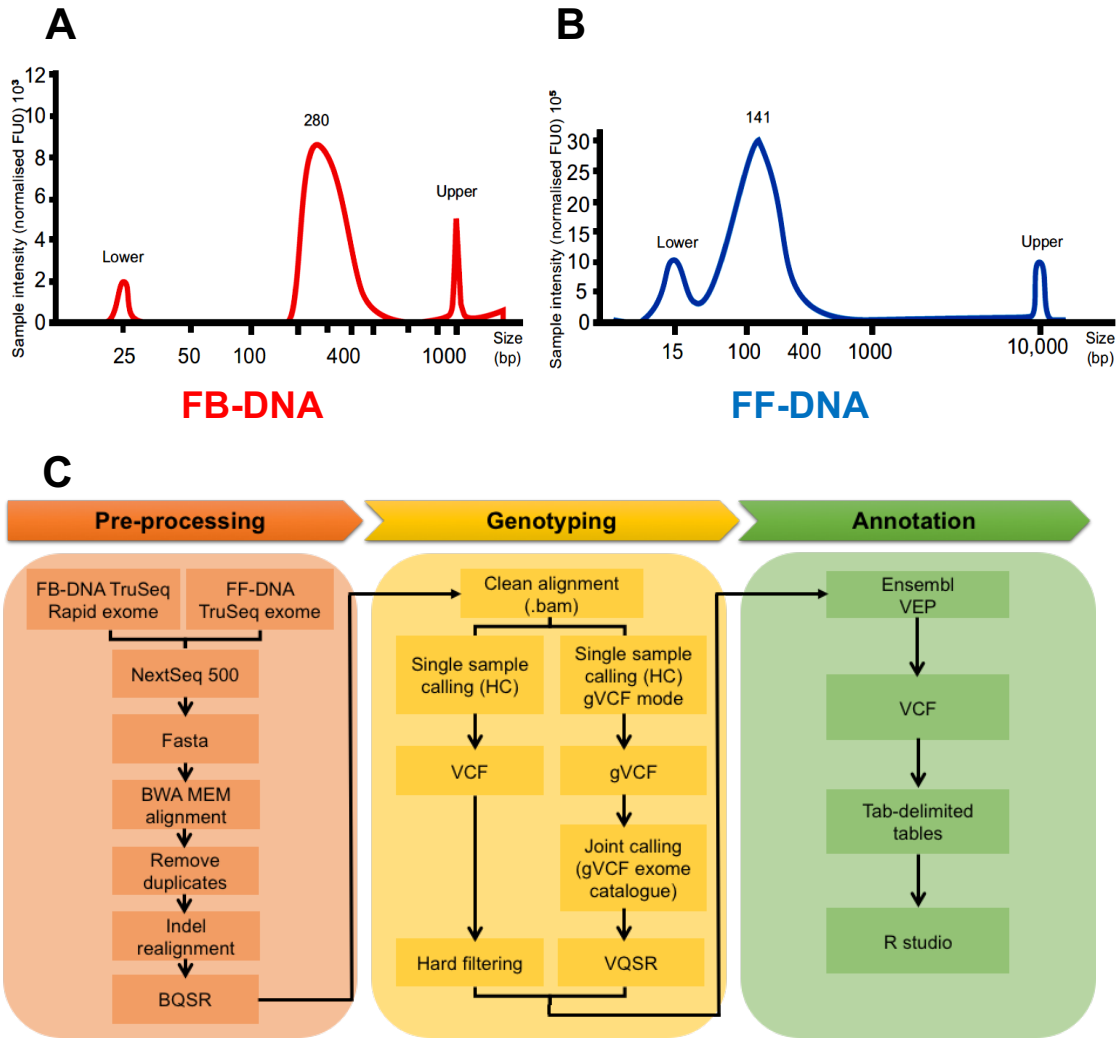

Figure 3.14: Next-generation sequencing analysis on FF-DNA and FB-DNA samples.
(A) quantification of gDNA integrity using automated electrophoresis system for FB-DNA and (B) FF-DNA. FB-DNA sample showed a fragment length product up to 3500bp, whereas FF-DNA sample only had a fragment length up to 141bp. (C) a flow chart indicating the process of sequencing date using an Illumina NextSeq500 and the analysis was performed using GATK (3.8) best practice. Pre-processing included the BWA-MEM alignment, duplicates removal, re-alignment of indel, and then base quality score recalibration (BQSR). The genotyping call was performed using the HaplotypeCaller (HC), which was run using two distinctive mode: Single sample calling and gVCF mode to examine the effect of different modes on improving calls from formalin-fixed tissues. The single sample calling was used the recommended hard filtering for filtering variants, whereas the joint calling with 216 exomes with different phenotypes used variant quality score recalibration (VQSR) to filter variants. Annotation of variants was made using Ensembl' variant effect predictor (VEP, v90) with two plugins: LOFTEE and dbnsfp. The VCF file was then converted to a tab-delimited table file using the GATK's VariantsToTable tool before it was exported to R studio for further analysis.

3.6.5.1 Genomic analysis of FB-DNA and FF-DNA: Coverage, depth, and GC content

The BAMQC, a quality control application, was run on the alignment .BAM files and reported a mean coverage of high-quality aligned reads of 78-fold with FB-DNA but only 15-fold with FF-DNA (**Figure 3.15 A**). This coverage was equally distributed throughout all chromosomes (**Figure 3.15 B**). Analysis of the GC content indicated lower reads gained from the FF-DNA sample compared to the FB-DNA sample (**Figure 3.15 C**). This might be because the GC-rich regions are prone to low coverage depth, partly due to their instability during amplification. Alternatively, this could be due to formalin-induced changes of G and C bases to A and T bases. This was then further analysed through inspecting the various single nucleotide polymorphisms (SNPs) found in the aligned .bam files compared to the original sequence in the initial .bam files generated by BWA-MEM. There were differences in the SNP frequency observed between the two samples, however this could be limited to the inconsistent coverage between samples and failure to recognise indels (**Figure 3.15 D**). An important aspect of NGS is the paired-end reads, which allows both ends of the DNA fragments to be sequenced. Hence it provides two reads for the same DNA fragment region, which enables identification of genomic rearrangements and repetitive elements within sequences. Therefore, comparison between read1 and read2 for FF-DNA sample was performed to detect whether the observed changes in SNP frequency was due to formalin and not to technical limitation of NGS. As anticipated, there was enrichment of G>A and C>T in read2 along with minor alterations between the

two reads (**Figure 3.15 E**) indicating induced-formalin damages. Strikingly, read2 data showed less distortion in SNPs suggesting misrecognition of the genomic positions of read1 leading to inability to correctly match read2 transcripts on the genomic scaffold.

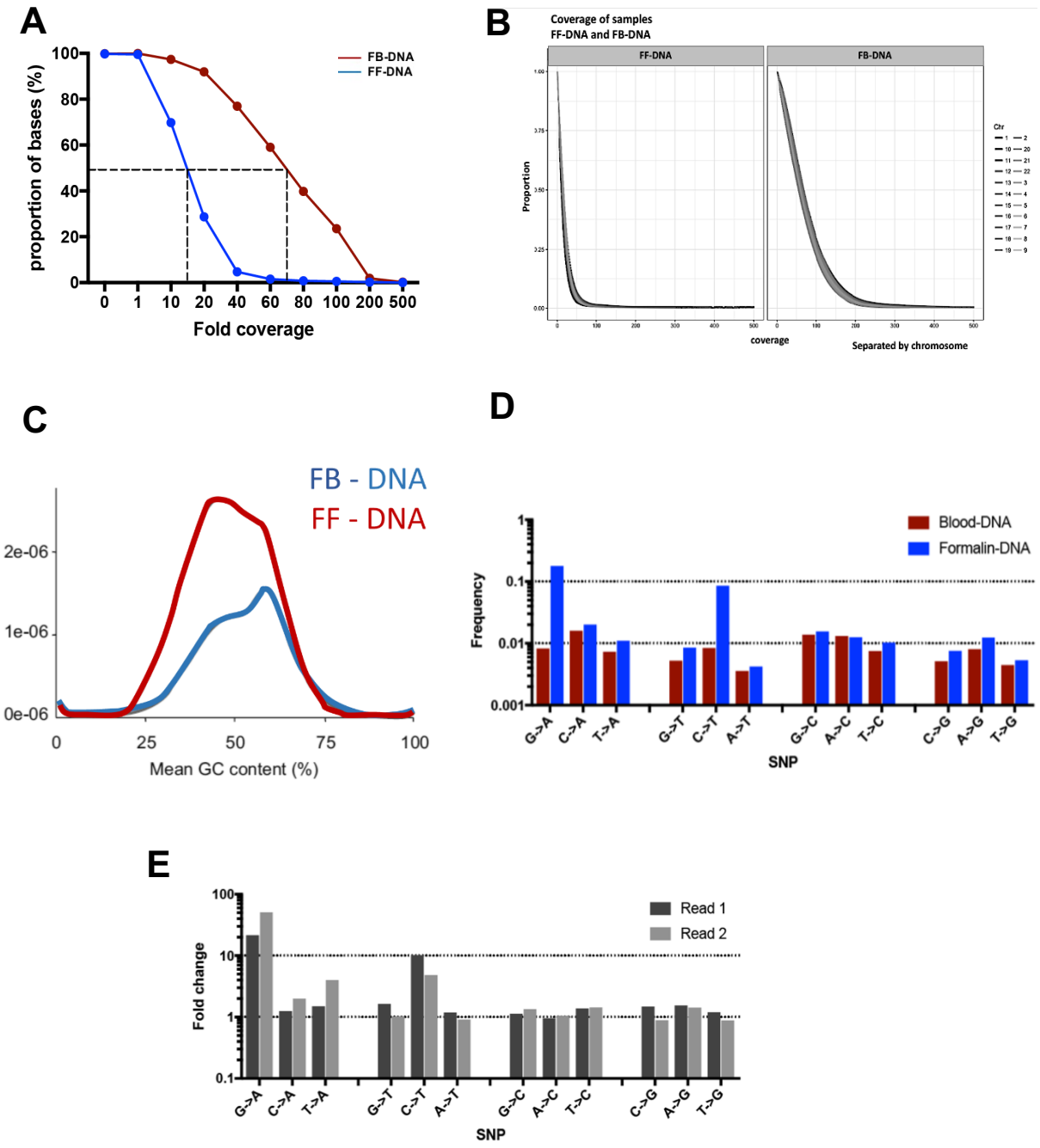

Figure 3.15: Validation of genomic data for FF-DNA sample through coverage, depth and GC content.
The mean coverage of FB-DNA sample was higher than FF-DNA sample by 78 folds (A), although the coverage was equally distributed throughout all chromosomes for both samples (B). (C) GC content for FF-DNA sample was lower than that for FB-DNA sample. (D) Comparison of the single nucleotide polymorphisms (SNPs) found in the aligned .bam files compared to the original sequence in the initial .bam file between FF-DNA and FB-DNA samples. (E) Comparison of the paired-end reads, read 1 and read2, in FF-DNA sample showed less distortion in SNPs between the two reads but enrichment of G>A and C>T in read2.

3.6.5.2 Variant calling pipelines for this study

After the quality metric analysis of FB-DNA and FF-DNA samples, it was important to consider whether the variant caller tool used in this study providing accurate information regarding filtering and SNP calling errors. Several potential variant calling pipelines were identified, but the GATK pipeline was favoured among other suggested pipelines (Hwang et. al., 2015). Therefore, the GATK pipeline was used for variant calling in combination with a BWA-MEM read aligner in this study. This is summarised in **Figure 3.14 C**. Initially, the reads were mapped to the reference genome Hg19 (http://grch37.ensembl.org/index.html), then duplicates were marked, sequence was re-aligned to known indels, and base score quality recalibration (BSQR) was conducted to generate the clean alignment .bam file. The .bam file was then processed either solely using HaplotypeCaller (HC), a variant caller tool, or in combination with a large exome group to permit joint calling. Joint calling is the analysis of variants simultaneously throughout all samples. This then generated variant call files (.vcf), which were subjected to hard filtering after simple HC, or to variant quality score recalibration (VQSR) after joint calling.

The single HC and hard filtering generated 5,239 variants from FB-DNA, compared to 13,079 variants generated by FF-DNA samples. Conversely, this data showed low specificity and sensitivity (13% and 32.5%, respectively) as more of variants (11,377 variants) were identified in FF-DNA sample but not in the FB-DNA sample (**Figure 3.16 B**). The joint calling and VQSR filtering, however, represented higher specificity and sensitivity (94.2% and 73.3%,

respectively) when variants between FB-DNA and FF-DNA samples were compared to the previous filtering. It showed 104,387 variants from the FF-DNA sample that was matched with the FB-DNA sample (**Figure 3.16 A**). Therefore, analysing the data using the joint calling with VQSR significantly improved the sensitivity and specificity of variant calling. This could be explained by the joint calling advantage of sharing information throughout all samples, which increases its sensitivity toward rescued genotype calls that located in low coverage regions, by searching for a consistent variant at that region found within other samples.

Lastly, analysis of base changes after the two variant calling methods was carried out. Both methods produced similar base change counts and the preference of formalin to produce G>A and C>T and other minor base changes observed in the initial analysis (**Figure 3.15 D**) were not presented by both filtering systems (**Figure 3.16 D**). Also, comparing the number of detected SNPs in FF-DNA to that in FB-DNA revealed similar call counts for both variant calling methods (**Figure 3.16 C**). This suggests that both single variant calling with hard filtering and joint calling with VQSR were able to reduce deviant calls produced from formalin-induced damage, but at the risk of losing real rare variants.

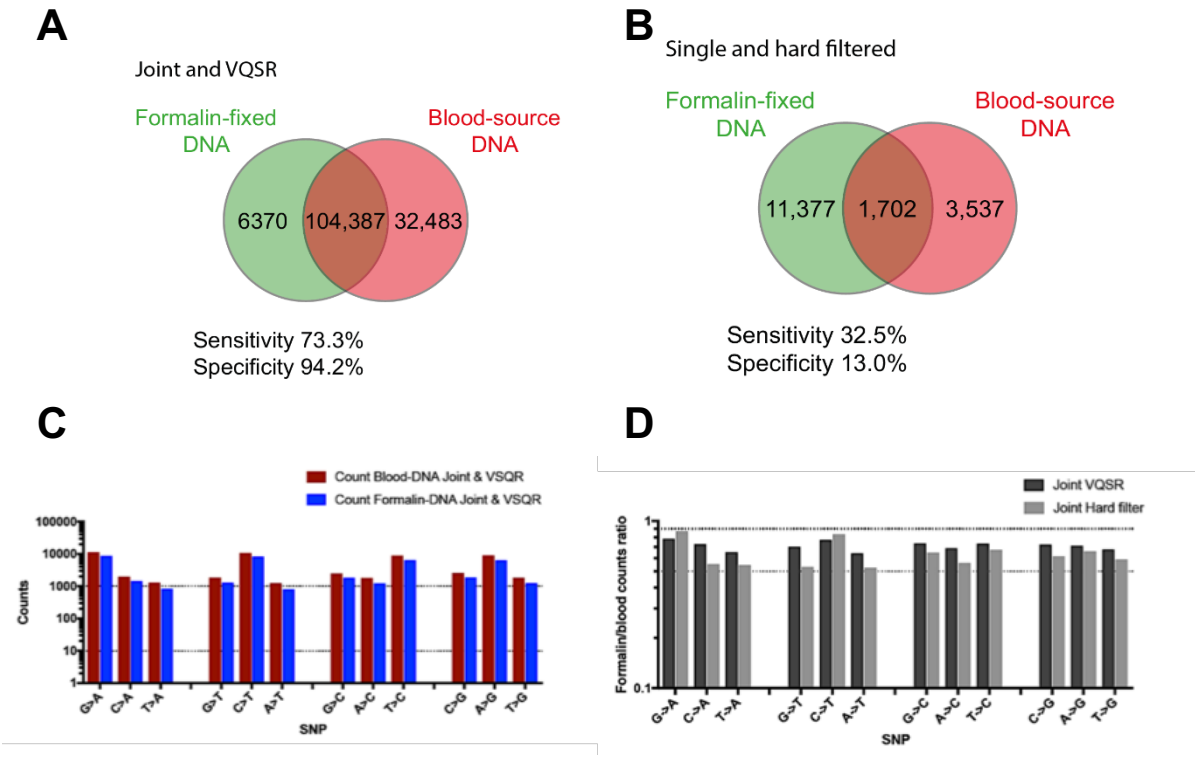

Figure 3.16: Assessment of FF-DNA sequencing reads using two modes of GATK best practice pipeline: joint calling with VQSR mode and single calling with hard filtering mode.
Comparison between the joint calling with VASR filtering (A) and the single calling with hard filtering (B) for FF-DNA and FB-DNA (Blood-source DNA) revealed higher read sensitivity and specificity when the joint calling with VQSR was applied. (C) Base change analysis between FF-DNA and FB-DNA using the joint calling with VQSR reads indicated similar base change counts between the two samples. (D) Comparison between the base changes in the joint VQSR and single with hard filtering for FF-DNA sample showed minor changes between the two modes indicating that both modes were able to reduce deviant calls produced from formalin-induced damage.

3.6.5.3 Phred Quality scoring

As a final assessment of the quality of sequencing reads in the FF-DNA compared to the FB-DNA, the Phred quality score (Q score) was used. It provides a logarithmic value to describe the probability of a base calling error during automated DNA sequencing (Kulkarni and Pfeife, 2015). When using this to filter results, this means that a higher cut-off Q score reduces the likelihood of reads containing a base-calling error and results in higher call accuracy. For example, A Phred Q score of 30 (Q30) refers to a base with an error probability of 1 in 1000, or conversely 99.9% accuracy, whereas the Q score of 10 (Q10) equates an error rate of 1 in 10 or 90% accuracy (Cliften, 2015).

In this study, intention was made to examine the effect of three different levels of base filtering using three different Phred Q scores; Q score of 10 (Q10; error rate of 1 in 10), 20 (Q20; error rate of 1 in 100) and 30 (Q30; error rate of 1 in 1000).

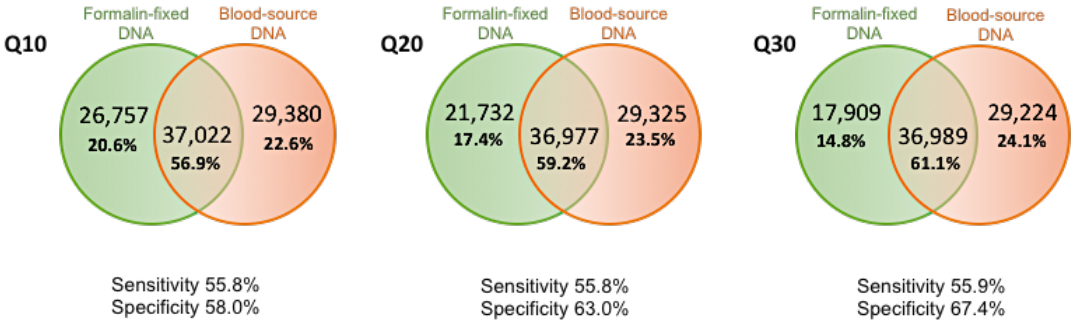

Figure 3.17: Venn diagrams showing relationship of reads obtained from formalin fixed DNA and blood using filtering of variants at different Phred scores.
At all Phred scores there was no difference in the number of variants detected in blood, but not in the formalin samples, and no difference between the variants that were discovered in the blood and the formalin sample. However, with increasing Phred score there was a reduction in the number of variants unique to the formalin DNA sample. Thus, the sensitivity of variant calling in formalin samples was unchanged, but the specificity increased from 58.0% to 67.4%.

The quantitative analysis with Phred Q score of 10 (Q10) generated 37,022 variants that were in common between FF-DNA and FB-DNA with 55.8% sensitivity and 58% specificity (**Figure 3.17**). Although the Phred Q score of 20 (Q20) revealed similar sensitivity (55.8%) to Q10, it showed higher specificity (63%) as 21,732 variants were identified in FF-DNA but not in FB-DNA. The Phred Q score of 30 (Q30), compared to both Q10 and Q20, illustrated comparable sensitivity (55.9%), but elevated specificity (67.4%) indicating less variability between FF-DNA and FB-DNA with only 17,909 variants found in FB-DNA (**Figure 3.17**). Therefore, the Q30 showed comparable sensitivity to both Q10 and Q20, but higher specificity demonstrating the best Phred Q score to analyse formalin fixed samples.

Overall, it is possible to extract DNA from tissues that had been fixed in formalin for up to 2 years using the iCH-120 method. Although Sanger sequencing and cloning showed less reliability sequencing data with tissues fixed in formalin for less than one year, NGS presented here a better option to generate a reliable sequencing data particularly when a specific filtering system is applied. Therefore, using the iCH-120 protocol to extract DNA from prolonged fixation period in formalin and to sequence DNA through NGS can produce high specificity with limited sensitivity data.

3.7 Discussion

This study investigated the possibility of extracting a good quality and quantity DNA from formalin-fixed tissues. In addition, the potential of sequencing the formalin fixed genomic DNA using the gold standard Sanger sequencing and Next Generation sequencing was investigated. In order to achieve this, an in-house and cheap method was developed to obtain large amounts of DNA with high purity, large fragment size and PCR products up to 400bp through using proteinase K digestion and heat treatment along with Chelex-100. The final method (iCH-120) described in this study provides a better and cost-effective system compared to the commercial QIAgen DNA extraction kit. This method, also, showed efficiency in extracting DNA from tissues that had been preserved in formalin for up to two years. Although treatment with UDG resulted in the removal of deamination incidences, alternative corruptions can arise. Even with the gold standard Sanger sequencing and cloning methods, there were still variants that appeared in most of the transcripts making determination of real rare variants from artefacts very difficult. In addition, it was demonstrated that NGS from formalin-fixed materials was successful and when the joint variant calling and VQSR pipeline along with the Phred Q score of 30 (Q30) were applied, high call specificity was obtained compared to the single calling with hard filtering, Q10 and Q20 systems. Conversely, sensitivity of calls ranged between 55% to 73% and therefore there would still be a chance of concluding false positive or false negative variants for inherited genetic defects using NGS on formalin-fixed tissues, but at the same time NGS provides more reliable data compared to the Sanger sequencing.

The rationale behind this study was to investigate whether it was possible to carry out genomic studies on long-term formalin-fixed archival human tissues, as this could be useful for the archival hypoplastic left heart syndrome hearts that were phenotyped in the previous chapter (Crucean, Alqahtani et al., 2017). Previously, there was a genomic study carried out on 31 formalin-fixed malformed hearts with either hypoplastic left or right ventricles (Reamon-Buettner et al., 2008). This study showed that 24/31 hearts had a deletion of G at position 376 in *HAND1* gene, causing a frameshift in the amino acid sequencing beginning at Alanine 126 in the basic Helix-Loop-Helix domain of *HAND1*. This frameshift mutation was predicted to lead to a truncated protein that was unable to regulate combinatorial interactions (Reamon-Buettner et al., 2008). Engineering a conditional Hand1A126fs mouse allele resulted in abnormalities of cardiac outflow tract and intraventricular septum, but definitely not HLHS. Moreover, this mutation led to lethality at E14.5 (Firulli et al., 2017). It was therefore concluded that this mutation was not causative for HLHS, but more importantly, this mutation was originally identified from HLHS formalin-fixed tissues using Cycle Sequencing, which had similar principles to Sanger sequencing. However, in the current study, it was shown that formalin-fixed tissues had a high preference for G>A artefacts when normal PCR and Sanger sequencing were used (**Figure 3.13**). Since the A126fs mutation resulted from G changing to A and in the current study, the high preference of G>A artefacts were illustrated; this therefore suggests, together with the absence of HLHS in the mutant mouse and the failure to replicate this finding in other HLHS patients, that this mutation could result from formalin-induced damage rather. Moreover, as illustrated previously, when NGS was used with joint calling, with

VQSR pipelines along with the Phred quality score of 30, most of the formalin artefacts including the G>A artefacts were excluded. Therefore, NGS produces more reliable data for DNA extracted from formalin fixed tissues compared to Sanger sequencing

Next-generation sequencing (NGS) technology is a powerful tool that can quantify expression levels, map diseases and, most importantly for this study, identify de novo and rare variants (Liu et al., 2013). To call variants using NGS, several aligners and variant callers have been established and combined into various pipelines. In a typical pipeline, an aligner or algorithm is required to map the NGS reads to a reference genome, and a variant caller to recognise variant locations and then allocate a genotype to the subjects. There are several aligners that have been extensively studied including Bowtie, BWA, SOAP and mrFAST (Ruffalo et al., 2011). In this study, the widely-used aligner BWA was utilised. This is because BWA provides mappings/reads with a quality score, which can be used to remove unsupported mappings or mappings with a high number of mismatches (Ruffalo et al., 2011; Liu et al., 2013). Moreover, the variant caller used in the study was the GATK best practice (Poplin et al., 2017). The GATK has a new single-sample calling pipeline, which allows combining per-sample gVCF and performs joint analysis of a cohort at an advance stage. The advantage of involving gVCF is to record all the variant sites regardless of variant presence or not and this subsequently provides a file of every represented site, which is necessary for performing a joint call analysis at the subsequent stage. Therefore, the chosen pipeline permits performing two distinct modes in order to compare the variant calls

between the FB-DNA and FF-DNA samples. The analysis of coverage, depth, and GC content revealed some differences between the FB-DNA and FF-DNA, which were most likely to be caused by the formalin-induced damage (**Figure 3.15**). However, after filtering the data by single HC with hard filtering or joint calling with VQSR, both methods generated less formalin-induced calls, although at the expense of losing real rare variants. Although both filtering modes increased the chances of producing correct variants, the joint calling with VQSR presented high specificity (94%) and sensitivity (73.3%) compared to the single HC with hard filtering mode. Moreover, assessment of the Phred quality score (Q score) for the FF-DNA and FB-DNA samples showed that a Q score of 30 yielded the highest specificity and sensitivity of the sequencing reads. Therefore, in order to obtain the maximum reliability sequencing reads from formalin materials, it is important to consider running the GATK best practice pipeline with the joint calling and VQSR filtering mode and to assess the sequencing quality with Q30.

Comparison between the reliability of sequencing data obtained from formalin-fixed tissue by the NGS or Sanger sequencing with cloning methods revealed that NGS could generate reliable results with a limited sensitivity. However, as the sensitivity of data ranged between 55% to 73%, which leaves only between a 27% to 45% chance of inaccurate identification of variants, it seemed to be acceptable as long as further investigation follows. This includes using the gold standard Sanger sequencing and the cloning method to confirm the identified variants. The advantages and disadvantage of using both NGS and Sanger sequencing are listed in the table below (Table 3.3).

Table 3.3: list of the pros and cons of using NGS and Sanger sequencing to analyse DNA from formalin-fixed tissues.

	pros	cons
Sanger sequencing	cheap	Produce persistence variants through different clone transcripts.
NGS	Reliable data	Limited sensitivity and expensive

Overall, it is possible to extract high quality and quantity DNA from long-term formalin-fixed materials using a cheap and scalable in-house method. It was previously reported that reliable NGS data could only be obtained from tissues that had been fixed in formalin for one day (Einaga et al., 2017). However, this study proved that it was possible to extract DNA and generate a reliable NGS data using the iCH-120 method. Although it was suggested that Sanger sequencing data generated from formalin-fixed DNA could not be used to discover new rare variants, it remained useful to use the Sanger sequencing data to confirm identified variants.

3.8 Conclusion

Formalin is an effective conservative medium for biological structures, but it damages DNA by crosslinking bases, fixing proteins, generating breaks and modifying bases. However, it is still possible to extract DNA from long-term up to two-year formalin fixed tissue and carry out PCR. In this chapter, a cheap scalable method for extracting DNA from formalin-fixed tissues was described. This method allowed efficient PCR to generate at least 400bp product length and this was comparable to the leading commercial kit. Nevertheless, the extracted DNA from formalin-fixed tissue was unreliable for Sanger sequencing, as it was not possible to separate formalin artefact from, for example, heterozygosity. It might be possible to improve discrimination through next generation sequencing and paired reads. Altogether, the current study proposes that the GATK best practice pipeline, with joint calling and VQSR, and assessing with Phred quality score of 30 is a good pipeline to obtain high specificity with moderate sensitivity sequencing reads from formalin-fixed materials. Whereas, Sanger sequencing data generated from formalin-fixed DNA cannot be used to discover new rare variants, but it remains useful to confirm identified variants.

Chapter 4: Implicated Genes in Hypoplastic Left Heart Syndrome

4.1 Overview

In the previous chapter, various methods to extract DNA from formalin fixed tissues (FFT) were described. Whilst isolation of DNA from FFT can be limited by DNA degradation, crosslinking with proteins and sequence unreliability, it is still possible to extract high quality DNA using the described optimal method. However, the determination of the accuracy and reliability of DNA sequences extracted from FFT is still variable. Therefore, using FFT to identify mutations can be achieved but it raises risks of producing false positive results. Henceforth, until a further advance in technology, FFT best remain a valuable source for mutation validation studies, rather than for primary identification of mutations. In fact, there have been several studies that suggested different genes to cause hypoplastic left heart syndrome (HLHS). Therefore, the following chapter will focus on analysing all the key genes reported for HLHS and provide a complete profile for their main roles and expression during heart development.

4.2 Main suggested genes involved in HLHS

The genetic aetiology of HLHS has been supported with a growing body of evidence throughout the years. Initially, in 1971, Shokeir described a transmission pattern of autosomal recessive inheritance for HLHS after analysing 13 patients from 5 independent families (Shokeir, 1971). A couple of years later, in 1974, Shokeir provided further evidence to support his hypothesis of the autosomal recessive inheritance through describing 6 families with 15 patients diagnosed with HLHS (Shokeir, 1974). However, in 1974, Brownell and Shokeir proposed the polygenetic inheritance hypothesis based on the recurrence of HLHS in the second generation of 42 families (Brownell and Shokeir, 1976). Slightly more recently, Gerboni et al. (1993) reported an autosomal dominant inheritance of HLHS rather than polygenetic inheritance. His hypothesis was based on a study of 5 members in three generation of a single family affected with various congenital heart defects, where first degree relatives of HLHS patients had a high risk of reoccurrence (Gerboni et al., 1993). Altogether, there are three suggested transmission patterns of HLHS: autosomal recessive, autosomal dominant and polygenic inheritance. Since there are three ventricular subgroups of HLHS described in this study, this may implicate different aetiologies for different HLHS subgroups.

Over the years, several genes have been suggested to either directly cause or associate with HLHS. These genes include *GJA1* (Dasgupta et al., 2001), *NKX2.5* (Elliott et al., 2003; McElhinney et al., 2003),

NOTCH1/NOTCH3/NOTCH4 (Garg et al., 2005; Yang et al., 2017; Durbin et al., 2017), *HAND1* (Reamon-Buettner et al., 2008*), FOXC2* (Iascone et al., 2012; Yu et al., 2010; Finegold et al., 2001), *ETS1* (Ye et al., 2010), *RBFOX2* (Verma et al., 2016) and *PCDHA13/SAP130* (Liu et al., 2017). Consequently, evaluation of these gene expressions during heart development will be discussed.

4.3 Limitation and restriction of involved genes

There are 15 genes that have been implicated in HLHS. This section will focus on discussing the main roles of the suggested genes for HLHS and describe the core mutations found in these genes.

4.3.1 *GJA1*

In normal heart development, *GJA1*, encoding connexin-43, is abundant and found in myocytes of ventricles and atria (Michela et al., 2015). The gap junction protein, connexin 43 (Cx43), is located at the intercalated disk; which are found at the longitudinal ends of cardiomyocytes, allowing intercellular communication between cardiomyocytes and metabolic interchange between contiguous cells (Dermietzel et al., 2000). Also, *Cx43* is essential for ensuring accurate regulation of vascular tone, cardiac rhythm, and endothelial function (Iwasaki et al., 2011). With all of these central roles in cardiac tissues, *GJA1* is one of the key genes in cardiomyocyte development. Homologous deletion of *Gja1* in mice causes death at birth due to stenotic pulmonary artery and hypertrophy of the ventricular outflow tract (Dermietzel et al., 2000).

Variations in *GJA1* were the first to be proposed to cause HLHS, as four substitution variations (2 missense and 2 polymorphisms) were identified in 8 children out of 14 cases diagnosed with HLHS (Dasgupta et al., 2001). However, Huang et al. (2011) carried out a screening study of 300 patients with various congenital heart defects (CHD) including four cases with HLHS. This screening study revealed that none of the previous suggested *GJA1*

variants were found, although two novel variants were identified. These two variants were then recreated as *Gja1* knock-in mice, to assess the relevance of these point mutations in CHD. However, the knock-in mice showed normal lifespan with no CHD. Therefore, both screening and knock-in model studies showed that mutations in *Gja1* gene were less significant for CHD in general and HLHS in particular. Overall, *GJA1* plays important roles in the cardiovascular system through regulating endothelial function and intercellular communication in ventricles (Huang et al., 2011). Although the suggested mutations in *GJA1* showed no cardiac abnormalities, *GJA1* remains an important gene that may be indirectly contributing to the ventricular cardiomyopathy observed in HLHS.

4.3.2 *NKX2.5*

NK2 homeobox5 (*NKX2.5*) is one of the critical cardiac transcription factors during cardiogenesis (Stanley et al., 2002; Akazawa and Komuro, 2005). Expression of *NKX2*.5 is abundant in the early cardiac progenitor cells of the first and second heart fields, which support a role in differentiation of myocardial lineages (Dupays et al., 2019). In addition, the fact that *NKX2*.5 is expressed in specialised myocardial conduction cells indicates a core role for *NKX2*.5 in conduction system development (Akazawa and Komuro, 2005). During embryogenesis, *NKX2*.5 is involved in cardiac morphogenesis through regulating rightward looping, consequent specification and septation of the chambers, and in functional maturation and maintenance of ventricular cardiomyocytes (Stanley et al., 2002). During adulthood, *NKX2*.5 is involved

in maintaining the homeostasis of cardiomyocytes (Akazawa and Komuro, 2005). More recently, *NKX2*.5 was found to play a direct role in the formation of atrioventricular junction through modulating BMP signalling by suppression of *Furin,* which is a secretory proprotein convertase (Dupays et al., 2019). Knockout mouse model of *Nkx2*.5 demonstrated disrupted growth and chamber specification as well as severe impaired regulatory transcriptional network during embryonic cardiogenesis, and eventually caused early embryonic lethality (Furtado et al., 2016). Therefore, *NKX2*.5 is a fundamental gene to ensure a normal cardiac formation.

Variations in *NKX2*.5 were initially suggested to cause HLHS by Elliott et al. (2003), as a missense mutation was found in one child out of 18 patients with HLHS (included both sporadic and familial cases; Elliott et al, 2003). McElhinney et al. (2003), likewise, reported a missense *NKX2*.5 mutation that was found in one patient out of 80 cases diagnosed with left-sided cardiac lesions included HLHS (McElhinney et al., 2003). Although the significance of this mutation was not clear, it was suggested to cause impairment of *NKX2*.5 protein dimerization leading to lower its ability to monomeric or dimeric DNA binding sites (McElhinney et al., 2003). However, the study of Esposito et al. (2011) on cardiac tissues of 24 HLHS patients identified no *NKX2*.5 mutations speculating that somatic *NKX2*.5 mutations were not the cause of HLHS (Esposito et al., 2011). Altogether, although these studies showed conflicting views on the importance of *NKX2.5* for HLHS, the significance of *NKX2*.5 during cardiac development makes it a possible contributor to HLHS.

4.3.3 NOTCH family

The NOTCH signalling pathway was firstly described by Morgan more than 90 years ago (Morgan and Bridges, 1916; Zhou and Liu, 2014), and ever since it has been well-documented to be a phylogenetically conserved signalling pathway (Borggrefe and Oswald, 2009). The NOTCH family consists of four genes (*NOTCH1, NOTCH2, NOTCH3*, and *NOTCH4*) encoding type 1 transmembrane proteins, that share similar structural properties with one another (Zhou and Liu, 2014). This section will discuss *NOTCH1*, *NOTCH3* and *NOTCH4* only, as the suggested mutations in HLHS were reported only in these genes.

4.3.3.1 *NOTCH* 1

The product of *NOTCH1* is linked to several crucial activities related to cell differentiation, proliferation, cell fate specification and survival (Zhou and Liu, 2014). *NOTCH1* is widely expressed in different organs including stomach, lungs and heart. In heart, it acts as a receptor, binding specific membrane-bound ligands including Delta1, Jagged1 and Jagged2, to regulate cell-specification processes. Therefore, the Notch1 receptor plays a major role during cardiac development through interactions with these ligands (Miazga and McLaughlin, 2009). In early cardiogenesis, *NOTCH1* modulates the timing of heart field specification, and is responsible for heart tube looping and left-right axis formation (Zhou and Liu, 2014). *NOTCH1* is also involved in valve primordia formation and trabeculation of the left ventricle (Grego-Bessa et al., 2007). Notch intracellular domain NICD1-activated mice showed several

cardiac abnormalities including atrioventricular myocardium defect, disrupted cardiomyocyte differentiation, and intraventricular septum shifting to the right. These mice then eventually died during embryogenesis (Watanabe et al., 2006). Therefore, Notch1 signalling is fundamental for proper cardiac development.

Several studies have suggested that variants in the *NOTCH1* gene are associated with HLHS. Garg et al. in 2005 reported the first *NOTCH1* variant, a frameshift mutation (H1505del), that proposed to cause bicuspid aortic valve (BAV) identified in a HLHS patient with a family history of different congenital heart diseases (Garg et al., 2005). Another three variants affecting the coding region of *NOTCH1* were identified in patients with HLHS along with other left ventricular outflow tract (LVOT) malformations including BAV (McBride et al., 2008). These variants were $NOTCH1^{G661S}$, $NOTCH1^{A683T}$, and $NOTCH1^{A1343V}$. Assessment of ligand-induced Notch1 activity by comparing the Notch1-dependent signalling induced by JAGGED1 between wild-type *NOTCH1* and mutant *NOTCH1* showed that the first and second variants significantly changed the level of JAGGED1-induced activation (McBride et al., 2008). However, the $NOTCH1^{A1343V}$ variants, which was present in controls and patients at similar rates, showed no significant difference in JAGGED1-induced activation level. This observed reduction in the ligand-induced signalling by $NOTCH1^{G661S}$ and $NOTCH1^{A683T}$ variants was speculated to cause the aortic valve defects observed in the patients through haploinsufficiency for the NOTCH1 receptor, which suggesting that Notch

signalling levels must be tightly regulated and sight changes to its activity level could cause abnormalities in the heart.

In another study, 53 HLHS patient; characterized according to Tchervenkov et al. 2006 classification of HLHS; were analysed (Iascone et al., 2012). It was reported that there were two *NOTCH1* de novo variants; one splicing (p.Asp1790Asp) and one frameshift (p.Gly1476Asp) identified in 30/53 HLHS patients (Iascone et al., 2012). Although the biological significance of these variants was unclear, it was suggested that the NOTCH1 signalling pathway might be implicated in HLHS, at least in the valve malformations observed in the syndrome. More recently, a novel *NOTCH1* germline frameshift/stop-gain mutation was identified in a HLHS patient with family history of both HLHS and hypoplastic right heart syndrome (HRHS). This study proposed that there is a strong association between *NOTCH1* mutations and HLHS based on the identification of this variant in multiple family members (Durbin et al., 2017).

According to animal studies, mutations in *NOTCH1* have been linked to impaired endothelial mesenchymal transformation (EMT) during early stages of valvulogenesis (Timmerman et al., 2004). Knocking out a large portion of *NOTCH1* gene in mice showed reduce ability to form endocardial cushions through EMT leading to hypoplastic endocardial cushions (Andersen et al., 2014; Timmerman et al., 2004). This illustrated that *NOTCH1* plays an important role during cardiovascular development, and mutations in this gene could promote cardiac defects including HLHS.

NOTCH1 signalling pathway is one of the most important pathways for heart development. Although there have been several *NOTCH1* mutations associated with congenital heart defects including HLHS, BAV and HRHS, none of these mutations were actually proved to be pathogenic or most importantly to cause HLHS.

4.3.3.2 *NOTCH3*

NOTCH3 receptors are located at the surface of vascular smooth muscle cells (VSMC) or pericytes that found around blood vessels and it has been reported that they play an important role in VSMC maturation and differentiation (Joutel et al., 2010). NOTCH3 receptors also have been implicated in the development of pulmonary artery SMC, as it involves in different cell activities including survival and function of vascular smooth muscle cells (Li et al., 2009). Expression of *NOTCH3* was detected in late embryonic brain tissue, and in most of the organs during adulthood, particularly the vagina. Interestingly, unlike *Notch1* knockout mouse models, homozygous *Notch3* mutant mice showed normal embryonic growth; and were fertile and viable in adulthood; suggesting that *Notch3* is not essential for mouse embryonic development (Krebs et al., 2003).

Mutations in *NOTCH3* have been associated with pulmonary arterial hypertension and cerebral autosomal dominant arteriopathy with subcortical infarcts and leukoencephalopathy (CADASIL). However, recently, a mutation in the *NOTCH3* coding region (exon 11: c.A1766C:p.Q589P) was reported in (3/5) induced pluripotent stem cells (iPSC) from HLHS patients (Yang et al.,

2017). Inducing this mutation to the iPSC derived from patient fibroblasts, which were differentiated to cardiomyocytes, enhanced the ability of these cell to differentiate into SMC, leading to disorganised sarcomeres and sarcoplasmic reticulum, and reduced beating rate. Consequently, it was suggested that mutations in *NOTCH3* could cause dysfunction of the left ventricle, leading to HLHS. Thus, *NOTCH3* might be a good candidate for HLHS.

4.3.3.3 *NOTCH4*

NOTCH4 is the most specific receptor as it is almost solely expressed in the vasculature, whereas other *NOTCH* family genes are found in most tissue types (James et al., 2014: Uyttendaele et al., 1996). *NOTCH4* plays a minor role in angiogenesis in embryos. Since *NOTCH4* is the least studied receptor, it is the least understood in term of its potential functions and signalling (James et al., 2014). Similar to homozygous *Notch3* mutant mouse model, *Notch4*-knockout mice showed no obvious mutant phenotype, indeed they were fertile and viable (Krebs et al., 2000).

Recently, there were three *NOTCH4* novel mutations (exon1:c.33_44del: p.11_15del, exon1:c.17_28del:p.6_10del and exon18:c.G2834A:p.C945Y) that were identified in (4/5) induced pluripotent stem cells (iPSC) from HLHS patients (Yang et al., 2017). These mutations were reported to reduce differentiation into mature cardiomyocytes and mesodermal cells and were speculated to subsequently diminish left ventricular growth and eventually lead

to dysfunctional left ventricle (Yang et al., 2017). Therefore, *NOTCH4* could have a potential association with HLHS.

4.3.4 *HAND1*

HAND1 is basic helix-loop-helix (bHLH) transcription factor of the Twist family (Vincentz et al., 2011). *HAND1* has an important role during cardiac morphogenesis. During cardiac looping in mice, *HAND1* is predominantly expressed in the outer curvature of the left ventricle and the myocardial cuff of the outflow tract suggesting its role in the expansion of chamber myocardium (McFadden et al., 2005). Also, *HAND1* was documented to modulate the morphogenesis of endocardial cushion through a myocardium-derived signal (McFadden et al., 2005; Barnes et al., 2010). Targeted mutation of *Hand1* in mice causes lethality of embryos at E8 to E8.5 with severe placental and extraembryonic membrane defects. This therefore reflects the important role for *Hand1* in differentiation of trophoblast and hence in embryogenesis (McFadden et al., 2005).

Mutations in *HAND1* have been implicated in congenital heart defects, including HLHS and tetralogy of Fallot (Reamon-Buettner et al., 2009). A frameshift mutation (A126fs) in the bHLH domain of *HAND1* was reported in 24 of 31 formalin-fixed hypoplastic left ventricles (Reamon-Buettner et al., 2008). This mutation resulted in a truncated and premature protein that is dysfunctional (Reamon-Buettner et al., 2008). However, modelling of the A126fs mutation in mice was embryonic lethal at E14.5, as mutant mice showed abnormalities in cardiac outflow tract, ventricular septal defect, and

thin myocardium; but at the same time they showed normal sized left ventricular chamber. This therefore suggested that this mutation did not cause HLHS, but instead it caused a dominant negative function of the vital *Hand1* role during cardiogenesis (Firulli et al, 2017). It is important to note that this mutation could be a consequence of formalin-induced changes to DNA, as it was originally identified in formalin-fixed paraffin embedded tissues of patients with hypoplastic left or right ventricles (Reamon-Buettner et al., 2008; chapter 4). Overall, *HAND1* plays a major role during embryogenesis in general and carcinogenesis in particular, hence it remains a candidate for HLHS despite having no definitive evidence.

4.3.5 *FOXC2/FOXL1*

The FOX gene family comprises of 50 members identified in human genomes and at least 43 members found in the mouse genome (Jackson et al., 2010). Several functions have been associated with the *FOX* gene family including modulation of cell senescence or proliferation, development of different organs, and metabolic homeostasis (Jackson et al., 2010). This section will only focus on the members of *FOX* family that have implicated in HLHS; *FOXC2* and *FOXL1*.

A great deal of attention has been paid to *FOXC2*, as it is closely related to FOXC1 transcription factor and both have important roles in heart formation (Kume et al., 2001). During embryonic development, *FOXC1* and *FOXC2* share similar expression patterns in overlapping domains in various tissues, suggesting complementary functions. In the heart, *FOXC2* is localised to

endothelial cells and neural crest cell-derived endocardial cushions (Seo and Kume, 2006). Likewise, *FOXL1* expressed in epithelial cells, mesoderm underlying the endoderm, in the mesenchyme of the palate, and in the lung (Wotton et al., 2008). It has been shown that the null mutation of *Foxc2* in mice leads to perinatal lethality, a skeletal malformation, lymphatic system defects, as well as severe cardiovascular defects including ventricular septal defects and aortic arch patterning defects (Iida et al., 1997; Uddin et al., 2015). However, the deletion of *Foxl1* in mice caused a delay in gastric gland and intestinal villi formation during foetal development and in adulthood, with the mice exhibiting gastric mucosa and intestinal villi hypoplasia (Takano-Maruyama et al., 2006). This therefore indicates that *FOXC2* has roles during heart development, whereas the role of *FOXL1* in the heart remains unclear.

It was reported that deletion of *FOXC2* and *FOXL1,* along with *FOXF1,* which were located close to each other on the same chromosome, in patients caused HLHS along with other distinct malformations including lung developmental disorder, urinary tract malformations, and gastrointestinal atresia (Stankiewicz et al., 2009). In addition, a de novo deletion of chromosome 16q24.1-q24.2 that contained the *FOXC2* gene was suggested to cause HLHS along with several other malformations, including polyhydramnios, pleural effusion and bilateral hydronephrosis, in a new born male baby (Yu et al., 2010). However, a study conducted by Iascone et al. (2012) based on screening 53 well-characterized HLHS patients showed no contributory effect of *FOXC2* and *FOXL1* on underdevelopment of the left ventricle in the HLHS patients (Iascone et al., 2012). Whilst *FOXL1* and *FOXC2* were both suggested to

associate with HLHS, it is still unclear how these genes were implicated during heart development. However, since *FOXC2* null mice showed defects in the heart but not *FOXL1* knock out mice, this suggests that *FOXC2* may be a better candidate for association with HLHS than *FOXL1*.

4.3.6 *SMAD3*

The protein encoded by *SMAD3* belongs to the SMAD family, which are intracellular proteins that transmit extracellular signals from the cell surface to the nucleus for activation of downstream transcription (OMIM: 603109). The signal transducer, SMAD3, acts through the transforming growth factor-beta (TGF-β) signalling pathway and plays an essential role in both cardiac and renal fibrosis (Liu et al., 2016). *SMAD3* is expressed in ovary, thyroid and heart. In heart, it was found to regulate formation of cardiac fibroblasts (Euler-Taimor and Heger, 2006). Knocking out *Smad3* in mice resulted in aortic aneurysms, colonic dilation, and renal fibrosis (Zanninelli et al., 2006).

Variants in *SMAD3* have been associated with several disorders including aneurysms-osteoarthritis syndrome, Loeys-Dietz Syndrome 3, and leukaemia (Van de Laar et al., 2011; Walfraim et al., 2004). Recently, a single study proposed an association of *SMAD3* with HLHS. A novel variant in *SMAD3* (c.3G>A, p. Met1Ile) was reported in a 14-year-old boy who was born with HLHS and developed progressive aortic aneurysm after completing staged palliation (Fitzgerald et al., 2014). However, this *SMAD3* variant was also found in two family members of the proband, although both had normal echocardiography and magnetic resonance angiography (MRA) with no

evidence of osteoarthritis (Fitzgerald et al., 2014). Therefore, it seems less likely for *SMAD3* to be associated with HLHS.

4.3.7 *TBX5*

The T-box transcription factor, *TBX5*, is a member of a large T-box family of transcription factors that plays a role in forelimb formation and identity as well as in cardiac development (OMIM: 601620). *TBX5* is expressed in retina, forelimb buds and heart. In early heart development, *TBX5* is found in the precardiac mesoderm, then becomes limited to the posterior region of the looping heart tube. After the specification of the cardiac chambers, *TBX5* is expressed in the atria, the left ventricle and the ventricular septum. Targeted mutation of *Tbx5* in mice ($Tbx5^{del/del}$) demonstrated cardiac and forelimb abnormalities that caused severe hypoplastic posterior domains during carcinogenesis. Interestingly, although these *Tbx5*-deficiency mice die during embryogenesis, they demonstrated that *Tbx5* is not important for heart formation; but rather in programming cardiac development particularly heart chamber patterning (Bruneau et al., 2001; Bimber et al., 2006).

Dominant mutations in *TBX5* have been associated with Holt–Oram syndrome, a developmental abnormality, which often includes cardiac defects including isolated atrial and ventricular septal defects, conduction system defects and HLHS (Steimle and Moskowitz, 2017). The association of HLHS with *TBX5* mutations resulted from reviewing the spectrum of cardiac defects reported in 240 patients with Holt-Oram syndrome and additional cases reported in literature (Bruneau et al., 1999). There was not enough evidence

to show that the reported case was HLHS, and not speculation of HLH. Therefore, *TBX5* seems less significant for HLHS since there is little evidence to link *TBX5* to HLHS.

4.3.8 *ETS1*

ETS1 belongs to the ETS family of transcription factors, which are known for their essential roles in different cellular functions, vascular development and angiogenesis, and cardiovascular development (Ye et al., 2010). Expression of *ETS1* is predominantly found in the lymphoid organs and brain. A murine expression study showed that *Ets1* expression increased after embryonic implantation and during organogenesis. However, in foetal stages, *Ets1* expression becomes restricted to the lymphoid tissues, branching organs, and brain (Kola et al., 1993). Expression of *Ets1* was also detected in embryonic heart, particularly in the neural crest cells and endocardium of developing mouse heart (Ye et al., 2010). The first implication of *Ets1* in heart development came from non-mammalian species such as chicks, frogs and fruit flies (Lie-Venema et al., 2003). Years later, the role of *Ets1* in mammalian heart development was demonstrated through deletion of *Ets1* in mice (Ye et al., 2010). This study showed that loss of *Ets1* functions caused impaired ventricular development (non-apex forming left ventricle), membranous ventricular septal defects, and mostly led to embryonic lethality.

Chromosomal microarray mapping of three patients with Jacobsen syndrome and heart defects, such as ventricular septal defects; double outlet right ventricle; and HLHS, *ETS1* gene was identified as a potential causative gene

for the heart defect observed in these patients. Based on the *Ets1* knockout mouse model, which showed underdevelopment/non-apex forming left ventricle, and expression of *Ets1* during heart development; it was suggested that *ETS1* was associated with HLHS (Ye et al., 2009). This, therefore, suggested that *ETS1* plays a critical role during heart development and manipulating its function could lead to congenital heart defects such as HLHS. Hence, *ETS1* might be a good candidate for HLHS.

4.3.9 *PCDHA9/SAP130*

PCDHA9 is a member of a 15 superfamily protocadherin alpha gene cluster that has similar genomic organization to B-cell and T-cell receptor gene groups (OMIM: 606315). The *PCDHA9* gene is an integral plasma membrane protein with a critical role in the formation and function of cell-cell communications (Wu and Maniatis, 1999). Over the years, the *PCDHA9* gene has been associated with different defects including autism, a dysfunctional nervous system and brain disorders (Anitha et al., 2013; Kohmura et al., 1998). Accordingly, expression of *PCDHA9* was reported in several brain tissue types during adulthood, including the forebrain and cerebellum (Kohmura et al., 1998), which supported the association between *PCDHA9* mutations with several brain disorders. Only recently, the expression of *Pcdha9* was studied in mouse heart. Whilst *Pcdha9* expression was reported to be weakly expressed in the developing heart ventricle and atrium at E9.5 (Liu et al, 2017), no specific role has been determined for this gene in the cardiovascular system.

The histone deacetylase subunit, *SAP130*, is a member of the SIN3A co-repressor complex, which functions as a transcriptional repressor or regulates interactions between the complex and another regulatory complex (Fleischer et al., 2003). There is limited information about the roles of *SAP130*, although it was reported to promote oncogenesis and tumorigenesis (Wardwell-Ozgo et al., 2014). Analysis of the expression pattern of *Sap130* in mice using Sap130-lacZ knockout (KO) showed ubiquitous expression of *Sap130* throughout the whole developing embryo (Liu et al, 2017). Moreover, homozygous and heterozygous mouse knockout of *Sap130* demonstrated peri-implantation lethality and hence suggesting its significant role in embryogenesis (Liu et al, 2017). Although *SAP130* was reported to be expressed in the developing heart, its specific roles during cardiogenesis remains unknown.

Recently, both *PCDHA9/SAP130* genes were implicated in the congenital heart defect, HLHS (Liu et al, 2017). Based on a large-scale analysis of ethylnitrosourea mutagenesis in mice, which aimed to recover mutations resulting in congenital cardiac defects, Cecelia Lo's group recovered eight mouse strains with a HLHS-related phenotype (Figure 4.1 A) (Liu et al., 2017; Benson et al., 2016). From screening these mice, it was suggested that HLHS was caused by digenetic interactions between *Pcdha9* and *Sap130* although this combination of genes was only seen in one mouse of the original recovered strains. It was also suggested that mutations in *Pcdha9* but not in *Sap130* resulted in a normal left ventricle size but a dysplastic aorta, whereas mutations in *Sap130* caused hypoplasia in the left ventricle. Therefore, combination of both genes together was required to cause all HLHS features

(Liu et al., 2017). However, the obtained phenotype from the proposed HLHS digenic model revealed a well-recognised, but rare form of double-outlet right ventricle (DORV) with both great arteries (aorta and pulmonary) arising from the right ventricle and intact ventricular septum (Figure 4.1 B) (Chaudhry et al., 2019). In addition, linking this finding to human HLHS patients revealed that one out of 68 HLHS patients had the rare mutations in *SAP130* and in *PCDHA13*, which was proposed to be homologous to *Pcdha9* identified in HLHS mice (Liu et al., 2017). Altogether, although a digenic model for HLHS was proposed, the interaction between these two genes was not necessarily causing HLHS; as a range of other cardiac malformations were also found (Cecilia et al., 2019). This included double-outlet right ventricle (DORV), aortic arch anomalies, outflow tract malalignment defect, and hypoplastic RV with tricuspid hypoplasia (Liu et al., 2017). Therefore, considering the multiple abnormalities that can arise from the interaction between these genes and the lack of homologous protocadherin mutations between humans and mice, suggested less significant roles for these genes in causing HLHS. However, for the purpose of this study, it is still important to identify *SAP130* and *Pcdha9* expression pattern in heart in order to understand their role during heart development.

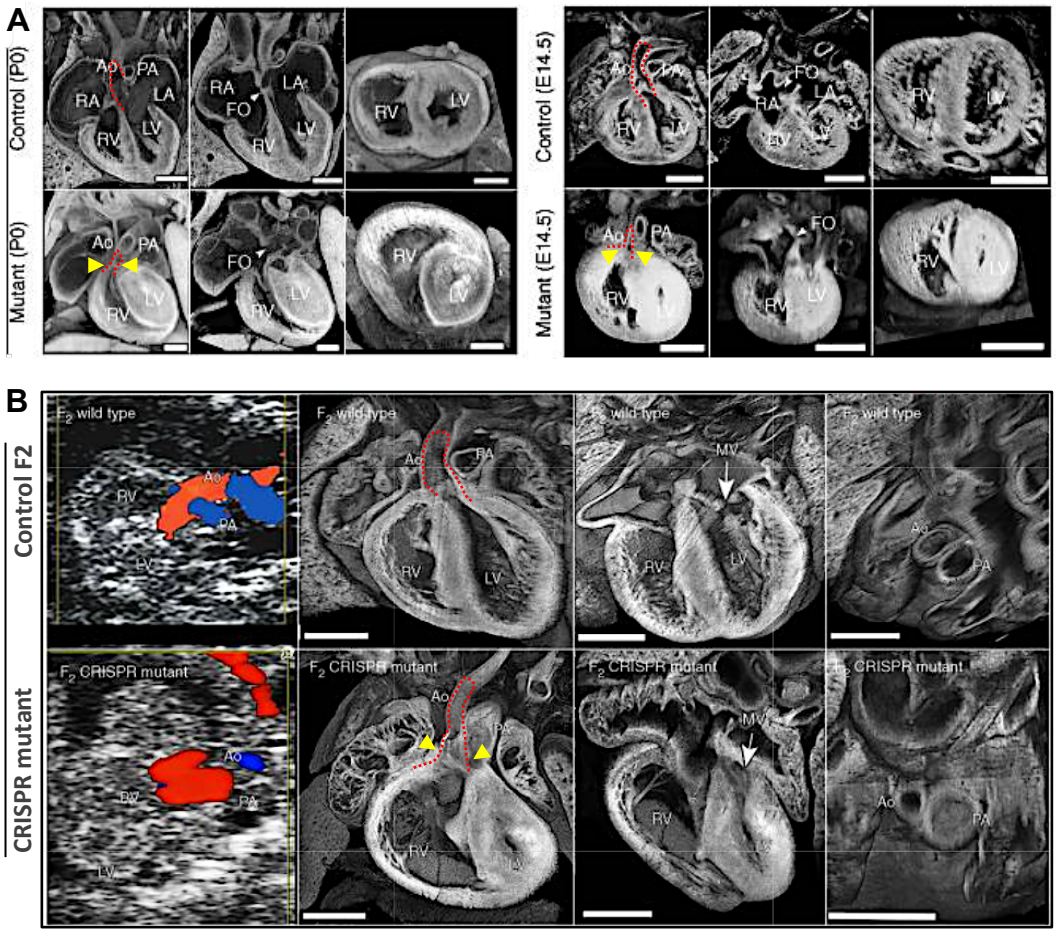

Figure 4.1: The proposed HLHS digenic model.
(A) The recovered mutant mouse line for a HLHS-related phenotype at P0 and E14.5. The mutant showed both aorta and pulmonary arteries connected to the right ventricle (red dashed lines: aorta, yellow arrows: connection point). Also, thickening in the left ventricular wall, which could be resulted from blocking blood flow though the transposition of aorta to the right ventricle. (B) CRISPR–Cas9 mutant of *Sap130*$^{m/m}$; *Pcdha9*$^{m/m}$ mouse model. The generated mouse model for the proposed genes also showed no HLHS features, instead it showed double-outlet right ventricle (DORV) phenotypes, as the aorta demonstrated right ventricular connection (Red dashed line). Images obtain from (Liu et al, 2017).

4.3.10 *RBFOX2*

RNA binding protein FOX2 or *RBFOX2* is a binding protein with high affinity for (U)GCAUG-rich sequences. One of the critical functions of *RBFOX2* is to control alternative splicing events, which are important for pluripotent stem cell differentiation and epithelial to mesenchymal transition during heart development (Venables et al., 2013). *RBFOX2* is widely expressed in brain, muscles, neurons and various progenitor cells (Partridge and Carter, 2017). Experimental non-mammalian model of *rbfox*-deficient in zebrafish exhibited severe abnormalities in heart, including decreased heart rate and myofibrillar disarray, and skeletal muscles that led to embryonic motility loss (Conboy, 2016). Also, conditional deletion of *Rbfox2* in mice caused an alternative splicing event that led to brain developmental disorders. Moreover, downregulation of *Rbfox2* in mice led to pressure overload that induced heart failure (Wei et al., 2016).

In a large cohort of congenital heart defect patients, *RBFOX2* was recognised as a key risk allele for HLHS, as three de novo loss of function mutations (splice site, nonsense and frameshift mutations) in *RBFOX2* and one de novo copy number loss *RBFOX2* mutation, were identified in four CHD proband with HLHS (Homsy et al., 2015). However, there were various speculations regarding the effect of each mutation. For example, the splice site mutation was predicated to include around 1.6kb of intron 10, which could lead to nonsense-mediated decay (NMD) of the *RBFOX2* mRNA. Similarly, the frameshift mutation was also predicted to induce a stop codon that would

eventually result in NMD of *RBFOX2* mRNA (Homsy et al., 2015). The effect of the de novo nonsense mutation (281 C>T), which was reported previously by Homsy et al (2015), was investigated. It was found that expression and localisation of Rbfox2 in cardiomyocytes of HLHS patient right ventricles (RV) was predominantly cytoplasmic with low level expressions in nucleus, compared to cardiomyocytes of RV controls that showed equal expression Rbfox2 in both the nucleus and cytoplasm (Verma et al., 2016). In addition, the effect of this mutation on protein levels was measured in cells infected with Rbfox2 nonsense mutation, using Western blotting with a Rbfox2 antibody. This showed that the Rbfox2 protein in the Rbfox2 mutant cells had ~3KDa reduced molecular weight compared to Rbfox2 wild type cells. Moreover, examination of transcriptome changes in HLHS RV patients revealed that the majority of transcripts in patients identified as Rbfox2 targets implicating its important function in RNA/protein metabolism. Therefore, it was suggested that the *RBFOX2* nonsense mutation resulted in incomplete formation of the *RBFOX2* C-terminal, leading to protein truncation and impair subcellular distribution, which affected its function in RNA metabolism contributing to early changes in transcriptome observed in HLHS patients (Verma et al., 2016). Overall, both studies highlighted the significance of *RBFOX2* mutations in HLHS, as these mutations resulted in major effects on *RBFOX2* functional protein. Therefore, *RBFOX2* seems to be a good candidate gene to investigate its relevant to HLHS.

4.4 Expression of HLHS-implicated genes in the relevant regions of the developing heart

The majority of the suggested genes seems to have a strong associated with HLHS. Therefore, the expression patterns for genes with strong significant for HLHS will be investigated in respect to the specific structures that are affected in HLHS.

All HLHS cases involve abnormalities in the development of the left ventricle and its communicating valves. These abnormalities might happen during the primary development of these regions and lead to the predominant malformations observed in the left side of the heart in HLHS patients. Alternatively, HLHS could occur in the window after the heart has formed, which at embryonic day E15.5 or Carnegie Stage CS23 (week 8), but before 15 weeks, when HLHS is earliest diagnosed antenatally (Hunter et al., 2003; Andrews et. al., 2004). This is important because it brings the argument of intact ventricular septum in HLHS patients, which means abnormalities in HLHS may occur after the completion of septation (Grossfeild et al., 2019). In order to address these possibilities, it is important to specifically identify the crucial stages involved in the development of the main affected regions including the left ventricle, aortic valve and mitral valve.

Since there is a window from the beginning of heart formation (week4) through ventricular and valve formation and development, and after septation to the time of HLHS diagnosis (week 15), HLHS can occur at any stage during this

period (Figure 4.2). Therefore, the stages between week 4 to week 15 will be investigated.

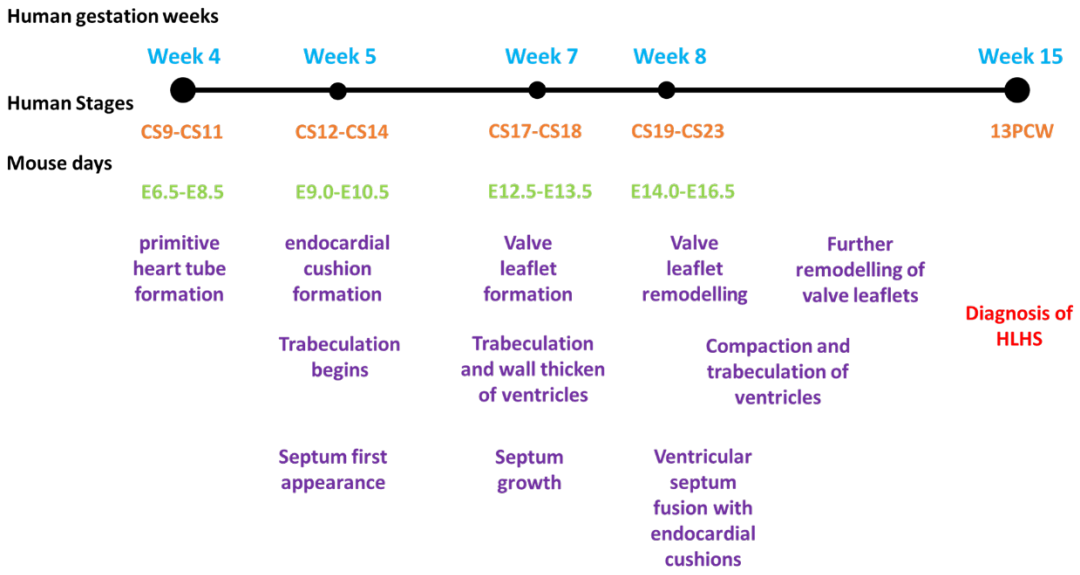

Figure 4.2: Main developmental stages in human and mouse for HLHS. CS: human Carnegie stages, E: mouse embryonic days, PCW: postconceptional weeks.

The initial formation of the primitive heart tube begins at week 4 (CS9-CS11 in human and E6.5-E8.5 in mouse), where cardiac progenitor cells undergo an epithelial to mesenchymal transition (EMT) in order to migrate and establish a cardiac crescent (Hunter et al., 2003). Through several signals and induction of cardiac transcription factors, the cardiac crescent folds and fuses at the midline forming a primitive cardiac tube, which swiftly begins to bump blood. The cardiac tube is composed of an outer myocardial layer surrounded by an inner endocardial cell layer and in between an extracellular matrix filled cardiac jelly (Vincent and Buckingham, 2010). As embryo development progresses, the heart tube suspends in the developing pericardial cavity where it

undergoes a rightward looping process causing the developing chambers to be placed into their adult positions (Kelly et al., 2014). After the poorly understood looping process and expansion of myocardium, the heart tube develops four-recognisable chambers at week 5 (CS12-CS14 and E9.0-E10.5). At the same time, the endocardial cells of the cardiac tube undergo EMT process to invade into the cardiac jelly, particularly at the proximal outflow tract and the atrioventricular canal, and initial the formation of endocardial cushions. The mitral valve is formed by the atrioventricular cushion and the aortic valve forms at the distal part of endocardial cushions located in the outflow tract (Henderson et al., 2018). After several developing processes and by week 7 (CS17-CS18 and E12.5-E13.5), the aortic three-leaflet and mitral two-leaflet valves are formed and permits unidirectional blood flow. However, by these stages, these valves have not matured yet, as they resemble solid bulky structures. Thus, over the later stages, the cushions grow and remodel to start forming mature valves with thin leaflets from CS19-CS23 and E14.0-E16.5 to Birth (Geng et al., 2017). By these stages E15.5, the ventricular septum has completely formed, and the left ventricular chamber becomes thickly packed with trabecular meshwork, in which the left ventricle can be distinguished from the right ventricle (Captur et al., 2016; Moorman et al., 2003). Therefore, all the highlighted developmental stages are essential for normal heart development and understanding the key genes for cardiogenesis may reflect their implications in HLHS.

Overall, the current study focused on using mouse tissues to study expression of HLHS implicated genes in the crucial stages of developing the main effected

regions in HLHS, including the mitral and aortic valves and left ventricle. Hence, mouse embryos at E10.5 were used to illustrate the expression pattern of the selected genes in the early stage of cushions (future valves) and ventricular developments. Also, in order to illustrate the roles of these genes during the remodelling of cushions to valve leaflets, E13.5 stage was selected. Finally, to understand these gene roles in further remodelling of valves into thin leaflets and after the completion of ventricular septum, E15.5 was selected. Thus, the expression of HLHS-implicated genes will be investigated in the mouse embryonic stages: E10.5, E13.5 and E15.5.

4.5 Aims of this chapter

Several genes have been described to be associated with HLHS. However, none of the mutations in these genes were confirmed as being pathogenic and a clear mechanism underpinning the development of HLHS delineated (Liu et al., 2017, Firulli et al., 2017). Therefore, this chapter intends to discuss the most significant genes for HLHS with respect to their potential functions and expressions during heart development. Although some of these gene expression patterns have been described previously, they have not been investigated in respect to the specific structures that are affected in HLHS neither been linked to HLHS subgroups.

To achieve this, this chapter will:

- Identify the expression pattern of HLHS-implicated genes in the mouse heart at various developmental stages including E10.5, E13.5 and E15.5 using *in situ* hybridisation
- Critically analyse the HLHS-implicated genes in HLHS based on these expression patterns and the published literature.

4.6 Materials and methods

4.6.1 Mouse lines

All mouse embryos used in this project were from the outbred CD1 mouse line to provide genetic diversity. Embryos were collected at embryonic days (E) 10.5, E13.5 and E15.5.

4.6.2 Paraffin wax embedding of mouse tissues

All collected embryos were fixed at 4°C in 4% paraformaldehyde made in DEPC water. Based on the embryo age, wax embedding time was altered (Table 4.1). All solutions used in the fixation and embedding processes were made in DEPC water.

Table 4.1: Steps for embryo paraffin wax embedding processes

	E10.5	E13.5	E15.5
4% PFA at 4°C	1 night	2 nights	2 nights
50% EtOH Shaking at RT	30 mins	2 hours	3 hours
70% EtOH (x2) Shaking at RT	30 mins 30 mins	2 hours 2 hours	3 hours 3 hours
Embryos could be stored at room temperature			
95% EtOH Shaking at RT	30 mins	2 hours	3 hours
100% EtOH (x2) Shaking at RT	30 mins 1 hour	2 hours O/N	3 hours O/N
Histoclear (x2) Shaking at RT	15 mins 15 mins	20 mins 20 mins	30 mins 30 mins
Histoclear/Wax Heat 60-65°C	20 mins	30 mins	1 hour
Wax (x3 or 4) Heat 60-65°C	30 mins 30 mins 30 mins	1 hour 1 hour 1 hour	1 hour 1 hour 1 hour 1 hour

4.6.3 Sectioning paraffin wax tissues

Paraffin wax tissues were sectioned at 10μm thickness using Leica RM2235 manual rotary microtome (Biosystems Swaziland). Before use, microtome surface was wiped with a RNaseZap solution (Invitrogen, AM9780). Tissue sections were lined up on microscope glass slides (Marienfeld Superior, 1000612) and adhered to the slides through heating the slides with water to 37°C. The slides were then left overnight in 37°C incubator. Next day, slides were kept in fridge at 4°C.

4.6.4 RNA in situ hybridisation

The RNA in situ hybridisation experiments were conducted in an RNase-free environment at room temperature unless otherwise stated.

4.6.4.1 Glassware and solution treatments

A glass funnel, 500ml measuring cylinder, 7 glass troughs and a metal slide holder were needed. All glassware were washed in a dish washing machine and wiped with the RNaseZap solution before use. The following table summarises the preparation method for *in situ* hybridisation stock solutions (Table 4.2).

Table 4.2: Preparation method for treatment solutions.

Solution	Preparation method	Storage conditions
DEPC-H_2O	2mL Diethyl pyrocarbonate dissolved in 2L dH_2O	incubate overnight in a fumehood then autoclave

1x PBS-DEPC	200mL 10x PBS-H_2O mixed with 2mL Diethyl pyrocarbonate, topped up to 2L dH_2O	incubate overnight in a fumehood then autoclave
20x Saline Sodium Citrate (SSC)	175.3g NaCl and 88.2g Trisodium Citrate dissolved in 800mL dH_2O, adjust to pH6 then make up to 1L dH_2O	Autoclaved prior to use, and stored at room temperature
2x SSC	4ml 20x SSC diluted in 36ml DEPC-H_2O	Stored at room temperature
5x MAB	29g Maleic acid, 21.9g NaCl, 19.5g NaOH pellets dissolved in 400mL dH_2O; the pH was adjusted to 8 then the solution was topped up to 500mL dH_2O	Autoclaved and stored at room temperature
200ml 1x MABT	40mL 5x MAB, 0.2mL tween-20 mixed with 160mL dH_2O	Stored at room temperature
400ml 1x MABT	80mL 5xMAB, 0.4mL tween-20, and 320mL dH_2O	Stored at room temperature
90% ethanol	315mL ethanol mixed with 35mL DEPC-H_2O	Stored at room temperature
70% ethanol	245ml ethanol mixed with 105ml DEPC-H_2O	Stored at room temperature
50% ethanol	175ml ethanol mixed with 175ml DEPC-H_2O	Stored at room temperature
Hybridisation buffer	25ml 50% formamide, 12.5ml 5x SSC (pH6), 100µl 200 µg/mL T-RNA, 50µl 100 µg/mL Heparin, and 0.5ml 0.1% tween-20, mixed with 11.85ml DEPC-H_2O	Stored at 20^0C
Post-hybridization buffer I	200mL formamide, 100mL 20X SSC (pH6), 20mL 20%SDS, made up to 400mL with dH_2O	Incubate at 60°C, only used once.
Post-hybridization buffer II	200mL formamide, 40mL 20X SSC (pH6), 4mL 20%SDS, made up to 400mL with dH_2O	Incubate at 60°C, only used once.
2% Blocking buffer	2g blocking agent dissolved in 100mL 1xMABT	Autoclaved and stored at 4°C
AP-buffer	10mL 5M NaCl (292.5g/L), 25mL 1M $MgCl_2$ (203g/L), 50mL 1M Tris HCL pH9.5 (121.1g/L), 500µL Tween-20, made up to 500mL with DEPC-H_2O	Must be made on Day 3 of the in situ; stored at -20°C

In situ hybridization method is a three-day experiment. Table 4.3 summarises the main steps that were performed in each day.

Table 4.3: a summary of the main steps of in situ hybridization.

Day 1	Day 2	Day 3
• Hydration • Fixation • Digestion • Post-fixation • Acetylation reaction • Pre-hybridization • Hybridization	• Post-hybridization wash • Blocking • Antibody detection	• Washing • Developing • Mounting

4.6.4.2 Hydration of wax sections

The slides were placed on a metal slide holder and were immersed in the following solutions for the indicated time periods (Table 4.4).

Table 4.4: Slides hydration.

Solution	Time (minute)
Histoclear	10
Histoclear	10
100% etOH	5
100% etOH	5
90% etOH	5
70% etOH	5
50% etOH	5
1st wash with PBS-DEPC	5
2nd wash with PBS-DEPC	5

4.6.4.3 Fixation

An RNase-cleaned slide box was humidified with DEPC-PBS socked tissues. 1ml of 4% PFA-DEPC was added to each slide and incubated for 20 minutes at room temperature away from the light in the humid chamber. The slides

were washed twice with PBS-DEPC each for 5 minutes then placed back in the humid chamber.

4.6.4.4 Digestion

In order to allow an efficient probe penetration; partial tissue digestion with proteinase K was conducted. The timing was critical for this step as less digestion time would result in a weak signal and prolonged digestion periods would damage the morphology of tissues. Proteinase K was prepared by diluting 10µl of 10mg/ml proteinase K in 10mL PBS-DEPC making a final concentration of 10µg/ml. 1ml proteinase K was added to the slides and incubated for 10 minutes at 37^0C then washed twice with PBS-DEPC each for 5 minutes. The slides were placed back in the dark humid chamber.

4.6.4.5 Post-fixation

This step is crucial for fixing proteinase K-digested tissue. 1ml 4% PFA-DEPC was added for each slide and incubated for 5 minutes at room temperature away from light in the humid chamber. The slides were washed twice with PBS-DEPC each for 5 minutes.

4.6.4.6 Acetylation reaction

Acetylation reaction was conducted to reduce background noise by acetylating any positive charge in tissues. This step was performed in a fumehood. Acetic anhydride buffer was kept at room temperature for 10 minutes with continuous stirring. In a glass trough with a magnetic stirrer, 392 mL PBS-DEPC, 5.31 mL

of 7.53M TEA, 1.4 mL HCl, and lastly 1mL acetic anhydride were added. Fresh PBS-DEPC was used to wash the slides twice for 5 minutes then a final wash with DEPC-dH_2O for 5 minutes.

4.6.4.7 Pre-hybridisation

To maintain humidity, the tissue rolls were replaced with newly 2x SSC-soaked ones. 500µL of hybridisation buffer was added to each slide and incubated for 2h at 68^0C. The time period could be extended up to 12h.

4.6.4.8 Hybridisation

Hybridisation buffer was warmed up to 68^0C for 10 minutes. The probes were defrosted on ice and 1:300 dilution was prepared in the hybridisation buffer (50ng probe/200µl buffer/slide). To denature secondary structures in probes, the hybridisation mix was incubated at 70^0C for 5 minutes then immediately placed on ice. 200µl hybridisation mix was added to each slide and covered with a coverslip. The slides were incubated overnight (12h to 16h) at 68^0C.

4.6.4.9 Post-hybridisation washes

This step was crucial for controlling stringency. The post-hybridisation buffers were incubated in water bath at 68^0C for 30 minutes. The slides were covered with post-hybridisation buffer I in the oven at 68^0C for 30 minutes. The buffer was discarded, and the slides were again covered with post-hybridisation buffer I at 68^0C for further 30 minutes. The slides were then incubated in post-hybridisation buffer II for 30 minutes at 68^0C. The buffer was discarded, and

the slides were once again incubated in the post-hybridisation buffer II at 68^0C for 30 minutes. The slides were washed with 1x MABT buffer three times each for 5 minutes at room temperature.

4.6.4.10 Blocking step

The slides were kept humidified by using blue tissue rolls soaked in 1x MABT in the humid chamber. 500µl of freshly made 2% blocking buffer was added to each slide and incubated for 2h at room temperature.

4.6.4.11 Antibody detection

A piece of paraffin film was used to cover the slides and ensure even spread of antibody. 1:1000 dilution of the antibody was prepared by diluting anti-DIG AP in 2% blocking solution and supplement it with 10% goat serum. 150µL of the antibody mix was added to each slide and incubated overnight at 4^0C.

4.6.4.12 Washing

The washing step was conducted to remove excessive background and was performed at room temperature on a shaker. Table 4.5 summarises the washing steps along with the appropriate length of time.

Table 4.5: Summary of the washing step and time required.

Solution	Volume (mL)	Time (minute)
1xMABT	60	10
1xMABT	60	10
1xMABT	60	60
1xMABT	60	60
1xMABT	60	60
AP-Buffer- 1st wash	60	10
AP-Buffer- 2nd wash	60	10
AP-Buffer- 3rd wash	60	10

4.6.4.13 Developing sections

100µL NBT/BCIP solution was diluted in 5mL AP buffer for a final concentration of 20µL/mL. 0.4mL was added to each slide. The slides were incubated in humid chamber away from light with tissue soaked in AP buffer to sustain humidity. The slides were allowed to develop until blue stain was visible. When the blue stain was sufficient enough, the slides were washed in 60mL 1x PBS twice for 5 minutes. The slides were placed back in the humid chamber with tissues soaked in PBS. 500µL 4% PFA was added to each slide for fixation and the slides were incubated for 15 minutes at room temperature. The slides were washed with 1x PBS twice, each for 5 minutes at room temperature and were dehydrated with non-DEPC ethanol as indicated in table 4.6.

Table 4.6: Dehydration procedure.

Solution	Volume (mL)	Time (minute)
100% Methanol	200	5
1x PBS	200	5
1% Eosin	200	7
1x PBS	200	5
50% ethanol	200	5
70% ethanol	200	5
90% ethanol	200	5
100% ethanol- 1st	200	5
100% ethanol- 2nd	200	5
Histoclear- 1st	200	10
Histoclear- 2nd	200	10

4.6.4.14 Mounting

Histomount was used to mount slides and coverslips were placed over it. The slides were allowed to dry and stored at room temperature. Brightfield imaging was used to capture images.

4.6.5 Preparation of RNA probes

RNA probes were made either from plasmid (Notch1) or PCR (all other genes).

4.6.5.1 Probe synthesis from plasmid

The plasmid of interest was identified in the plasmid library. Synthesizing probes from plasmid involved three main steps: transformation, digestion and clean-up of digested fragments.

4.6.5.1.1 Transformation

Two LB agar plates were prepared for ligation reactions. The agar plates were supplemented with 100µg/ml ampicillin, 100µl 100mM IPTG, 50µl 20mg/ml X-Gal by spreading those on the surface of the plates and allow absorption for 30 minutes at 37^0C. Tubes containing ligation mix were briefly centrifuged and 5µl of ligation mix was added to a 1.5ml eppendorf tube on ice. JM109 High Efficiency Competent Cells were briefly thawed on ice for 5 minutes and the cells were gently mixed by flicking the tube. 50µl of competent cells were transferred to the eppendorf containing the ligation mix and mixed gently then placed on ice for 20 minutes. In a 42^0C water bath, the cells were heat-shocked for 45-50 seconds then immediately placed on ice for 2 minutes. 950µl of warm SOC medium was added to the cells and incubated shaking (approximately 150rpm) at 37^0C for 1.5 hours. The cells were centrifuged at 1000xg for 10 minutes and the pellet was resuspended in 125µl SOC medium. The cells were plated on the agar plates and incubated overnight (16h-24h) at 37^0C.

Using a sterile tip, the colonies were transferred to LB broth supplemented with 1% 100mg/ml ampicillin (a single colony per 5ml LB broth for miniprep or 50ml LB broth per colony for midiprep) and incubated overnight at 37^0C, shaking at 225rpm.

The 5ml bacterial culture was centrifuged at 3000xg for 10 minutes at room temperature, the supernatant was discarded, and the pellet was resuspended in 250µl buffer P1. The suspension was transferred to a fresh eppendorf and 250µl buffer P2 was added and mixed thoroughly by inverting the tube up and

down until the suspension turned blue in colour. This step should not exceed a 5-minute time limit. 350µl buffer N3 was added to the tube to end the reaction and the suspension became colorless. This step should not exceed 5 minutes. The cells were centrifuged for 10 minutes at 17,900xg (13,000rpm). 800µl of the supernatant was pipetted into QIAprep 2.0 spin column and centrifuged for 30-60 seconds. The flow through was discarded and the QIAprep 2.0 spin column was washed with 0.5ml buffer PB and centrifuged again for 30-60 seconds. The flow through was discarded and the column was washed again with 0.75ml buffer PB and centrifuged for 30-60 seconds. A final 1-minute centrifugation was performed to remove all residual buffer PB. The QIAprep 2.0 spin column was placed in a fresh 1.5ml eppendorf and 50µl buffer EB (10mM trisCL, pH 8.5) or H_2O was added to the spin column and allowed to stand for 1 minute at room temperature. The column was centrifuged for 1 minute then stored at -20^{0}C.

4.6.5.1.2 Digestion of plasmid

DNA in plasmid was quantified using NanoDrop spectrophotometer. The restriction digestion mix was calculated as indicated in table 4.7. the reaction mix was incubated overnight at 37^{0}C. A mixture of 10µl digestion mix plus 3µl loading dye was detected on 1% agarose gel.

Table 4.7: Reagents for restriction digestion.

Reagent	Volume (µl)
DNA (5ng-10ng)	X µl
Buffer (e.g cutsmart)	8µl
Enzyme	2µl
dH2O	Up to 80µl

4.6.5.1.3 Clean-up of digested fragments

Equal volumes of phenol, chloroform and isopropanol were added to the digestion mix and vortexed. The tube was centrifuged at 12,000rpm for 3 minutes, the upper layer was transferred to a fresh tube and an equal volume of chloroform was added then vortexed. The tube was centrifuged for at 12,000rpm for 5 minutes and the upper was transferred to a fresh tube. 200µl ice-cold 100% ethanol plus 8µl 3M sodium acetate was added to the tube. The tube was gently mixed and stored at -80^{0}C for 1h prior to centrifugation at 13,000rpm for 5 minutes at 4^{0}C. The supernatant was discarded and 500µl ice-cold 70% ethanol was added. The tube was centrifuged at 4^{0}C for 5 minutes at 13,000rpm. The ethanol was discarded and the pellet was allowed to air-dry for 1 minute. The pellet was resuspended in 15µl DEPC-H_2O and stored at -20^{0}C. Nanodrop quantifications were conducted prior to proceeding to the synthesis of DIG-labelled probe (see section 2.2).

4.6.5.2 Probe synthesis from PCR

Primers were designed using ensemble or primer 3. After designing the primers, T7 primer was added to the reverse primer for antisense probe (AS) and the forward primer for the sense (S) probe. See example below:

Black-font sequence is the gene primers and Red-font sequence is the T7 primers.
Gene_AS_F: GTACAGCTCGGGTCCTAGAC
Gene_AS_R: TAATACGACTCACTATAGGGGGGGCATGGTCATTGATGTC

Gene_S_F: TAATACGACTCACTATAGGGGTACAGCTCGGGTCCTAGAC
Gene_S_R: GGGGCATGGTCATTGATGTC

All the designed probe primers were listed in the table below (Table 4.8).

Table 4.8: List of probe primers used as antisense and sense in this study.

genes	Product size	Forward primer	Reverse primer
Gja1	1149bp	ATGGGTGACTGGAGCGCCT	TTAAATCTCCAGGTCATCAG
Nkx2.5	753bp	CAGAACCGTCGCTACAAGTG	GCGCACTCACTTTAATGGGA
Notch3	646bp	GCTATACTGGACCTCGCTGT	CCATCACGGCAAACTCCAAA
Notch4	641bp	AGTGTCTCCCAGGCTTTGAA	GAAAGTGCCAGGCTTGTTCA
Hand1	526bp	CAGCTACGCACATCATCACC	CTCCCTTTTCCGCTTGCTTT
Foxc2	1315bp	GAGCAAAACTACTACCGGGC	ACGAGTTGTCCAGTCCTAGC
Pcdha9	414bp	GCTACTCTGCCTCGCTAAGA	TCGTGCTGTTCCCTTTCTCT
Sap130	925bp	CGGCCCACTTTATCTATCCA	CATCTGCCAACACCACTGA
Rbfox2	1141bp	CCAGGAGCCAACAACAACTC	TCACGTCACTTCAGTAGGGG

After that, PCR was conducted using the newly designed primers and the PCR reaction in (Table 4.9). The PCR cycles and annealing temperature were carried out as described in (Table 4.10).

Table 4.9: PCR volumes for the newly designed primers.

Component	Volume (µl)
Forward primer	1µl
Reverse primer	1µl
dNTPs	0.4µl
5x reaction buffer	4µl
Taq DNA polymerase	0.2µl
Template cDNA	2µl
Nuclease-free H2O	11.4µl

Table 4.10: Temperature and time for PCR cycles.

Temperature (°C)	Time (minute)
95	4
95	1
60	0.5
72	1
72	6
4	∞

Finally, 2% gel electrophoresis was performed using 2g of agarose (Genaxxon bioscience, M3044.0250) to 100mL of 1x TAE, ran for 25mins at 125V and the PCR products were cleaned from gel agarose (see section 4.5.5.1.3). DIG-labelled probes were synthesised as demonstrated in the next section.

4.6.6 Synthesis of Digoxiogenin-labelled (DIG) probes

The table below summarizes the reagents and volumes used in DIG-labelled probe synthesis (Table 4.11). All buffers were defrosted on ice and briefly vortexed before use.

Table 4.11: Reagents and volumes used in DIG-labelled probe synthesis.

Reagent	Volume (µl)	Manufacturer
DNA	10	-
10X DigNTPs (DIG-labelling mix)	2	Roche; Cat#17109820
Buffer X5	4	Promega; Cat#P1188
RNase inhibitor	1	ThermosScientific; Cat#EO0381
100mM DTT	1	Promega; Cat#P1178
Enzyme T7	2	Promega; Cat#P207E

The probe mix was incubated in a water bath at 37^0C for 3h. 2µl DNA product mixed with 3µl nuclease-free water plus 1µl loading buffer were used for detection on a 2% agarose gel, ran at 150 volts for 10 minutes. 3µl 100bp ladder was used as a size marker. The probe could be stored at -20^0C at this stage. 31µl DEPC-H_2O, 5µl ammonium acetate, and 165µl ice-cold 100% ethanol were added to the probe and incubated for a minimum of 1h at -80^0C. The probe was then centrifuged at 4^0C for 30 minutes at 13,000rpm. The

supernatant was discarded, and the pellet was washed twice with 500µl 70% ethanol-DEPC, each time the pellet was centrifuged at 4^0C for 15 minutes at 13,000rpm and supernatant was discarded. The pellet was allowed to air-dry for 2 minutes prior to resuspension in 50µl nuclease-free H_2O-DEPC depending on the size of the pellet. For detection, a 1.5% agarose gel was run at 125 volts for 10 minutes. 3µl DNA product mixed with 6µl loading buffer were loaded on the gel. The DNA was denatured at 65^0C for 5 minutes then incubated on ice for a few seconds prior to loading on the gel. The remaining probes were stored at -80^0C.

4.7 Results

4.7.1 Assessment of the suggested genes for HLHS during development of the crucial regions in heart

The fact that HLHS can be prenatally diagnosed by the 15th week of gestation, shows that it must, by definition, have occurred during stages of embryonic and fetal development prior to this, and perhaps early in gestation. Therefore, mapping the expression of the predicted HLHS genes at early cardiac developmental stages, particularly in the main parts of the heart affected in HLHS, may provide insight into their likely participation in HLHS. The following section, hence, will look at the expression pattern of the implicated genes for HLHS including *Gja1, Nkx2.5, Notch family, Hand1, Foxc2, Ets1, Pcdha9, Sap130,* and *Rbfox2*, at different developmental stages (E10.5, E13.5 and E15.5) and focussing on the regions of the heart affected by HLHS. This includes the atrioventricular (AV) junction, mitral valve, outflow tract (OFT), aortic valve, and left ventricle. Since abnormalities in the aorta werw found to be secondary to defects in the aortic valve, the aorta was excluded. Presence of these gene expressions in well-established and previously reported regions, where is applicable, was used as control.

4.7.1.1 *Gja1*

Expression of *Gja1* was mapped to the main regions of the heart affected in HLHS, including left ventricle, mitral valve and aortic valve. These regions were investigated at three different time-points: E10.5, E13.5 and E15.5 (**see section 4.3**).

4.7.1.1.1 Left ventricle

At E10.5, *Gja1* was expressed in the left and right ventricles, specifically in the myocardium. However, it expressed higher in the left than right ventricular myocardium (Figure 4.3 A). At E13.5, *Gja1* expressed in both the left and right ventricles, particularly in the ventricular endocardium. Also, *Gja1* expressed at higher level than that observed in E10.5 (Figure 4.3 B). Likewise, at E15.5, *Gja1* showed a similar expression pattern to that at the previous stage (Figure 4.3 C). Remarkably, expression of *Gja1* was higher in the left ventricle than the right ventricle throughout heart development. No expression was observed in the *Gja1* sense probe (Figure 4.3 D).

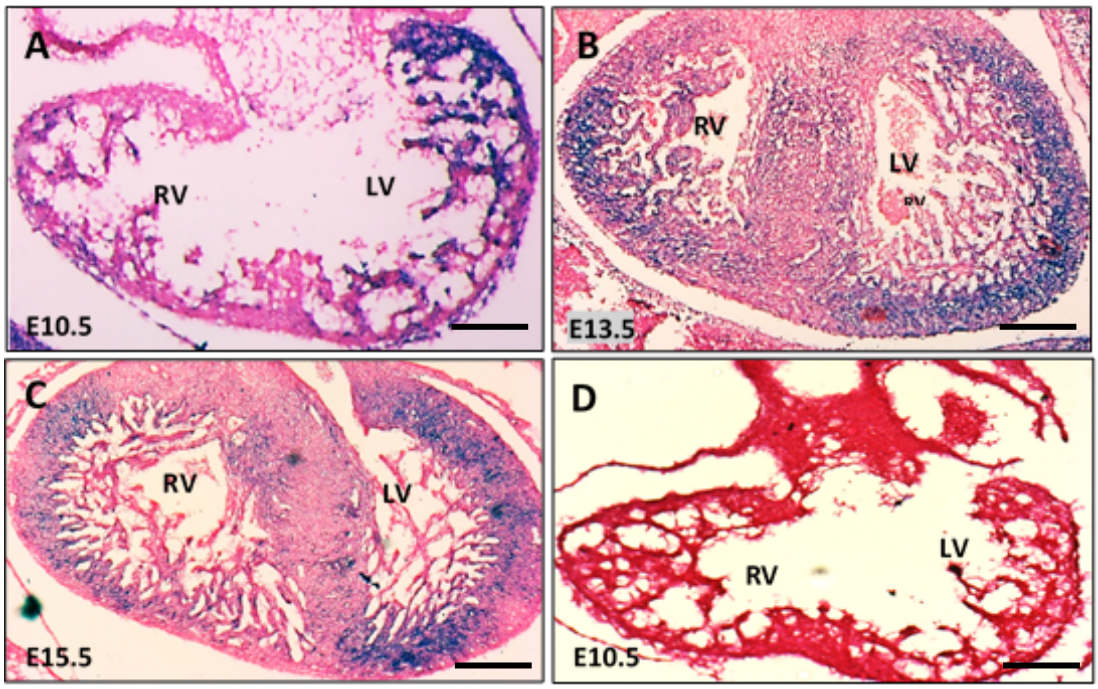

Figure 4.3: Restricted expression of *Gja1* to the ventricular cambers through different developmental stages.
(A) *Gja1* was expressed in the left and right ventricles at E10.5, with higher expression in the left than the right ventricles. Also, expression of *Gja1* was observed in both ventricular endocardium at (B) E13.5 and (C) E15.5. (D) *Gja1* sense probe showed no expression in the heart at E10.5. Scale bar = 200μm.

4.7.1.1.2 Mitral valve

Expression of *Gja1* was not detected in the endocardial cushion of the atrioventricular canal at E10.5 (Figure 4.4 A). Similarly, it was not detected in the mitral valve leaflets at E13.5 and E15.5 (Figure 4.4 B, C). No expression was observed in the *Gja1* sense probe (Figure 4.4 D).

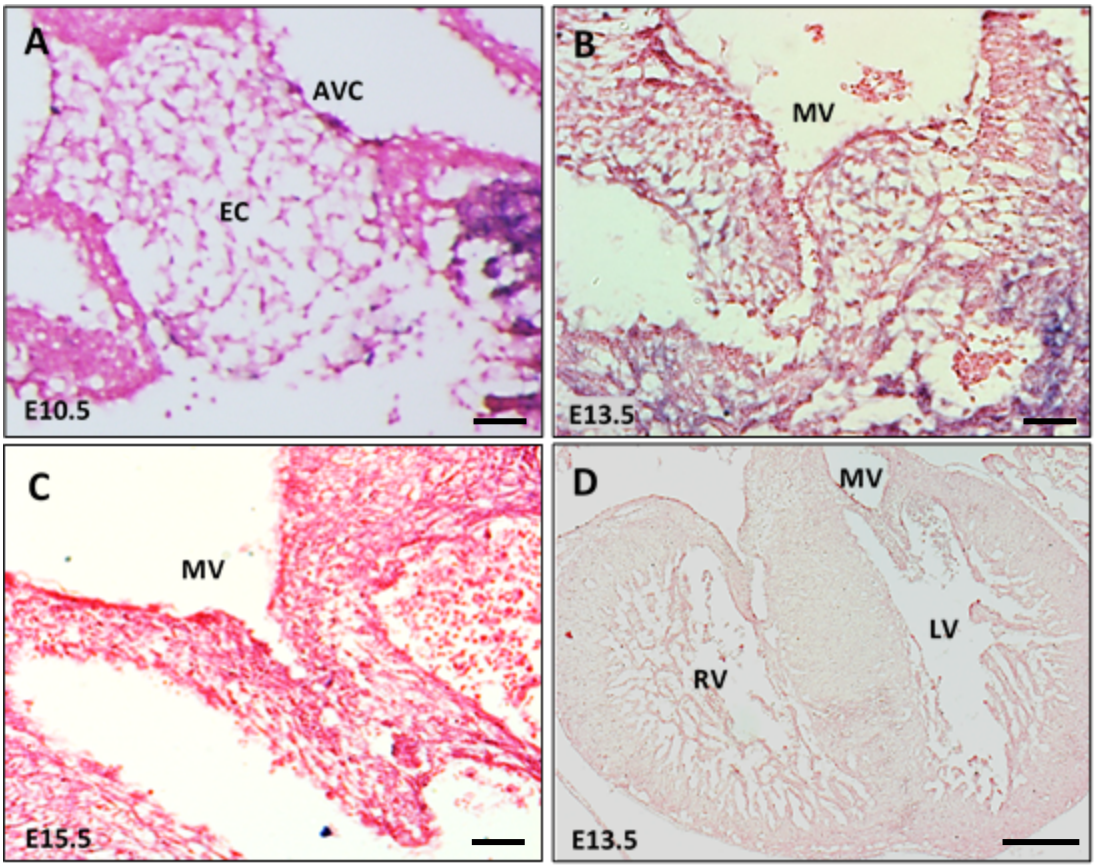

Figure 4.4: No expression of *Gja1* in the mitral valve.
(A) *Gja1* was not expressed in the endocardial cushions of the atrioventricular canal at E10.5. No expression was observed in the mitral valve leaflets at (B) E13.5 and (C) E15.5. (D) *Gja1* sense probe showed no expression in the heart at E13.5. Scale bar: A-C= 100μm, D= 200μm.

4.7.1.1.3 Aortic valve

Expression of *Gja1* was not detected in the endocardial cushion of the outflow tract at E10.5 (Figure 4.5 A). Similarly, it was not detected in the aortic valve leaflets at E13.5 and E15.5 (Figure 4.5 B, C). No expression was observed in the *Gja1* sense probe (Figure 4.5 D).

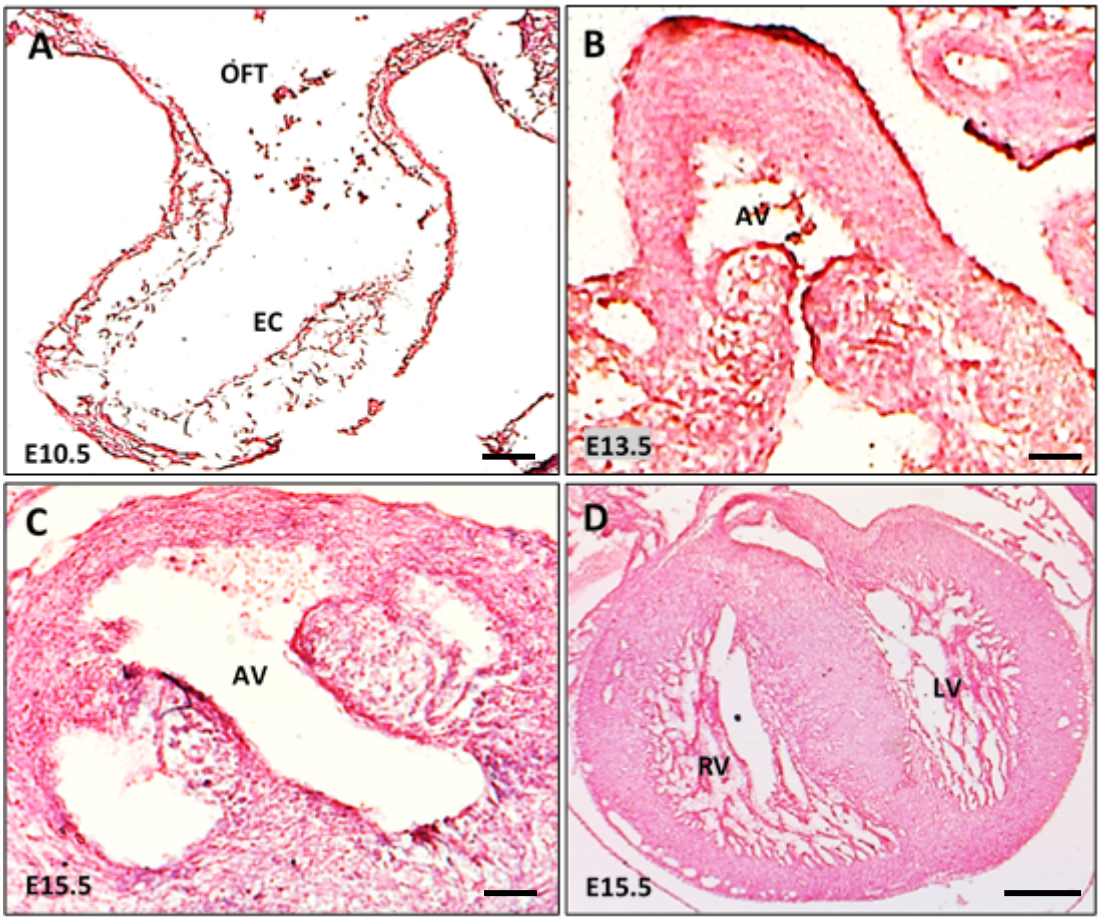

Figure 4.5: No expression of *Gja1* in the aortic valve.
(A) *Gja1* was not expressed in the endocardial cushions of the outflow tract at E10.5. No expression was observed in the aortic valve leaflets at (B) E13.5 and (C) E15.5. (D) *Gja1* sense probe showed no expression in the heart at E15.5. Scale bar: A-C= 100μm, D= 200μm.

4.7.1.1.4 Summary

Overall, *Gja1* expression showed restricted expression to the left and right ventricles, although at all stages the expression was higher in the left than the right ventricles. Expression of *Gja1* in this study was consistent to that previously reported (Christoffels et al., 2004). The fact that *Gja1* was expressed higher in the left ventricle than the right ventricle indicated a specific role for *Gja1* in the early development of the left ventricular chamber. This therefore suggested that *Gja1* contributed to the initial process of the left ventricle formation and hence could associate with hypoplasia of the left ventricle that observed in HLHS cases.

4.7.1.2 *Nkx2.5*

Expression of *Nkx2.5* was mapped to the main regions of the heart affected in HLHS, including left ventricle, mitral valve and aortic valve. These regions were investigated at three different time-points: E10.5, E13.5 and E15.5.

4.7.1.2.1 Left ventricle

Expression of *Nkx2.5* was localised in both left and right ventricles at E10.5 (Figure 4.6 A). However, this expression was decreased in the ventricular chambers at E13.5 (Figure 4.6 B). By E15.5, the expression of *Nkx2.5* was undetectable in both cardiac chambers (Figure 4.6 C). No expression was observed in the *Nkx2.5* sense probe (Figure 4.6 D). Altogether, *Nkx2.5* was widely expressed in the left and right ventricles at the early stages of heart development, specifically at E10.5, but this expression reduced as the ventricles fully formed (E15.5).

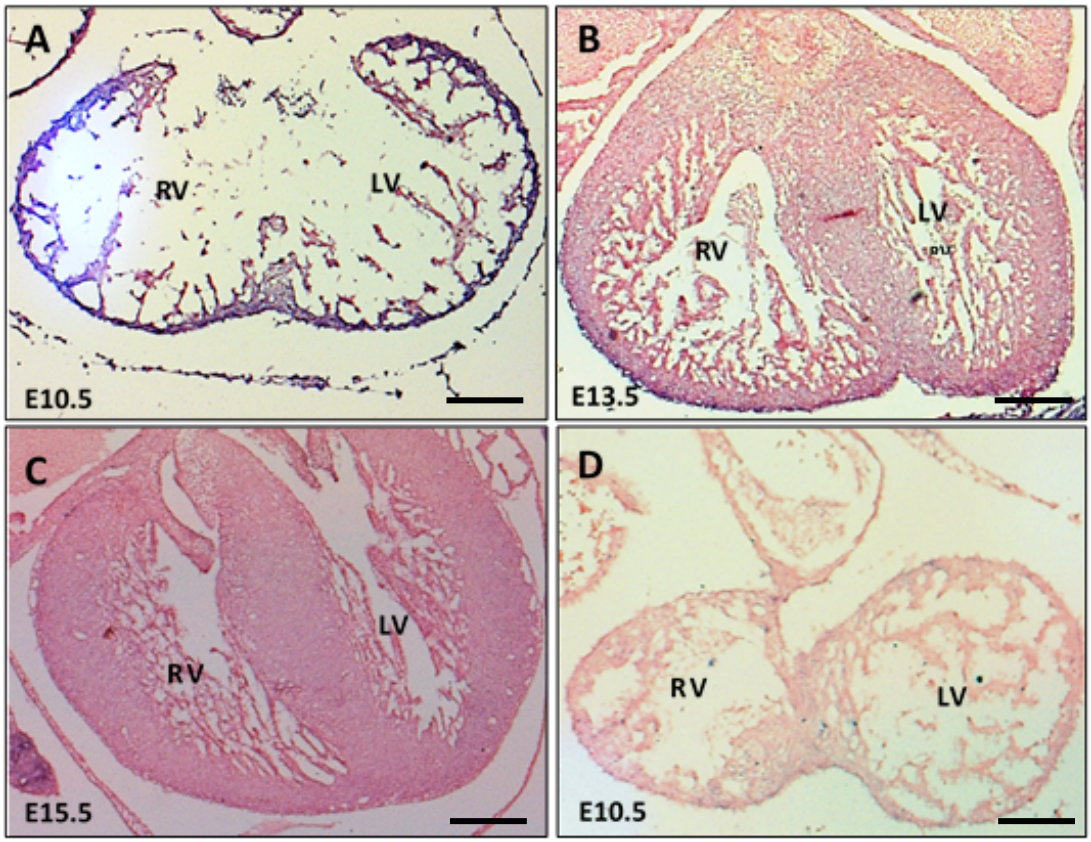

Figure 4.6: Broad expression of *Nkx2*.5 in the early heart developmental stage.
(A) *Nkx2*.5 expressed in both left and right ventricles at E10.5. However, it was not expressed in both ventricles at (B) E13.5 and (C) E15.5. (D) *Nkx2*.5 sense probe showed no expression in the heart at E10.5. Scale bar = 200μm.

4.7.1.2.2 Mitral valve

The expression of *Nkx2.5* at E10.5 was broadly observed in the endocardial cushions of the atrioventricular canal (Figure 4.7 A). However, *Nkx2*.5 expression was not detected in the mitral valve at E13.5 and E15.5 (Figure 4.7 B, C). No expression was observed in the *Nkx2.5* sense probe (Figure 4.7 D).

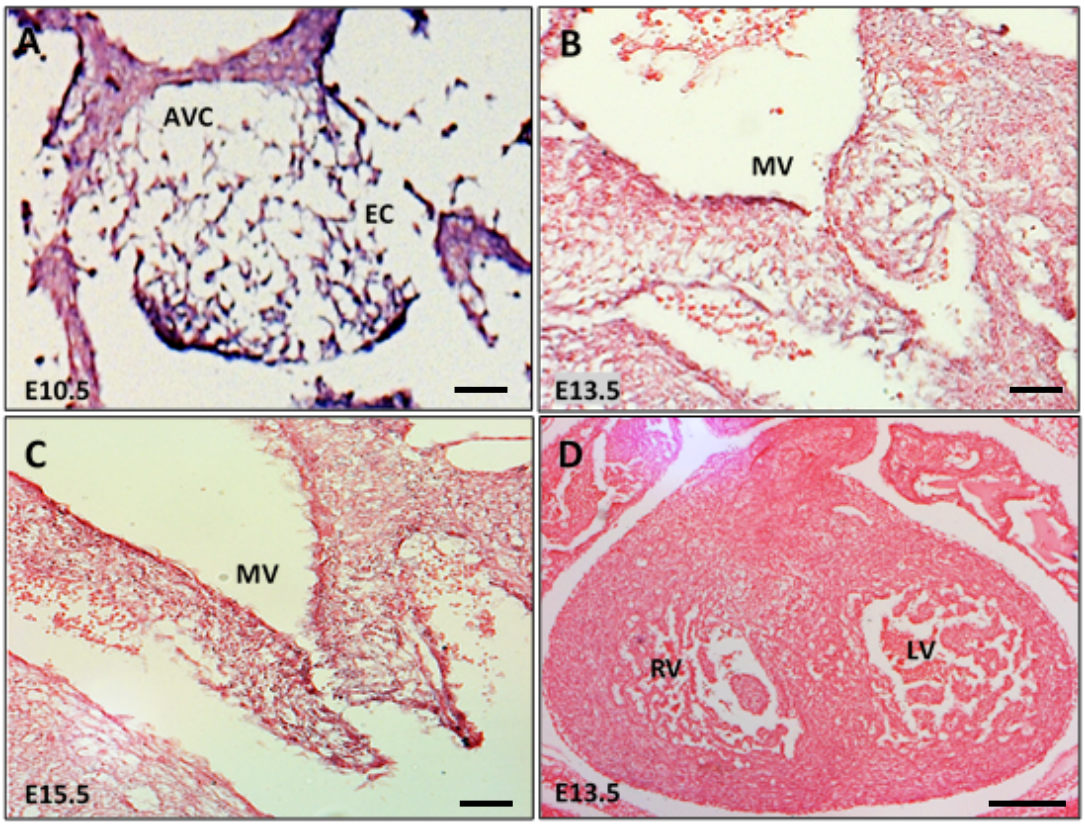

Figure 4.7: Broad expression of *Nkx2*.5 in the early heart developmental stage.
(A) *Nkx2*.5 expressed in the endocardial cushions of the atrioventricular canal. However, *Nkx2*.5 was not expressed in the mitral valve at (B) E13.5 and (C) E15.5. (D) *Nkx2*.5 sense probe showed no expression in the heart at E13.5. Scale bar: A-C= 100μm, D= 200μm.

4.7.1.2.3 Aortic valve

At E10.5, Nkx2.5 was found in most of the heart regions including the outflow tract, particularly the myocardial cells and mesenchymal cells lining the outflow tract (arrows) (Figure 4.8 A). However, *Nkx2*.5 expression was not detected in the aortic valve at E13.5 and E15.5 (Figure 4.8 B, C). No expression was observed in the *Nkx2.5* sense probe (Figure 4.8 D).

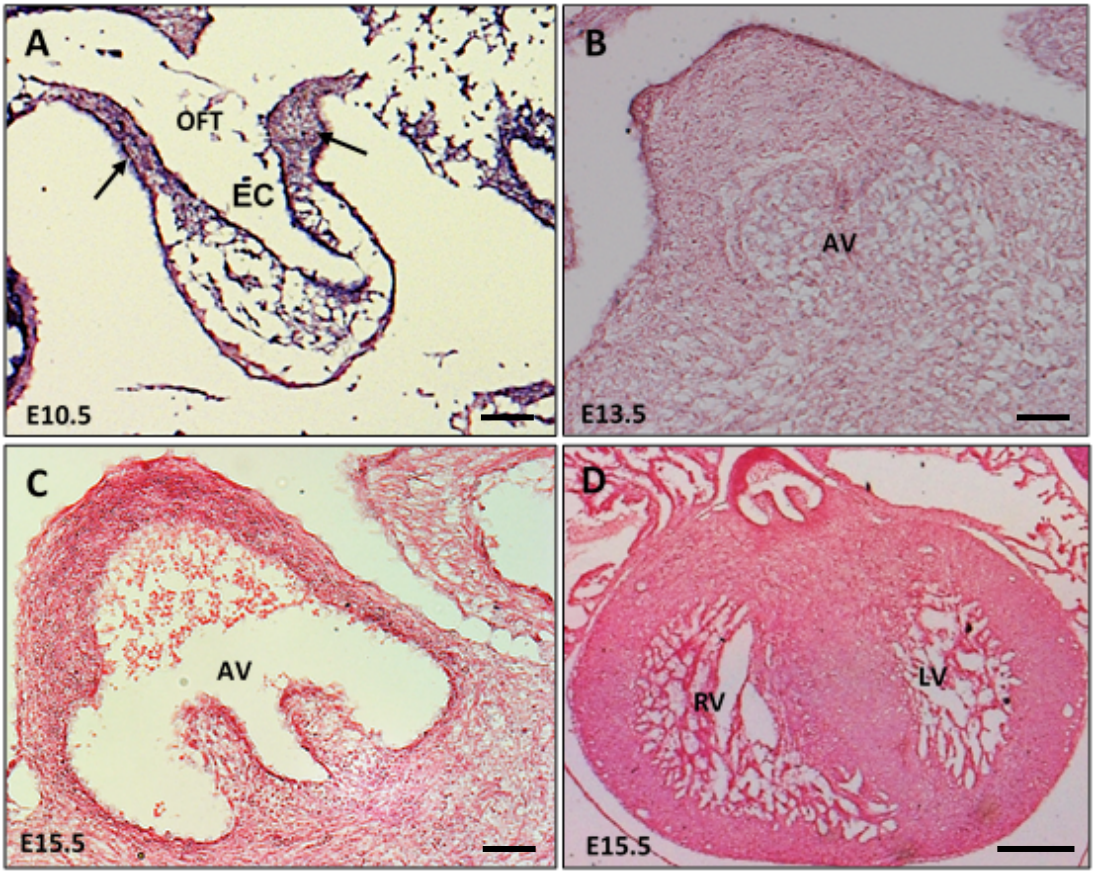

Figure 4.8: Broad expression of *Nkx2*.5 in the early heart developmental stage.
(A) *Nkx2*.5 expressed in the endocardial cushions of the outflow tract. However, *Nkx2*.5 was not expressed in the aortic valve at (B) E13.5 and (C) E15.5. (D) *Nkx2*.5 sense probe showed no expression in the heart at E15.5. Scale bar: A-C= 100μm, D= 200μm.

4.7.1.2.4 Summary

Overall, *Nkx2*.5 showed high expression in the endocardial cushions that form the future mitral and aortic valves as well as the left and right ventricular chambers in the early heart formation (E10.5). Nevertheless, this expression disappeared from these regions as the heart developed (E13.5 and E15.5). This therefore indicates a significant role for *Nkx2*.5 during the initial formation stage of these regions.

Similar expression patterns of *Nkx2*.5 in mouse heart was previously reported (Tanaka et al., 1999; Scherptong et al., 2012), and beside its expression in heart it was also reported to express in head fold at E10.5 (Pu et al., 2013) (Figure 4.9 A) and in mantle layer of spinal cord, but not marginal layer at E13.5 and E15.5 (Visel et al., 2004) (Figure 4.9 B,C), this therefore was used as control in this section.

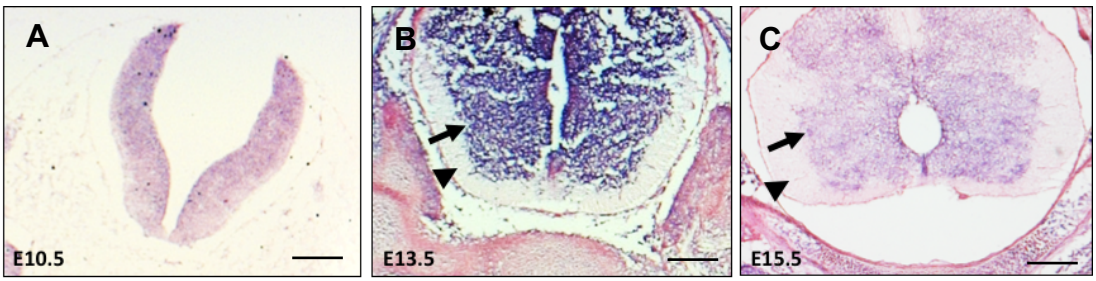

Figure 4.9: *Nkx2*.5 expression at different stges.
Nkx2.5 expression in embryonic mouse head fold at E10.5, and in the mantle layer (arrow), but not in the marginal layer (arrow head) at both E13.5 and E15.5. Scale bar = 70μm.

The fact that *Nkx2*.5 expressed in the cardiac regions that affected in HLHS suggested that variations in *Nkx2*.5 could lead to the abnormalities observed in HLHS. However, at the same time, because the expression was not limited to the left-side structures, this also implicated that variations in this gene could affecting the left as well as the right-side structures at the same level, which could lead to abnormalities without HLHS features.

4.7.1.3 *Notch1*

The Notch family member, *Notch1,* was mapped to find the expression pattern in the selected cardiac regions including atrioventricular canal, outflow tract, mitral valve, aortic valve, and the left ventricle at E10.5, E13.5 and E15.5.

4.7.1.3.1 Left ventricle

At E10.5, *Notch1* was found in both the left and right ventricles, particularly in the endocardium of the left ventricle and epicardium and myocardium of the right ventricle (Figure 4.10 A). At E13.5, *Notch1* expression was highly detected in the right more than the left ventricular endocardium (Figure 4.10 B). At E15.5, however, *Notch1* was reduced in both left and right ventricles (Figure 4.10 C). No expression was observed in the *Notch1* sense probe (Figure 4.10 D).

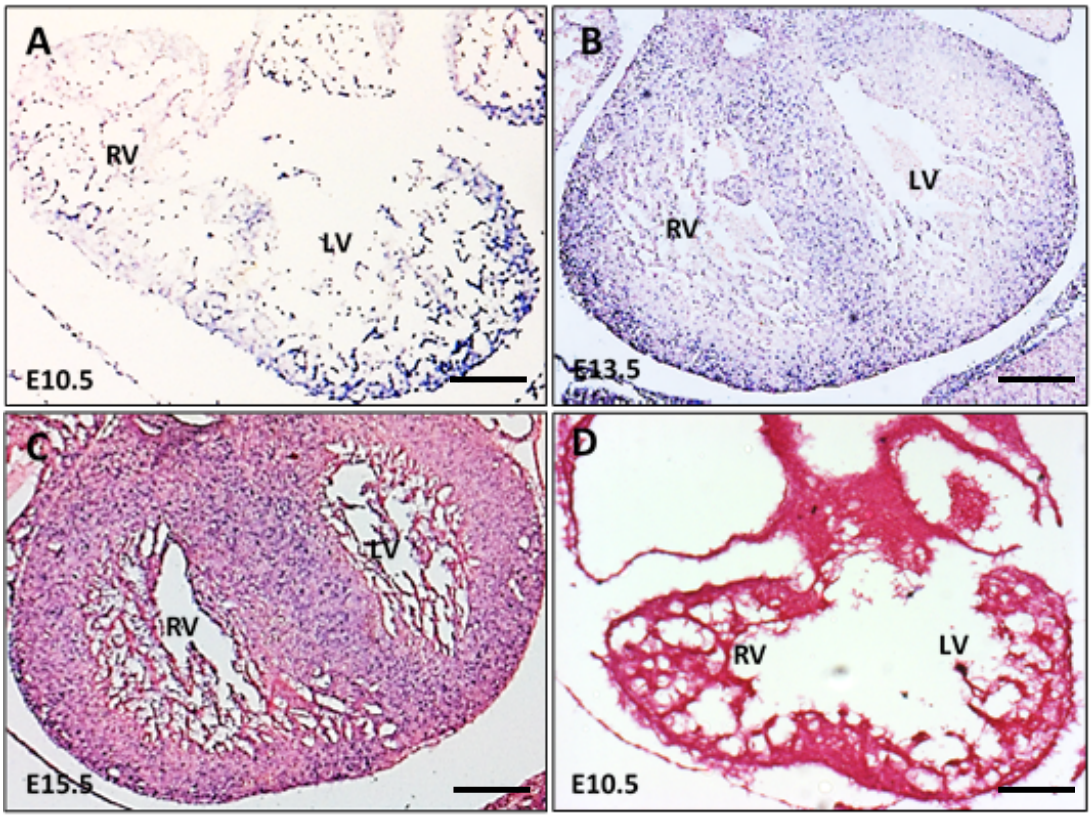

Figure 4.10: *Notch1* expression in ventricles throughout the developmental stages.
(A) *Notch1* was expressed in the endocardium of the left ventricle and myocardium of the right ventricle at E10.5. Also, expression of *Notch1* was observed in both the left and right ventricles at both (B) E13.5 and (C) E15.5, but higher in E13.5 than E15.5. (D) Notch1 sense probe showed no expression in the heart at E10.5. Scale bar = 200μm.

4.7.1.3.2 Mitral valve

Notch1 expression was localised to the endocardial cushions found in the atrioventricular canal (AVC), but not in the wall of AVC at E10.5 (Figure 4.11 A). At E13.5, *Notch1* was observed in the endothelial cells (arrows) and interstitial cells (asterisks) found in both posterior and anterior leaflets of the mitral valve (Figure 4.11 B). However, at E15.5, the expression of *Notch1* was reduced from the endothelial and interstitial cells located in the mitral valve compared to that observed at E13.5 (Figure 4.11 C). No expression was observed in the *Notch1* sense probe (Figure 4.11 D).

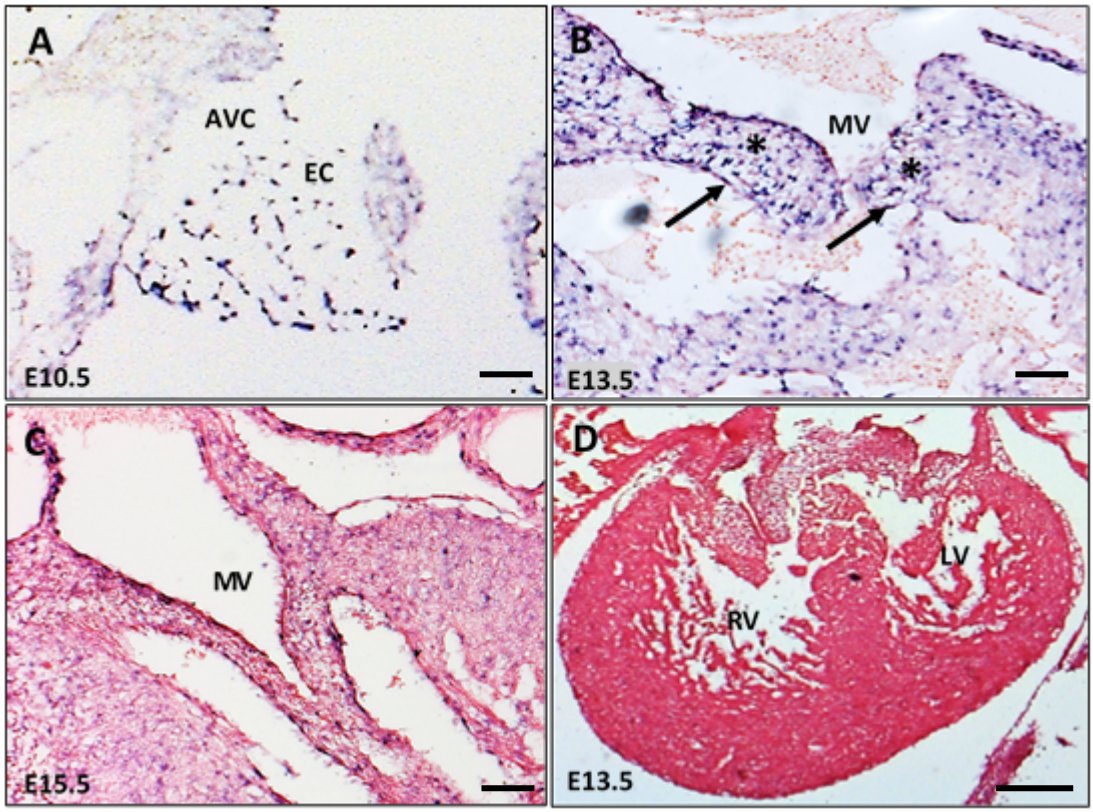

Figure 4.11: *Notch1* expression in the mitral valve throughout the developmental stages.
(A) *Notch1* was expressed in the endocardial cushion found in the atrioventricular canal at E10.5, but its expression was not identified in the wall of AVC. (B) At E13.5, *Notch1* expressed in the endothelial cells (arrows) and interstitial cells (asterisk) of mitral valve leaflets. (C) Similarly, at E15.5, expression of *Notch1* was detected in the leaflets of the mitral valve, but at low level than that seen in E13.5. Scale bar: A-C= 100μm, D= 200μm.

4.7.1.3.3 Aortic valve

At E10.5, *Notch1* transcripts were found to be expressed in the endothelial cells lining the outflow tract as well as in the pericardium (Figure 4.12 A). At E13.5, *Notch1* was expressed in the leaflets of the aortic valve, specifically in the subendothelial cells and weakly in the endothelial cells lining the leaflets (Figure 4.12 B). Likewise, at E15.5, *Notch1* showed similar expression to that observed at E13.5 in the aortic valve leaflets (Figure 4.12 C). No expression was observed in the *Notch1* sense probe (Figure 4.12 D).

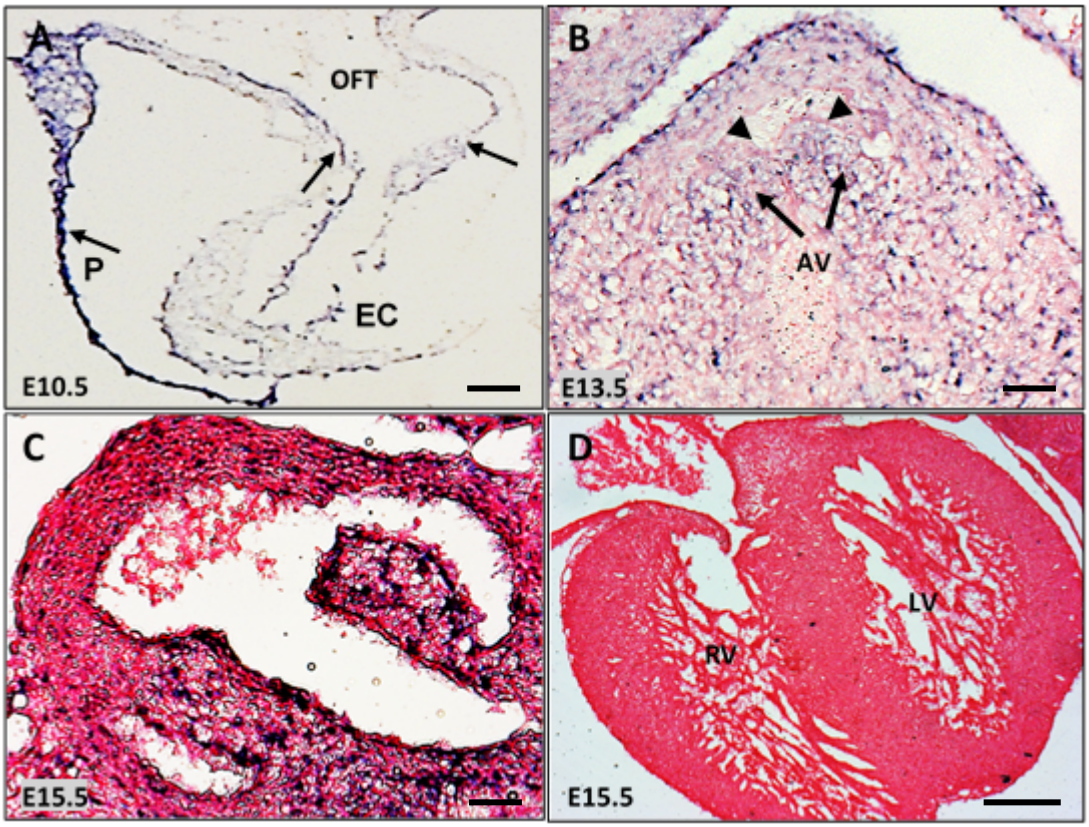

Figure 4.12: *Notch1* expression in the aortic valve throughout the developmental stages.
(A) At E10.5, restricted expression of *Notch1* to the endocardium and endothelial cells (arrow) lining the outflow tract (OFT) tube, and pericardium (P, arrow), was observed. (B) At E13.5, *Notch1* expression was in the subendothelial cells (arrows), but not in the endothelial cells (arrow heads). (C) At E15.5, *Notch1* expression was observed in the aortic valve, but at reduced level compared to that observed in E13.5. (D) *Notch1* sense probe showed no expression in the heart at E15.5. Scale bar: A-C= 100μm, D= 200μm.

4.7.1.3.4 Summary

Overall, *Notch1* expressed in the early stage (E10.5) at the endocardial cushions of the atrioventricular canal and the outflow tract, and the left ventricular endocardium. In later stages (E13.5 and E15.5), *Notch1* was expressed in the mitral and aortic valves, as well as the left ventricle. Similar expression patterns of *Notch1* were reported by Del Monte et al (2007). Altogether, *Notch1* was expressed throughout the different developmental stages although the expression was higher at E10.5 and E13.5 than E15.5.

The fact that *Notch1* was mapped to the left ventricle and both the mitral and aortic valves indicates its significant roles in formations of these regions. Therefore, *Notch1* could contribute to abnormalities observed in all the affected regions in HLH.

4.7.1.4 *Notch3*

The Notch family member, *Notch3,* was mapped to find the expression pattern in the selected cardiac regions including atrioventricular canal, outflow tract, mitral valve, aortic valve, and the left ventricle at E10.5, E13.5 and E15.5.

4.7.1.4.1 Left ventricle

Notch3 was found to be mainly expressed in the epicardium of the left ventricle at E15.5 with very minor expression in the right ventricle (Figure 4.13 C). However, no expression was detected in the left ventricle at E10.5, neither at E13.5 (Figure 4.13 A,B). No expression was observed in the *Notch3* sense probe (Figure 4.13 D).

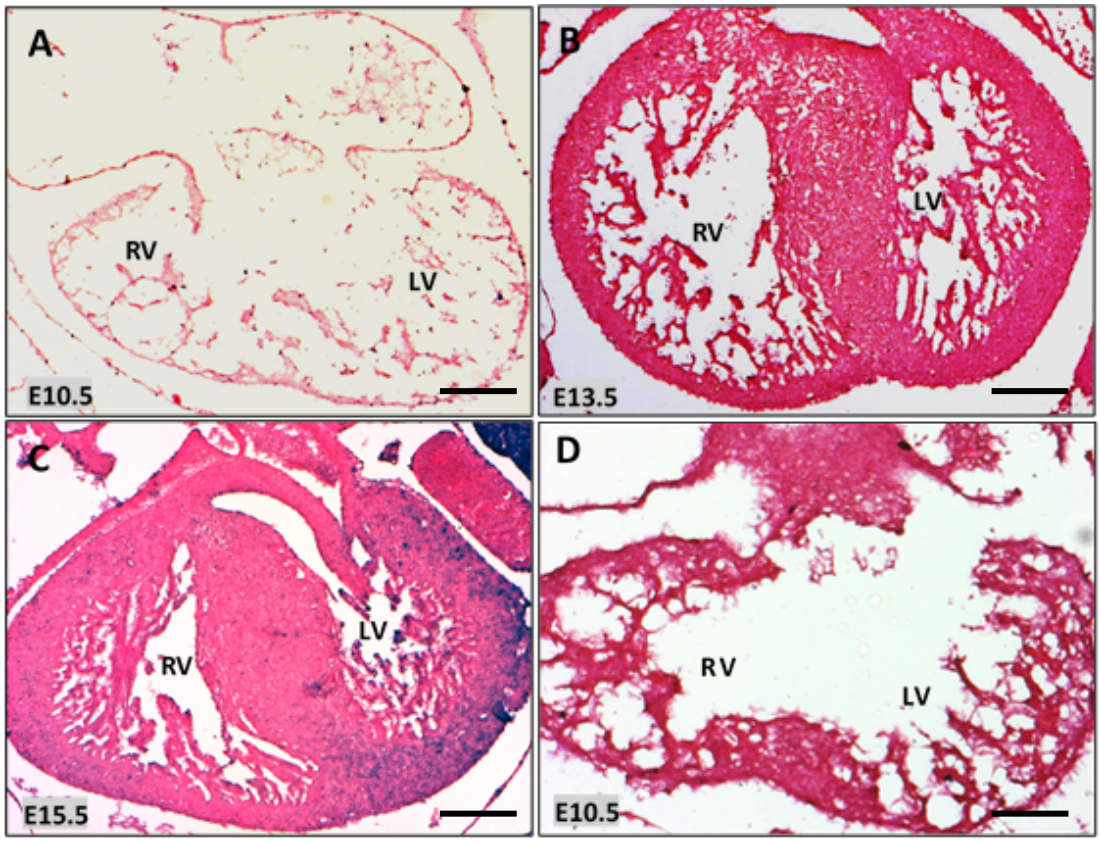

Figure 4.13: Restricted expression of *Notch3* to the left ventricle at E15.5. *Notch3* was found to express in the left ventricle at E15.5 with low level expression in the right ventricle (C). No expression was found in the left ventricle at (A) E10.5 and (B) E13.5. (D) *Notch3* sense probe showed no expression in the heart at E10.5. Scale bar = 200μm.

4.7.1.4.2 Mitral valve

Notch3 was not expressed in the endocardial cushions of the atrioventricular canal at E10.5 (Figure 4.14 A). Similarly, no expression was detected in the mitral valve leaflets at E13.5 (Figure 4.14 B), neither at E15.5 (Figure 4.14 C). No expression was observed in the *Notch3* sense probe (Figure 4.14 D).

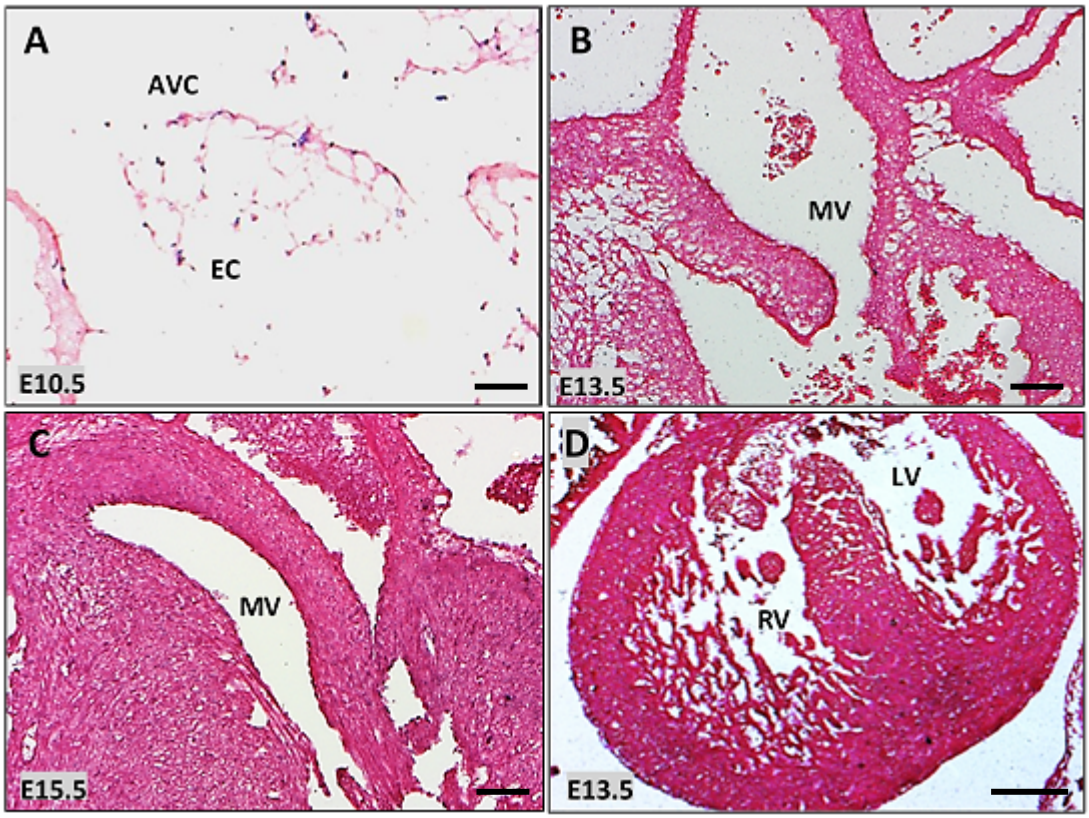

Figure 4.14: No expression of *Notch3* in the mitral valve.
(A) No expression was found in the endocardial cushion of the atrioventricular canal (AVC) at E10.5. Also, no expression was detected in the mitral valve at (B) E13.5 nor (C) at E15.5. (D) *Notch3* sense probe showed no expression in the heart at E13.5. Scale bar: A-C= 100μm, D= 200μm.

4.7.1.4.3 Aortic valve

Notch3 was not expressed in the endocardial cushions of the outflow tract at E10.5 (Figure 4.15 A). Similarly, no expression was detected in the aortic valve leaflets at E13.5 (Figure 4.15 B), neither at E15.5 (Figure 4.15 C). No expression was observed in the *Notch3* sense probe (Figure 4.15 D).

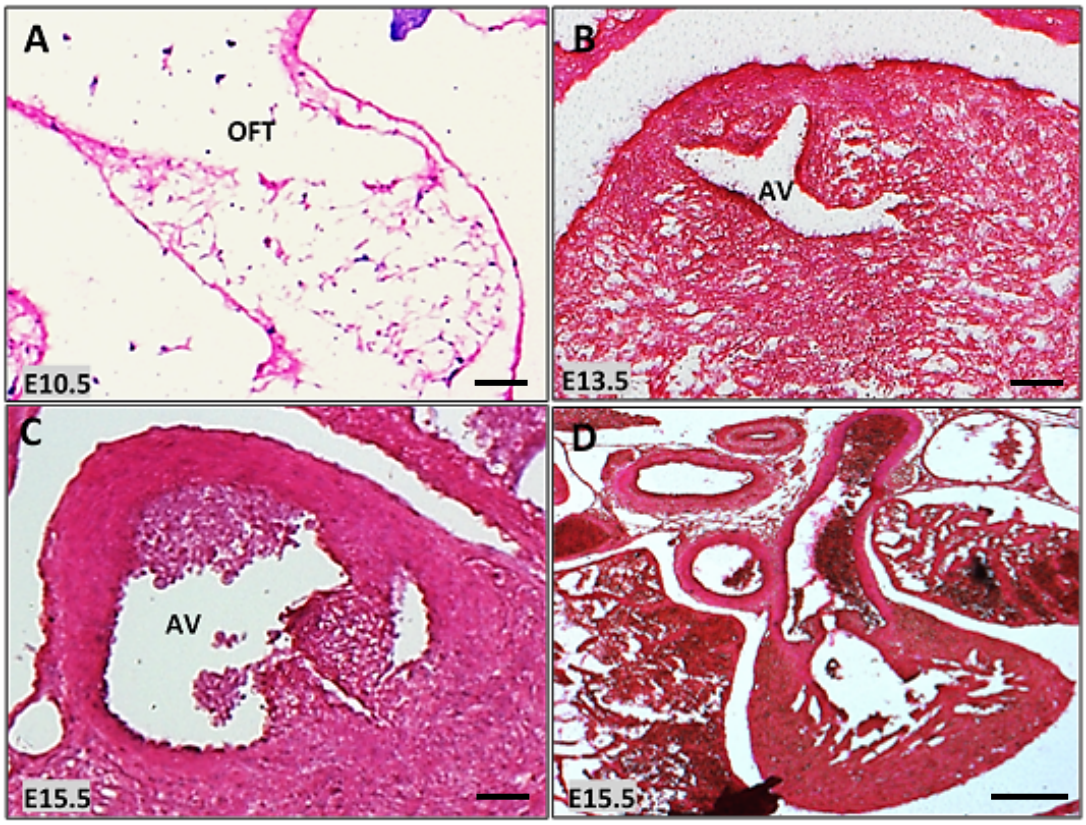

Figure 4.15: No expression of *Notch3* in the aortic valve.
(A) No expression was found in the endocardial cushion of the outflow tract (OFT) at E10.5. Also, no expression was detected in the aortic valve at (B) E13.5 nor (C) at E15.5. (D) Notch3 sense probe showed no expression in the heart at E15.5. Scale bar: A-C= 100μm, D= 200μm.

4.7.1.4.4 Summary

Altogether, *Notch3* did not express at the early developmental stages (E10.5 and E13.5), whereas at E15.5 it expressed exclusively to the left ventricle. Although *Notch3* expression was not previously reported in mouse heart at E10.5, it was reported in head fold at E10.5 (Mason et al., 2005) (Figure 4.16 A) and in pulmonary artery and valve at E13.5 and E15.5 (Visel et al., 2004) (Figure 4.16 B,C) in which these regions were used here as controls.

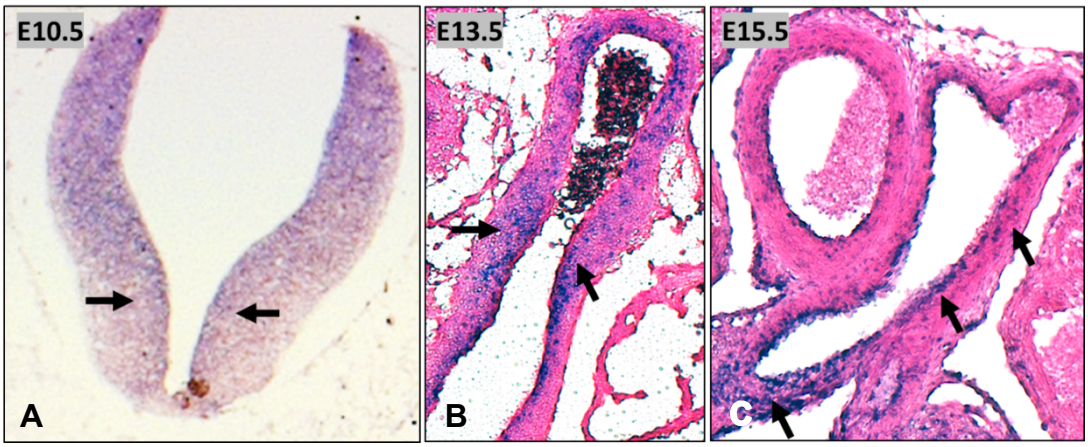

Figure 4.16: expression of *Notch3* in the head fold at E10.5 and pulmonary artery and valve at E13.5 and E15.5.
Scale bar: A=μm 50μm B,C= 100μm.

Overall, the specific expression of *Notch3* in the left ventricle at E15.5 suggested that variations in *Notch3* could cause abnormalities in the left ventricle, hence contributed to the left ventricular hypoplasia observed in HLHS.

4.7.1.5 *Notch4*

The Notch family member, *Notch4,* was mapped to find the expression pattern in the selected cardiac regions including atrioventricular canal, outflow tract, mitral valve, aortic valve, and the left ventricle at E10.5, E13.5 and E15.5.

4.7.1.5.1 Left ventricle

At E10.5, *Notch4* was found in the left and right ventricular chambers, particularly localised to the ventricular endocardium (Figure 4.17 A). However, at E13.5 and E15.5, *Notch4* expression was not detected in the left and right ventricles (Figure 4.17 B, C). No expression was observed in the *Notch4* sense probe (Figure 4.17 D).

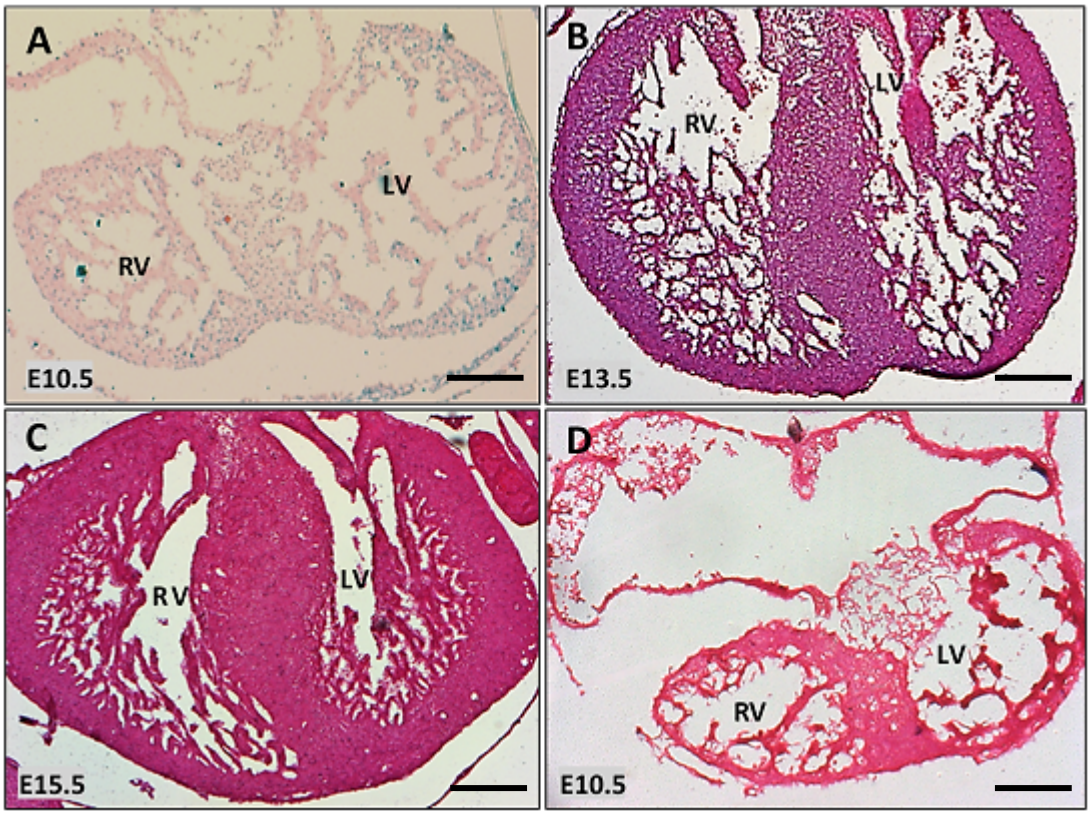

Figure 4.17: Restricted expression of *Notch4* to the ventricles at E10.5. (A) At E10.5, *Notch4* expression was detected in the left and right ventricles. However, no expression was detected in the ventricles at (B) E13.5 and (C) E15.5. (D) *Notch4* sense probe showed no expression in the heart at E10.5. Scale bar = 200μm.

4.7.1.5.2 Mitral valve

At E10.5, no expression of *Notch4* was detected in the endocardial cushions of the atrioventricular canal (Figure 4.18 A). Similarly, at E13.5 and E15.5, the expression of *Notch4* was not detected in the mitral valve leaflets (Figure 4.18 B, C). No expression was observed in the *Notch4* sense probe (Figure 4.18 D).

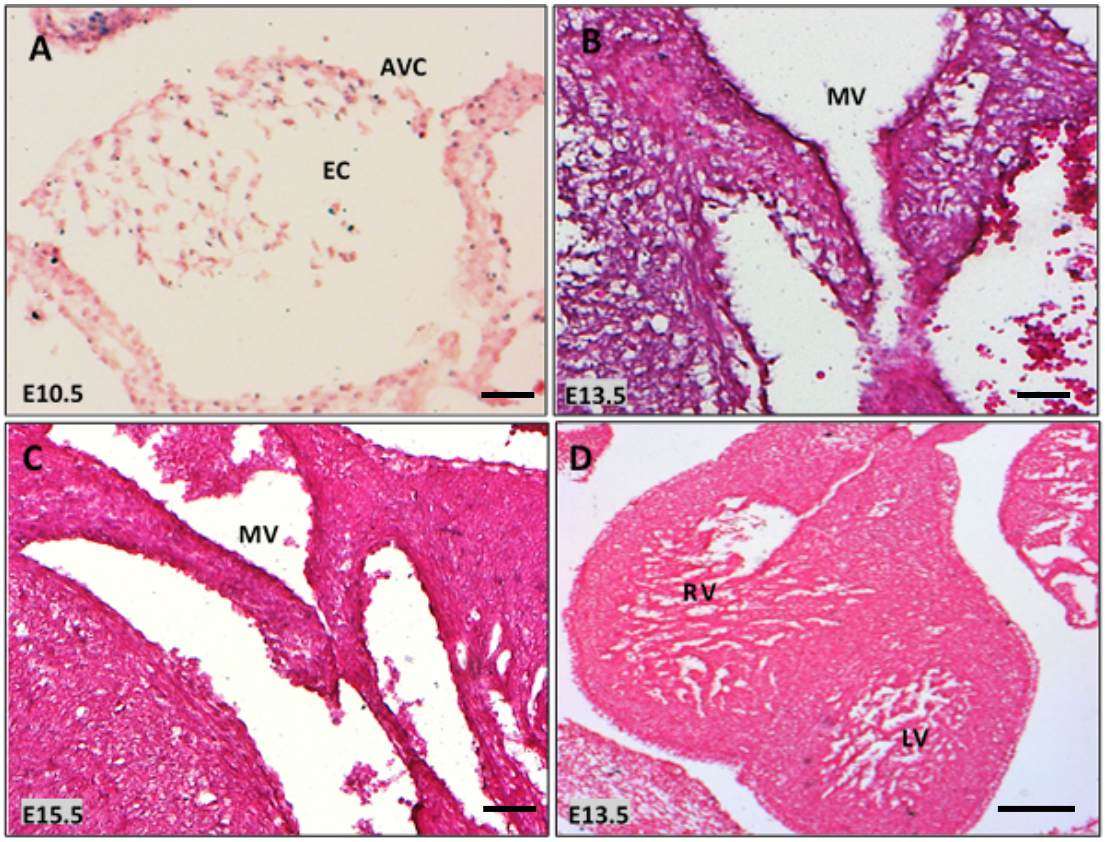

Figure 4.18: No expression of *Notch4* in the mitral valve.
(A) No expression was found in the endocardial cushion of the atrioventricular canal (AVC) at E10.5. Also, no expression was detected in the mitral valve at (B) E13.5 nor (C) at E15.5. (D) *Notch4* sense probe showed no expression in the heart at E13.5. Scale bar: A-C= 100μm, D= 200μm.

4.7.1.5.3 Aortic valve

At E10.5, no expression of *Notch4* was detected in the endocardial cushions of the outflow tract (Figure 4.19 A). Similarly, at E13.5 and E15.5, the expression of *Notch4* was not detected in the aortic valve leaflets (Figure 4.19 B, C). No expression was observed in the *Notch4* sense probe (Figure 4.19 D).

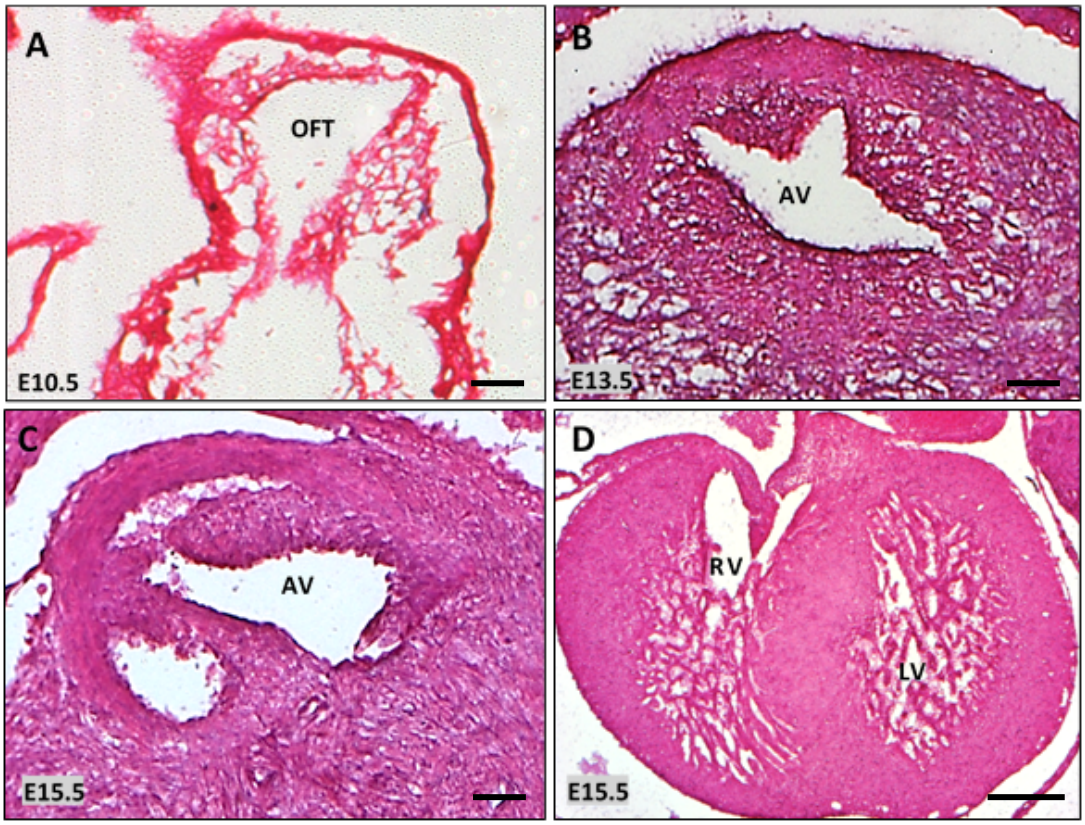

Figure 4.19: No expression of *Notch4* in the aortic valve.
(A) No expression was found in the endocardial cushion of the outflow tract (OFT) at E10.5. Also, no expression was detected in the aortic valve at (B) E13.5 nor (C) at E15.5. (D) *Notch4* sense probe showed no expression in the heart at E15.5. Scale bar: A-C= 100μm, D= 200μm.

4.7.1.5.4 Summary

Altogether, *Notch4* was highly expressed in the left and right ventricle at E10.5 while no expression was detected in other cardiac regions in later developmental stages. Previous study had shown a general expression of *Notch4* in mouse embryo at E11.5 and E15.5, where *Notch4* was expressed in the spinal cord and brain while no expression in the heart was detected (Magdaleno et al., 2006). Other studies showed that *Notch4* was expressed in the aorta and pulmonary arteries at E13.3 (Villa et al., 2001) and in the brain at E10.5 (Shirayoshi et al., 1997). Therefore, *Notch4* expression in brain at E10.5 (Figure 4.20 A), aorta and pulmonary arteries at E13.5 (Figure 4.20 B), and spinal cord at E15.5 (Figure 4.20 C) was used as controls.

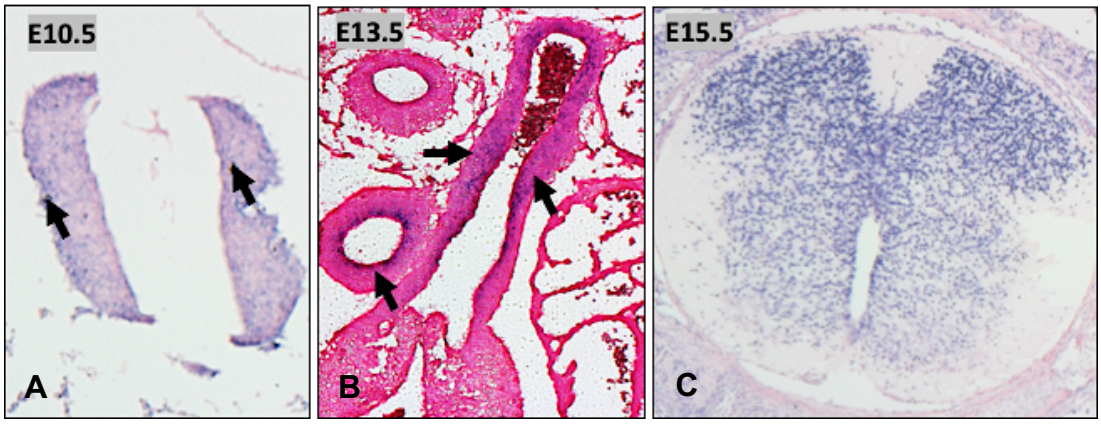

Figure 4.20: Expression of *Notch4* in the brain at E10.5, aorta and pulmonary arteries at E13.5 and spinal cord at E15.5.
Scale bar: A= 50μm, B=150μm, C= 70μm.

Overall, *Notch4* demonstrated a specific expression in the left and right ventricles, which suggested that *Notch4* played a role during early development of the ventricles and thus could contribute to the hypoplasia observed in the left ventricle of HLHS.

4.7.1.6 *Hand1*

Expression of *Hand1* was mapped to the main regions of the heart affected in HLHS, including left ventricle, mitral valve and aortic valve. These regions were investigated at three different time-points: E10.5, E13.5 and E15.5.

4.7.1.6.1 Left ventricle

At E10.5, *Hand1* demonstrated expression in the developing left ventricle (Figure 4.21 A) and the outer curvature of the developing right ventricle at low level (Figure 4.21 A arrow). At E13.5, *Hand1* was expressed in endocardium and myocardium of the left and right ventricles but at a low level in the right ventricle compared to the left ventricular expression (Figure 4.21 B). Moreover, at E15.5, *Hand1* was exclusively expressed in the endocardium of the left ventricle, whereas no expression was detected in the myocardium of the left ventricle, or in the right ventricle (Figure 4.21 C). No expression was observed in the *Hand1* sense probe (Figure 4.21 D).

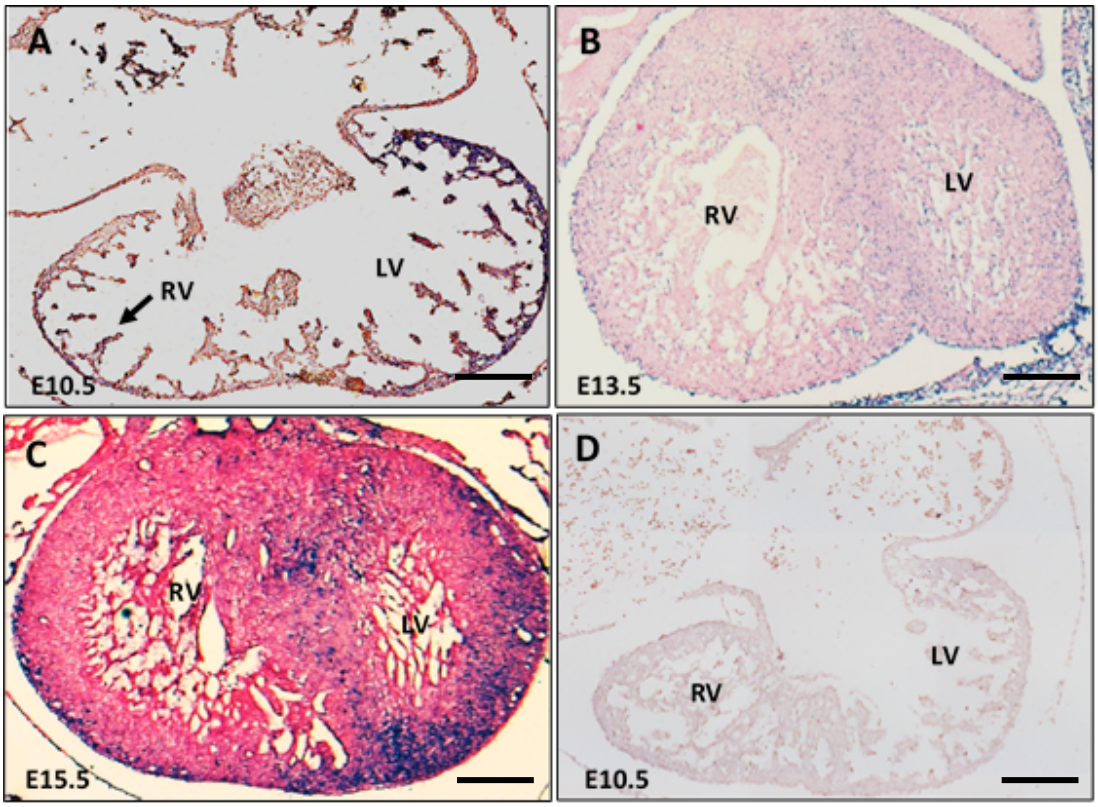

Figure 4.21: *Hand1* expressed in the left ventricle at different developmental stages.
(A) At E10.5, *Hand1* expressed in the endocardium of the left ventricle with low expression level in the right ventricle (arrow). Similarly, (B) at E13.5 and (C) E15.5, expression of *Hand1* observed in the left ventricle and right ventricle. (D) *Hand1* sense probe showed no expression in the heart at E10.5. Scale bar = 200μm.

4.7.1.6.2 Mitral valve

At E10.5, no expression of *Hand1* was detected in the endocardial cushions of the atrioventricular canal at this stage (Figure 4.22 A). At E13.5, *Hand1* was expressed in the mitral valve, particularly in the endothelial cells covering the leaflets as well as in the interstitial cells found at the distal tip of developing primordia (Figure 4.22 B). At E15.5, *Hand1* showed similar expression pattern to that seen in E13.5 as it was found in the endothelial cells and the interstitial cells of anterior and posterior leaflets of the mitral valve (Figure 4.22 C). No expression was observed in the *Hand1* sense probe (Figure 4.22 D).

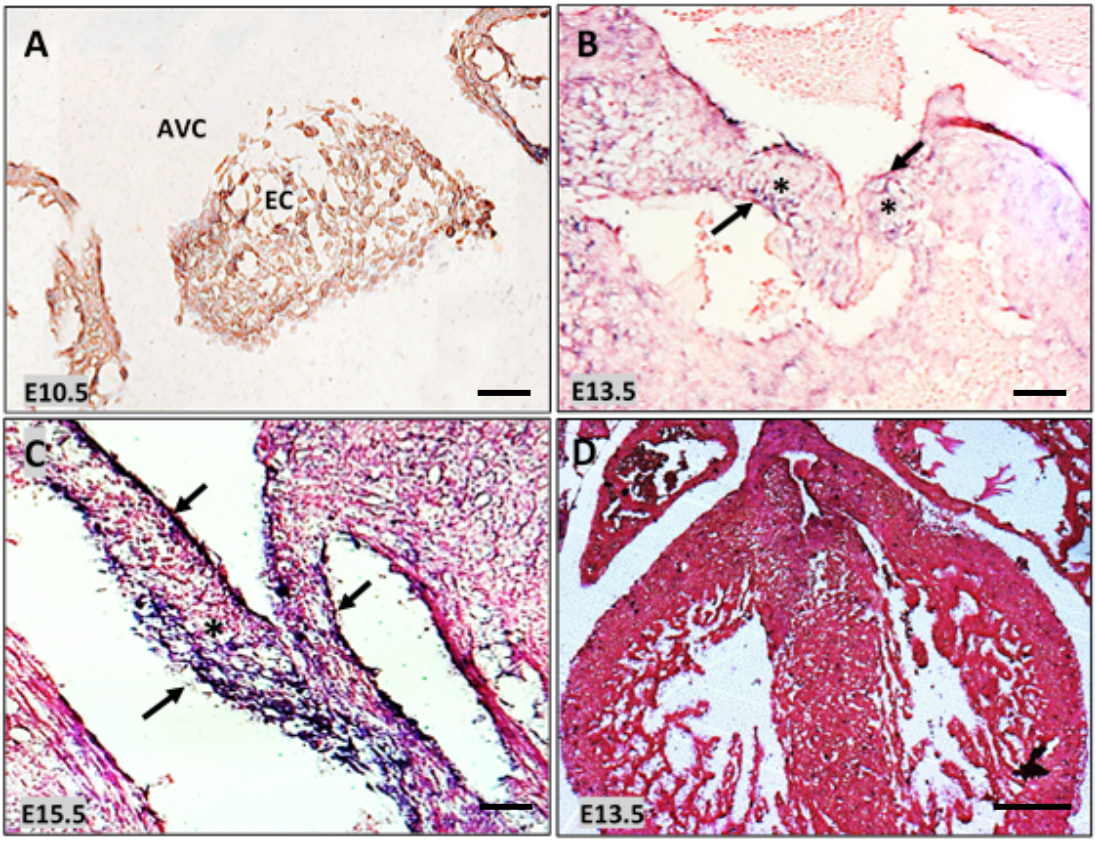

Figure 4.22: *Hand1* expressed in the mitral valve at E13.5 and E15.5.
(A) At E10.5, *Hand1* was not expressed in the endocardial cushions of the atrioventricular canal (AVC). However, (B) at E13.5, *Hand1* was expressed in the endothelial cells (arrows) covering the leaflets of the mitral valve and the interstitial cells (asterisks) in the distal tip of developing primordia. (C) Similarly, at E15.5, both endothelial (arrows) and interstitial cells (asterisks) of the mitral valve leaflets expressed *Hand1*. (D) Hand1 sense probe showed no expression in the heart at E13.5. Scale bar: A-C= 100μm, D= 200μm.

4.7.1.6.3 Aortic valve

At E10.5, *Hand1* was expressed in the in the early development of the outflow tract, particularly throughout the aortic sac at the distal end of the outflow tract (Figure 4.23 A). At E13.5, *Hand1* was expressed in the wall of the aortic valve. Although Hand1 was not found in the endothelial cells lining the aortic valve leaflets (Figure 4.23 B arrows), it was found in the sub-endothelial cells located in the aortic valve leaflets. At E15.5, there was no expression of *Hand1* in the sub-endothelial cells found in the aortic valve leaflets, whereas high expression was seen in the endothelial cells covering these leaflets (Figure 4.23 C). No expression was observed in the *Hand1* sense probe (Figure 4.23 D).

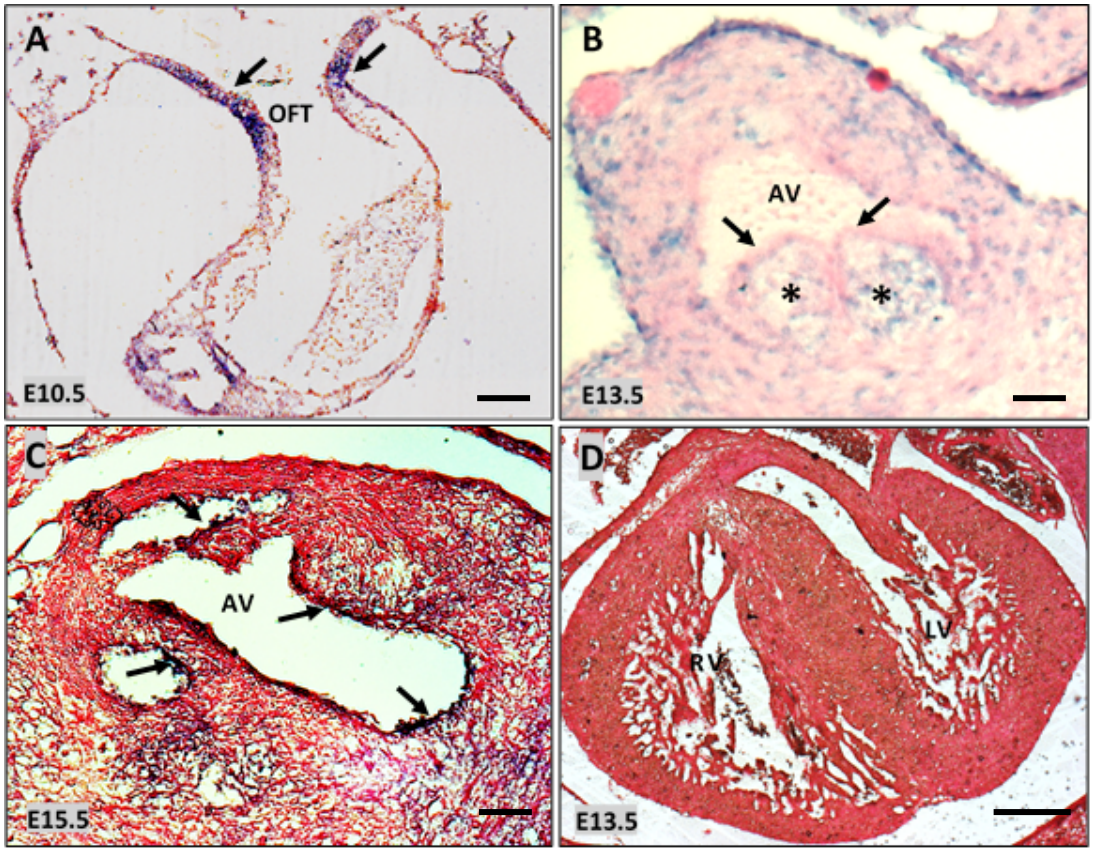

Figure 4.23: *Hand1* expressed in the aortic valve throughout the different developmental stages.
(A) Expression of *Hand1* at E10.5 was detected in the in the mesenchymal cells (arrows) covering the outflow tract (OFT). (B) At E13.5, expression of *Hand1* was detected in the sub-endothelial cells of the aortic valve leaflets (asterisks), but not in the endothelial cells covering the leaflets (arrows). (C) At E15.5, *Hand1* expression was restricted to the endothelial cells covering aortic valve leaflets. (D) *Hand1* sense probe showed no expression in the heart at E15.5. Scale bar: A-C= 100μm, D= 200μm.

4.7.1.6.4 Summary

Altogether, *Hand1* demonstrated high expression in the left ventricle and its associated valves throughout the different cardiac developmental stages. The expression patterns of *Hand1* in this section was consistent with the previously reported expression (Huanget al, 2004; McFadden et al., 2005), as *Hand1* expression was observed in the early development of the outflow tract and left ventricle. The fact that *Hand1* expressed highly in the left-side structures with minor expression in the right side indicated its essential role during early cardiogenesis. Since HLHS mainly affects the left side structures, *Hand1* can contribute to the defects observed in the affected regions in HLHS, and hence it seems a significant gene for HLHS. Although the previously reported variation in this gene showed no HLHS features, but instead caused embryonic lethality, *Hand1* has been implicated in survival of the embryo and thus *Hand1* is important for cardiogenesis as well as embryogenesis.

4.7.1.7 *Foxc2*

Expression of *Foxc2* was mapped to the main regions of the heart affected in HLHS, including left ventricle, mitral valve and aortic valve. These regions were investigated at three different time-points: E10.5, E13.5 and E15.5.

4.7.1.7.1 Left ventricle

At the early development stage E10.5, *Foxc2* was not expressed in the left and right ventricles (Figure 4.24 A). Likewise, at E13.5 and E15.5, there was no expression of *Foxc2* in the left and right ventricles (Figure 4.24 B C). No expression was observed in the *Foxc2* sense probe (Figure 4.24 D).

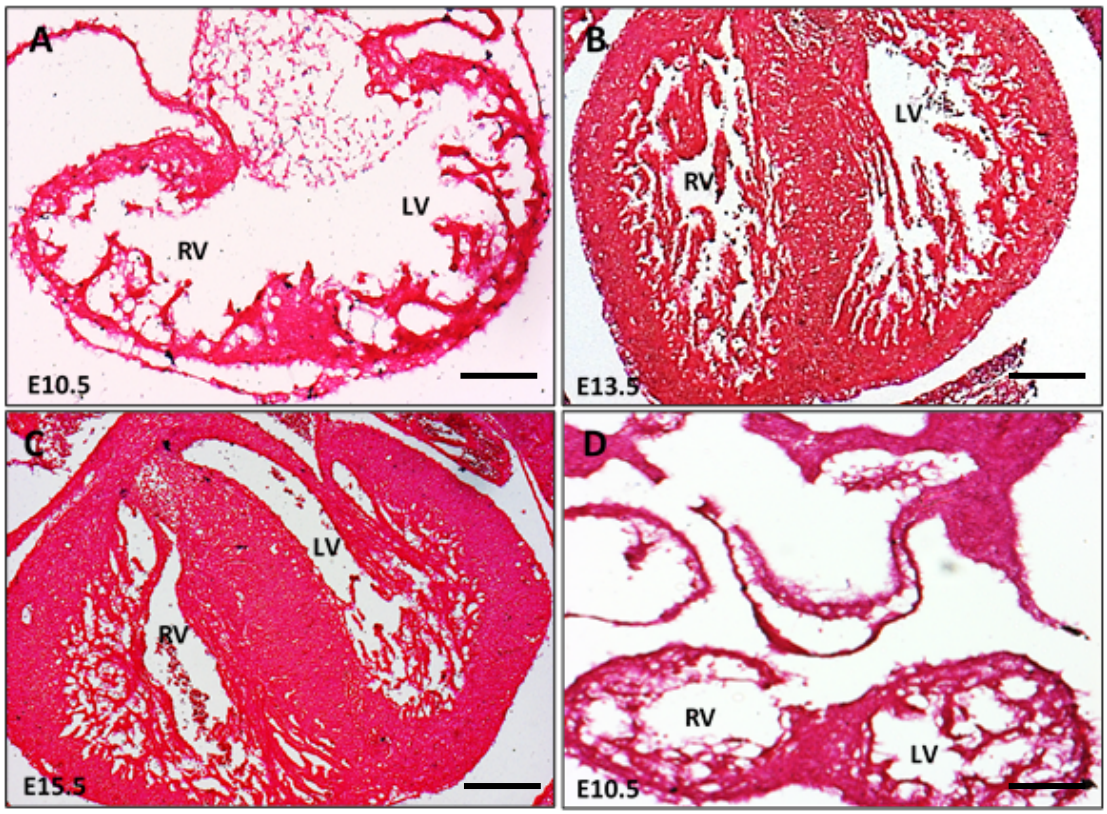

Figure 4.24: No expression of *Foxc2* in the left ventricle throughout the different developmental stages.
(A) At E10.5, *Foxc2* expression was not detected in the left and right ventricles. Also, no expression was detected in the ventricles at (B) E13.5 and (C) E15.5. (D) *Foxc2* sense probe showed no expression in the heart at E10.5. Scale bar = 200μm.

4.7.1.7.2 Mitral valve

At E10.5, no expression of *Foxc2* was observed in the atrioventricular endocardial cushions (Figure 4.25 A). Also, *Foxc2* was not expressed in the mitral valve at E13.5 and E15.5 (Figure 4.25 B C). No expression was observed in the *Foxc2* sense probe (Figure 4.25 D).

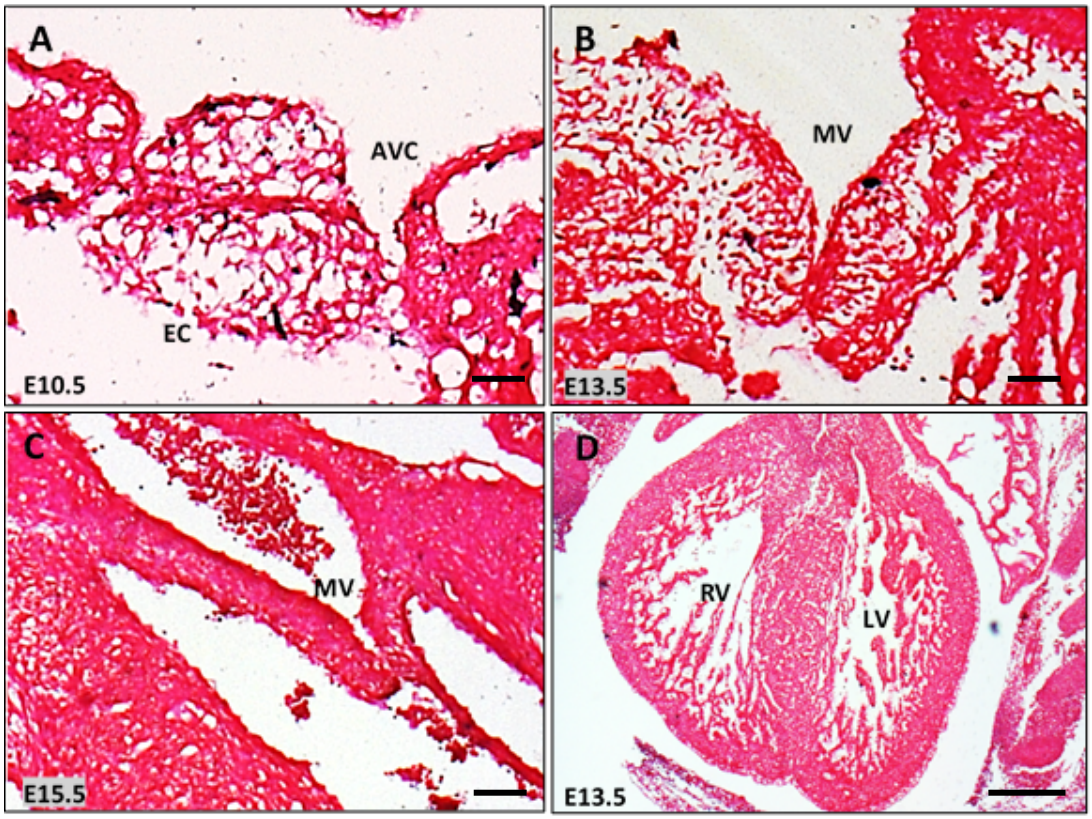

Figure 4.25: No expression of *Foxc2* in the mitral valve throughout the different developmental stages.
(A) At E10.5, *Foxc2* expression was not observed in the endocardial cushions (EC) of the atrioventricular canal (AVC). Similarly, no expression of *Foxc2* was detected in the mitral valve at (B) E13.5 and (C) E15.5. (D) *Foxc2* sense probe showed no expression in the heart at E13.5. Scale bar: A-C= 100μm, D= 200μm.

4.7.1.7.3 Aortic valve

The early expression of *Foxc2* was detected at E10.5 in the mesenchymal cells covering the cardiac tube (Figure 4.26 A). After that, *Foxc2* became restricted to the aortic valve, as it was found in the endothelial cells covering the leaflets of the aortic valve at E13.5 (Figure 4.26 B) and sub-endothelial cells of the aortic valve leaflets as well as the wall of the aortic valve at E15.5 (Figure 4.26 C). No expression was observed in the *Foxc2* sense probe (Figure 4.26 D).

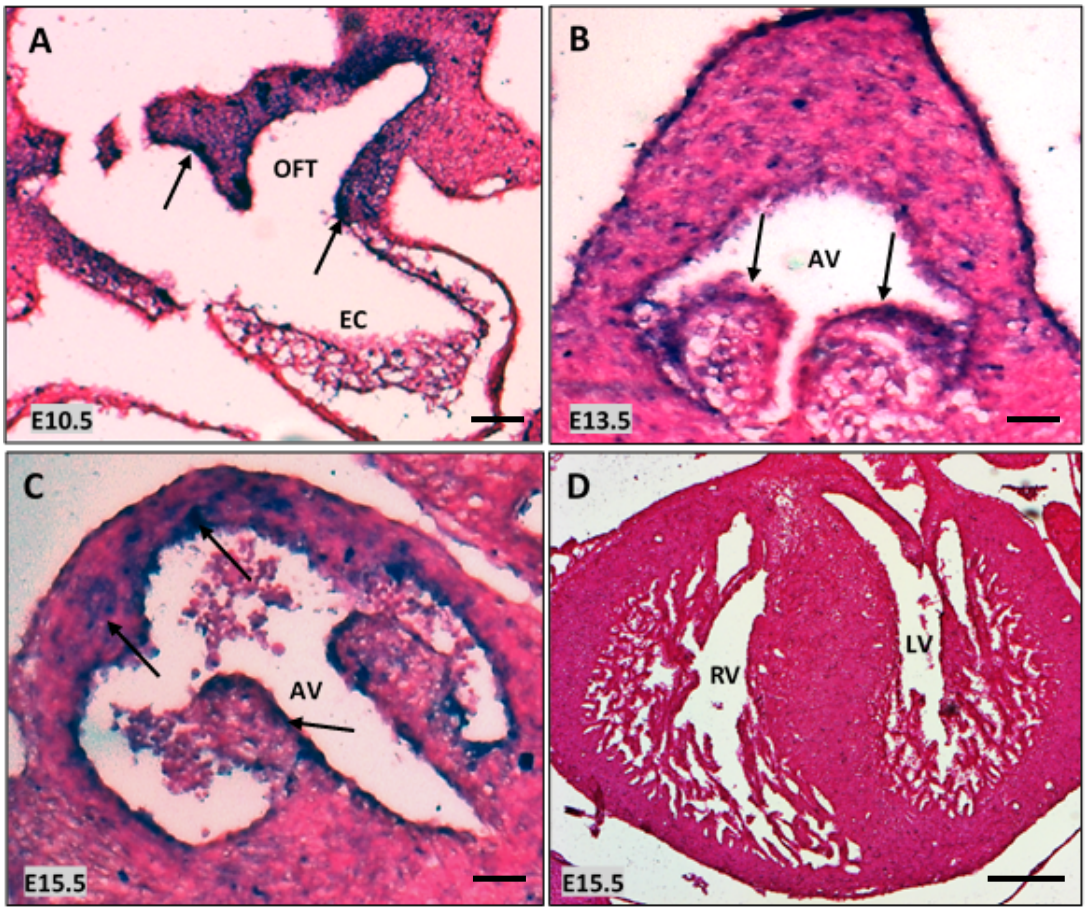

Figure 4.26: Restricted expression of *Foxc2* to the aortic valve during heart development.
(A) At E10.5, Expression of *Foxc2* was observed in the mesenchymal cells (arrows) covering the outflow tract (OFT). (B) At E13.5, *Foxc2* was expressed in the endothelial cells (arrows) covering the aortic valve leaflets. (C) At E15.5, *Foxc2* was detected in the endothelial cells (arrows) found in the aortic valve leaflets and wall. (D) *Foxc2* sense probe showed no expression in the heart at E15.5. Scale bar: A-C= 100μm, D= 200μm.

4.7.1.7.4 Summary

Overall, *Foxc2* expressed in the mesenchymal cells in the outflow tract at E10.5, before it became restricted to the aortic valve at E13.5 and E15.5. The expression of *Foxc2* in this section was consistence with the previously reported expression of *Foxc2* (Gitler et al., 2003; Uddin et al., 2016). Also, it was previously reported that expression of *Foxc2* in endothelial cells covering the pulmonary and aorta arteries at E13.5 and E16.5, and hence it was used as controls (Figure 4.27 A,B) (Gitler et al., 2003). Altogether, *Foxc2* is found mainly in the mesenchymal cells and then expressed exclusively in the aortic valve, which implicates its essential roles in early formation of the aortic valve. Particularly, during remodelling of valve leaflets, as aortic valve undergoes an endothelial–mesenchymal transformation (EMT) process during maturation of the valve leaflets and mesenchymal cells play important role during this process. Therefore, Foxc2 could contribute to the defects observed in the aortic valve of HLHS.

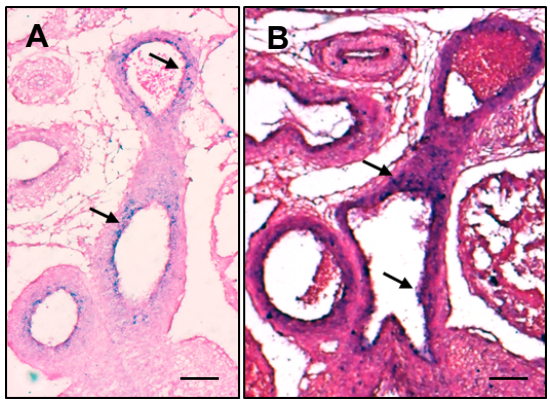

Figure 4.27: Expression of Foxc2 at different stges.
Expression of *Foxc2* in endothelial cells covering the pulmonary and aorta arteries at E13.5 and E15.5. Scale bar = 150μm.

4.7.1.8 *Ets1*

Expression of *Ets1* was mapped to the main regions of the heart affected in HLHS, including left ventricle, mitral valve and aortic valve. These regions were investigated at three different time-points: E10.5, E13.5 and E15.5.

4.7.1.8.1 Left ventricle

At E10.5, no expression of *Ets1* was detected in the left and right ventricles (Figure 4.28 A). However, at E13.5, *Ets1* expressed in the left and right ventricles (Figure 4.28 B). It was reported that *Ets1* expressed in the epicardial and the myocardial cell membranes of the ventricles, which reflected the expression observed here (Figure 4.28) (Cao et al., 2010). At E15.5, the expression of *Ets1* was completely absent from both ventricles (Figure 4.28 C). No expression was observed in the *Ets1* sense probe (Figure 4.28 D).

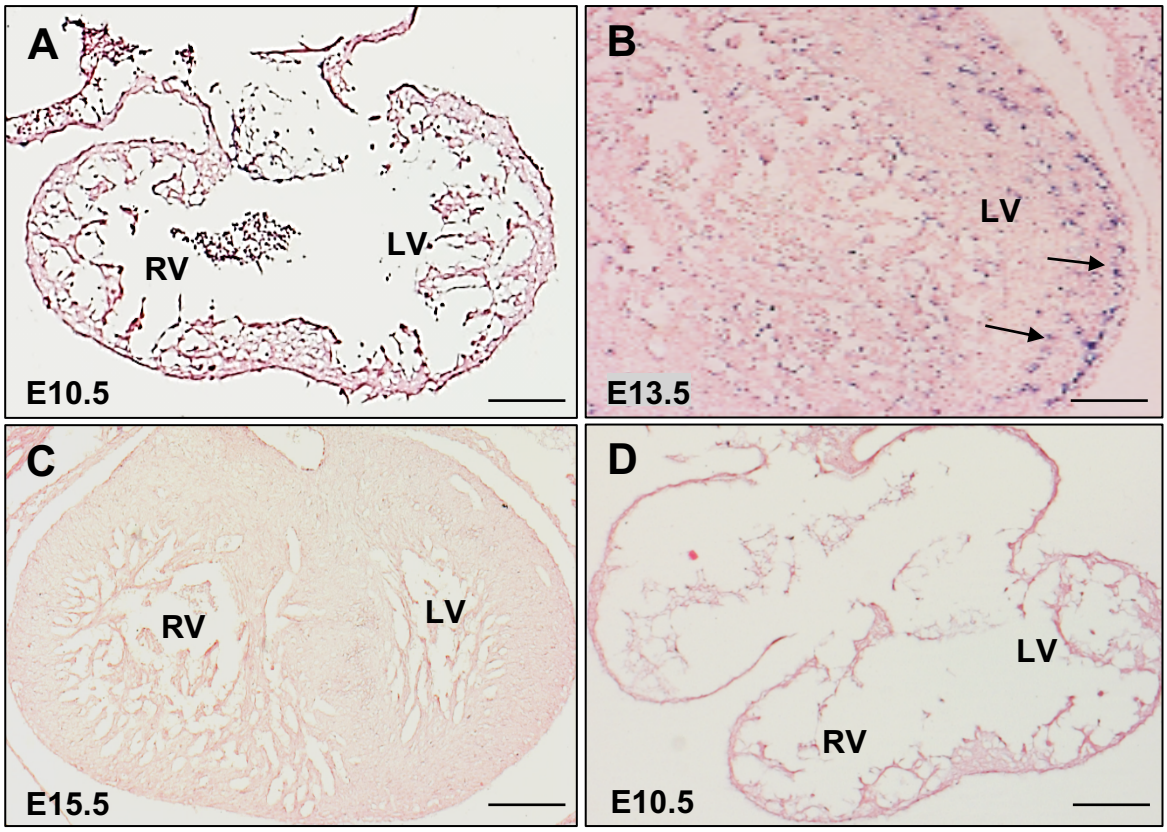

Figure 4.28: Expression of *Ets1* in the left ventricle at E13.5.
(A) No expression of *Ets1* in the left ventricle at E10.5. (B) A membrane-like expression of *Ets1* was found in the left and right ventricles at E13.5 (arrows = high power image of the left ventricle. (C) At E15.5, no expression of *Ets1* was observed in the left and right ventricles. (D) *Ets1* sense probe showed no expression in the heart at E10.5. Scale bar = 200μm.

4.7.1.8.2 Mitral valve

At E10.5, *Ets1* was expressed in the endocardial cushions of the atrioventricular canal (Figure 4.29 A). At E13.5, strong expression of *Ets1* was observed in the endothelial cells and the interstitial cells of the posterior leaflet of the mitral valve, whereas it was found only in the endothelial cells of the mitral valve anterior leaflet (Figure 4.29 B). At E15.5, the expression of *Ets1* was completely absent from the mitral valve (Figure 4.29 C). No expression was observed in the *Ets1* sense probe (Figure 4.29 D).

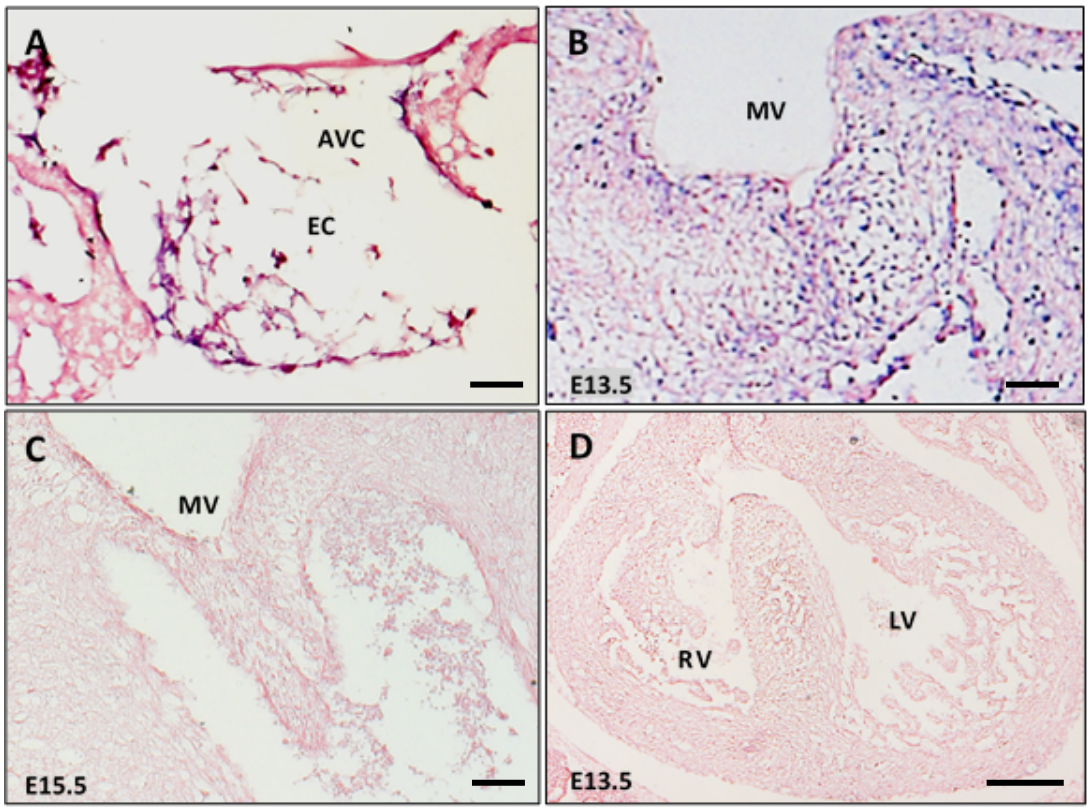

Figure 4.29: Expression of *Ets1* in the mitral valve at E10.5 and E13.5. (A) At E10.5, *Ets1* expressed in the endocardial cushions (EC) of the atrioventricular canal (AVC) and in the wall of AVC. (B) Expression of *Ets1* was detected in in the endothelial cells lining the anterior and posterior leaflets of the mitral valve as well as in the interstitial cells in the distal tip of developing primordia at E13.5. (C) At E15.5, *Ets1* was not expressed in the mitral valve. (D) *Ets1* sense probe showed no expression in the heart at E13.5. Scale bar: A-C= 100μm, D= 200μm.

4.7.1.8.3 Aortic valve

At E10.5, *Ets1* was expressed in the outflow tract (Figure 4.30 A). Also, as previously reported (Cao et al, 2010), high level expression of *Ets1* was observed in the mesenchymal cells located in the aortic sac at E10.5 (Figure 4.30 A). At E13.5, *Ets1* was strongly expressed in the endothelial cells covering the aortic leaflets, but not in the subendothelial cells of the leaflets (Figure 4.30 B). At E15.5, the expression of *Ets1* however was completely absent from the aortic valve (Figure 4.30 C). No expression was observed in the *Ets1* sense probe (Figure 4.30 D).

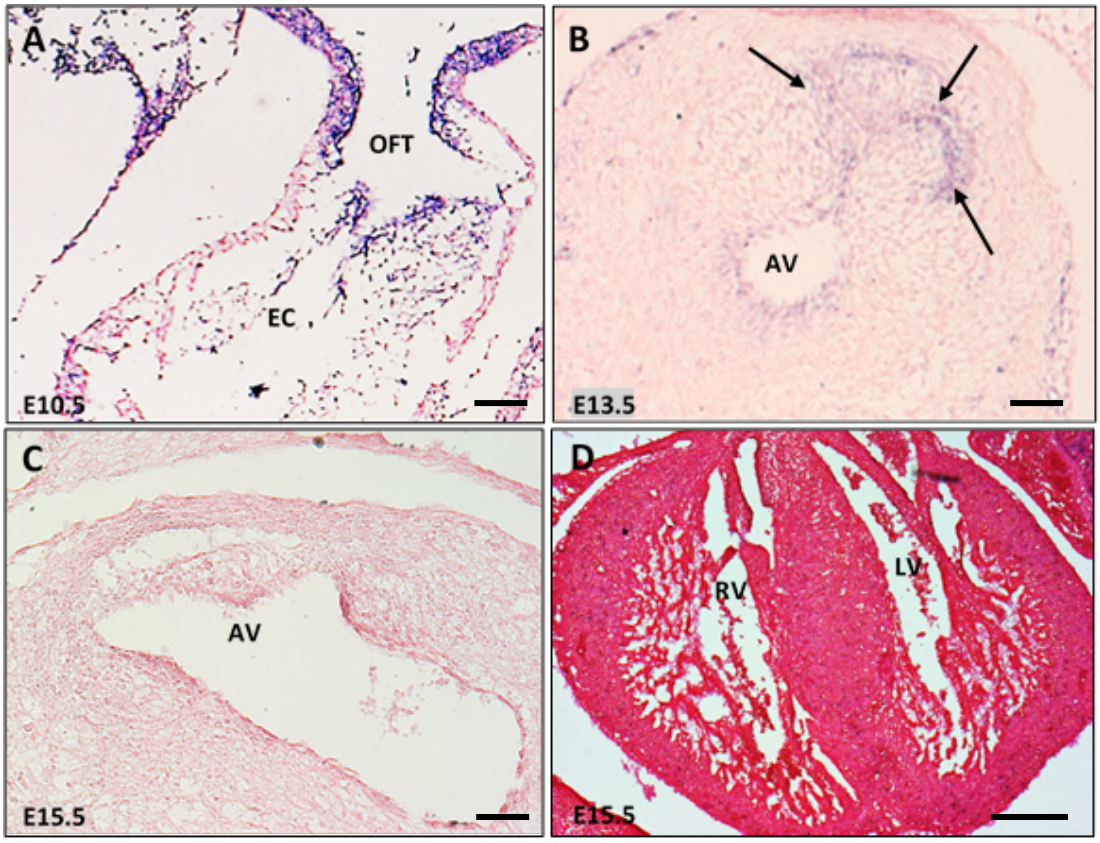

Figure 4.30: Expression of *Ets1* in the aortic valve at E10.5 and E13.5.
(A) *Ets1* was expressed in the mesenchymal cells covering the outflow tract tube and the endocardial cushion (EC) of the outflow tract (arrows). (B) At E13.5, *Ets1* expressed in the endothelial cells (arrows) covering the leaflets of the aortic valve, but not in the sub-endothelial cells. (C) At E15.5, no expression of *Ets1* was detected. (D) *Ets1* sense probe showed no expression in the heart at E15.5. Scale bar: A-C= 100μm, D= 200μm.

4.7.1.8.4 Summary

Altogether, *Ets1* showed strong expression in the early stages (E10.5 and E13.5) of the mitral and aortic valve formation as well as in the developing right and left ventricles at E13.5. However, this expression completely reduced as heart developed E15.5. Similar expression of *Ets1* was previously reported in mouse and chick embryos (Lie-Venema et al., 2003; Cao et al., 2010). Overall, *Ets1* shows essential roles during early heart development, which illustrated through its expression patterns at E10.5 and E13.5. These two stages are important for initial formation of valves and left ventricle, therefore *Ets1* could contribute to the abnormalities observed in the aortic and mitral valves as well as the left ventricle hypoplasia of HLHS.

4.7.1.9 *Pcdha9*

Expression of *Pcdha9* was mapped to the main regions of the heart affected in HLHS, including left ventricle, mitral valve and aortic valve. These regions were investigated at three different time-points: E10.5, E13.5 and E15.5.

4.7.1.9.1 Left ventricle

Pcdha9 expression was absent from the left and right ventricles at E10.5 (Figure 4.31 A). Similarly, the expression of *Pcdha9* was absent from both left and right ventricles at E13.5 and E15.5 (Figure 4.31 B C). No expression was observed in the *Pcdha9* sense probe (Figure 4.31 D).

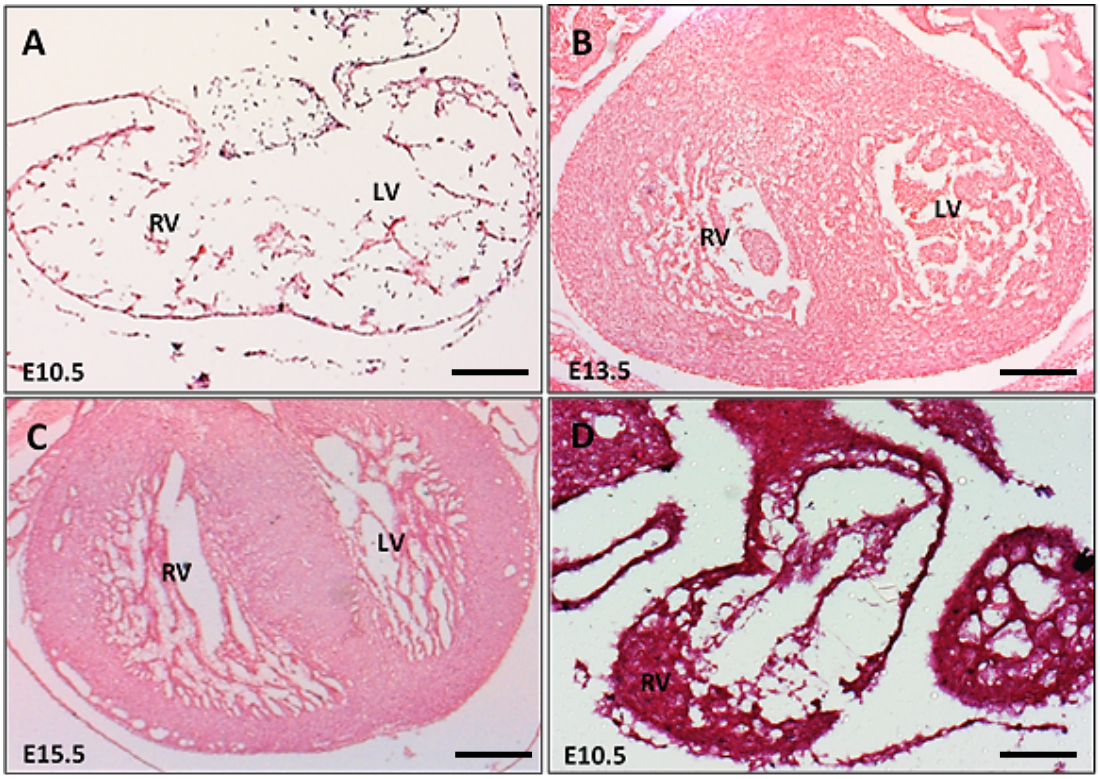

Figure 4.31: No expression of *Pcdha9* in the left ventricle at different developmental stages.
No expression of *Pcdha9* was detected in the left and right ventricles at (A) E10.5, (B) E13.5, and (C) E15.5. (D) *Pcdha9* sense probe showed no expression in the heart at E10.5. Scale bar = 200μm.

4.7.1.9.2 Mitral valve

At E10.5, *Pcdha9* expression was strongly detected in the endocardial cushions of the atrioventricular canal (Figure 4.32 A). However, at later stages (E13.5 and E15.5) the expression of Pcdha9 was absent from the mitral valve (Figure 4.32 B C). No expression was observed in the *Pcdha9* sense probe (Figure 4.32 D).

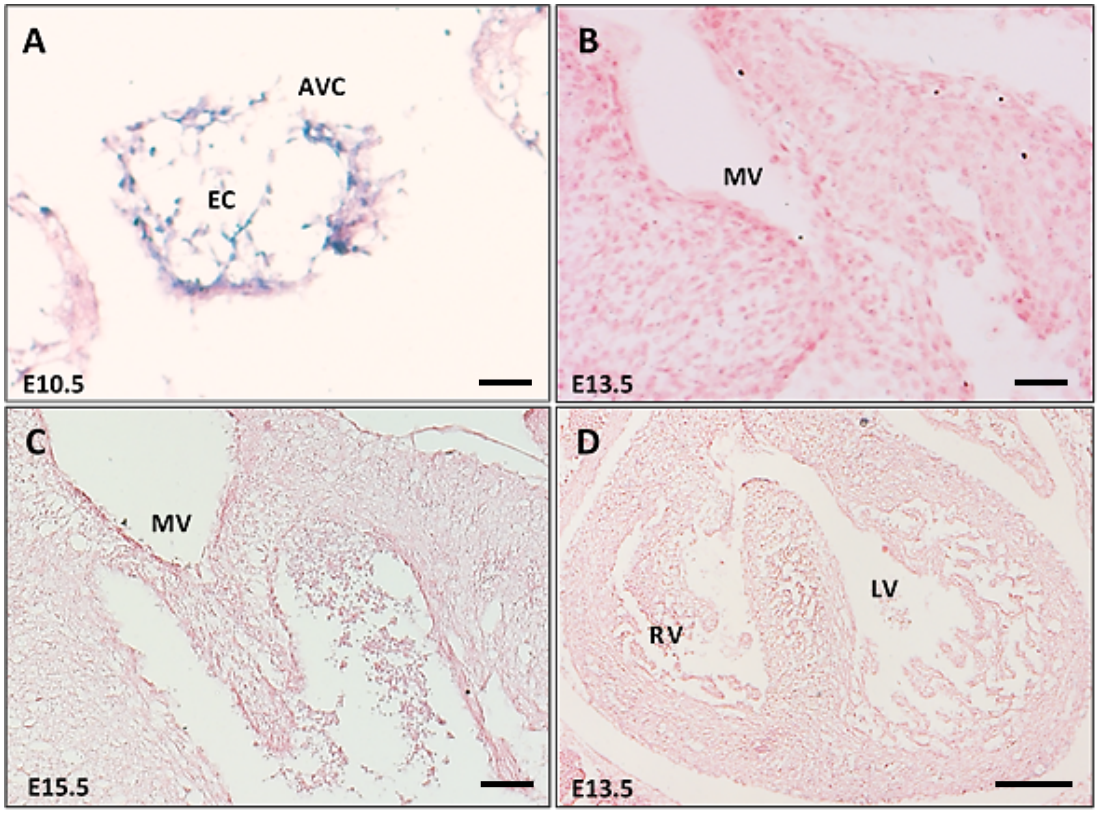

Figure 4.32: Restricted expression of *Pcdha9* in the endocardial cushions at E10.5.
(A) *Pcdha9* expressed in the endocardial cushions (EC) of the atrioventricular canal (AVC). No expression of *Pcdha9* was detected in the mitral valve (B) at E13.5, nor (C) at E15.5. (D) *Pcdha9* sense probe showed no expression in the heart at E13.5. Scale bar: A-C= 100μm, D= 200μm.

4.7.1.9.3 Aortic valve

Strong expression of *Pcdha9* was identified at E10.5 in the outflow tract and the mesenchymal cells found in the aortic sac (Figure 4.33 A). However, this expression was absent from the developed aortic valve at E13.5 and E15.5 (Figure 4.33 B C). No expression was observed in the *Pcdha9* sense probe (Figure 4.33 D).

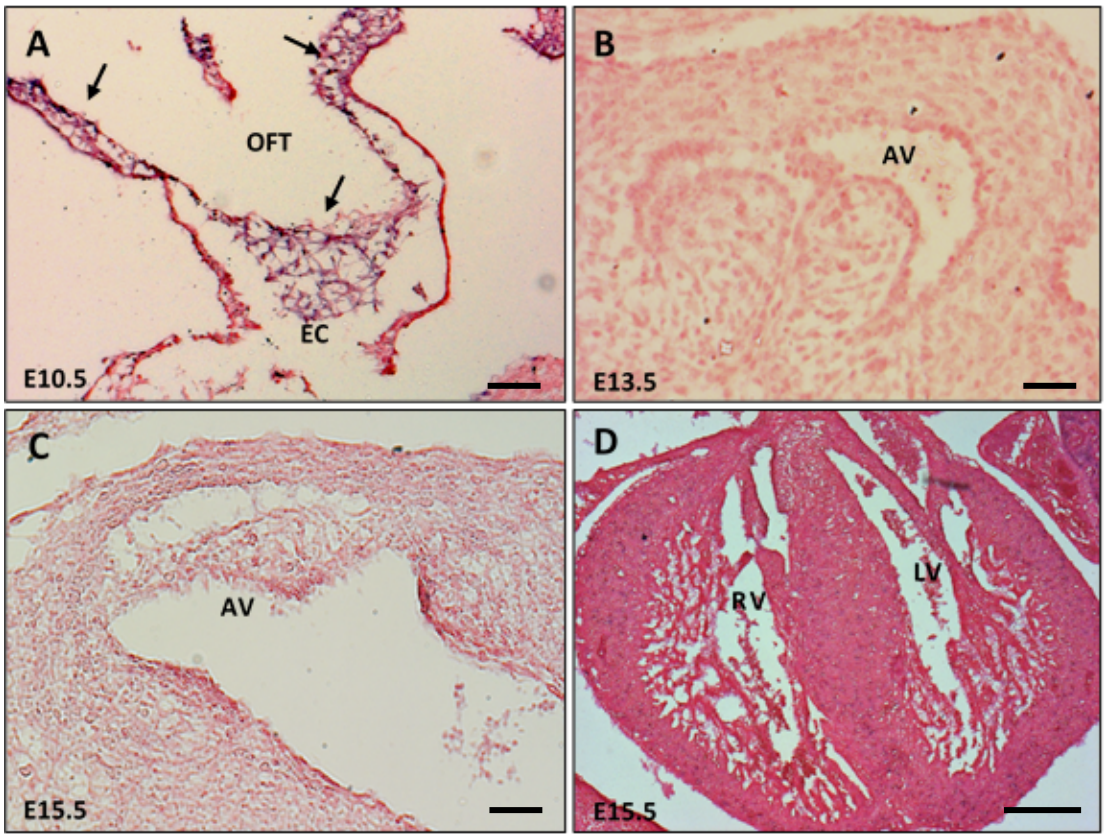

Figure 4.33: Restricted expression of *Pcdha9* in the endocardial cushions at E10.5.
(A) *Pcdha9* expressed in the endocardial cushion (EC) of the outflow tract (arrows) and *Pcdha9* was expressed in the mesenchymal cells covering the outflow tract (OFT) tube. *Pcdha9* was not expressed in the aortic valve at (B) E13.5 and (C) E15.5. (D) *Pcdha9* sense probe showed no expression in the heart at E15.5. Scale bar: A-C= 100μm, D= 200μm.

4.7.1.9.4 Summary

Altogether, *Pcdha9* is strongly expressed in the early cardiac developmental stage E10.5 and absent from the later stages of heart development E13.5 and E15.5. Expression of *Pcdha9* was previously reported using a quantitative PCR analysis, where *Pcdha9* expressed the highest in heart at E9.5. However, *Pcdha9* showed low expressions at E10.5, E13.5 and E15.5 (Liu et al., 2017). Expression study of *Pcdha9* using in situ hybridization in E9.5 mouse embryo showed localisation of its transcripts in brain and spinal cord; thus these regions were used as controls for this study (Figure 4.34 A,B,C) (Liu et al., 2017). Overall, expression of *Pcdha9* in the endocardial cushions during early development of the aortic and mitral valves suggests that *Pcdha9* can contribute to the valve abnormalities associated with HLHS.

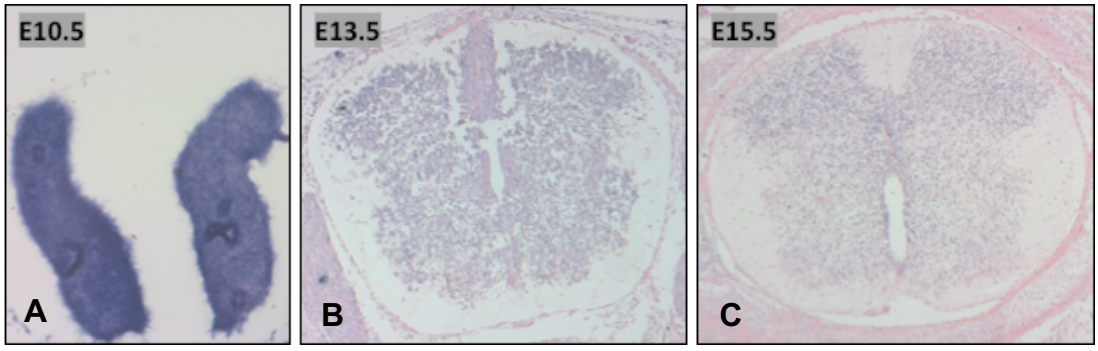

Figure 4.34: Expression of *Pcdha9* at different stges.
Expression of *Pcdha9* in the brain at E10.5, and spinal cord at E13.5 and E15.5. Scale bar: A= 50μm, B,C= 70μm.

4.7.1.10 *Sap130*

Expression of *Sap130* was mapped to the main regions of the heart affected in HLHS, including left ventricle, mitral valve and aortic valve. These regions were investigated at three different time-points: E10.5, E13.5 and E15.5.

4.7.1.10.1 Left ventricle

At E10.5, *Sap130* was not expressed in the left and right ventricles (Figure 4.35 A). However, *Sap130* expression was highly found in both the endocardium and myocardium of the left and right ventricles at E13.5 (Figure 4.35 B). Likewise, at E15.5, *Sap130* was highly expressed in the endocardium with low expression in the myocardium of left and right ventricles (Figure 4.35 C). No expression was observed in the *Sap130* sense probe (Figure 4.35 D).

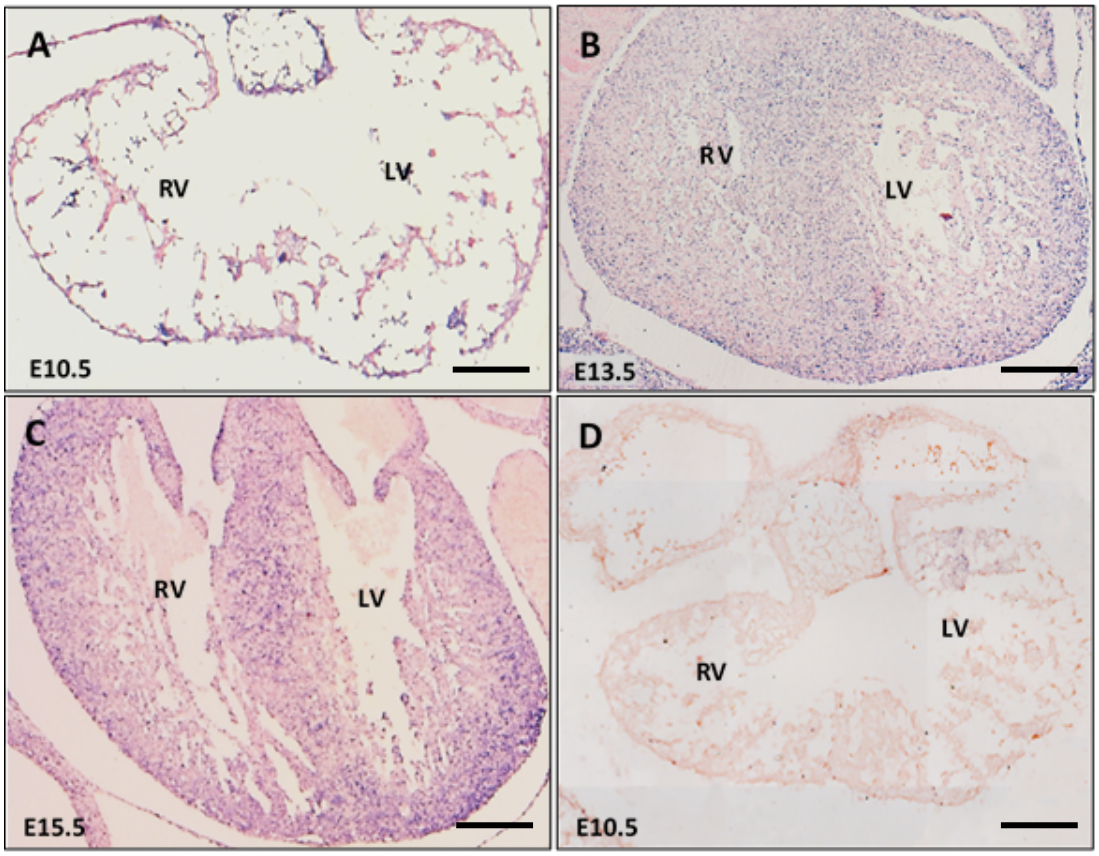

Figure 4.35: Expression of *Sap130* in the left ventricle during development of heart.
(A) No expression of *Sap130* detected in the left and right ventricles at E10.5. However, *Sap130* expression was detected in the left and right ventricular myocardium and endocardium at (B) E13.5, whereas only in the endocardium at (C) E15.5. (D) *Sap130* sense probe showed no expression in the heart at E10.5. Scale bar = 200μm.

4.7.1.10.2 Mitral valve

At E10.5, Sap130 was expressed in the endocardial cushions of the atrioventricular canal (Figure 4.36 A). At E13.5, *Sap130* expression was observed in the interstitial cells filling the mitral valve leaflets, but not in the endothelial cells covering the leaflets (Figure 4.36 B). However, at E15.5, the expression of *Sap130* was seen in both interstitial and endothelial cells of the mitral valve leaflets (Figure 4.36 C). No expression was observed in the *Sap130* sense probe (Figure 4.36 D).

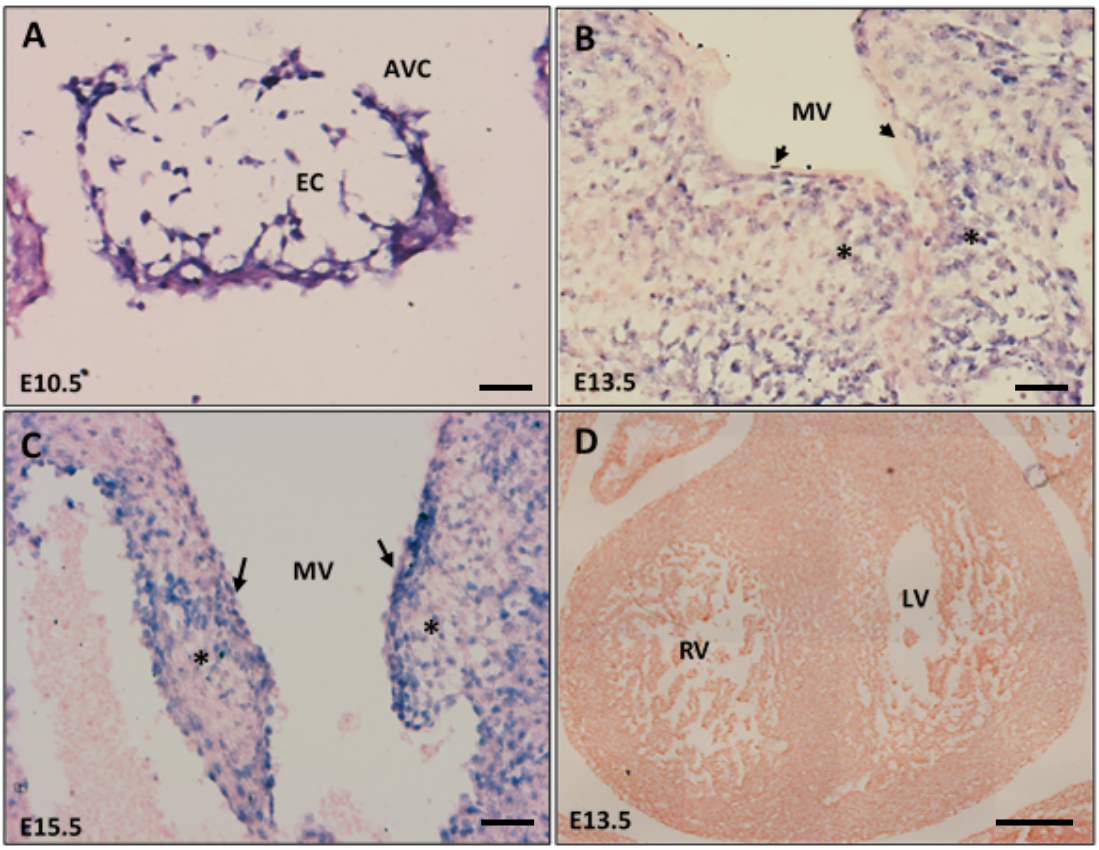

Figure 4.36: Expression of *Sap130* in the mitral valve during development of heart.
(A) *Sap130* expressed in the endocardial cushions (EC) of the atrioventricular canal (AVC). (B) At E13.5, expression of *Sap130* was detected in the interstitial cells (asterisk), but not in the endothelial cells (arrow heads) of the mitral valve leaflets. (C) However, at E15.5, *Sap130* was expressed in the interstitial cells (asterisk) and the endothelial cells (arrows) of the mitral valve leaflets. (D) *Sap130* sense probe showed no expression in the heart at E13.5. Scale bar: A-C= 100μm, D= 200μm.

4.7.1.10.3 Aortic valve

At E10.5, *Sap130* expression was seen in the outflow tract and the mesenchymal cells found in the aortic sac (Figure 4.37 A). Expression of *Sap130* in the aortic valve at E13.5 was localised to both endothelial and subendothelial cells of covering the leaflets (Figure 4.37 B), whereas at E15.5 it was only localised to the endothelial cells covering the leaflets (Figure 4.37 C). No expression was observed in the *Sap130* sense probe (Figure 4.37 D).

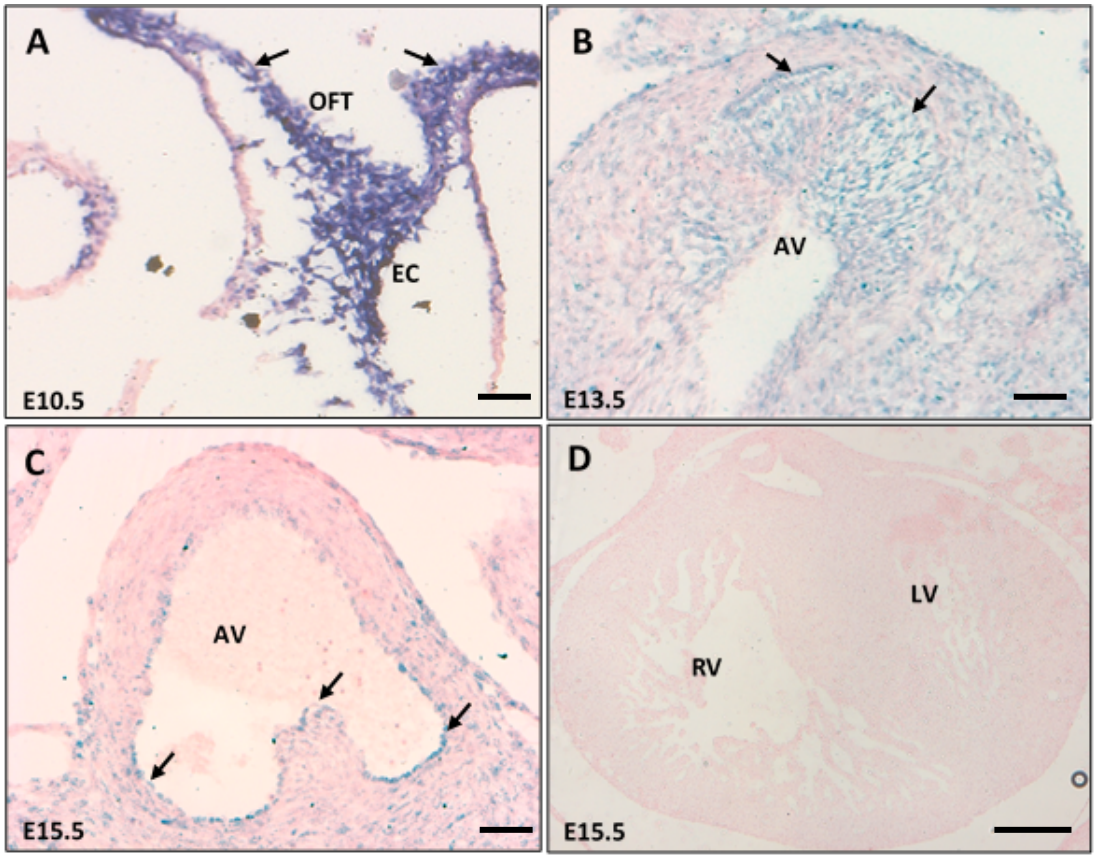

Figure 4.37: Expression of *Sap130* in the aortic valve during development of heart.
(A) At E10.5, *Sap130* was expressed in mesenchymal cells (arrows) and the endocardial cushion (EC) of the outflow tract. (B) At E13.5, *Sap130* was expressed in endothelial cells (arrow) and subendothelial cells of the aortic valve leaflets. (C) At E15.5, on the other hand, expression of *Sap130* was detected in the endothelial cells (arrows) covering the leaflets of the aortic valve. (D) *Sap130* sense probe showed no expression in the heart at E15.5. Scale bar: A-C= 100μm, D= 200μm.

4.7.1.10.4 Summary

Altogether, expression of *Sap130* was detected throughout the different developmental stages. *Sap130* expression was previously reported using a quantitative PCR analysis, where *Sap130* expressed the highest in heart at E9.5, whereas other stages including E10.5, E13.5 and E15.5 showed lower expression level than that at E9.5 (Liu et al., 2017). Also, expression study of *Sap130* using in *Sap130*-lacZ knockout (KO)-first allele in E9.5 and E13.5 mouse embryo showed that ubiquitous LacZ expression throughout the whole embryo (Liu et al., 2017). The fact that *Sap130* expresses in the cardiac cushions and mesenchymal cells at E10.5 and then become localised to the endothelial cells in the valves at later stages, suggesting it important role during initial formation and remodelling of valve leaflets. Also, because it expresses in the left and right ventricular endocardium, this suggests a role in the developing the ventricles. Therefore, *Sap130* could contribute to abnormalities observed in the ventricle and valves of HLHS.

4.7.1.11 *Rbfox2*

Expression of *Rbfox2* was mapped to the main regions of the heart affected in HLHS, including left ventricle, mitral valve and aortic valve. These regions were investigated at three different time-points: E10.5, E13.5 and E15.5.

4.7.1.11.1 Left ventricle

At E10.5, *Rbfox2* was not expressed in the right and left ventricles (Figure 4.38 A). However, at E13.5, *Rbfox2* highly expressed in the left and right ventricles (Figure 4.38 B). The expression of *Rbfox2* became more in the left than the right ventricular endocardium at E15.5 (Figure 4.38 C). No expression was observed in the *Rbfox2* sense probe (Figure 4.38 D).

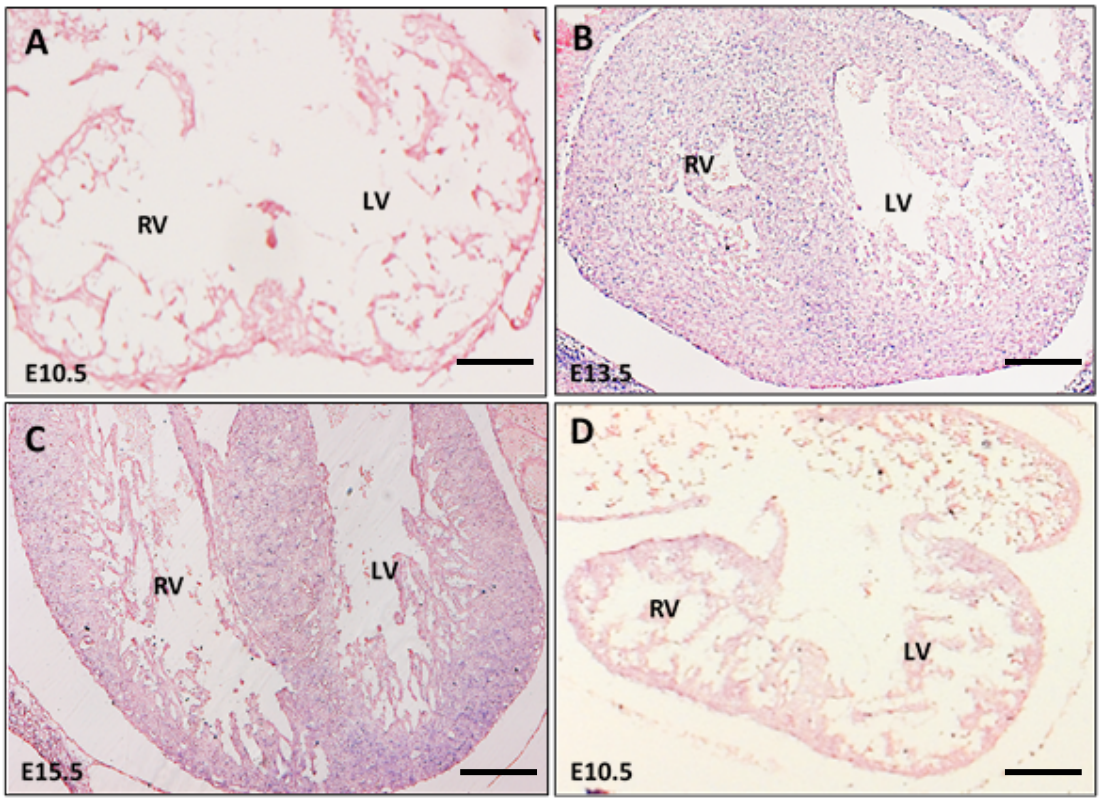

Figure 4.38: Expression of *Rbfox2* in the left ventricle at E13.5 and E15.5. (A) *Rbfox2* expression was not detected in the left and right ventricles at E10.5. However, *Rbfox2* was highly expressed in the left and right ventricles at (B) E13.5 and (C) E15.5; higher expression in the left ventricle compared to the right ventricle was detected, particularly in the endocardium. (D) *Rbfox2* sense probe showed no expression in the heart at E10.5. Scale bar = 200μm.

4.7.1.11.2 Mitral valve

Expression of *Rbfox2* was expressed in the endocardial cushions of the atrioventricular canal at E10.5 (Figure 4.39 A). At E13.5, *Rbfox2* was expressed in the interstitial cells, but not in the endothelial cells of mitral valve leaflets (Figure 4.39 B). Similarly, at E15.5, the expression of *Rbfox2* was detected in the interstitial cells in the tips of mitral valve leaflets (Figure 4.39 C). No expression was observed in the *Rbfox2* sense probe (Figure 4.39 D).

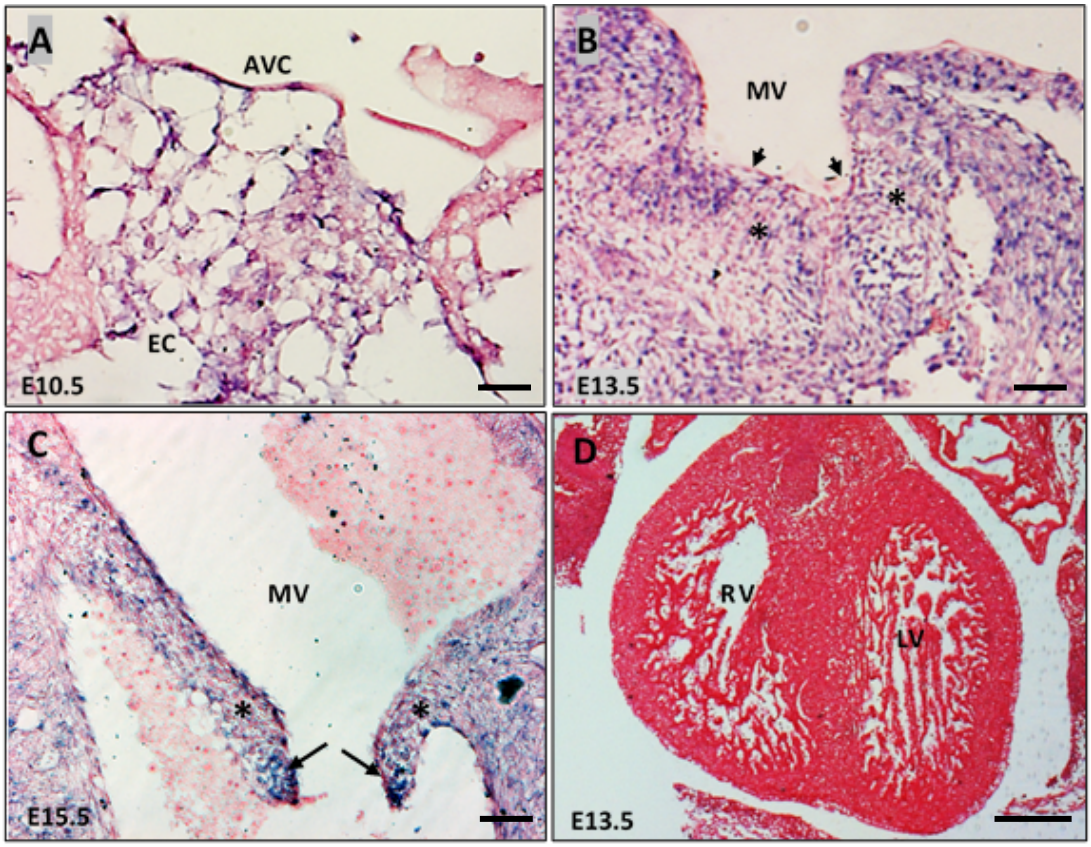

Figure 4.39: Expression of *Rbfox2* in the mitral valve during different developmental stages.
(A) *Rbfox2* expressed in the endocardial cushions (EC) of the atrioventricular canal (AVC) at E10.5. (B) Expression of *Rbfox2* was detected in the interstitial cells (asterisk), but not in the endothelial cells (arrow heads) covering the mitral valve leaflets at E13.5. (C) Similarly, at E15.5, *Rbfox2* was expressed in the interstitial cells (asterisk) found in the tips (arrows) of the mitral valve leaflets. (D) *Rbfox2* sense probe showed no expression in the heart at E13.5. Scale bar: A-C= 100μm, D= 200μm.

4.7.1.11.3 Aortic valve

At E10.5, *Rbfox2* expressed in the endocardial cushions of the outflow tract (Figure 4.40 A). At E13.5, it expressed in the sub-endothelial cells of the aortic valve leaflets and aortic valve wall (Figure 4.40 B), whereas at E15.5 *Rbfox2* expression became restricted to the sub-endothelial cells found in the aortic valve leaflets (Figure 4.40 C). No expression was observed in the *Rbfox2* sense probe (Figure 4.40 D).

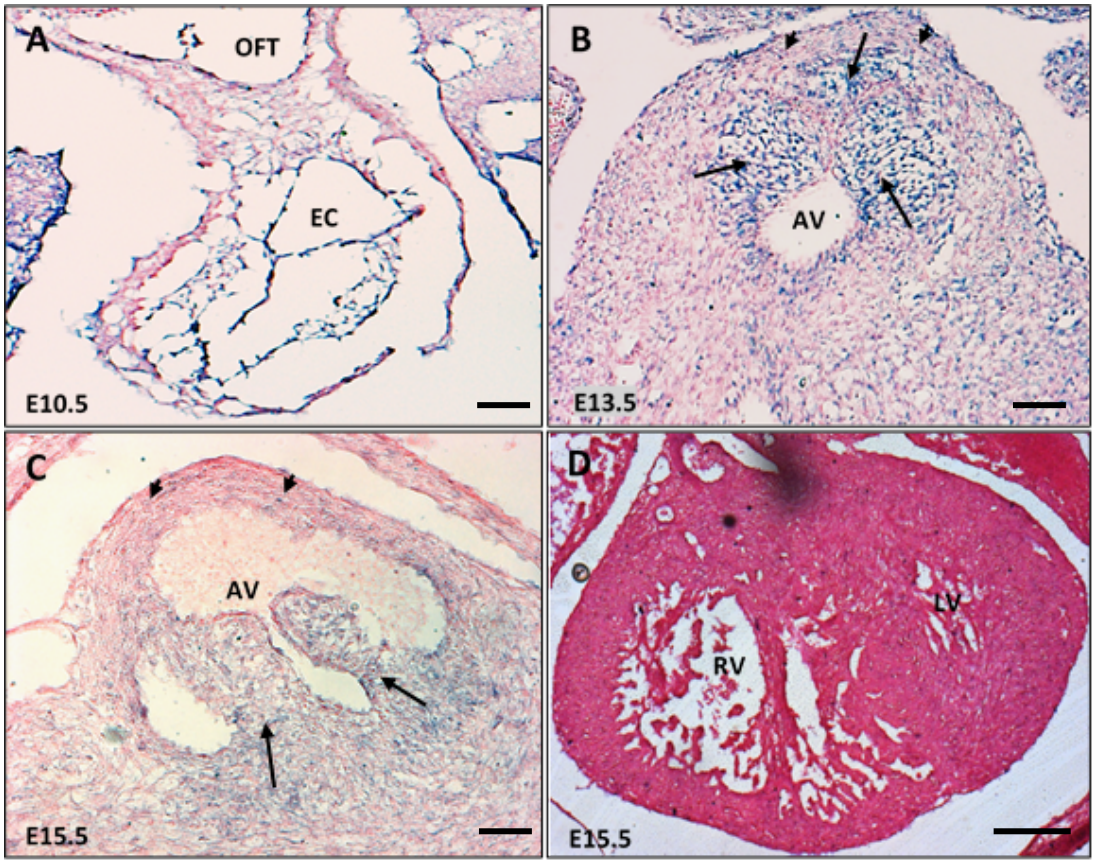

Figure 4.40: Expression of *Rbfox2* in the aortic valve during different developmental stages.
(A) At E10.5, *Rbfox2* was expressed in the endocardial cushion (EC) of the outflow tract. (B) At E13.5, *Rbfox2* was expressed in the sub-endothelial cells of the aortic valve leaflets as well as the wall of the aortic valve (arrows). (C) At E15.5, while expression of *Rbfox2* was detected in the sub-endothelial cells found in the leaflets of the aortic valve (arrows), no expression was seen in the aortic valve wall (arrow heads) (D) *Rbfox2* sense probe showed no expression in the heart at E15.5. Scale bar: A-C= 100μm, D= 200μm.

4.7.1.11.4 Summary

Altogether, *Rbfox*2 showed a strong expression in the endocardial cushion of the future mitral and aortic valves at E10.5, whereas no expression was seen in the ventricles at the same stage. At E13.5, high expression of *Rbfox2* in the ventricles was observed, which then restricted to the left ventricle at E15.5. Expression of *Rbfox2* was reported to be broadly expressed throughout the embryo including brain and cartilage at E14.5 (Visel et al., 2004). Thus, expression of *Rbfox2* at these regions was used as control (Figure 4.41 A-C). Overall, the fact that *Rbfox2* expressed in the endocardial cushions and in the left ventricle, the affected regions in HLHS, implicates its roles during the initial formation of these regions. This, therefore, suggests that *Rbfox2* can contribute to the abnormalities observed in HLHS.

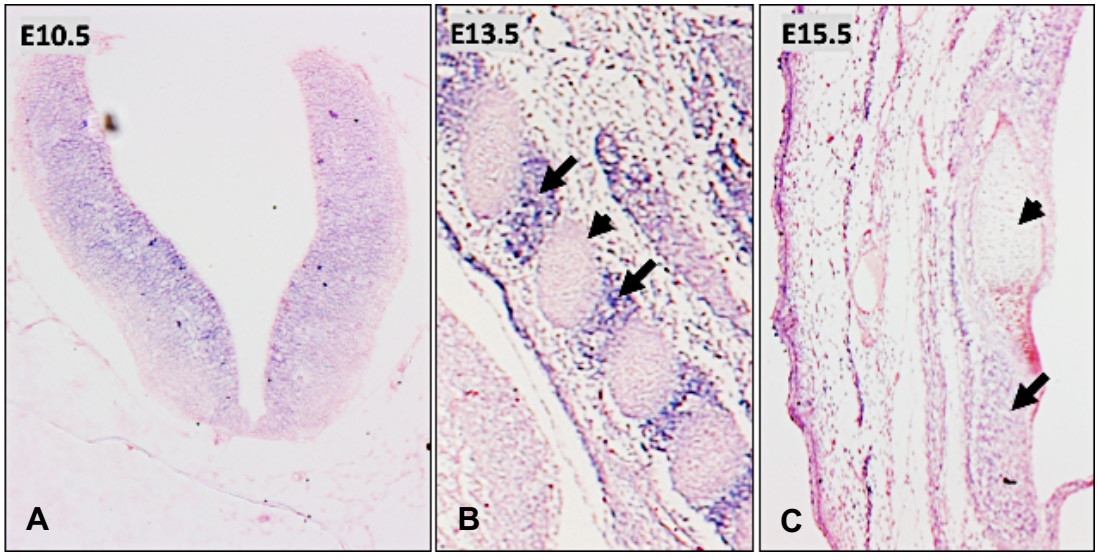

Figure 4.41: Expression of *Rbfox2* at different stges.
Expression of *Rbfox2* in the Brian at E10.5 and cartilage at E13.5 and E15.5 (arrows). A= 50μm, B,C= 70μm.

4.7.2 Critical analysis of HLHS-implicated genes

In summary, there are several genes that were suggested to implicate in HLHS including *Gja1, Nkx2.5, Notch* family, *Hand1, Foxc2, Ets1, Pcdha9, Sap130* and *Rbfox2*. The expression pattern for these genes was mapped during the crucial time points of development of the important cardiac regions in HLHS. A summary of these genes and where they expressed at different developmental stages as well as how they relevant to HLHS is illustrated in the table below (Table 4.12).

Table 4.12: HLHS implicated genes.

	E10.5				E13.5				E15.5				Comments
	OFT	AVC	LV	RV	AoV	MV	LV	RS	AoV	MV	LV	RS	
Gja1	✗	✗	✓	✓	✗	✗	✓	RV	✗	✗	✓	RV	*Gja1* expressed at the initial stages of ventricular formations, which could indicate its fundamental roles in hypoplasia of the left ventricle found in HLHS. However, since this gene was mapped to both left and right ventricles, it suggests that variations in this gene would affect both ventricles equally. Therefore, this gene seems less significant to HLHS.
Nkx2.5	✓	✓	✓	✓	✗	✗	✗	✗	✗	✗	✗	✗	*Nkx2.*5 expressed during early developmental stage of valves and both ventricles. This suggested that *Nkx2.5* could affect early cardiac development with no specification to the left-side structure of the heart. Thus, *Nkx2.5* seems less significant to HLHS.
Notch1	✓	✓	✓	✓	✓	✓	✓	RV PulV TV	✓	✓	✓	RV PulV	*Notch1* expressed during all developmental stages with no specification to one side. Although this suggested the importance of *Notch1* for heart development, it also suggested that *Notch1* could lead to defects in

												both sides of the heart. Hence, *Notch1* seems less significant to HLHS.
Notch3	✗	✗	✗	✗	✗	✗	✗	✗	✗	✗	✓	RV PulV	*Notch3* expressed in the left ventricle at E15.5 with minor expression in the right ventricle, which suggested that *Notch3* played roles in the later developmental stage of the left ventricle. This therefore highlights its significant for defects associated with the left ventricle in HLHS, particularly in the miniturised group or the thick-walled ventricle group of HLHS. Hence, *Notch3* seems significant for HLHS.
Notch4	✗	✗	✓	✓	✗	✗	✗	✗	✗	✗	✗	✗	Expression of *Notch4* was found in the left and right ventricles at E10.5, with no expression at later stages. This indicated its roles in the early developing of the ventricles. Since *Notch4* expressed in the left and right ventricles, it could contribute to defects in both ventricles equally. This therefore makes *Notch4* less significant for HLHS.
Hand1	✓	✗	✓	✓	✓	✓	✓	RV TV	✓	✓	✓	RV TV	*Hand1* expressed in most of the interesting regions in HLHS except the atrioventricular cushions, which suggested its important roles in developing the left sided structures of the heart. However, the fact that modeling the suggested *Hand1* mutation in mice produced severe heart abnormalities but normal left

													ventricle size; and knocking out *Hand1* completely caused embryonic lethality; illustrated the important of maintaining its regulation during heart development. Nevertheless, the expression patterns of *Hand1* makes it an interesting gene that needs to be investigated further in order to understand the mechanisms behind its functions. Therefore, *Hand1* seems to be significant for HLHS.
Foxc2	✓	✗	✗	✗	✓	✗	✗	✗	✓	✗	✗	✗	*Foxc2* expressed in the outflow tract at E10.5 and then restricted to the aortic valve, which suggested its essential roles in the formation and developing of the aortic valve. Thus, Foxc2 could contribute to the malformation affecting the aortic valve in HLHS, particularly HLHS subgroup with severe aortic valve malformation, such as the thick-walled ventricle group. Therefore, Foxc*2* seems significant for HLHS.
Ets1	✓	✓	✗	✗	✓	✓	✓	RV TV	✗	✗	✗	✗	Expression of *Ets1* was mapped at E10.5 to the endocardial cushions and E13.5 to the aortic and mitral valves and left ventricle, but no expression was seen at E15.5. This suggested that *Ets1* could involve in the original development of the valves as well as

													the ventricular morphogenesis. However, the fact that *Ets1* expressed in these regions and in the right-side regions indicated that this gene could also cause abnormalities in both sides equally. Therefore, *Ets1* seems less significant to HLHS.
Pcdha9	✓	✓	✗	✗	✗	✗	✗	✗	✗	✗	✗	✗	Expression of *Pcdha9* was mapped to the endocardial cushions at E10.5, but not to the left ventricle, nor in any other cardiac regions at later developmental stages. This suggested that *Pcdha9* played roles in the early formation of valves through endocardial cushions. Thus, *Pcdha9* could contribute to the abnormalities associated with the mitral and aortic valves in HLHS. Since *Pcdha9* affects both endocardial cushions of the outflow tract (future aortic valve) and atrioventricular canal (future mitral valve) at the same level, this suggests that *Pcdha9* contributes to the abnormalities associated with HLHS subgroup that has similar defect level of mitral and aortic valve; such as the miniaturized ventricle group. Therefore, *Pcdha9* seems significant to HLHS.
Sap130	✓	✓	✗	✗	✓	✓	✓	RV	✓	✓	✓	RV	Expression of *Sap130* was mapped to most of the regions in the heart throughout the different stages, excluding the left/right ventricles at

							PulV TV				PulV TV	E10.5. The fact that *Sap130* expressed in the left and right sides of heart and also throughout the embryonic body (Liu et al, 2017), suggested that this gene had multiple roles throughout the heart and the rest of the body, and thus losing its functions could not only lead to heart defects, but also to embryonic lethality. Therefore, this gene seems less significant for HLHS.
Rbfox2	✓	✓	✗	✗	✓	✓	✓	RV PulV TV	✓	✓	✓	PulV	Expression of *Rbfox2* was mapped in all the heart regions of HLHS throughout the different stages, excluding left/right ventricle at E10.5. The ubiquitous expression of *Rbfox2* suggested essential roles for this gene during heart development. However, since this gene was also expressed outside the heart, suggested a significant role for *Rbfox2* not only in the heart but in normal development of embryo. Therefore, *Rbfox2* seems less significant for HLHS.

OFT: outflow tract, AVC: atrioventricular canal, LV: left ventricle, RV: right ventricle, AoV: aortic valve, MV: mitral valve, RS: right structure of the heart, PulV: pulmonary valve, TV: tricuspid valve.

4.8 Discussion

Although several genes have been proposed to implicate in hypoplastic left heart syndrome (HLHS), none of these genes were confirmed as being pathogenic with a clear mechanism underpinning the development of HLHS delineated (Liu et al., 2017, Firulli et al., 2017). In this study, however, the most significant genes for HLHS were highlighted and their potential functions and expressions during heart development, particularly in the specific structures that are affected in HLHS were described. The analysed genes in this study included *Gja1, Nkx2.5, Notch1,3,4, Hand1, Foxc2, Ets1, Pcdha9, Sap130*, and *Rbfox2*. Investigation of their expression patterns during development of the affected regions in HLHS illustrated their potential involvement in formation/functionality of these regions. Although some of these genes presented broad expression throughout the developmental stages, some genes, such as *Notch3, Hand1, Foxc2,* and *Pcdha9*, showed specific expression to the cardiac regions of HLHS. Hence, this demonstrated their essential roles in developing these regions and at the same time suggesting the subgroup of HLHS that could potentially cause.

As yet, no genetically engineered animal models have been generated for HLHS. Although several animal models have been proposed for HLHS, none of them showed left ventricular hypoplasia in the setting of an intact ventricular septum with maintaining the ventriculoarterial and atrioventricular connections (Grossfeld et al., 2019). The difficulty in generating appropriate animal model was explained for specific epigenetic factors, such as *NKx2*.5, by a

combination of genetic, environmental and epigenetic factors, which proposed to be necessary to cause HLHS (Schulkey et al., 2015). However, conditional deletion of *Nkx2*.5 in murine ventricle generated a cardiomyopathic phenotype accompanied with BMP10 upregulation. This over-expression of BMP10 in murine left/right ventricles produced a thinned compact layer with increased ventricular trabeculations, and hence loss of chamber cavity. Although this model had proposed that the hypoplastic left ventricular cavity was caused by overgrowth of the trabecular layer, rather than the compact layer (Pashmforoush et al., 2004). This model also affected the right ventricular cavity, which suggested less specificity for left ventricular hypoplasia. Therefore, *Nkx2*.5 is less significance for HLHS.

Previous studies have implicated *Notch1* as one cause of hypoplastic left ventricle in HLHS (Garg et al., 2005; McBride et al., 2008). It was reported that loss-of-function mutations in *Notch1* in *Drosophila* led to increase cardiac myocytes and a total loss of pericardial cells. Hence, it generated an abnormal bifid heart with a diminished chamber volume (Hartenstein et al., 1992). The investigation in this chapter showed that *Notch1* expressed in endocardial cushions, endocardium and myocardium during murine cardiac development. This suggested that defects in one or all of these cell lines could lead to produce the phenotypic findings of HLHS. Nevertheless, knocking out the Notch intracellular domain (NICD1), which is important for subcellular localisation, in mice did not show the anticipated phenotypes of HLHS (Watanabe et al., 2006). Instead, several cardiac abnormalities including atrioventricular myocardium defect, disrupted cardiomyocyte differentiation,

and intraventricular septum shifting to the right were generated (Watanabe et al., 2006). Hence, *Notch1* has a very high penetrance and can produce various cardiac defects.

Similar to *Notch1*, loss-of-function mutations in *Ets1* in *Drosophila* demonstrated an increased number of cardiomyocytes with a loss of pericardial cells in the posterior aspect of the heart tube, which thought to resemble the left ventricle in mammalian heart (Alvarez et al, 2003). In addition to that, the expression patterns for *Ets1,* in this chapter and consistent with (Ye et al., 2010) study, was mapped to the endocardial cushions, neural crest cells and endocardium. This therefore suggested that abnormalities in these cells, or at least one of them, could produce HLHS phenotypic features. Nevertheless, *Ets1* neural crest cells knockout embryos and *Ets1* cardiac mesodermal knockdown embryos did not generate the anticipated features of HLHS. Instead these embryos exhibited either various cardiac defects including double outlet right ventricle and isolated dilation of the ascending aorta, or growth arrest in the left ventricle leading to small and thin-wall looking ventricle and eventually die at E11 (Kelle et al., 2015; Snider et al., 2014). Therefore, Ets1 seems less significance for HLHS.

There were other suggested genes for HLHS including *Gja1*, *Notch3* and *Notch4* that showed specific expressions in the ventricles. Expression of *Gja1* was found mainly in the myocardial cells of left and right ventricles and thus knocking down *Gja1* in mice caused a reduction in myocardial gap junctions and altered the structure and function of both ventricles, yet did not cause HLHS phenotypic features (Flenniken et al., 2005). Similarly, although *Notch4*

was mapped to the early heart development (E10.5) of the left and right ventricles and in vascular endothelial cells (Costa et al., 2013), knocking out its expression did not cause HLHS. In fact, it did not even lead to any detectable abnormalities, but rather mice developed normally. Conversely, homozygous loss of *Notch1* and *Notch4* in mice caused vascular abnormalities and embryonic lethality, which compared to the homozygous *Notch1* null mice that developed the same abnormalities but less severity than that observed in the combination (Krebs et al., 2000; Costa et al., 2013). This suggested that *Notch4* plays a role in vascular development, which remains unknown, but it definitely exacerbated the consequence of *Notch1* deficiency. However, the consequences of knocking out *Notch3* was found to decrease the progenitor cells and resulted in small arterioles with abnormal vessels on the cardiac ventricular wall (Tao et al. 2017). Although these changes were reported in adult mice (7-9 month-old), this implicated a significant role for *Notch3* in vascular maturation during embryogenesis. There is less knowledge about the specific roles of *Notch3* during heart development, but its expression in the late developmental stage of the left ventricle suggested an interesting role for *Notch3* during the left ventricle formation. Therefore, Notch3 may contribute to the left ventricular abnormalities associated with HLHS.

Other genes, such as *Foxc2*, which were found to express in the aortic valve and associated with HLHS and other congenital heart defects (CHD). The fact that *Foxc2* was mapped to mesenchymal cells of the outflow tract highlighted the possibility of producing HLHS phenotypic features through abnormalities in these cells. Association of *FOXC2* with HLHS patients has been suggested.

A study using high-resolution oligonucleotide array identified variants in *FOXC2* in 2 out of 7 patients with HLHS (Stankiewicz et al., 2009). Likewise, variants in *FOXC2* were identified in 23 out of 53 patients with HLHS (Iascone et al., 2012), although the biological significance of these *Foxc2* variants remains unknown. These findings in addition to *Foxc2* expression pattern, suggest that *Foxc2* may contribute to at least abnormalities in the aortic valve observed in HLHS. Further investigation of *Foxc2* roles, particularly in the mesenchymal cells, remains important, as it is quite possible that *Foxc2* may have other yet to be determined impacts on HLHS.

Some of the implicated genes in HLHS showed very similar expression pattern including *Rbfox2* and *Sap130*, as they expressed in the regions of interest for HLHS at different developmental stages and also in various regions of the body, particularly in brain. In addition to *Rbfox2* embryonic expression in the heart, it expressed postnatally during heart remodelling; which suggested an important role for *Rbfox2* in embryonic and postnatal heart development (Partridge and Carter, 2017; Ye et al, 2017). Double knockdown of *Rbfox1l*/*Rbfox2* in zebrafish embryos labelled with GFP myocardial cells showed ventricular defects in these embryos. Nevertheless, injection of these embryos with *rbfox2* alone rescued the heart ventricle, which indicated its significant roles in the left ventricular growth (Gallagher et al., 2011). Similarly, *Sap130* was reported to express in the embryonic heart and new-born heart. Knockdown of *sap130a* in Zebrafish revealed a reduce in ventricular cardiomyocytes at 72 h postfertilization, when the first heart field cells found in the heart (Cordero-Espinoza et al., 2013). Hence, *Sap130* was suggested to

involve in cardiomyocyte cell proliferation and cell cycle arrest. However, the cellular and molecular mechanisms driving the hypoplastic left ventricle through Rbfox2 and Sap130 remain unknown. Therefore, further investigation is needed to understand their roles in hypoplasia of the left ventricle.

The fact that *Hand1* was mapped to the left side structures of the heart, particularly to epicardium, endocardium and outflow tract neural crest cells indicated essential roles for *Hand1* during cardiogenesis (Barnes et al., 2010). The suggested causation of HLHS was a mutation in $HAND1^{A126fs}$ (Reamon-Buettner et al, 2008), which was directly tested in mice. Although neither *Mef2CAHF-Cre* (targeting endothelial SHF) and *Nkx2.5Cre* (targeting SHF) resulted in HLHS when crossed to the $HAND1^{SFA126fs}$ allele, these *Cre* drivers caused elongated outflow tract and eventually led to early embryonic lethality (Firulli et al., 2017). Therefore, it was suggested that the $HAND1^{A126fs}$ mutation was not biologically relevant to HLHS, yet mutations within *Hand1* enhancer domain that changes its spatiotemporal expression and led to less deleterious effects would be more likely to associate with HLHS. The association of *Pcdha9* with HLHS has been suggested, although its roles in cardiogenesis remains largely unknown. Nonetheless, expression patterns of *Pcdha9* implicated roles for this gene in formation of valves as it was found in the endocardial cushions of the outflow tract (future aortic valve) and atrioventricular canal (future mitral valve). Therefore, further investigation on the significant of *Pcdha9* during heart development is required to understand its association with HLHS.

Together, these data suggest that some HLHS implicated genes showed very specific expression patterns, particularly at the regions of HLHS, whereas other genes showed broad expression throughout the embryo. Although the genes with broad expressions showed significant roles during cardiogenesis and possible association with HLHS, the likelihood of these genes to be the main causative of HLHS seems low. It is speculated that *Notch3, Hand1, Foxc2,* and *Pcdha9* would be more likely to correlate, based on their expression patterns, with the abnormalities associated with various subgroups of HLHS.

4.9 Summary

In summary, there have been several genes implicated for HLHS in which some of them showed low significance for being a HLHS causative. This indeed can be explained by the low prevalence of HLHS, which makes many genetic studies pooling HLHS cases with other phenotypically related heart malformations and this hence raises questions about relevance of these genes to HLHS. Also, from the current study, it is well-recognised that HLHS has various subgroups that can be caused by different genes and these subgroups need to be analysed separately to avoid implication of insignificant genes to HLHS. In this chapter, evaluation of all the suggested genes for HLHS was performed. Description of HLHS-implicated genes roles and detecting their expression patterns were carried out using the main developmental stages for HLHS. Some genes showed very broad and less significant association with HLHS including *Gja1* and *Sap130,* whereas other genes showed specific expression to the affect regions of HLHS. Further, these genes were linked to the potential subgroup of HLHS that could be resulted from mutations within that gene.

Chapter 5: General Discussion

Hypoplastic left heart syndrome (HLHS) is a severe form of congenital heart defect that affects multiple regions of the hearts to a varying degree. In this study, a series of 78 hearts from the Birmingham Children's Hospital (using the standard valve-based classification method), classified as having HLHS, was re-analysed and a novel classification method was proposed, based on the ventricular phenotypes. Hence, three distinctive ventricular morphologies were identified: slit-like ventricle, thick-walled ventricle and miniaturised ventricle. Although the standard valve-based classification reflects the clinical approach to treatment, it does not demonstrate the genetic aspect of HLHS. However, the proposed ventricular classification provides possible explanations for HLHS developmental origins and hence reveals a route for genetic studies via the perspective of progenitor contributions to particular affected structures in HLHS. In addition, the fact that the thick-walled ventricular group has resulted in categorising the AA/MS and severe AS/MS clinical groups that showed identical anatomical features as one group, while presenting great differences between the other clinical groups. This demonstrates the advantage of the ventricular-based classification, as it presents the HLHS hearts with similar ventricular morphology together to highlight parallel genetic causes for both the AA/MS and severe AS/MS subgroups. Moreover, although HLHS is routinely diagnosed through echocardiogram; which provides high frequency sound waves to generate moving images of heart structure and blood flow; classification of HLHS subgroups using the valve-based classification can be misleading. For example, severe aortic stenosis could be misclassified because imperceptible blood flow through the aortic valve would categorise as aortic atresia. Whereas

this could be due to the left ventricle being unable to pump blood to the aortic valve and with the aortic valve being severely affected the blood would not appear to flow through it. Therefore, utilizing the ventricular-based classification should provide accurate indication of HLHS subgroups. Altogether, the ventricular-based classification demonstrates a good basis for exhibiting the different HLHS subgroups.

The current study not only suggested a novel classification of HLHS, it also showed the importance of archival heart collections in understanding the morphological appearances of HLHS in the different subgroups. On the basis of the close similarity of hearts in the three identified subgroups, it is suggested that it could be used as a basis for genetic studies of HLHS. However, because formalin was used to preserve the archival hearts, using these hearts for molecular studies would be a challenge. This is because formalin disrupts the chromosomal DNA in these tissues, resulting in corrupt and short sequencing reads from that DNA. This hence generates sequences with various artefacts that cannot be distinguished from heterozygosity. This current study described a cheap and scalable in-house method that allowed the extraction and sequencing of high-quality DNA from long-term formalin-fixed materials. It was previously reported that reliable sequencing data could only be obtained from tissues that had been fixed in formalin for no longer than one day (Einaga et al., 2017). However, this study proved that it was possible to extract DNA and generate a reliable sequencing data from tissues fixed for up to 2 years using the improved method. Using Next Generation Sequencing (NGS) with the GATK best practice pipeline, described in chapter 4, generated high specificity

for detecting variants in DNA sequencing, with moderate sensitivity. However, using Sanger sequencing generated unreliable data that cannot be used to discover new rare variants, but it remains useful to confirm identified variants. Altogether, both NGS and Sanger sequencing demonstrated variable degree of accuracy for detecting variants in DNA extracted from formalin-fixed tissues, and hence it would not be recommended to use archival tissues except to check for variants that were previously identified in fresh tissues.

The genetic aetiology of HLHS has been supported with a growing body of evidence throughout the years (Shokeir, 1974, Hinton et al., 2008). To date, there are three suggested transmission patterns of HLHS: autosomal recessive, autosomal dominant and polygenic inheritance. Since there are three ventricular subgroups of HLHS described in this study, it may be that there are different aetiologies for different HLHS subgroups. Therefore, in this study, evaluation of the HLHS-implicated genes was carried out in respect to their potential functions and expression during heart development, in the specific structures that are affected in HLHS. The analysed genes in this study included *Gja1, Nkx2.5, Notch1-4, Hand1, Foxc2, Ets1, Pcdha9, Sap130*, and *Rbfox2*. There were some genes that demonstrated broad expression and did not appear to be good candidates for causing the very specific and reproducible phenotypes seen in HLHS. In contrast, other genes showed specific expression to the regions affected by HLHS. Further, these genes could be linked to a potential subgroup of HLHS, based on the precise ventricular and valve phenotypes seen in each group. Further investigation is needed to gather additional evidence for an association between these genes

and a particular subgroup of HLHS. Even though numerous reports have implicated some of these genes in HLHS, identification of specific genes or variants remains challenging. This can be explained by the low prevalence of HLHS, which meant that several genetic studies pooled HLHS cases with other phenotypically related (and sometimes unrelated) heart malformations and this hence raises questions about relevance of these genes to HLHS. Also, from the current study, it is well-recognised that HLHS has various subgroups that could be caused by different genes, suggesting that it might be a good idea to analyse the subgroups separately. For example, a study carried out by Zuffardi group (2012), which used a defined-group of HLHS based on Tchervenkov et al. 2006 classification of HLHS, identified most of the HLHS-implicated genes (Iascone et al., 2012). Hence, further subgrouping of HLHS could lead to identify the specific gene(s) for the desired HLHS subgroup. Altogether, the current study highlighted the potential importance of using a unique subgroup of HLHS in order to find the causative genes for HLHS.

Therefore, future work will involve using a well-defined, carefully phenotyped and homogeneous subgroup of HLHS, ideally the slit-like ventricular group of HLHS (SLV-HLHS). This is because the SLV-HLHS group showed atresia or absence of both mitral and aortic valves as well as a highly uniform slit-like ventricular cavity, suggesting that all the HLHS regions are equally affected. Hence, speculation about the causative gene(s) for the SLV-HLHS group suggests that they might influence the remodelling of the valves, together with left ventricular growth, if each region is affected primarily, or just the valves if this is a sequence with the ventricular phenotype secondary to the valve

defects. Therefore, collecting samples from patients with the SLV-HLHS and performing exome sequencing on these sample will allow the identification of genes that are specific for this subgroup. In order to filter the data and home in on likely relevant genes, one strategy would be to generate a list of specific genes (from RNaseq at relevant stages of development, for examples when the valves are remodelling) that are only found in the HLHS-affected cardiac regions, from normal human embryonic heart. These regions would include the mitral valve, aortic valve and left ventricle, collected from human embryonic heart at CS14, CS17 and CS22, equivalent to the mouse embryonic stages of E10.5, E13.5 and E15.5 respectively. Filtering the exome patient data according to the RNAseq data of the normal heart regions will allow identification of genes that are variant in the patients and expressed in the regions of interest. This could provide a useful approach to identify the gene(s) that cause the SLV subgroup of HLHS.

Chapter 6: Conclusion

In summary, the aims of the current thesis were to establish on morphological grounds, using archival specimens, whether it was possible to devise an alternative way of classifying HLHS, which could be related to how the phenotypes seen in HLHS develop, that might be useful for genomic studies. As archived hearts were used to develop this new classification, it was then desirable to establish an improved method to extract high quality DNA with reliable and reproducible sequence information, from formalin-fixed tissues, so that the archived hearts with HLHS could themselves be used for genomic studies. Finally, as it was concluded that DNA obtained from formalin-fixed studies was best suited to confirming genes implicated from other methods, rather than for primary gene detection, the expression patterns of genes previously implicated in HLHS were examined, taking into account their localisation to both the valves and the ventricular chambers.

Analysis of the HLHS archival collection demonstrated three distinctive ventricular subgroups of HLHS including slit-like ventricle, thick-walled ventricle and miniaturised ventricle. The proposed ventricular-based classification of HLHS in this study not only provided easy and firm approach to subgroup HLHS, but also facilitated the identification of causative genes for different HLHS subgroup through linking each HLHS subgroup to its possible origins of defect.

It was also hypothesised that it would be possible to extract high quality DNA with reliable and reproducible sequence information from archival formalin fixed tissues and this would eventually be useful for identifying causative genes of specific HLHS subgroup by using the archival specimens. In fact, it

was possible to extract DNA from tissue fixed in formalin and carry out PCR using the proposed method in chapter 4. This proposed method allowed to generate high quality DNA from tissues fixed in formalin for up to two years. Since elevated quantity of DNA was obtained from the two-year tissues, it was speculated that it was possible to obtain DNA from tissues that were fixed in formalin for longer than two years. However, using the formalin extracted DNA to perform next generation sequencing (NGS) led to generate high specificity with moderate sensitivity sequencing reads. Whereas, with Sanger sequencing, unreliable reads that could not be possible to separate formalin artefacts from, for example, heterozygosity were obtained. Thus, both NGS and Sanger sequencing demonstrated variable degree of accuracy for detecting variants in DNA extracted from formalin-fixed tissues, and hence it would not be recommended to use archival tissues except to check for variants that were previously identified in fresh tissues

Finally, it was hypothesised that the implicated HLHS genes showed expression patterns that reflected their potential functions during heart development, and this therefore would allow linking these genes to HLHS subgroups. Although some HLHS-implicated genes, including *Gja1* and *Sap130,* showed very broad expression patterns, and thus it was hard to associate them with the HLHS phenotypes, other genes showed specific expression to the affected regions of HLHS. It was speculated that *Notch3, Hand1, Foxc2,* and *Pcdha9* would be more likely to correlate with, based on their expression patterns, the abnormalities associated with various subgroups of HLHS.

Together, these data suggest that HLHS is a well-recognised defect that composes of various distinctive subgroups. These HLHS subgroups can be caused by different genes and therefore they have to be analysed separately to avoid implicating irrelevant genes to HLHS.

Chapter 7: References

Agay-Shay K, Friger M, Linn S, Peled A, Amitai Y, Peretz C. (2013). Air pollution and congenital heart defects. Environ Res. 124:28–34.

Ahmed, H. (2004). Principles and Reactions of Protein Extraction, Purification, and Characterization, CRC Press.

Ai, Z., Fischer, A., Spray, D., Brown, A.M.C. and Fishman, G.I. (2000). Wnt-1 regulation of connexin43 in cardiac myocytes. J Clin Invest. 105(2): 161–171.

Akazawa, H and Komuro, I (2005). Cardiac transcription factor Csx/Nkx2-5: Its role in cardiac development and diseases. Pharmacology & Therapeutics. 107(2):252-268.

Al Yaqoubi HN, Al Badi MM, Ambu Saidi FM, Al Shafouri NST. (2018). A Case of Sirenomelia Associated with Hypoplastic Left Heart with a Healthy Co-Twin: A Rare Entity. Case Rep Pediatr. 2018:9361745. doi: 10.1155/2018/9361745. eCollection 2018.

Alaeddini, R. (2012). Forensic implications of PCR inhibition--A review. Forensic Sci Int Genet. 6(3):297-305. doi: 10.1016/j.fsigen.2011.08.006.

Alboliras ET, Mavroudis C, Pahl E, Gidding SS, Backer CL, Rocchini AP. Left ventricular growth in selected hypoplastic left ventricles. Ann Thorac Surg 1999; 68: 549–555.

AlRais, F., Feldstein VA, Srivastava D, Gosnell K, Moon-Grady AJ. (2011). Monochorionic twins discordant for congenital heart disease: a referral center's experience and possible pathophysiologic mechanisms. Prenat Diagn. 31(10):978-84. doi: 10.1002/pd.2819. Epub 2011 Jul 11.

Alvarez, A. D., Shi, W., Wilson, B. A. and Skeath, J. B. (2003). pannier and Andersen, T.A., Troelsen, K.D.L.L. and Larsen, L.A. (2014). Of mice and men: molecular genetics of congenital heart disease. Cell Mol Life Sci. 71(8): 1327–1352.

Anderson, RH. and Shirali, G. (2009). Sequential segmental analysis. Ann Pediatr Cardiol. 2(1): 24–35. doi: 10.4103/0974-2069.52803

Andrews RE, Yates RW, Sullivan ID, Cook AC, Anderson RH, Lees CC. (2004) Early fetal diagnosis of monochorionic twins concordant for hypoplastic left heart syndrome. Ultrasound Obstet Gynecol. 24(1):101-2.

Andrews, R.E., Yates ,R.W., Sullivan ID, Cook AC, Anderson RH, and Lees, C.C. (2004). Early fetal diagnosis of monochorionic twins concordant for hypoplastic left heart syndrome. Ultrasound Obstet Gynecol. 24(1):101-2.

Andrews,R.E., Cook, A.C. and Yates, R.W.M (2003). Concordance for hypoplastic left heart syndrome in a monochorionic twin pregnancy. Heart. 89(4): e13. PMID: 12639890

Anitha, A., Thanseem, I., Nakamura, K., Yamada, K., Iwayama, Y, Toyota T, Iwata Y, Suzuki K, Sugiyama T, Tsujii, M, Yoshikawa, T, and Mori, N. (2013). Protocadherin α (PCDHA) as a novel susceptibility gene for autism. J Psychiatry Neurosci. 38(3):192-8. doi: 10.1503/jpn.120058.

Baffa JM, Chen SL, Guttenberg ME, Norwood WI, Weinberg PM. Coronary artery abnormalities and right ventricular histology in hypoplastic left heart syndrome. J Am Coll Cardiol. 1992;20(2):350–8. doi: 10.1016/0735-1097(92)90101-R.

Baffa, J.M., Chen, S.L., Guttenberg, M.E., Norwood, W.I., Weinberg, P.M. (1992). Coronary artery abnormalities and right ventricular histology in hypoplastic left heart syndrome. J Am Coll Cardiol, 20: pp. 350-358

Bao, X., Chen, Y., Lee, S.H., Lee, S.C., Reuss, L. and Altenberg, G.A. (2005). Membrane Transport Proteins with Complete Replacement of Transmembrane Helices with Polyalanine Sequences Remain Functional. The Journal of Biological Chemistry. 280, 8647-8650.

Barbara Uhl, Verena Sailer, Emily Eva Holmes, Maria Jung, Sebastian Meller, and Glen Kristiansen. (2013). Improved PCR Performance Using Template DNA from Formalin-Fixed and Paraffin-Embedded Tissues by Overcoming PCR Inhibition Dimo Dietrich, PLoS One. 8(10):e77771

Barnes, R. M., Firulli, B. A., Conway, S. J., Vincentz, J. W., & Firulli, A. B. (2010). Analysis of the Hand1 cell lineage reveals novel contributions to cardiovascular, neural crest, extra-embryonic, and lateral mesoderm derivatives. Developmental dynamics : an official publication of the American Association of Anatomists, 239(11), 3086–3097. doi:10.1002/dvdy.22428

Barnes, R. M., Firulli, B. A., Conway, S. J., Vincentz, J. W., and Firulli, A. B. (2010). Analysis of the Hand1 cell lineage reveals novel contributions to cardiovascular, neural crest, extra-embryonic, and lateral mesoderm derivatives. Dev Dyn. 239(11), 3086-3097. doi:10.1002/dvdy.22428

Benson D.W., Martin, L.J., and Lo, C.W. (2016). Genetics of Hypoplastic Left Heart Syndrome. J Pediatr. 173:25-31. doi: 10.1016/j.jpeds.2016.02.052.

Bergwerff M, Verberne ME, DeRuiter MC et al (1998) Neural crest cell contribution to the developing circulatory system: implications for vascular morphology? Circ Res 82:221–231

Bimber, B., Dettman, R. W., & Simon, H. G. (2006). Differential regulation of Tbx5 protein expression and sub-cellular localization during heart development. Developmental biology, 302(1), 230–242. doi:10.1016/j.ydbio.2006.09.023

Bjornstad, P. G., & Michalsen, H. (1974). Coexistent mitral and aortic valve atresia with intact ventricular septum in sibs. British heart journal, 36(3), 302–306.

Blitzer D, Yedlicka G, Manghelli J, Dentel J, Caldwell R, Brown JW. (2017). Twin-to-Twin Heart Transplantation: A Unique Event With a 25-Year Follow-Up. Ann Thorac Surg. 103(4):e341-e342. doi: 10.1016/j.athoracsur.2016.09.060.

Bockman DE and Kirby ML (1984) Dependence of thymus development on derivatives of the neural crest. Science 223:498–500

Bohlmeyer, T. J., Helmke, S., Ge, S., Lynch, J., Brodsky, G., Sederberg, J.H., Robertson, A.D., Minobe, W., Bristow, M.R, and Perryman, B. (2003). Hypoplastic left heart syndrome myocytes are differentiated but possess a unique phenotype. Cardiovasc Pathol 12(1): 23-31.

Bohlmeyer, T.J., Helmke, S., Ge, S., Lynch J, Brodsky G, Sederberg JH, Robertson AD, Minobe W, Bristow MR, Perryman, M.B. (2003). Hypoplastic left heart syndrome myocytes are differentiated but possess a unique phenotype. Cardiovasc Pathol. 12(1):23-31.

Borggrefe T, and Oswald F. (2009). The Notch signaling pathway: Transcriptional regulation at Notch target genes. Cell Mol Life Sci. 66:1631–1646. doi: 10.1007/s00018-009-8668-7.

Bray SJ (2006) Notch signalling: a simple pathway becomes complex. Nat Rev Mol Cell Biol 7: 678–89.

Bremer, J.L. (1948). Coarctation of the aorta and the aortic isthmuses. Archives ofPathology 45, 425-434.

Brenner J.I and Kuehl, K. (2011) Hypoplastic left heart syndrome and other left heart disease: evolution of understanding from population-based analysis to molecular biology and back again – a brief overview. Cardiology in the Young. 21(Suppl. 2): 23–27.

Brenner JI, Berg KA, Schneider DS, Clark EB, Boughman JA. (1989). Cardiac malformations in relatives of infants with hypoplastic left-heart syndrome. Am J Dis Child.143(12):1492–4.

Brownell LG, Shokeir MH. (1976). Inheritance of hypoplastic left heart syndrome (HLHS): further observations. Clin Genet. 9(2):245-9.

Brownell, L. G. and Shokeir, M. H. K. (1976). Inheritance of hypoplastic left heart syndrome (HLHS): further observations. Clin. Genet. 9: 245-249.

Bruneau BG, Nemer G, Schmitt JP et al (2001) A murine model of Holt-Oram syndrome defines roles of the T-box transcription factor Tbx5 in cardiogenesis and disease. Cell 106:709–721

Bruneau BG, Nemer G, Schmitt JP, Charron F, Robitaille L, Caron S, Conner DA, Gessler M, Nemer M, Seidman CE, Seidman JG (2001). A murine model of Holt-Oram syndrome defines roles of the T-box transcription factor Tbx5 in cardiogenesis and disease. Cell.106(6):709-21.

Bruneau, B.G., Burn, J., and Srivastava, D. (2010). CHAPTER 9: Aetiology of Congenital Cardiac Disease. Paediatric Cardiology (Third Edition). Pages 161-171

Bruneau, B.G., Logan, M., Davis, N., Levi, T., Tabin, C.J., Seidman, J.G., Seidman, C.E. (1999). Chamber-specific cardiac expression of Tbx5 and heart defects in Holt-Oram syndrome. Dev Biol. 211 (1):100-8.

Buckingham M and Rigby PW (2014) Gene regulatory networks and transcriptional mechanisms that control myogenesis. Dev Cell 28:225–238.

Buckingham M, Meilhac S, Zaffran S (2005) Building the mammalian heart from two sources of myocardial cells. Nat Rev Genet 6:826–835

Buckingham, M. (2016). First and Second Heart Field. Congenital Heart Diseases: The Broken Heart. pp 25-40.

Butcher, J.T and Markwald, R.R (2007). Valvulogenesis: the moving target. Phil. Trans. R. Soc. B. 362, 1489–1503

Chen, P., Xie, L.J., Huang, G.Y., Zhao, X.Q., and Chang, C. (2005). Mutations of connexin43 in fetuses with congenital heart malformations. Chin Med J (Engl). 118(12):971-6.

Chester, A.H, El-Hamamsy, I., Butcher, J.T., Latif, N., Bertazzo, S., and Yacoub, M.H. (2014). The living aortic valve: From molecules to function. Glob Cardiol Sci Pract. 2014(1): 52–77.

Christoffels VM, Hoogaars WM, Tessari A, Clout DE, Moorman AF, and Campione M. (2004). T-box transcription factor Tbx2 represses differentiation and formation of the cardiac chambers. Dev Dyn. 229(4):763-70.

Christoffels VM, Hoogaars WM, Tessari A, Clout DE, Moorman AF, Campione M. (2004). T-box transcription factor Tbx2 represses differentiation and formation of the cardiac chambers. Dev Dyn. 229(4):763-70.

Clark, M.D, Marcum, R., Graveline, R., Chan, D.W., Xie, T., Chen, Z., Ding, Y., Yongbo Zhang, Alfonso Mondragón, David, G., and Radhakrishnan, S. (2015). Structural insights into the assembly of the histone deacetylase-associated Sin3L/Rpd3L corepressor complex. PNAS. 112(28): E3669-E3678.

Coceani, F. and Baragatti, B. (2012). Mechanisms for ductus arteriosus closure. Semin Perinatol. 36(2):92-7. doi: 10.1053/j.semperi.2011.09.018.

Colombo, S., de Sena-Tomás, C., George, V., Werdich, A. A., Kapur, S., MacRae, C. A., & Targoff, K. L. (2018). Nkx genes establish second heart field cardiomyocyte progenitors at the arterial pole and pattern the venous pole through Isl1 repression. *Development (Cambridge, England)*, *145*(3), dev161497. doi:10.1242/dev.161497

Colquitt, J.L., Morris, S.A., Denfield, S.W., Fraser, C.D., Wang, W., and Kyle, B. (2016). Survival in Children With Down Syndrome Undergoing Single-Ventricle Palliation. The Annals of Thoracic Surgery. 101 (5): 1834 – 1841

Conboy J. G. (2016). Developmental regulation of RNA processing by Rbfox proteins. Wiley interdisciplinary reviews. RNA, 8(2), 10.1002/wrna.1398. doi:10.1002/wrna.1398

Cordero-Espinoza, L., & Hagen, T. (2013). Regulation of Cullin-RING ubiquitin ligase 1 by Spliceosome-associated protein 130 (SAP130). Biology open, 2(8), 838–844. doi:10.1242/bio.20134374

Costa, M. J., Wu, X., Cuervo, H., Srinivasan, R., Bechis, S. K., Cheang, E., … Wang, R. A. (2013). Notch4 is required for tumor onset and perfusion. Vascular cell, 5(1), 7. doi:10.1186/2045-824X-5-7

Currarino G, Edwards FK, Kaplan S. (1959). Hypoplasia of the left heart complex. AMA J Dis Chil. 97: 839–844.

Dadvand P, Rankin J, Rushton S, Pless-Mulloli T. (2011). Ambient air pollution and congenital heart disease: aregister-based study. Environ Res. 111:435–441.

Daimei, T., Devi, N.D., and Sinam, V. (2014). Difference between the left and right ventricular thickness in fetal heart. IOSR Journal of Dental and Medical Sciences. 13(4). PP 21-24. e-ISSN: 2279-0853, p-ISSN: 2279-0861.

Danyal H., Adrian C. Grimes, Huai-Jen Tsai, Margaret L. and Kirby. (2011). Zebrafish cardiac development requires a conserved secondary heart field. Development. 138(11): 2389–2398. doi: 10.1242/dev.061473

Dasgupta, C., Martinez, A.M., Zuppan, C. W., Shah, M. M., Bailey, L. L., Fletcher, W. H. (2001). Identification of connexin43 (alpha-1) gap junction gene mutations in patients with hypoplastic left heart syndrome by denaturing gradient gel electrophoresis (DGGE). Mutat. Res. 479: 173-186.

D'Aurizio, R., Russo, F., Chiavacci, E., Baumgart, M., Groth, M., D'Onofrio, M., Arisi, I., Rainaldi, G, Pitto, L., and Pellegrini, M. (2016). Discovering miRNA Regulatory Networks in Holt-Oram Syndrome Using a Zebrafish Model. Front Bioeng Biotechnol. 4:60. doi: 10.3389/fbioe.2016.00060.

Davidson, B., Shi, W., Beh, J., Christiaen, L. and Levine, M. (2006). FGF signaling delineates the cardiac progenitor field in the simple chordate, Ciona intestinalis. Gene Dev. 20(19):2728-38.

Dawson AL, Tinker SC, Jamieson DJ, Hobbs CA, Berry RJ, Rasmussen SA, Anderka M, Keppler-Noreuil KM, Lin AE, Reefhuis J (2016). National Birth Defects Prevention Study. Twinning and major birth defects, National Birth Defects Prevention Study, 1997-2007. J Epidemiol Community Health. 70(11):1114-1121. doi: 10.1136/jech-2015-206302. Epub 2016 Jun 20.

Deely WJ, Ehlers KH, Levin AR, Engle MA. Hypoplastic left heart syndrome. Anatomic, physiologic, and therapeutic considerations. Am J Dis Child 1971; 121: 168–175.

Del Monte G, Grego-Bessa J, González-Rajal A, Bolós V, and De La Pompa JL. (2007). Monitoring Notch1 activity in development: evidence for a feedback regulatory loop. Dev Dyn. 236(9):2594-614.

del Río M, Martínez JM, Galindo A, Figueras F, Palacio M, Borrell A, Puerto B, Coll O, de la Fuente P. (2005). Successful selective termination at 17 weeks' gestation in monochorionic monoamniotic twin pregnancy affected by twin-twin transfusion syndrome and discordant for hypoplastic left heart syndrome. Prenat Diagn. 25(13):1223-5.

Dermietzel R, Gao Y, Scemes E, Vieira D, Urban M, Kremer M, Bennett MV, and Spray DC. (2000). Connexin43 null mice reveal that astrocytes express multiple connexins. Brain Res Brain Res Rev. 32(1):45-56.

Digilio MC1, Marino B, Giannico S, Giannotti A, Dallapiccola B. (1999). Atrioventricular canal defect and hypoplastic left heart syndrome as discordant congenital heart defects in twins. Teratology. 1999 Oct;60(4):206-8.

Dolk H, Armstrong B, Lachowycz K, Vrijheid M, Rankin J, Abramsky L, Boyd PA, Wellesley D. (2010). Ambient air pollution and risk of congenital anomalies in England, 1991–1999. Occup Environ Med. 67:223–227.

Donald C., Fyler, MD Talner CN (1980) Report of the New England Regional Infant Cardiac Program. Pediatrics, 65:375-461.

Doty DB, Marvin WJ, Schieken RM, and Lauer RM. (1980). Hypoplastic leftheart syndrome. Successful palliation with a new operation. J Thorac Cardiovasc Surg. 80: 148–152.

Dupays, L., Towers, N., Wood, S., David, A., Stuckey, D.J., and Mohun, T. (2019). Furin, a transcriptional target of NKX2-5, has an essential role in heart development and function. PLoS One. 6;14(3):e0212992. doi: 10.1371/journal.pone.0212992.

Durbin MD, Cadar AG, Williams CH, Guo Y, Bichell DP, Su YR, and Hong, C.C. (2017). Hypoplastic Left Heart Syndrome Sequencing Reveals a Novel NOTCH1 Mutation in a Family with Single Ventricle Defects. Pediatr Cardiol. 38(6):1232-1240. doi: 10.1007/s00246-017-1650-5.

Durbin, M.D., Cadar, A.G., Williams, C.H. et al. (2017). Hypoplastic Left Heart Syndrome Sequencing Reveals a Novel NOTCH1 Mutation in a Family with Single Ventricle Defects Pediatr Cardiol. 38: 1232. https://doi.org/10.1007/s00246-017-1650-5

Edwards,J.E.(1960).Congenitalmalformationsoftheheartandgreatvessels.InPathologyoftheHeart(ed S.E.Gould), pp.260-496.Springfield, Ilinois:C.C.Thomas.

Ehebauer, M.T, Chirgadze, D.Y., Hayward, P., Arias, A.M. and Blundell, T.L. (2005). High-resolution crystal structure of the human Notch 1 ankyrin domain. Biochem J. 392(Pt 1): 13–20.

Einaga, N., Yoshida, A., Noda, H., Suemitsu, M., Nakayama, Y., Sakurada, A., Kawaji, Y., Yamaguchi, H., Sasaki, Y., Tokino, T., … Esumi, M. (2017). Assessment of the quality of DNA from various formalin-fixed paraffin-embedded (FFPE) tissues and the use of this DNA for next-generation sequencing (NGS) with no artifactual mutation. PloS one, 12(5), e0176280. doi:10.1371/journal.pone.0176280

Elliott, D,A, Kirk, E.P., Yeoh, T., Chandar, S., McKenzie, F., Taylor, P., Grossfeld, P., Fatkin, D., Jones, O., Hayes, P., Feneley, M., and Harvey, R.P. (2003). Cardiac homeobox gene NKX2-5 mutations and congenital heart disease: associations with atrial septal defect and hypoplastic left heart syndrome. J Am Coll Cardiol. 41(11):2072-6.

Esposito G, Butler TL, Blue GM, Cole AD, Sholler GF, Kirk EP, Grossfeld P, Perryman BM, Harvey RP, and Winlaw, D.S. (2011). Somatic mutations in NKX2–5, GATA4, and HAND1 are not a common cause of tetralogy of Fallot or hypoplastic left heart. Am J Med Genet A. 155A(10):2416-21.

Euler-Taimor, g. and Heger, J. (2006). The complex pattern of SMAD signaling in the cardiovascular system. Cardiovascular Research. 69(1): 15–25.

Evans, W. (1964). Diseases of the Heart and Arteries, p. 209. Edinburgh, London: E. & S. Livingstone.

Farrugia, A., Keyser, C. and Ludes, B. (2010). Efficiency evaluation of DNA extraction and purification protocol on archival formalin-fixed and paraffin-embedded tissue. Forensic science international. 194(2010):e25-e28.

Feinstein JA, Benson DW, Dubin AM, Cohen MS, Maxey DM, Mahle WT, Pahl E, Villafañe J, Bhatt AB, Peng LF, Johnson BA, Marsden AL, Daniels CJ, Rudd NA, Caldarone CA, Mussatto KA, Morales DL, Ivy DD, Gaynor JW, Tweddell JS, Deal BJ, Furck AK, Rosenthal GL, Ohye RG, Ghanayem NS, Cheatham JP, Tworetzky W, Martin GR. (2012). Hypoplastic left heart

syndrome: current considerations and expectations. J Am Coll Cardiol. 59(1 Suppl):S1–42.

Felker, A, Prummel KD, Merks AM, Mickoleit M, Brombacher EC, Huisken J, Panáková D, Mosimann C. (2018). Continuous addition of progenitors forms the cardiac ventricle in zebrafish. Nat Commun. 9(1):2001. doi: 10.1038/s41467-018-04402-6.

Ferreira CR, Aiello VD, Melo AMAGP, et al. (2014). Classic form of hypoplastic left heart syndrome diagnosed post-natally: an autopsy report. Autopsy Case. 4(3):21-30. http://dx.doi.org/10.4322/acr.2014.025

Finegold, D.N, Kimak MA, Lawrence EC, Levinson KL, Cherniske EM, Pober BR, Dunlap JW, and Ferrell R.E. (2001) Truncating mutations in FOXC2 cause multiple lymphedema syndromes. Hum Mol Genet. 10(11):1185-9.

Firulli, B.A, Toolan, K.P, Harkin, J., Millar, H., Pineda, S., and Firulli, A.B. (2017). The HAND1 frameshift A126FS mutation does not cause hypoplastic left heart syndrome in mice, Cardiovascular Research, 113 (14). Pages 1732–1742, https://doi.org/10.1093/cvr/cvx166

Firulli, B.A., Toolan, K.P., Harkin, J., Millar, H., Pineda, S., and Firulli, A.B. (2017). The HAND1 frameshift A126FS mutation does not cause hypoplastic left heart syndrome in mice. Cardiovasc Res. 113(14):1732-1742. doi: 10.1093/cvr/cvx166.

Fitzgerald, K.K., Bhat, A.M., Conard, K., Hyland, J. and Pizarro, C. (2014). Novel SMAD3 Mutation in a Patient with Hypoplastic Left Heart Syndrome with Significant Aortic Aneurysm. Case Reports in Genetics. Article ID 591516, 4 pages.

Fleischer, T.C., Yun, U.J, and Ayer, D.E. (2003). Identification and Characterization of Three New Components of the mSin3A Corepressor Complex. Mol Cell Biol. 23(10): 3456–3467. doi: 10.1128/MCB.23.10.3456-3467.2003

Forencz C, Rubin JD, McCarter RJ, et al (1985) Congenital heart disease: prevalence at livebirth: The Baltimore-Washington infant study. Am J Epidemiol: 121:31–6.

Fox, C. H., et al. (1985). "Formaldehyde fixation." J Histochem Cytochem 33(8): 845-853.

Frandon, J., Bricq, S., Miquerol, L., Bernard, M., Lalande, A., and Jacquier, A. (2016). Transgenic mice with mutations in Nkx2.5 gene: animal model proposal to study non compaction. J Cardiovasc Magn Reson. 18. doi: [10.1186/1532-429X-18-S1-Q34]

Franklin RCG, Béland MJ, Colan SD, Walters HL, Aiello VD, Anderson RH, Bailliard F7, Boris JR, Cohen MS, Gaynor JW, Guleserian KJ9, Houyel L, Jacobs ML, Juraszek AL, Krogmann ON, Kurosawa H, Lopez L9, Maruszewski BJ, St Louis JD, Seslar SP, Srivastava S, Stellin G, Tchervenkov CI, Weinberg PM, Jacobs JP. (2017). Nomenclature for congenital and paediatric cardiac disease: the International Paediatric and Congenital Cardiac Code (IPCCC) and the Eleventh Iteration of the International Classification of Diseases (ICD-11). Cardiol Young. 27(10):1872-1938. doi: 10.1017/S1047951117002244.

Fruitman DS (2000). Hypoplastic left heart syndrome: Prognosis and management options. Paediatr Child Health. 5(4): 219–225.

Furtado MB, Wilmanns JC, Chandran A, Tonta M, Biben C, Eichenlaub M, Coleman HA, Berger S, Bouveret R, Singh R, Harvey RP, Ramialison M, Pearson JT, Parkington HC, Rosenthal NA, and Costa MW. (2016). A novel conditional mouse model for Nkx2-5 reveals transcriptional regulation of cardiac ion channels. Differentiation. 91(1-3):29-41. doi:10.1016/j.diff.2015.12.003.

Gallagher, T. L., Arribere, J. A., Geurts, P. A., Exner, C. R., McDonald, K. L., Dill, K. K., … Conboy, J. G. (2011). Rbfox-regulated alternative splicing is critical for zebrafish cardiac and skeletal muscle functions. Developmental biology, 359(2), 251–261. doi:10.1016/j.ydbio.2011.08.025

Gao, Z., Kim, G. H., Mackinnon, A. C., Flagg, A. E., Bassett, B., Earley, J. U., & Svensson, E. C. (2010). Ets1 is required for proper migration and differentiation of the cardiac neural crest. Development (Cambridge, England), 137(9), 1543–1551. doi:10.1242/dev.047696

Garg, V., Muth, A., Ransom, J., Burdine, M., Barnes, R., King, I., Grossfeld, P., and Srivastava, D. (2005). Mutations in NOTCH1 cause aortic valve disease. Nature. 437. 270-4. 10.1038/nature03940.

Garg, V., Muth, A.N., Ransom, J.F, et al. (2005). Mutations in NOTCH1 cause aortic valve disease. Nature. 437:270–4.

Geng, X., Cha, B., Mahamud, M.R., Srinivasan, R.S. (2017). Intraluminal valves: development, function and disease. Disease Models & Mechanisms. 10: 1273-1287; doi: 10.1242/dmm.030825

Gerboni, S., Sabatino, G., Mingarelli, R., and Dallapiccola, B. (1993). Coarctation of the aorta, interrupted aortic arch, and hypoplastic left heart syndrome in three generations. J Med Genet. 30(4): 328–329.

Gilboa SM, Mendola P, Olshan AF, Langlois PH, Savitz DA, Loomis D, Herring AH, Fixler DE. (2005). Relation between ambient air quality and selected birth defects, seven county study, Texas,1997–2000. Am J Epidemiol. 2005;162:238–252.

Gioli-Pereira, L., Pereira, A.C., Mesquita, S.M., Xavier-Neto, J., Lopes, A.A., and Krieger, J.E. (2010). NKX2.5 mutations in patients with non-syndromic congenital heart disease. Int J Cardiol. 138(3):261-5. doi: 10.1016/j.ijcard.2008.08.035.

Gitler AD, Lu MM, Jiang YQ, Epstein JA, Gruber PJ. (2003). Molecular markers of cardiac endocardial cushion development. Dev Dyn. 228(4):643-50.

Gładki, M., Składzień, T. & Skalski, J. (2015). The impact of environmental factors on the occurrence of congenital heart disease in the form of hypoplastic left heart syndrome. Kardiochirurgia i Torakochirurgia Polska/Polish Journal of Thoracic and Cardiovascular Surgery, 12(3), 204-207.

Glatz, J.A., Fedderly R.T., Ghanayem, J.S., weddell, T (2008). Impact of mitral stenosis and aortic atresia on survival in hypoplastic left heart syndrome. Ann Thorac Surg,85: pp. 2057-2062.

Goetz, T.L., Gu, T.L., Speck NA, and Graves, B.J. (2000). Auto-inhibition of Ets-1 is counteracted by DNA binding cooperativity with core-binding factor alpha2. Mol Cell Biol. 20(1):81–90.

Goldmuntz E. (2003) The Epidemiology and Genetics of Hypoplastic Left Heart Syndrome. In: Rychik J., Wernovsky G. (eds) Hypoplastic Left Heart Syndrome. Developments in Cardiovascular Medicine, vol 246. Springer, Boston, MA

Gordon BM, Rodriguez S, Lee M, Chang RK (2008) Decreasing number of deaths of infants with hypoplastic left heart syndrome. J Pediatr. 153(3):354.

Grech, V. Pediatr Cardiol (1999) Decreased Prevalence of Hypoplastic Left Heart Syndrome in Malta. 20(5): 355- 357. https://doi.org/10.1007/s002469900484

Grego-Bessa, J., Luna-Zurita, L., Monte, G., Bolós, V., Melgar, P., Arandilla, A., Garratt, N.A, Zang, H., Mukouyama, Y., Chen, C., Shou, W., Balles, W., Esteller, M., Rojas, A., Pérez-Pomares, A., Pompa, J. (2007). Notch Signaling Is Essential for Ventricular Chamber Development. Developmental cell. 12(3): 415-429.

Hamblet NS, Lijam N, Ruiz-Lozano P et al (2002) Dishevelled 2 is essential for cardiac outflow tract development, somite segmentation and neural tube closure. Development 129:5827–583

Hansen CA, Barnett AG, Jalaludin BB, Morgan GG. (2009). Ambient air pollution and birth defects in Brisbane, Australia. PLoS One. 4:e5408.

Hassell, J. and Hand, A.R. (1973). Tissue Fixation with diimidoesters as an alternative to aldehydes. J of histochemistry and cytochemistry. 22(4):pp 223-239.

Hatcher, C. J., & Basson, C. T. (2009). Specification of the cardiac conduction system by transcription factors. Circulation research, 105(7), 620–630. doi:10.1161/CIRCRESAHA.109.204123

Hill, M.A. (2018, April 12) Embryology Advanced Cardiac Embryology. Retrieved from https://embryology.med.unsw.edu.au/embryology/index.php/Advanced_Cardiac_Embryology

Hinton RB, Martin LJ, Tabangin ME, Mazwi ML, Cripe LH, Benson DW. (2007). Hypoplastic left heart syndrome is heritable. J Am Coll Cardiol. 50(16):1590–5.

Ho, S. Yen and Anderson, R. H. (1979). Coarctation, tubular hypoplasia, and the ductus arteriosus. British HeartJournal 41, 268-274.

Holmes, L. B., Rose, V., Child, A. H., and Kratzer, W. (1974). Commentary on the inheritance of the hypoplastic left heart syndrome. Birth Defects Orig. Art. Ser. X(4): 228-230.

Homsy J, Zaidi S, Shen Y, Ware JS, Samocha KE, Karczewski KJ, DePalma SR, McKean D, Wakimoto H, Gorham J, Jin SC, Deanfield J, Giardini A, Porter GA Jr, Kim R, Bilguvar K, López-Giráldez F, Tikhonova I, Mane S, Romano-Adesman A, Qi H, Vardarajan B, Ma L, Daly M, Roberts AE, Russell MW, Mital S, Newburger JW, Gaynor JW, Breitbart RE, Iossifov I, Ronemus M, Sanders SJ, Kaltman JR, Seidman JG, Brueckner M, Gelb BD, Goldmuntz E, Lifton RP, Seidman CE, and Chung WK (2015). De novo mutations in congenital heart disease with neurodevelopmental and other congenital anomalies. Science. 350(6265):1262-6

Huang F, Wagner M, Siddiqui MA. (2004). Ablation of the CLP-1 gene leads to down-regulation of the HAND1 gene and abnormality of the left ventricle of the heart and fetal death. Mech Dev. 121(6):559-72.

Huang GY, Xie LJ, Linask KL, Zhang C, Zhao XQ, Yang Y, Zhou GM, Wu YJ, Marquez-Rosado L, McElhinney DB, Goldmuntz E, Liu C, Lampe PD, Chatterjee B, and Lo CW. (2011). Evaluating the role of connexin43 in congenital heart disease: Screening for mutations in patients with outflow tract anomalies and the analysis of knock-in mouse models. J Cardiovasc Dis Res. 2(4):206-12. doi: 10.4103/0975-3583.89804.

Huelke, D. F. (1998). An Overview of Anatomical Considerations of Infants and Children in the Adult World of Automobile Safety Design. Annu Proc Assoc Adv Automot Med. 42: 93-113.

Hunter, A., Kaufman, M. H., McKay, A., Baldock, R., Simmen, M. W., & Bard, J. B. (2003). An ontology of human developmental anatomy. Journal of anatomy, 203(4), 347–355. doi:10.1046/j.1469-7580.2003.00224.x

Hutson MR, Zeng XL, Kim AJ et al (2010) Arterial pole progenitors interpret opposing FGF/BMP signals to proliferate or differentiate. Development 137:3001–3011

Iascone M, Ciccone R, Galletti L, Marchetti D, Seddio F, Lincesso AR,Pezzoli L, Vetro A, Barachetti D, Boni L, Federici D, Soto AM, ComasJV, Ferrazzi P, and Zuffardi O. (2012). Identification ofde novomutations and rarevariants in hypoplastic left heart syndrome. Clin Genet: 81: 542–554.

Iascone, M., Ciccone R, Galletti L, Marchetti D, Seddio F, Lincesso AR, Pezzoli L, Vetro A, Barachetti D, Boni L, Federici D, Soto AM, Comas JV, Ferrazzi P, and Zuffardi O. (2012). Identification of de novo mutations and rare variants in hypoplastic left heart syndrome. Clin Genet. 81(6):542-54.

Idris, B. and Goodwin, W. (2015). Comparison of Chelex-100 with two solid phase DNA extraction techniques. Forensic science international: genetics supplement serier. 5(2015): e274-e275.

Iida K, Koseki H, Kakinuma H, Kato N, Mizutani-Koseki Y, Ohuchi H, Yoshioka H, Noji S, Kawamura K, Kataoka Y, Ueno F, Taniguchi M, Yoshida N, Sugiyama T and Miura N (1997) Essential roles of the winged helix transcription factor MFH-1 in aortic arch patterning and skeletogenesis. Develop- ment 124, 4627–4638.

Iwasaki, Y.K., Nishida, K., Kato, T. and Nattel, S. (2011). Atrial fibrillation pathophysiology: implications for management. Circulation, 124: pp. 2264-2274.

Jackson, B.C., Carpenter, C., Nebert, D.W., and Vasiliou, V. (2010). Update of human and mouse forkhead box (FOX) gene families. Hum Genomics. 4(5):345-52.

Jain R, Engleka KA, Rentschler SL et al (2011) Cardiac neural crest orchestrates remodeling and functional maturation of mouse semilunar valves. J Clin Invest 121:422–430

James, A.C., Szotac, J.O., Iyera, K., Majora, L.A, Pursglovea, S.E., Chapmana, G., and Dunwoodie, S.L. (2014). Notch4 reveals a novel mechanism regulating Notch signal transduction. Biochimica et Biophysica Acta (BBA) - Molecular Cell Research.1843 (7): Pages 1272-1284.

Jin, C, Marsden I, Chen X, and Liao, X. (1999). Dynamic DNA contacts observed in the NMR structure of winged helix protein-DNA complex. J Mol Biol. 289(4):683-90.

Jour (1950). Heart Size Estimations in Infants, Acta Radiologica. 33 (82): 30-44. doi:10.1177/0284185150033S8204

Joutel A, Monet-Lepretre M, Gosele C, et al. (2010) Cerebrovascular dysfunction and microcirculation rarefaction precede white matter lesions in a mouse genetic model of cerebral ischemic small vessel disease. J Clin Invest.120:433–445.

Karbassi A, Nair K, Harris L, Wald RM, Roche SL. Atrial tachyarrhythmia in adult congenital heart disease. *World J Cardiol*. 2017;9(6):496–507. doi:10.4330/wjc.v9.i6.496.

Karamlou T, Diggs BS, Ungerleider RM, Welke KF (2010). Evolution of treatment options and outcomes for hypoplastic left heart syndrome over an 18-year period. J Thorac Cardiovasc Surg. 139(1):119.

Katritsis, D.G. (2014). Cardiac Electrophysiology: From Cell to Bedside (Sixth Edition): Causes of Progressive Conduction Disease. Saunders. ISBN: 978-1-4557-2856-5

Kelle AM, Qureshi MY, Olson TM, Eidem BW, O'Leary PW. (2015). Familial incidence of cardiovascular malformations in Hypoplastic left heart syndrome. Am J Cardiol. 116(11):1762–6.

Kelly RG (2012) The second heart field. Curr Top Dev Biol 100:33–65

Kelly, K. (2006) Path to Effective Recovering of DNA from Formalin-Fixed Samples in Natural History Collection, (pp. 5–14). Washington, DC: The National Academies Press.

Kerkdijk, H., de Kant, E. and DeRuiter, M. C. (2003). Ets-1 and Ets-2

Keyte A, and Hutson MR (2012) The neural crest in cardiac congenital anomalies. Differentiation 84:25–40

Kiernan, J.A. (2000). Formaldehyde, formalin, paraformaldehyde and glutaraldehyde: What they are and what they do. Microscopy Today. 1:8–12

Kirby ML, Turnage KL 3rd, Hays BM (1985) Characterization of conotruncal malformations following ablation of “cardiac” neural crest. Anat Rec 213:87–93

Kirklin JW and Barratt-Boyes BG. (1993). Coarctation of the aorta and inter- rupted aortic arch. In: Kirklin JW, Barratt-Boyes BG (eds). Cardiac Surgery, 2nd ed. Churchill Livingstone, New York. pp 1269–1270.

Kiserud, T. and Acharya, G. (2004). "The fetal circulation". Prenatal Diagnosis. 24 (13): 1049–59. doi:10.1002/pd.1062.

Kohmura, N., Senzaki, K., Hamada, S., Kai, N., Yasuda, R., Watanabe, M., Ishii, H., Yasuda, M., Mishina, M., Yagi, T. (1998). Diversity revealed by a novel family of cadherins expressed in neurons at a synaptic complex. Neuron. 20(6):1137-51.

Kola, I., Brookes, S., Green, A.R., Garber, R., Tymms, M., Papas, T.S., and Seth, A. (1993). The Ets1 transcription factor is widely expressed during

murine embryo development and is associated with mesodermal cells involved in morphogenetic processes such as organ formation. Proc Natl Acad Sci U S A. 90(16): 7588–7592.

Krebs LT, Xue Y, Norton CR, Shutter JR, Maguire M, Sundberg JP, Gallahan D, Closson V, Kitajewski J, Callahan R, Smith GH, Stark KL, Gridley T (2000). Notch signaling is essential for vascular morphogenesis in mice. Genes Dev. 14(11):1343-52.

Krebs LT, Xue Y, Norton CR, Sundberg JP, Beatus P, Lendahl U, Joutel A, Gridley T. (2003). Characterization of Notch3-deficient mice: normal embryonic development and absence of genetic interactions with a Notch1 mutation. Genesis. 37(3):139-43.

Krebs, L. T., Xue, Y., Norton, C. R., Shutter, J. R., Maguire, M., Sundberg, J. P., … Gridley, T. (2000). Notch signaling is essential for vascular morphogenesis in mice. Genes & development, 14(11), 1343–1352.

Krenning,G., Zeisberg, E.Z, and Kalluri, R. (2010). The Origin of Fibroblasts and Mechanism of Cardiac Fibrosis. J Cell Physiol. 225(3): 631–637.

Kume, T., Jiang, H., Topczewska, J.M., and Hogan, B.L. (2001).The murine winged helix transcription factors, Foxc1 and Foxc2, are both required for cardiovascular development and somitogenesis. Genes Dev. 15: 2470-2482.

Laird, D.W. and Revel, J.P. (1990). Biochemical and immunochemical analysis of the arrangement of connexin43 in rat heart gap junction membranes. J Cell Sci. 97 (Pt 1):109-17.

Lamers WH, Viragh S, Wessels A, Moorman AF, and Anderson RH. (1995). Formation of the tricuspid valve in the human heart. Circulation 91: 111 – 121.

Lapierre, C., Dery, J., Guerin, R., Viremouneix, L., Dubois, J., & Garel, L. (2010). Segmental approach to imaging of congenital heart disease. Radiographics, 30(2), 397-411.

Larson Gedman, A., Chen, Q., Kugel Desmoulin, S., Ge Y, LaFiura K, Haska CL, Cherian C, Devidas M, Linda SB, Taub JW, and Matherly, L.H. (2009). The impact of NOTCH1, FBW7 and PTEN mutations on prognosis and downstream signaling in pediatric T-cell acute lymphoblastic leukemia: a

report from the Children's Oncology Group. Leukemia. 23(8):1417-25. doi: 10.1038/leu.2009.64. Epub 2009 Apr 2.

Leake, R.D., Strimling, B., Emmanouilides, G.C. (1973). ntrauterine cardiac failure with hydrops fetalis. Case report in a twin with the hypoplastic left heart syndrome and review of the literature. Clin Pediatr (Phila). 12(11):649-51.

Legrand B., Mazancourt P., Durigon M., Khalifat V., Crainic K. (2002). DNA genotyping of unbuffered formalin fixed paraffin embedded tissues. Forensic Science International. 125: 205–211.

Lev M. (1952). Pathologic anatomy and interrelationship of hypoplasia of the aortic tract complexes. Lab Invest. 1(1):61-70

Lev, M. (1966). Some Newer Concepts of the Pathology of Congenital Heart Disease. Medical Clinics of North America. 50(1):pp 3-14.

Li, X., Zhang, X., Leathers, R., Makino, A., Huang, C., Parsa, P., Macias, J., Yuan, J. X.-J., Jamieson, S. W., and Thistlethwaite, P. A. (2009). Notch3 signalling promotes the development of pulmonary arterial hypertension. Nature Med. 15: 1289-1297.

Lieb, W.R., Stein, W.D. (1986). "Chapter 2. Simple Diffusion across the Membrane Barrier". Transport and Diffusion across Cell Membranes. San Diego: Academic Press. pp. 69–112.

Lie-Venema H, Gittenberger-de Groot AC, van Empel LJ, Boot MJ, Kerkdijk H, de Kant E, DeRuiter MC. (2003). Ets-1 and Ets-2 transcription factors are essential for normal coronary and myocardial development in chicken embryos. Circ Res. 92(7):749-56.

Lie-Venema, H., Gittenberger-de Groot, A.C., van Empel, L.J., Boot M.J., Kerkdijk H., de Kant E., DeRuiter M.C. (2003). Ets-1 and Ets-2 transcription factors are essential for normal coronary and myocardial development in chicken embryos. Circ. Res. 92:749–756.

Lie-Venema, H., Gittenberger-de, Groot, A. C., van Empel, L. J., Boot, M. J., Liu L, Liu X, Ren X, Tian Y, Chen Z, Xu X, Du Y, Jiang C, Fang Y, Liu Z, Fan B, Zhang Q, Jin G, Yang X, Zhang X. (2016). Smad2 and Smad3 have differential sensitivity in relaying TGFβ signaling and inversely regulate early lineage specification. Sci Rep. 6:21602. doi: 10.1038/srep21602.

Liu, C.M., Liu, Y.L., Fann, C.S., Chen, W.J., Yang, W.C., Ouyang, W.C., Chen, C.Y., Jou, Y.S., Hsieh, M.H., Liu. S.K., Hwang, T.J., Faraone, S.V., Tsuang, M.T., and Hwu. H.G. (2007). Association evidence of schizophrenia with distal genomic region of NOTCH4 in Taiwanese families. Genes Brain Behav. 6(6):497-502. Epub 2006 Oct 19

Liu, X., Yagi, H., Saeed, S., Bais, A. S., Gabriel, G. C., Chen, Z., Peterson, K. A., Li, Y., Schwartz, M. C., Reynolds, W. T., Saydmohammed, M., and 23 others. (2017). The complex genetics of hypoplastic left heart syndrome. Nature Genet. 49: 1152-1159.

Liu, X., Yagi, H., Saeed, S., Bais, A. S., Gabriel, G. C., Chen, Z., Peterson, K. A., Li, Y., Schwartz, M. C., Reynolds, W. T., Saydmohammed, M., and 23 others. (2017). The complex genetics of hypoplastic left heart syndrome. Nature Genet. 49: 1152-1159.

Liu, Z., Brunskill, E., Varnum-Finney, B., Zhang, C., Zhang, A., Jay, P.Y., Bernstein, I., Morimoto, M., and Kopan, R. (2015). The intracellular domains of Notch1 and Notch2 are functionally equivalent during development and carcinogenesis. Development. 142(14): 2452–2463.

Liu, Z., Lia, T., Li, Y., Zhang, C., Chen, P., Ma, K., Affara, N., and Zhou, C. (2008). WNT signaling promotes Nkx2.5 expression and early cardiomyogenesis via downregulation of Hdac1. Biochimica et Biophysica Acta (BBA) - Molecular Cell Research.1793 (2): Pages 300-311.

Liu,X., Han, S., Wang,Z., Gelernter, J., and Yang, B. (2013). Variant Callers for Next-Generation Sequencing Data: A Comparison Study. PLOS ONE, 8(9): e75619.

Lopriore, E, Bökenkamp, R., Rijlaarsdam, M., Sueters, M., Vandenbussche, F., and Walther FJ. (2007).Congenital heart disease in twin-to-twin transfusion syndrome treated with fetoscopic laser surgery. Congenit Heart Dis;2(1):38-43. doi: 10.1111/j.1747-0803.2007.00070.x.

Lurie, P.R. (2010). Changing concepts of endocardial fibroelastosis. Cardiology in the Young. 20, 115–123

Macgrogan, D., Gaetano, D., Amato, M.A., Travisano, S.I., Martínez-Poveda, B., Luxán, G., Monte-Nieto, G.D., Papoutsi, T., Sbroggió, M., Bou, V., Arco, P.G., Gómez, M.M., Zhou, B., Redondo, J.M., Jiménez-Borreguero, L.J., & Pompa, J.L. (2016). Results Distinct and Overlapping Expression Patterns of Dll 4 , Jag 1 , and Notch 1 Intracellular Domain During Valve Development.

Magdaleno, S., Jensen, P., Brumwell, C. L., Seal, A., Lehman, K., Asbury, A., Curran, T. (2006). BGEM: an in situ hybridization database of gene expression in the embryonic and adult mouse nervous system. PLoS biology, 4(4), e86. doi:10.1371/journal.pbio.0040086

Markwald RR, Fitzharris TP, and Manasek FJ. (1977) Structural development of endocardial cushions. Am J Anat 148: 85 – 119.

Martinovic, J., Encha-Razavi, F., Vekemans, F., Fermont, L., Bonnet, D., Jouannic, J.M. and Benachi, A. (2003). Occurrence of left versus right heart hypoplasia in a pair of dizygotic twins. Am J Med Genet A. 122A(2):183-5

Mason HA, Rakowiecki SM, Raftopoulou M, Nery S, Huang Y, Gridley T, Fishell G. (2005). Notch signaling coordinates the patterning of striatal compartments. Development. 132(19):4247-58.

Mason J.T. And O'Leary T.J. (1991). Effects of formaldehyde fixation on protein secondary structure: a calorimetric and infrared spectroscopic investigation. J Histochem Cytochem. 39(2):225-9.

Mathew R., Steffensen TS, Gilbert-Barness E. (2009). Discordant omphalocele-exstrophy-imperforate anus-spinal defects (OEIS) complex and cardiac malformations in monochorionic twins. Fetal Pediatr Pathol. 28(6):279-86.

McBride, K.L., Riley, M., Zender, G.A., Fitzgerald-Butt, S.M., Towbin, J.A., Belmont, J.W. and Cole, S.E. (2008). NOTCH1 mutations in individuals with left ventricular outflow tract malformations reduce ligand-induced signalling. Hum Mol Genet. 17(18): 2886–2893.

McCulley, D.J. and Black, B.L. (2012) Transcription factor pathways and congenital heart disease. Curr Top Dev Biol.100():253-77

McElhinney, D.B, Geiger, E., Blinder, J., Benson, D.W., and Goldmuntz, E. (2003). NKX2.5 mutations in patients with congenital heart disease. J Am Coll Cardiol. 42:1650–5.

Miazga, C.M. and McLaughlin, K.A. (2009). Coordinating the timing of cardiac precursor development during gastrulation: A new role for Notch signalling. Developmental Biology. 333(2): 285-296.

Michela, P., Velia, V., Aldo, P. and Ada, P. (2015). Role of connexin 43 in cardiovascular diseases. European Journal of Pharmacology. 768:71-76.

Mitchell, M.E., Sander TL, Klinkner DB, Tomita-Mitchell A. (2007). The molecular basis of congenital heart disease. Semin Thorac Cardiovasc Surg. 19:228–237.

Moore, K.L., Persaud, T.V.N. & Torchia, M.G. (2015). The developing human: clinically oriented embryology (10th ed.). Philadelphia: Saunders, Ch14: p304-349

Moorman, A., Webb, S., Brown, N.A., Lamers, W. and Anderson, R.A. (2003). Development of the heart: (1) formation of the cardiac chambers and arterial trunks. Heart. Jul; 89(7): 806–814.

Mu TS, McAdams RM, Bush DM. (2005). A case of hypoplastic left heart syndrome and bicuspid aortic valve in monochorionic twins. Pediatr Cardiol. 26(6):884-5.

Murphy, P.J. (2005). The fetal circulation, Continuing Education in Anaesthesia Critical Care & Pain, 5 (4): 107–112, https://doi.org/10.1093/bjaceaccp/mki030

Negishi H, Okuyama K, Sagawa T, Makinoda S, Fujimoto S. Two cases of monozygotic twins, in each of which one fetus was prenatally diagnosed as having a heart anomaly. J Obstet Gynaecol. 21(3):293-8.

Nelson, J. D., Denisenko O. and Bomsztyk K. (2006). "Protocol for the fast chromatin immunoprecipitation (ChIP) method." Nature Protocols 1(1): 179-185.

Ni J, Bowles NE, Kim YH, Demmler G, Kearney D, Bricker JT, Towbin JA. Viral infection of the myocardium in endocardial fibroelastosis. Molecular evidence for the role of mumps virus as an etiologic agent. Circulation. 1997;95(1):133–9.

Norwood WI, Kirklin JK, and Sanders SP. (1980). Hypoplastic left heart syndrome. Experience with palliative surgery. Am J Cardiol. 45: 87–91.

Norwood WI, Lang P, Castaneda AR, and Campbell DN. (1981). Experience with operations for hypoplastic left heart syndrome. J Thorac Cardiovasc Surg. 82: 511–519.

Ohye RG, Sleeper LA, Mahony L, Newburger JW, Pearson GD, Lu M, Goldberg CS, Tabbutt S, Frommelt PC, Ghanayem NS, Laussen PC, Rhodes JF, Lewis AB, Mital S, Ravishankar C, Williams IA, Dunbar-Masterson C, Atz AM, Colan S, Minich LL, Pizarro C, Kanter KR, Jaggers J, Jacobs JP,

Krawczeski CD, Pike N, McCrindle BW, Virzi L, Gaynor JW. (2010). Comparison of shunt types in the Norwood procedure for single-ventricle lesions. N Engl J Med. 362(21):1980.

OMIM: MOTHERS AGAINST DECAPENTAPLEGIC, DROSOPHILA, HOMOLOG OF, 3

Page, D.A, and Levine, M.M. (1995). Left ventricular growth in a patient with critical coarctation of the aorta and hypoplastic left ventricle. Pediatr Cardiol.16(4):176-8.

Pandey, R., Mehrotra, D., Kowtal, P., Mahdi, A.A, Sarin, R. (2014). Mitochondrial DNA from archival tissue samples kept in formalin for forensic odontology studies. Journal of oral biology and craniofacial research. 4(2014): 109-113.

Papangeli I and Scambler P (2013) The 22q11 deletion: DiGeorge and velocardiofacial syndromes and the role of TBX1. Wiley Interdiscip Rev Dev Biol 2:393–403

Partridge, L., & Carter, D. A. (2017). Novel Rbfox2 isoforms associated with alternative exon usage in rat cortex and suprachiasmatic nucleus. Scientific reports, 7(1), 9929. doi:10.1038/s41598-017-10535-3

Pashmforoush, M., Lu, J.T., Chen, H., Amand, T.S., Kondo, R., Pradervand, S., Evans, S.M., B. Clark, J.R. Feramisco, W. Giles, S.Y. Ho, D.W. Benson, M. Silberbach, W. Shou, Chien, K.R. (2004). Nkx2–5 pathways and congenital heart disease; loss of ventricular myocyte lineage specification leads to progressive cardiomyopathy and complete heart block. Cell, 117: pp. 373-386

Peach, M., Marsh, N., Miskiewicz, E.I., and MacPhee, D.J. (2015). Solubilization of proteins: the importance of lysis buffer choice. Methods Mol Biol. 1312:49-60. doi: 10.1007/978-1-4939-2694-7_8.

Pelt-Verkuil, E., Belkum, A., & Hays, J. P. (2008). Principles and technical aspects of pcr amplification. Springer Science + Business Media B.V. Re-trieved from http://www.springerlink.com/index/10.1007/978-1-4020-6241-4{%}5Cnhttp://dx.doi.org/10.1007/978-1-4020-6241-4{_}5 doi: 10.1007/ 978-1-4020-6241-4_5.

Phillips HM, Mahendran P, Singh E et al (2013) Neural crest cells are required for correct positioning of the developing outflow cushions and pattern the arterial valve leaflets. Cardiovasc Res 99:452–460

Playford, David; Weyman, Arthur (2001). "Mitral valve prolapse: time for a fresh look". Reviews in Cardiovascular Medicine. 2 (2): 73–81. PMID 12439384

Poplin, R., Ruano-Rubio, V., DePristo, M.A., Fennell, T.J., Carneiro, M.O, Geraldine A. Auwera, V., Kling, E., Gauthier, L.D., Ami Levy-Moonshine, David Roazen, Khalid Shakir, Joel Thibault, Sheila Chandran, Chris Whelan, Monkol Lek, Stacey Gabriel, Daly, M.J., Neale, B., MacArthur, M.G., and Banks, E. (2017). Scaling accurate genetic variant discovery to tens of thousands of samples. bioRxiv, doi: https://doi.org/10.1101/201178

Pradhan, L., Genis, G., Scone, P., Weinberg, E.O., Kasahara,and Nam, H. (2012). Crystal Structure of the Human NKX2.5 Homeodomain in Complex with DNA Target. Biochemistry. 51(32): 6312–6319. doi:10.1021/bi300849c

Pu D, Du JL, Zhang J, Li XQ, Weng MJ, Liu YJ, Gao LZ, Xia S, Chen YQ, She Q. (2013). An economical and practical method for whole-mount in situ hybridization for mouse embryos and organs. Biotech Histochem. 88(1):27-37. doi: 10.3109/10520295.2012.724712.

Puchtler, H. and S. N. Meloan (1985). On the chemistry of formaldehyde fixation and its effects on immunohistochemical reactions. Histochemistry. 82(3): 201-204.

Qi X, Yang G, Yang L, et al. (2007) Essential role of Smad4 in maintaining cardiomyocyte proliferation during murine embryonic heart development. Dev Biol 311, 136–146.

Quach, N., Goodman, M.F. and Shibata, D. (2004). In vitro mutation artifacts after formalin fixation and error prone translesion synthesis during PCR BMC Clinical Pathology

Reamon-Buettner, S., Cirbilli, Y., Inga, A., and Borlak, J. (2008). A loss-of-funtion mutation in the binding domain of HAND1 predicts hypoplasia of the Human hearts. Human molecular genetics. 17(10): 1397- 1405.

Reamon-Buettner, S.M, Ciribilli, Y., Inga, A, Borlak, J. (2008). A loss-of- function mutation in the binding domain of HAND1 predicts hypoplasia of the human hearts. Hum Mol Genet. 17:1397– 405.

Reamon-Buettner, S.M., Ciribilli, Y., Traverso, I., Kuhls, B., Inga, A., and Borlak, J. (2009). A functional genetic study identifies HAND1 mutations

in septation defects of the human heart. Hum Mol Genet. 18(19):3567-78. Epub 2009 Jul 7.

Reaume, A. G., de Sousa, P. A., Kulkarni, S., Langille, B. L., Zhu, D., Davies, T. C., Juneja, S. C., Kidder, G. M., Rossant, J. (1995). Cardiac malformation in neonatal mice lacking connexin43. Science 267: 1831-1834.

Reid K. (1970). The anatomy of the sinus of Valsalva. Thorax. 1970. 25:79–85

Reller MD, Strickland MJ, Riehle-Colarusso T, Mahle WT, Correa A (2008) Prevalence of congenital heart defects in metropolitan Atlanta, 1998-2005. J Pediatr.153(6):807.

Ruffalo, M, LaFramboise T, Koyutürk M (2011) Comparative analysis of algorithms for next-generation sequencing read alignment. Bioinformatics 27: 2790-2796. doi:10.1093/bioinformatics/btr477. PubMed: 21856737.

Saied, A., and Folger, G.M. (1972). Hypoplastic left heart syndrome. Clinicopathologic and hemodynamic correlation. Am J Cardiol. 29: 190–196.

Saleem, R. A., Banerjee-Basu, S., Murphy, T. C., Baxevanis, A. and Walter, M. A. (2004). Essential structural and functional determinants within the forkhead domain of FOXC1. Nucleic Acids Res. 32(14): 4182–4193.

Santos, M.C.L.G, Saito, C.P.B., and Line, S.R.P. (2008). Extraction of genomic DNA from paraffin-embedded tissue sections of human fetus fixed and stored in formalin for long period. Pathology: Research and practice. 204 (2008): 633-636.

Sauka-Spengler T, Bronner-Fraser M (2008) A gene regulatory network orchestrates neural crest formation. Nat Rev Mol Cell Biol 9:557–568

Scherptong RW, Jongbloed MR, Wisse LJ, Vicente-Steijn R, Bartelings MM, Poelmann RE, Schalij MJ, Gittenberger-De Groot AC. (2012) Morphogenesis of outflow tract rotation during cardiac development: the pulmonary push concept. Dev Dyn. 241(9):1413-22. doi: 10.1002/dvdy.23833.

Schmiedeberg, L., Skene, P., Deaton, A., and Bird, A. (2009) A Temporal Threshold for Formaldehyde Crosslinking and Fixation. PLoS ONE 4(2): e4636. doi:10.1371/journal.pone.0004636

Seo, S. and Kume, T. (2006). Forkhead transcription factors, Foxc1 and Foxc2, are required for the morphogenesis of the cardiac outflow tract. Developmental Biology. 296(2):421-436.

Shao, Q., Liu, q.,Lorentz, R., Gong, X., Bai, D., Shaw, G.S., and Laird, D.W. (2012). Structure and functional studies of N-terminal Cx43 mutants linked to oculodentodigital dysplasia. Mol Biol Cell. 23(17): 3312–3321.

Shi, S., Cote, R.J., Wu, L., Datar, R., Shi, Y., Liu, D., Lim, H., and Tylor, C.R. (2002). DNA extraction from archival formalin-fixed paraffin embedded tissue sections based on the antigen retrieval principle: heating under the influence of pH. Rapid communication. 50(8): 1005-1011.

Shinebourne, EA., Macartney,FJ., and Anderson, RH. (1976). Sequential chamber localization logical approach to diagnosis in congenital heart diseases. British Heart Journal, 38: 327-340.

Shokeir, M. H. K. (1972). Hypoplastic left heart syndrome: an autosomal recessive disorder. Clin. Genet. 2: 7-14.

Shokeir, M.H. (1974). Hypoplastic left heart. Evidence for possible autosomal recessive inheritance. Birth Defects Orig Artic Ser.10(4):223-7.

Shone JD, Sellers RD, Anderson RG, Adams P, Lillehei CW, Edwards JE. (1963). The developmental complex of “parachute mitral valve”, supravalvar ring of left atrium, subaortic stenosis, and coarctation of the aorta. Am J Cardiol. 11: 714–725.

Shrivastava, K., Thakur, M.s., Tomar, M.P.S., Shrivastav, A.B., and Parmar, S.N.S. (2012). Extraction of genomic DNA from formalin fixed tissues of different wild avian species. Annals of Biological research. 3 (7): 3174-3177.

Shrivastava, T., Mino, K., Babayeva, N.D., Baranovskaya, O.I., Rizzino, A., and Tahirov, T.G. (2014). Structural basis of Ets1 activation by Runx1. Leukemia. 28(10): 2040–2048. doi: 10.1038/leu.2014.111

Siffel, C., Riehle-Colarusso, T., Oster, M. E., & Correa, A. (2015). Survival of Children With Hypoplastic Left Heart Syndrome. Pediatrics, 136(4), e864–e870. doi:10.1542/peds.2014-1427

Simsic, J.M., Bradley, S.M., Stroud, M.R., and Atz, A.M. (2005). Risk factors for interstage death after the Norwood procedure. Pediatr Cardiol, 26, pp. 400-403

Skalicky, J.J., Donaldson, L.W, Petersen JM, Graves BJ, and McIntosh, L.P. (1996). Structural coupling of the inhibitory regions flanking the ETS domain of murine Ets-1. Protein Sci. 5(2):296–309.

St. Geme JW Jr, Noren GR, Adams P Jr. (1966). Proposed embryopathic relation between mumps virus and primary endocardial fibroelastosis. N Engl J Med. 275: 340–347.

Stankiewicz, P., Sen, P., and Bhatt, S.S. (2009). Genomic and genic deletions of the FOX gene cluster on 16q24.1 and inactivating mutations of FOXF1 cause alveolar capillary dysplasia and other malformations. Am J Hum. 84(6):780-791.

Stankiewicz, P., Sen, P., Bhatt, S. S., Storer, M., Xia, Z., Bejjani, B. A., … Shaw-Smith, C. (2009). Genomic and genic deletions of the FOX gene cluster on 16q24.1 and inactivating mutations of FOXF1 cause alveolar capillary dysplasia and other malformations. American journal of human genetics, 84(6), 780–791. doi:10.1016/j.ajhg.2009.05.005

Stanley, E.G., Biben, C., Elefanty, A., Barnett, L., Koentgen, F., Robb, L. et al. (2002). Efficient Cre-mediated deletion in cardiac progenitor cells conferred by a 3′UTR-ires-Cre allele of the homeobox gene Nkx2-5. Int J Dev Biol, 46. pp. 431-439.

Steimle, J.D. and Moskowitz, I.P. (2017).TBX5: A Key Regulator of Heart Development. Curr Top Dev Biol. 122: 195–221.

Strehl, S., Glatt, K., Liu, Q.M., Glatt, H., and Lalande, M. (1998). Characterization of two novel protocadherins (PCDH8 and PCDH9) localized on human chromosome 13 and mouse chromosome 14. Genomics. 53(1):81-9.

Sugiyama, H., Yutani, C., Iida, K., Arakaki, Y., Yamada, O., and Kamiya, T. (1999). The relation between right ventricular function and left ventricular morphology in hypoplastic left heart syndrome: angiographic and pathological studies. Pediatr Cardiol, 20: pp. 422-427.

Sun, R., Liu, M., Lu, L. Zheng, Y., and Zhang, P. (2015). Congenital Heart Disease: Causes, Diagnosis, Symptoms, and Treatments. Cell Biochem Biophys. 72 (3): 857-860. https://doi.org/10.1007/s12013-015-0551-6

T.H. Morgan, C.B. Bridges (1916). Sex-linked inheritance in Drosophila pointedP2 act sequentially to regulate Drosophila heart development.

Takano-Maruyama, M., Hase, K., Fukamachi, H., Kato, Y., Koseki, H., and Ohno, H. (2006). Foxl1-deficient mice exhibit aberrant epithelial cell positioning resulting from dysregulated EphB/EphrinB expression in the small intestine. Am J Physiol Gastrointest Liver Physiol. 291(1):G163-70. Epub 2006 Feb 9.

Tanaka M, Wechsler SB, Lee IW, Yamasaki N, Lawitts JA, Izumo S. (1999). Complex modular cis-acting elements regulate expression of the cardiac specifying homeobox gene Csx/Nkx2.5. Development. 126(7):1439-50.

Tang, P. Y. E.(2006) Editor, National Research Council. Path to Effective Recovering of DNA from Formalin-Fixed Biological Samples in Natural History Collections: Workshop Summary, Washington, ISBN: 0-309-66399-7, 64 pages, 6 x 9DC: The National Academies Press. https://doi.org/10.17226/11712.

Tao, Y. K., Zeng, H., Zhang, G. Q., Chen, S. T., Xie, X. J., He, X., … Chen, J. X. (2017). Notch3 deficiency impairs coronary microvascular maturation and reduces cardiac recovery after myocardial ischemia. International journal of cardiology, 236, 413–422. doi:10.1016/j.ijcard.2017.01.096\

Tchervenkov CI, Jacobs JP, Weinberg PM, Aiello VD, Béland MJ, Colan SD, Elliott MJ, Franklin RC, Gaynor JW, Krogmann ON, Kurosawa H, Maruszewski B, Stellin G. (2006). The nomenclature, definition and classification of hypoplastic left heart syndrome. Cardiol Young. 2006 Aug;16(4):339-68.

Tchervenkov CI, Tahta SA, Jutras L, Béland MJ. (1998). Biventricular Thorac Surg. 66: 1350–1357.

Tchervenkov, C.I., Jacob, M.L., and Tahta, S.A. (2000). Congenital Heart Surgery Nomenclature and Database Project: hypoplastic left heart syndrome. The Annals of Thoracic Surgery. 69(3):pp 170-179.

Thattaliyath B., and Hutson M. (2016) Neural Crest. In: Rickert-Sperling S., Kelly R., Driscoll D. (eds) Congenital Heart Diseases: The Broken Heart. Springer, Vienna

Thavarajah, R., Mudimbaimannar, V. K., Elizabeth, J., Rao, U. K., & Ranganathan, K. (2012). Chemical and physical basics of routine formaldehyde fixation. Journal of oral and maxillofacial pathology : JOMFP, 16(3), 400-5.

Theis JL, Zimmermann MT, Evans JM, Eckloff BW, Wieben ED, Qureshi MY, O'Leary PW, and Olson TM. (2015). Recessive MYH6 Mutations in Hypoplastic Left Heart With Reduced Ejection Fraction. Circ Cardiovasc Genet. 8(4):564-71.

Tian Y, Morrisey EE. Importance of myocyte-nonmyocyte interactions in cardiac development and disease. Circ Res. 2012;110(7):1023–1034. doi: 10.1161/CIRCRESAHA.111.243899.

Timmerman, L.A, Grego-Bessa J, Raya A, Bertrán E, Pérez-Pomares JM, Díez J, Aranda S, Palomo S, McCormick F, Izpisúa-Belmonte JC, and de la Pompa, JL. (2004). Notch promotes epithelial-mesenchymal transition during cardiac development and oncogenic transformation. Genes Dev.18(1):99-115.

Tirosh-Finkel L, Zeisel A, Brodt-Ivenshitz M et al (2010) BMP-mediated inhibition of FGF signaling promotes cardiomyocyte differentiation of anterior heart field progenitors. Development 137:2989–3000

Toth, J. and Biggin, M.D. (2000).The specificity of protein–DNA crosslinking by formaldehyde: in vitro and in Drosophila embryos Nucleic Acids Res. 28(2): e4.

Tynan, M. J., Becker, A. E., Macartney, F. J., Jimenez, M. Q., Shinebourne, E. A., & Anderson, R. H. (1979). Nomenclature and classification of congenital heart disease. Br Heart J, 41(5), 544-553.

Uddin MKM, Kimura W, Amin MB, Nakamura K, Islam MJ, Yamagishi H, Miura N. (2016). The Loss of Foxc2 Expression in the Outflow Tract Links the Interrupted Arch in the Conditional Foxc2 Knockout Mouse. SourceEtiology and Morphogenesis of Congenital Heart Disease: From Gene Function and Cellular Interaction to Morphology [Internet]. Tokyo: Springe. Chapter 27.

Uddin, M.K., Kimura, W., Ishikura, T., Koseki, H., Yoshida, N., Islam, M.J., Amin, M.B., Nakamura, K., Wu, Y.X., Sato, K., Aoto, K., and Miura, N. (2015). Foxc2 in pharyngeal arch mesenchyme is important for aortic arch

artery remodelling and ventricular septum formation. Biomed Res. 36(4):235-45. doi: 10.2220/biomedres.36.235.

Ungaro, C., Mazzei, R., Conforti, F.L., Sprovieri, T., Servillo, P., Liguori, M., Citrigno, L., Gabriele, A.L., Magariello, A., Patitucci, A., Muglia, M., and Quattrone, A. (2009). CADASIL: extended polymorphisms and mutational analysis of the NOTCH3 gene. J Neurosci Res. 87(5):1162-7. doi: 10.1002/jnr.21935

Uyttendaele, H., Marazzi, G., Wu, G., Yan, Q., Sassoon, D., and Kitajewski, J. (1996). Notch4/int-3, a mammary proto-oncogene, is an endothelial cell-specific mammalian Notch gene. Development, 122: pp. 2251-2259

Van de Laar, I. M. B. H., Oldenburg, R. A., Pals, G., Roos-Hesselink, J. W., de Graaf, B. M., Verhagen, J. M. A., Hoedemaekers, Y. M., Willemsen, R., Severijnen, L.-A., Venselaar, H., Vriend, G., Pattynama, P. M., and 14 others. (2011). Mutations in SMAD3 cause a syndrome form of aortic aneurysms and dissections with early-onset osteoarthritis. Nature Genet. 43: 121-126.

van den Hoff MJ, Moorman AF, Ruijter JM et al (1999) Myocardialization of the cardiac outflow tract. Dev Biol 212:477–490

Verma, S.K., Deshmukh, V., Nutter, C.A., Jaworski, E, Jin, W., Wadhwa, L., Abata, J., Ricci, M., Lincoln, J., Martin JF, Yeo GW, and Kuyumcu-Martinez, M.N. (2016). Rbfox2 function in RNA metabolism is impaired in hypoplastic left heart syndrome patient hearts. Sci Rep. 3 (6):30896. doi: 10.1038/srep30896.

Vida, V.L., Bacha, E.A, Larrazabal, A., Gauvreau, K., Dorfman, A.L., Marx, G. et al. (2008). Surgical outcomes for patients with the mitral stenosis–aortic atresia variant of hypoplastic left heart syndrome. J Thorac Cardiovasc Surg.135: pp. 339-346

Vincent SD and Buckingham ME (2010) How to make a heart: the origin and regulation of cardiac progenitor cells. Curr Top Dev Biol 90:1–41

Vincentz, J. W., Barnes, R. M., and Firulli, A. B. (2011). Hand factors as regulators of cardiac morphogenesis and implications for congenital heart defects. Birth Defects Res A Clin Mol Teratol, 91(6), 485-494. doi:10.1002/bdra.20796

Visel, A., Thaller, C., & Eichele, G. (2004). GenePaint.org: an atlas of gene expression patterns in the mouse embryo. Nucleic acids research, 32(Database issue), D552–D556. doi:10.1093/nar/gkh029

Waldo K, Miyagawa-Tomita S, Kumiski D et al (1998) Cardiac neural crest cells provide new insight into septation of the cardiac outflow tract: aortic sac to ventricular septal closure. Dev Biol 196:129–144

Waldo KL, Lo CW, Kirby ML (1999) Connexin 43 expression reflects neural crest patterns during cardiovascular development. Dev Biol 208:307–323

Walsh, P.S. Metzger, D.A. Higuchi,R. (1991). Chelex 100 as a medium for simple extraction of DNA for PCR-based typing from forensic material, Biotechniques 10 (4): 506–513.

Wang, J. H., Gouda-Vossos, A., Dzamko, N., Halliday, G., & Huang, Y. (2013). DNA extraction from fresh-frozen and formalin-fixed, paraffin-embedded human brain tissue. Neuroscience bulletin, 29(5), 649–654. doi:10.1007/s12264-013-1379-y

Wardwell-Ozgo J, Dogruluk T, Gifford A, et al. (2014). HOXA1 drives melanoma tumor growth and metastasis and elicits an invasion gene expression signature that prognosticates clinical outcome. Oncogene. 33:1017-1026

Waterhouse, A.M., Procter, J.B., Martin, D.M.A, Clamp, M. and Barton, G. J. (2009) Jalview Version 2 - a multiple sequence alignment editor and analysis workbench. Bioinformatics. 25(9): 1189-1191 doi: 10.1093/bioinformatics/btp033

Wei, C., Qiu, J., Zhou, Y., Xue, Y., Hu, J., Ouyang, K., … Fu, X. D. (2015). Repression of the Central Splicing Regulator RBFox2 Is Functionally Linked to Pressure Overload-Induced Heart Failure. Cell reports, 10(9), 1521–1533. doi:10.1016/j.celrep.2015.02.013

Wessels A, Sedmera D. (2003). Developmental anatomy of the heart: a tale of mice and man. Physiol Genomics. 15(3):165-76.

Wessels, A. and Sedmera, D. (2003). Developmental anatomy of the heart: a tale of mice and man. Physiol Genomics 15: 165–176.

Whitaker, Kent (2001). "Fetal Circulation". Comprehensive Perinatal and Pediatric Respiratory Care. Delmar Thomson Learning. pp. 18–20. ISBN 978-0-7668-1373-1.

Wiszniak, S.E., and Schwarz, Q.P. (2014). Neural Crest Cells in Vascular Development. Neural Crest Cells: Evolution, Development and Diseases. Pp. 313-333.

Wolfraim, L. A., Fernandez, T. M., Mamura, M., Fuller, W. L., Kumar, R., Cole, D. E., Byfield, S., Felici, A., Flanders, K. C., Walz, T. M., Roberts, A. B., Aplan, P. D., Balis, F. M., Letterio, J. J. (2004). Loss of Smad3 in acute T-cell lymphoblastic leukemia. New Eng. J. Med. 351: 552-559.

Wollins DS, Ferencz C, Boughman JA, Loffredo CA. (2001). A population-based study of coarctation of the aorta: comparison of infants with and without associated ventricular septal defect. Teratology. 64: 229–236.

Wotton, K.R., Mazet, F.O. and Shimeld, S.M. (2008). Expression of FoxC, FoxF, FoxL1, and FoxQ1 Genes in the Dogfish Scyliorhinus canicula Defines Ancient and Derived Roles for Fox Genes in Vertebrate Development. Developmental dynamics. 237:1590–1603

Wu, Q. and Maniatis, T. (1999). A striking organization of a large family of human neural cadherin-like cell adhesion genes. Cell. 97(6):779-90.

Xu X, Friehs I, Zhong Hu T, Melnychenko I, Tampe B, Alnour F, Iascone M, Kalluri R, Zeisberg M, Del Nido PJ, Zeisberg EM. Endocardial fibroelastosis is caused by aberrant endothelial to mesenchymal transition. Circ Res. 2015;116(5):857–866. doi: 10.1161/CIRCRESAHA.116.305629.

Yamada, S., Samtani, R. R., Lee, E. S., Lockett, E. , Uwabe, C. , Shiota, K. , Anderson, S. A. and Lo, C. W. (2010), Developmental atlas of the early first trimester human embryo. Dev. Dyn., 239: 1585-1595. doi:10.1002/dvdy.22316

Yabrodi, M., & Mastropietro, C. W. (2017). Hypoplastic left heart syndrome: from comfort care to long-term survival. *Pediatric research*, *81*(1-2), 142–149. doi:10.1038/pr.2016.194

Yang, C., Xu, Y., Yu M, Lee D, Alharti S, Hellen N, Ahmad Shaik N, Banaganapalli B, Sheikh Ali Mohamoud H, Elango R, Przyborski S, Tenin G, Williams S, O'Sullivan J, Al-Radi OO, Atta J, Harding SE, Keavney B, Lako M, Armstrong L. (2017). Induced pluripotent stem cell modelling of HLHS

underlines the contribution of dysfunctional NOTCH signalling to impaired cardiogenesis. Hum Mol Genet. 26(16):3031-3045. doi: 10.1093/hmg/ddx140.

Ye, M., Coldren, C., Liang, X., Mattina T, Goldmuntz E, Benson DW, Ivy D, Perryman MB, Garrett-Sinha LA, and Grossfeld, P. Deletion of ETS-1, a gene in the Jacobsen syndrome critical region, causes ventricular septal defects and abnormal ventricular morphology in mice. (2010). Hum Mol Genet. 19(4):648-56.

Ye, M., Coldren, C., Liang, X., Mattina, T., Goldmuntz, E., Benson, D. W., Ivy, D., Perryman, M. B., Garrett-Sinha, L. A., … Grossfeld, P. (2009). Deletion of ETS-1, a gene in the Jacobsen syndrome critical region, causes ventricular septal defects and abnormal ventricular morphology in mice. Human molecular genetics, 19(4), 648-56.

Young BK, Roqué H, Abdelhak Y, Timor-Tristch I, Rebarber A, Rosen R. (2001). Endoscopic ligation of umbilical cord at 19 week's gestation in monoamniotic monochorionic twins discordant for hypoplastic left heart syndrome. Fetal Diagn Ther. 16(1):61-4.

Yu, S., Shao, L., Kilbride, H., and Zwick, D.L. (2010). Haploinsufficiencies of FOXF1 and FOXC2 genes associated with lethal alveolar capillary dysplasia and congenital heart disease. Am J Med Genet A. 152A(5):1257-62.

Zaffran S, Kelly RG, Meilhac SM et al (2004) Right ventricular myocardium derives from the anterior heart field. Circ Res 95:261–268

Zaffran, S and Frasch, M. (2002). Early signals in cardiac development. Circ. Res. pp. 457-469.

Zhou, X.L. and Liu, J.C. (2014). Role of Notch signaling in the mammalian heart. Braz J Med Biol Res. 47(1): 1–10

Zweifel, M.E., Leahy, D.J., Hughson, F.M., Barrick, D. (2003). Structure and stability of the ankyrin domain of the Drosophila Notch receptor. Protein Sci. 12(11):2622-32.

Almekhlafi MA, Wilton SB, Rabi DM, Ghali WA, Lorenzetti DL, Hill MD. (2009). Recurrent cerebral ischemia in medically treated patent foramen ovale: a meta-analysis. Neurology. 14;73(2):89-97. doi: 10.1212/WNL.0b013e3181aa2a19

Chapter 8: Appendicies

Table 8.1: The reported frequency of HLHS occurring over the last 40 years.

Study region	Time period	population incidence*	CHD incidence*	Phenotypes	Comment	Reference
Birmingham, UK	??	0.03%		Not indicated		Barron et. al, 2009
Malta	1977-1994		0.4 % classical HLHS 0.6% HLHS variants	Classical HLHS and HLHS variants.	National Paediatric Cardiology Database	Grech, 1999
USA	1979-1988	0.016-0.036% cases in USA & Canada	2-9% HLHS	Not indicated	National Center for Health Statistics.	Fruitman, 2000
Bohemia	1980		1.4–3.8%	stenotic and atretic mitral and aortic valves	Autopsy study	Samánek et.al, 1989
Baltimore Washington	1981-1982		3.8%	Not indicated	No phenotype was given	Goldmuntz, 2003
California, USA	1995 and 1999		2-3%	No phenotype was given	Hospital discharge database	Gordon et. al, 2008
Atlanta, USA	1998 to 2005		2- 3%	Not indicated	Metropolitan Atlanta Congenital Defects Program.No phenotype was given	Reller et. al, 2008
Cincinnati, USA	2004-2006	0.02% of HLHS	2% of HLHS associated with CVM	Atresia and stenosis of left-side valves with intact atrial septum. Other HLHS group with associated with cardiovascular malformation (CVM).	Cardiology departmental data	Hinton et. al., 2007

Table 8.2: List of HLHS hearts used in the study including the measurements performed.

Case#	Groups	EFE	Hypertrophy	Mitral valve	Aortic valve	LV size	LV free wall (mm)	RV free wall (mm)	EFE size (mm)	LV length (mm)	RV length (mm)	Aortic size (mm)	pul size (mm)	LCC to SCA (mm)	LCC to duct (mm)	clinical classification
83-101	slit-like	no	no	absent	absent	Slit-like	1.17	5		24	42	3	13.4	6	10.72	AA/MA
6032-92	slit-like	no	no	absent	absent	slit like	3.1	5.8		25.3	34.6	4	15.4	8.6	8.6	AA/MA
66-183	slit-like	no	no	absent	absent	slit-like	4.33	5.46		28.14	38	2.7	14.6	2.5	8.6	AA/MA
67-153	slit-like	no	no	absent	absent	slit like	2.2	2.6	-	18.2	32.8	1.5	13.8	-	-	AA/MA
68-100	slit-like	no	no	absent	absent	slit like	5	3.8	-	31	39	2.54	13.3	7.4	8.1	AA/MA
70-132	slit-like	no	no	absent	absent	Slit-like	3.26	7.6		35	48	4.68	17	7.4	6.5	AA/MA
76-71	slit-like	no	no	absent	absent	Slit-like	3	4.9	-	26.05	33.7	3.9	16.7	4.08	12.9	AA/MA
79-39	slit-like	no	no	absent	absent	slit-like	1.53	3.9		28.8	34.9	4.1	13.97	-	-	AA/MA
79-73	slit-like	no	no	absent	absent	slit like	1.95	3		29	36	2.9	16	1.8	10.7	AA/MA
79-76	slit-like	no	no	absent	absent	slit like	4.25	7.6		24.5	31.6	4.3	15	6.9	12.2	AA/MA
74-106	slit-like	no	no	small	absent	slit-like	2.2	4.5	-	25.3	30.5	3.3	13.1	2	14	AA/MA
4-94	slit-like	no	no	absent	absent	slit-like	3.8	4.9	-	30.5	38.4	5.2	17.8	5	13.8	AA/MA
57-149	slit-like	no	no	absent	absent	slit-like	2.4	3.4	-	24	29.5	2.1	13.3	4.8	7	AA/MA
59-317	slit-like	no	no	absent	absent	slit-like	2.6	4.2	-	22	36	1.9	12	-	-	AA/MA
60-4	slit-like	no	no	normal	absent	slit-like	2.4	3.8	-	18	25	2.1	12.9	1.4	5.5	AA/MA
62-261	slit-like	no	no	absent	absent	slit-like	3.5	4.8	-	27	34	2.8	14.7	10	12.5	AA/MA
69-140	slit-like	no	no	absent	bicupsid	slit-like	4.1	6.9	-	25	36	4.7	15.6	-	-	AA/MA

70-75	slit-like	no	no	absent	absent	slit-like	3.6	3.6	-	22	32	1.86	14.4	3.4	11.5	AA/MA
73-10	slit-like	no	no	absent	absnet	slit-like	2.5	4.2	-	23.1	27	3.9	14.9	5.7	6.3	AA/MA
68-159	Thick walled ventricle	yes	yes	Image	absent	small	6.5	4.5	1.9	23.5	37.2	4.7	13.5	3	10.6	AA/MS
68-190	Thick walled ventricle	yes	yes	normal	absent	Small	12.4	4.3	1.7	26	34	5.3	13.7	4.7	6.7	AA/MS
69-148	Thick walled ventricle	yes	no	normal	absent	small	5.3	6.2	1	20.2	38	3	16.3	7.2	6.8	AA/MS
69-89	Thick walled ventricle	yes	yes	normal	absent	moderate	8.35	4.2	1.2	22	33	6.6	12.59	6	12.2	AA/MS
71-119	Thick walled ventricle	yes	yes	Image	Dysplastic	moderate	7.5	6.1	2.1	25	33	4.2	13	1.4	11.9	AA/MS
77-09	Thick walled ventricle	yes	yes	normal	absent	small	7.1	7.17	1	16	33	6.5	14.4	5.6	12.3	AA/MS
77-55	Thick walled ventricle	yes	yes	normal	absent	small	6.8	4	0.1	21	37	5.9	12.2	1.2	6.8	AA/MS
77-70	Thick walled ventricle	yes	yes	normal	not opened	small	9.74	4.8	1.81	27	35.3	6.7	13.15	4.5	4.5	AA/MS
79-111	Thick walled ventricle	yes	yes	normal	absent	small	4.6	3.25	26.8	33.3	43		-	-	-	AA/MS
79-51	Thick walled ventricle	yes	yes	normal	unicuspid	small	4.37	4.4	0.5	18.09	32	7.23	12.2	2.4	10.5	AA/MS
79-89	Thick walled ventricle	yes	yes	normal	unicuspid	small	11.3	7	1.7	22	41	9.85	16.4	5.3	12.4	AA/MS
80-42	Thick walled ventricle	yes	yes	normal	absent	small	11.8	5.9	0.3	23.7	41.3	6	16	6	15	AA/MS
84-06	Thick walled ventricle	yes	yes	normal	absent	small	4.8	5	0.9	28.4	49	6.1	13.6	4.1	12.6	AA/MS
55-186	Thick walled ventricle	yes	yes	normal	absent	small	9.8	4.6	1	24.5	34	3.7	14.6	-	-	AA/MS
62-300	Thick walled ventricle	yes	yes	normal	absent	small	7.5	4.7	1.8	26	37	5.7	14.2	3.6	10.7	AA/MS
62-32	Thick walled ventricle	yes	yes	normal	absent	small	6.2	3.2	0.9	17.9	29.6	4.7	12.4	-	-	AA/MS
64-106	Thick walled ventricle	yes	yes	normal	absent	small	9.7	4.5	2.8	22.6	31.5	6.1	12.5	-	-	AA/MS
66-216	Thick walled ventricle	yes	yes	normal	absent	small	9.3	3.3	1.6	23.3	37.9	5.5	16.8	-	-	AA/MS
67-144	Thick walled ventricle	yes	yes	normal with nodules	absnet	small	6.9	5.1	1.1	19.8	31	3	13	3.6	9.5	AA/MS

69-105	Thick walled ventricle	yes	yes	normal	absent	small	6	5.2	1	24	35	4.35	17.1	3.5	12.9	AA/MS
70-11	Thick walled ventricle	yes	yes	normal	absent	small	7.7	4.9	1.9	24.6	33.7	2.8	14.1	5.3	8.2	AA/MS
70-31	Thick walled ventricle	yes	yes	normal	absent	small	6.6	3.7	0.9	20.7	31.9	3.3	15.3	3.3	11.3	AA/MS
72-143	Thick walled ventricle	yes	yes	normal	absent	small	11	6.9	1	23.7	33.2	3.8	16.7	1.4	13	AA/MS
74-92	Thick walled ventricle	yes	yes	normal	absent	small	9.8	5.4	0.9	28	34.3	2.4	12.5	1.5	8.2	AA/MS
75-8	Thick walled ventricle	yes	yes	normal	absent	small	6.1	3.7	0.8	19.4	30.5	4.5	13.4	1.7	13.5	AA/MS
75-96	Thick walled ventricle	yes	yes	normal dysplastic	absent	small	6.4	5.7	1.3	26.6	37.7	5.4	15.1	1.9	6.6	AA/MS
76-111	Thick walled ventricle	yes	yes	normal	absent	Small	8.2	4.6	-	24.7	32.8	4.4	13.2	1.88	9.9	AA/MS
77-25	Thick walled ventricle	yes	yes	dysplastic	absent	small	7.3	4.6	2.3	19.8	37.4	4.7	11.7	5.5	6.6	AA/MS
56-188	Thick walled ventricle	yes	yes	dysplastic	absent	small	4.5	3.4	0.85	18.2	29	3.6	13.1	-	-	AA/MS
62-362	Thick walled ventricle	yes	yes	dysplastic	absent	small	8.5	5.2	1.6	28.2	38.8	5	17.4	14	13.5	AA/MS
50-273	Thick walled ventricle	yes	yes	dysplastic	absent	small	7.3	3.4	1.1	24	33.2	5.7	14.1	-	-	AA/MS
60-354	Thick walled ventricle	yes	yes	dysplastic	absent	moderate	8	4.3	1.5	20	27	8.9	15	3.3	9.6	AA/MS
79-124	Thick walled ventricle	no	no	normal	absent	small	3.45	3.05	-	22.5	30.9	4.18	14.3	5.9	5.9	AA/MS
8-91	Thick walled ventricle	no	yes	dysplastic	absent	small	6.2	4.7	-	29.37	37	5.7	12.4	2	12	AA/MS
80-85	Thick walled ventricle	no	yes	normal	absent	small	8.2	4	-	31	36	4.2	14.3	0.1	13	AA/MS
71-68	Thick walled ventricle	yes	yes	normal	small	small	6.8	5.4	1.4	25	38	6.7	14.6	1.6	12	AS/MS
74-66	Thick walled ventricle	yes	yes	normal	small	Small	7.7	5	2	26.4	37.3	4.3	11.7	4	15	AS/MS
75-81	Thick walled ventricle	yes	yes	normal	normal	moderate	7.3	5.9	1	33	39	5.6	13	2	2	AS/MS
84-81	Thick walled ventricle	yes	yes	normal	bicuspid	moderate	6	5.1	2	32	36.5	8.5	13.9	18	26	AS/MS

85-44	Thick walled ventricle	yes	yes	normal	bicuspid	small	5.3	6.9	1.5	24.8	33	6.5	13.6	-	-	AS/MS
-26	Thick walled ventricle	yes	yes	normal	dysplastic	moderate	6.1	3.8	2.2	25	33.8	7.2	16.2	10.1	11	AS/MS
42-77	Thick walled ventricle	yes	yes	normal	dysplastic (bicuspid)	small	6.2	5.1	1.2	25	37.4	3.2	10.9	-	-	AS/MS
49-260	Thick walled ventricle	yes	yes	normal	dysplastic	small	3.8	2.7	1.2	14.9	33	3.4	10.4	4.8	8.8	AS/MS
82-59	Thick walled ventricle	yes	yes	small	small	small	4.5	6.9	0.8	23	40.1	5.4	10.7	4.6	9.6	AS/MS
42-109	Thick walled ventricle	yes	yes	dysplastic	normal dysplastic	moderate	5.3	5.4	1.7	30	42	8.9	15.2	3.3	15.2	AS/MS
80-55	Thick walled ventricle	no	no	normal	dysplastic	small	6.9	5.4	-	26	41	5.9	16.8	13.8	13.8	AS/MS
59-14	Thick walled ventricle	no	yes	normal with nodules	bicupsid	moderate	9.9	6.9	?	34	42	9.9	14.5	0.9	14.1	AS/MS
71-170	Thick walled ventricle	yes	yes	normal	normal	moderate	3.4	6.3	1.3	23	30	8	13.3	9	17	AS/MS
73-132	Thick walled ventricle	yes	yes	normal	normal	small	6.9	4.4	2.5	23	34	7.2	12.2	4	4	AS/MS
73-57	Thick walled ventricle	yes	yes	normal	normal	small	4.5	5	0.8	26.4	37.5	7.35	14.9	2	12	AS/MS
74-105	Thick walled ventricle	yes	yes	normal	normal	small	8	3.3	4.8	30.4	42.3	8.4	12.1	3.1	15	AS/MS
74-109	Thick walled ventricle	yes	yes	normal	normal	large	7.2	4.4	2	27.7	33.5	7.8	13	1.5	8.4	AS/MS
63-136	Thick walled ventricle	yes	no	normal	normal	well-formed	8.4	5.6	2.7	40	40	9.3	18	6.3	17.6	AS/MS
63-113	Thick walled ventricle	yes	yes	normal	normal	small	7.7	3.8	1.8	24	34	5.5	13.1	1.3	8.5	AS/MS
67-187	Miniaturised ventricle	no	no	normal	normal	well-formed	4.5	4.35	-	26	32.5	4.9	13.3	-	-	AS/MS
69-35	Miniaturised ventricle	no	yes	normal	normal	small	4.7	5.3	-	31	36	7.7	12.2	6.5	9.5	AS/MS
75-48	Miniaturised ventricle	no	no	normal	normal	large	3.5	3.3	-	38	45.5	7.7	13.7	6.8	14	AS/MS
75-90	Miniaturised ventricle	no	small	normal	normal	Small	4.7	4.9	-	26	31	4.7	14.5	6.5	6	AS/MS
73-47	Miniaturised ventricle	no	no	normal	normal	moderate (well formed)	4.9	5.6	-	21	27.6	6.4	13.1	2	11.4	AS/MS